SANDIA REPORT
SAND88—2154 • UC—94cb
Unlimited Release
Printed August 1988

Exploratory Battery Technology Development and Testing Report for 1987

Nicholas J. Magnani, Ronald B. Diegle, Jeffrey W. Braithwaite,
Donald M. Bush, Paul C. Butler, James M. Freese,
Kenneth R. Grothaus, Kevin D. Murphy

Prepared by
Sandia National Laboratories
Albuquerque, New Mexico 87185 and Livermore, California 94550
for the United States Department of Energy
under Contract DE-AC04-76DP00789

Issued by Sandia National Laboratories, operated for the United States Department of Energy by Sandia Corporation.

Printed in the United States of America
Available from
National Technical Information Service
U.S. Department of Commerce
5285 Port Royal Road
Springfield, VA 22161

NTIS price codes
Printed copy: A09
Microfiche copy: A01

SAND88-2154
Unlimited Release
Printed August 1988

Distribution
Category UC - 94cb

Exploratory Battery Technology Development and Testing Report for 1987

Nicholas J. Magnani
Power Sources Department
Ronald B. Diegle, Jeffrey W. Braithwaite,
Donald M. Bush, Paul C. Butler, James M. Freese,
Kenneth R. Grothaus, and Kevin D. Murphy
Storage Batteries Division

Sandia National Laboratories
Albuquerque, NM 87185

Prepared by Dan W. Scott
Tech Reps, Inc.

Abstract

Sandia National Laboratories, Albuquerque, has been designated as Lead Center for the Exploratory Battery Technology Development and Testing Project, which is sponsored by the U.S. Department of Energy's Office of Energy Storage and Distribution. In this capacity, Sandia is responsible for the engineering development of advanced rechargeable batteries for both mobile and stationary energy storage applications. This report details the technical achievements realized in pursuit of the Lead Center's goals during calendar year 1987.

Contents

Figures

Tables

Acronyms and Abbreviations

ABS	Advanced Battery Systems
ADL	Analysis & Diagnostic Laboratory
ANL	Argonne National Laboratory
BBC	Brown, Boveri, and Cie
BEST	Battery Energy Storage Test Facility
BET	Brunauer, Emmett, Teller method for determining particle surface area
BSI	British Standards Institute
COMSAT	Communications Satellite Corporation
CPVC	chlorinated polyvinyl chloride
CSPL	Chloride Silent Power, Ltd.
CTE	coefficient of thermal expansion
DCOV	discharge cutoff voltage
DMA	dynamic mechanical analysis
DMF	dimethylformamide
DOD	depth of discharge
DOE	Department of Energy
DSEP	Dual Shaft Electric Propulsion Program
EHP	Electric and Hybrid Propulsion (a branch of DOE/OTS)
EPD	electrophoretic deposition
EPI	Eagle-Picher Industries
EPRI	Electric Power Research Institute
ERC	Energy Research Corporation
ETD	Exploratory Battery Technology Development and Testing Project
ETX	Electric Transaxle Experimental Test Vehicle Project
EV	electric vehicle
FACC	Ford Aerospace and Communications Corporation
F/T	freeze/thaw
FTIR	Fourier transform infrared analysis
FUDS	Federal Urban Driving Schedule
GPC	gel permeation chromatography
HNEI	Hawaii Natural Energy Institute
IDSEP	improved DSEP
IEC	ion exchange capacity
IR	internal resistance; infrared analysis
JCI	Johnson Controls, Inc.
LL	load leveling
LVDT	linear variable differential transformer
M	molar
NBTL	National Battery Test Laboratory
NMR	nuclear magnetic resonance
OCV	open-circuit voltage
OESD	DOE Office of Energy Storage and Distribution
OTS	DOE Office of Transporation Systems
PAA	polyacrylic acid
PASTF	Photovoltaic Advanced Systems Test Facility
PB	designation for the standard CSPL sodium/sulfur cell
PTA	posttest analysis
PV	photovoltaic

Acronyms and Abbreviations (continued)

PVC	polyvinylchloride
QC	quality control
RH	relative humidity
S^4D	seeded, slurry-solution spray drying
SAE	Society of Automotive Engineers
SAIC	Science Applications International Corporation
SEM	scanning electron microscopy
SFUDS	simplified FUDS
SNL	Sandia National Laboratories
SOC	state-of-charge
SPS	sulfonated polysulfone resins
TBR	Technology Base Research Project
TD	designation for a prototype CSPL sodium/sulfur cell (technology demonstration)
UK	United Kingdom
WEBS	wind energy battery storage model
XPB	extended (larger capacity) PB sodium/sulfur cell

Exploratory Battery Technology Development and Testing Report for 1987

Chapter 1. Executive Summary

Introduction

This report documents the activities of the Exploratory Battery Technology Development and Testing (ETD) Lead Center for calendar year 1987, ETD's seventh program year. (See SAND87-3094, *Exploratory Technology Development and Testing Report for 1986*, for a description of the previous year's activities.) The ETD Project, directed by Sandia National Laboratories (SNL), is supported by the U. S. Department of Energy, Office of Energy Systems Research, Energy Storage and Distribution Division (DOE/OESD). This project is operated in conjunction with the Technology Base Research (TBR) Project, which is under the direction of Lawrence Berkeley Laboratory. Together, these two projects seek to establish the scientific feasibility of advanced electrochemical energy storage systems and to conduct the initial engineering development on systems suitable for mobile and stationary commercial applications.

The ETD Project assumes responsibility for the engineering development of electrochemical couples whose feasibility has been demonstrated by either the TBR Project or other technically sound investigations. These systems will be incorporated into batteries for use in electric and hybrid vehicles, utility and commercial load leveling, and photovoltaic and wind-based electricity-generating systems. Battery development is accomplished through cost-sharing contracts with industrial partners. SNL is responsible for the technical direction of the development contracts and lead-center project management. Additionally, SNL conducts various applied-research activities (advanced membrane development, solid electrolyte fracture analysis, material durability studies, and container-plating development). Testing and analysis of the resulting batteries or components are performed either at SNL or, with SNL's guidance, at Argonne National Laboratory (ANL). SNL also undertakes a variety of battery cost-and-performance studies and analyses in connection with the ETD Project.

The ETD Lead Center is directed by Dr. Nicholas J. Magnani, manager of SNL's Power Sources Department. Lead Center operations are managed by Dr. Ronald B. Diegle, supervisor of SNL's Storage Batteries Division.

The organization of the ETD project for 1987 is illustrated in Figure 1-1. Its technical work is divided into three elements:

- Battery Technology Development
- Battery Technology Evaluation
- Battery Technology Improvement.

Supporting activities are grouped under two additional headings: Project Analysis and Planning, Budgeting, and Reporting. Each element is headed by an element manager who bore technical responsibility for all the activities within that element, including technical supervision of contracts outside SNL.

This report divides the ETD Project into four chapters. Two chapters are dedicated to the Battery Technology Development element, and

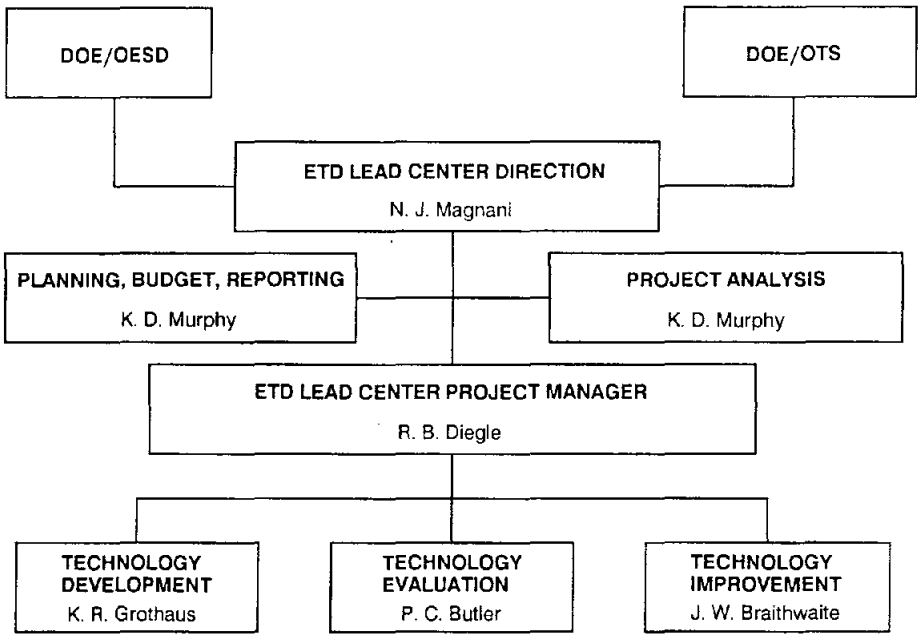

Figure 1-1. 1987 ETD Project Organization

the Battery Technology Evaluation and Improvement elements each have one chapter:

- Aqueous Battery Development (Chapter 2)
- Nonaqueous Battery Development (Chapter 3)
- Battery Technology Evaluation (Chapter 4)
- Battery Technology Improvement (Chapter 5).

In 1987, the ETD Project focused on four advanced secondary-battery technologies:

- sodium/sulfur
- zinc/bromine
- nickel/hydrogen
- aluminum/air.

A summary of the progress of the ETD Project in 1987, organized by battery technology, follows. More detailed information is found in Chapters 2 through 5.

Sodium/Sulfur Technology

In 1987, more of the ETD resources were directed to the sodium/sulfur technology than any one of the other three technologies. Two prime contractors and one national laboratory were involved in sodium/sulfur technology development, two national laboratories evaluated sodium/sulfur cells, and three Technology Improvement tasks supported this technology.

Technology Development

The primary developer of the sodium/sulfur technology for the ETD project in 1987 was Chloride Silent Power, Ltd., (CSPL), which completed the first two years of a four-year contract to continue research and development of core sodium/sulfur technology for both stationary and electric vehicle applications. Science Applications International Corporation (SAIC), a major subcontractor to CSPL, conducted work in battery engineering and testing. Ceramatec continued its evaluation of improvements to the beta"-alumina electrolyte, and ANL conducted posttest analysis of CSPL sodium/sulfur cells.

CSPL Technology Development

In 1987, CSPL continued to scale-up its electrolyte production. There was a four-fold increase in the fabrication of zero-defect electrolytes. PB electrolyte yields averaged 37%, and 50% yields were projected for 1988. Though this growth was achieved without adding zirconia to the electrolyte for microstructural improvement, cycle-life data indicate that further benefits can be derived from zirconia, providing a solution can be found to zirconia's increased moisture sensitivity. In addition, techniques for alcohol and powder reclamation were successfully developed.

CSPL implemented two important improvements in 1987:

- The MkIII metal-to-ceramic seal, which was developed to overcome the problems with the corrosion resistance of the previous seal design (MkIIA). The MkIII seal should increase cell reliability by preventing premature cell failure.

- The automatic sodium-filling machine, which lowers initial cell resistance, thus improving cell performance.

Science Applications International Corporation (SAIC), a major subcontractor to CSPL, developed a data acquisition and control apparatus that uses real-time X-ray radiography to observe sodium/sulfur cells during electrical cycling. This device was used to observe the behavior of two CSPL PB cells during freeze/thaw cycling, cell break-in, and electrical cycling. X-ray radiography has proven to be a valuable tool for understanding the behavior of the sodium/sulfur cell.

CSPL continued to make progress in the development of its standard PB cell, which is for electric vehicle applications. By the end of 1987, 1575 PB cells had been tested, and 282 of these cells had completed over 500 cycles. Compared to the 1984 technology, the 1987 PB cell has demonstrated a 16-fold improvement in cycle time required to fail one percent of the cells.

Work continued on the extended PB (XPB) cell (for load-leveling applications), which was in the early stages of development in early 1987. This year 235 XPB cells were tested, and 12 cells have exceeded 500 cycles.

There were several significant developments in module testing at CSPL:

- A 120-MkIII-PB-cell module (which features the more reliable metal-to-ceramic seal) was constructed, and testing is scheduled to begin in early 1988.

- The 120-PB-cell module completed 630 cycles before it was removed from testing, with 52 Ah of its original 120-Ah capacity. Its capacity decline matched SAIC computer predictions.

- A 16-XPB-cell module with improved thermal management was constructed to test the design of the final deliverable, a 240-XPB-cell battery.

SAIC was instrumental in creating the conceptual design of the SNL-deliverable XPB-cell battery. After several iterations, a baseline design consisting of six 40-cell battery segments was established. Because each segment will provide 8 V and 100 A, the battery can be configured to operate between 8 and 48 V and between 100 and 600 A. Flowing heated air will be used for battery thermal management. SAIC also conceptualized a cell-failure detection device that could be used with a thermal fuse to electrically remove bad cells.

Ceramatec Technology Development

Ceramatec continued comparative testing of beta"-alumina electrolytes. Zeta, S^{4}D (seeded, slurry-solution spray dried), and zirconia-toughened (unstabilized and partially stabilized) electrolytes were installed into sodium/sulfur cells, electrically cycled, visually inspected, cut, and burst-tested. None of the cells with the partially stabilized zirconia-toughened electrolytes or the Zeta electrolytes failed during electrical cycling. In addition, these two types of electrolytes had the least rise in resistance. The low resistance rise in the partially stabilized zirconia-toughened electrolytes was attributed to the gettering capability of zirconia. The burst tests, however, were inconclusive, apparently because of defects created by sectioning the

electrolytes. In order to make a fully valid evaluation of subcritical electrolyte degradation during cell cycling, Ceramatec has recommended testing of larger populations of electrolytes and of complete (uncut) electrolytes.

Posttest Analysis at ANL

In 1987, ANL performed posttest analysis of nine CSPL cells with the new MkIII metal-to-ceramic seal. Six cells had accumulated 63 cycles or less, one accumulated 242 cycles, one accumulated 520 cycles, and one cell was uncycled. Morphology of the sulfur electrode, gas formation in the sulfur electrode, and seal and electrolyte integrity were examined.

Significant findings included the following:

- It was found that higher-density felts in the cylindrical portion of the sulfur electrode could prevent slumping of active materials.
- Voids in the sulfur electrode at the base of the electrolyte tube were found to increase discharge polarization.
- Gas analysis revealed that water on the graphite felt of the sulfur electrode causes formation of hydrogen sulfide and carbon dioxide during electrical cycling. Hydrogen sulfide can corrode the sulfur seal, adversely affecting cell reliability.
- The MkIII seal was adequate in all but one cell.
- Measurable levels of calcium were detected on the interior of all electrolytes. Calcium can impede sodium transport through the electrolyte, reducing cell efficiency.

Technology Evaluation

ANL Evaluations

Eight CSPL PB cells were tested in 1987 at ANL. Seven of the eight cells continue life-cycle testing, with between 524 and 807 accrued cycles. Average capacity degradation was measured to be 0.1 Ah per 100 cycles, though degradation usually occurred in increments of 0.2 Ah to 0.3 Ah. The one cell failure was caused by a breach in the top seal. Simplified Federal Urban Driving Schedule (SFUDS) tests measured an average range of 258 miles for the CSPL-PB technology. In terms of specific energy versus specific power and peak power, CSPL PB cells exceeded FACC electric vehicle cells by ≈20%.

SNL Evaluations

In 1987, SNL tested three FACC cells (one for load leveling and two for electric vehicles) and eight CSPL PB cells. In addition, SNL began testing on two Powerplex cells this year.

All three FACC cells remained at above 97% operating capacity after accumulating between 393 and 798 cycles. However, installation of new test equipment suspended testing during almost half the year.

Of the eight CSPL cells, one was voluntarily removed from testing, five failed, and two were still on test by the end of 1987. One of the failures was caused by an overdischarge during an SFUDS test; the other four failures were attributed to leaks in the sodium and sulfur seals. The two CSPL cells still on test have completed 1140 and 781 cycles, with ≈85% of original capacity. Parametric testing highlighted the significant effect of temperature on cell capacity.

Technology Improvement

Failure Analysis of the Beta"-Alumina Electrolyte

SNL examined fractured electrolytes from two CSPL sodium/sulfur cells. It was found that one electrolyte was overfired during production, which caused the formation of numerous large grains. Cracking initiated at the large grains on or near the interior electrolyte surface, and sodium pressure caused the cracks to propagate during charging. In the second electrolyte, there apparently was nonuniform sodium wetting on the interior surface, and tensile stresses caused cracking in regions of poor wetting.

In addition, electromechanical degradation experiments were conducted at high

temperatures. These experiments indicate that the electrolyte may have to be free of both tensile and compressive stresses and that transformation toughening may not be desirable.

Component Stress During Freeze/Thaw Cycling of Sodium/Sulfur Cells

Because sodium/sulfur cells in both electric vehicle and load-leveling applications will be subjected to numerous freeze/thaw cycles, SNL is formulating a mathematical model that predicts stress within cell components caused by thermal cycling. This model will make it possible to determine the susceptibility of various cell designs to failure mechanisms.

This task's important accomplishments and findings in 1987 included the following:

- The feasibility and usefulness of modeling the freeze/thaw behavior of sodium/sulfur cells was demonstrated.
- It was determined that electrolyte stress is most influenced by the thermal expansion coefficient of the positive electrode.
- Localized volumetric changes caused by nonthermal amorphous-to-crystalline phase transformation were shown to cause electrolyte tensile stresses.
- The first strain measurements on functioning cells were completed. These measurements will be used to validate mathematical models.
- In support of the modeling effort, thermomechanical properties of sulfur and sulfur/graphite composites were measured using a variety of techniques.

Development of Improved Chromium Plating of Sodium/Sulfur Cell Containers

Because the present corrosion-resistant barrier on the interior of the CSPL cell container has limited durability (which can limit cell life) and high cost, development of a high-quality electroplated chromium layer was initiated in 1987. In 1985, SNL had developed a method of electroplating chromium on FACC cells that achieved a crack-free deposit, and two FACC cells with this chromium layer completed over 1200 cycles without failing. By the end of 1987, a chromium-plating facility for CSPL cell containers had been assembled and four different plating electrolytes were prepared for evaluation.

Zinc/Bromine Technology

Technology Development

Energy Research Corporation (ERC) was the primary developer of the zinc/bromine technology for the ETD project. By the end of 1987, ERC had completed two years of a four-year contract. The goals of this contract are to continue development of ERC's zinc/bromine core technology and to demonstrate a proof-of-concept 50-kWh stationary battery. Johnson Controls, Inc., (JCI), the other developer, fabricated and tested a 20-kWh load management battery in 1987.

ERC Technology Development

ERC continued work on improving the design of the zinc/bromine battery. A description of the more significant improvements in 1987 follows.

- A flow frame with 1500 cm^2 of active area was designed, and prototypes were fabricated and tested. This frame will replace the 872-cm^2 flow frame. The new design improves system reliability by reducing clogging in the flow channels, frame cracking from misalignment during assembly, electrolyte leakage, high pumping pressure requirements, and poor cell-to-cell flow uniformity.
- A two-loop flow system was designed and tested. This new flow system will also improve system reliability significantly, since it eliminates the third polybromide loop. Mixing and separation of the catholyte and polybromide fluids now

takes place in the catholyte tank. The two-loop system no longer requires a polybromide pump, which was extremely unreliable because of the high viscosity and corrosivity of the polybromide.

- Testing showed that ruthenia catalyst and activated felts lower the discharge polarization of the bromine electrode, that high-chloride electrolytes enhance zinc deposition, and that electrolyte iron concentration can be reduced to 1 ppm.

ERC tested three five-cell stacks and one 30-cell stack. All four stacks were built with 872-cm^2 flow frames. The two-loop flow system and the improved electrolyte cleaning process worked well; however, problems were encountered with cracking of the electrode end plates and clogging of the flow channels. Solutions to these problems were identified and implemented.

JCI Technology Development

The JCI load-management battery, a 20-kWh battery made from Exxon piece-parts, demonstrated better-than-expected performance after 97 cycles. Its projected life is now 150 cycles. The experience gained from this battery will be used for new designs that are being considered for various applications.

Technology Evaluation and Improvement

In support of zinc/bromine development, ANL and SNL evaluated Exxon and ERC zinc/bromine battery systems. In addition, the Battery Technology Improvement element worked on developing separator membranes with reduced bromine permeability and investigated the durability of candidate polyvinyl chloride materials for flow frames in the zinc/bromine battery.

ANL and SNL Evaluations

ANL completed tests on an Exxon 30-kWh, 124-cell zinc/bromine battery. It was found that this battery undergoes increased self-discharge at high operating temperatures. In addition, component failures and electrolyte leakage were found to be significant problems with this technology.

SNL completed tests on an Exxon 500-Wh battery, which was cycled over 2000 times. Posttest analysis of this battery has provided valuable new insight regarding the longevity of zinc/bromine batteries. Current-collector corrosion was the cause of a decline in efficiency after 2000 cycles, and electrode warpage caused a gradual degradation. Further posttest analysis is planned for 1988.

SNL tested four five-cell zinc/bromine stacks from ERC. Problems were encountered with control of the electrolyte level, blockage of flow channels, cracks in the end electrodes, and electrolyte leaks. ERC had proposed solutions to these reliability problems by year's end.

Membrane Development and Materials-Durability Studies

Because bromine permeation through the separator adversely affects the coulombic efficiency of zinc/bromine batteries, SNL studied the impregnation of separator membranes with cationic polymers. The purpose of impregnation is to reduce the bromine permeation rate without significantly increasing area resistivity. The best performance improvements were achieved with a 0.635-mm (25-mil) Daramic separator vacuum-impregnated with sulfonated polysulfone resins (SPS). This technique yielded a 23-fold decrease in bromine permeation rate with only a 2.5-fold increase in area resistivity.

The degradation of PVC (polyvinyl chloride) exposed to bromine-containing electrolytes was studied to characterize the effect of bromine on PVC materials, from which the ERC zinc/bromine flow frames are fabricated. Two PVC formulations were investigated. Both formulations demonstrated more stability to bromine than polyolefin thermoplastics.

Nickel/Hydrogen Technology

Technology Development

JCI, the sole developer of nickel/hydrogen technology for the ETD project, designed, built, and tested a 7-kWh nickel/hydrogen battery system in 1987. This battery was delivered to SNL for evaluation in late 1987. In addition, JCI continued its cost analysis of the nickel/hydrogen battery system.

The 7-kWh battery, which consists of four 12-V, 150-Ah modules, features:

- thicker electrodes, which lower the number of cell components per cell module (reducing costs) and increase specific energy;
- an electrolyte absorber wick, which improves electrolyte management, thus increasing cycle life;
- additives to the electrolyte and a change in electrolyte concentration, which improve high-temperature performance, thus allowing the battery to be operated without the added expense of active cooling;
- a common pressure vessel for the battery modules, which permits better thermal management and easy configuration to different capacities and voltages.

Reducing the high costs of nickel/hydrogen technology, which was originally developed for satellite applications, is a primary objective of the JCI development effort. Cost studies showed that technology improvements in 1987 brought about an additional 12% reduction in cost at the lowest production level. Calculations show that the programmatic goal of $375 per kWh can be reached after cumulative sales of 11,000 units.

Technology Evaluation

SNL evaluated six nickel/hydrogen cells and two nickel/hydrogen batteries from JCI in 1987. All eight units underwent cycle testing. In addition, the performance of one of the batteries interfaced to a photovoltaic array and a load was evaluated.

Principal findings from the cycling tests included the following:

- Thicker (70-mil) positive electrodes yielded increased capacity in the same-size cell case. However, when the thickness was increased to 90 mils, the actual capacity of the positive electrode did not reach theoretical capacity. This was attributed to the problems encountered from uniformly impregnating thicker (90-mil) plaques with active material.
- Electrolyte-loss problems were identified, which prompted design changes (electrolyte absorber/wick).
- Tests without Gore-Tex backing on negative electrode showed that lack of hydrophobic backing inhibits the hydrogen reaction, reducing cycle life. The Gore-Tex backing was therefore retained as part of the cell design.
- Tests on cells containing electrolytes with low potassium hydroxide concentrations and lithium additives showed that operation without active cooling is possible.

The solar tests indicated that, because the nickel/hydrogen battery is tolerant of overcharge and even cell reversal, there is no need for a costly controller. And because hydrogen pressure indicates state-of-charge, it is possible to shed loads during discharge based on hydrogen pressure. Such a load-shedding system would be nonparasitic; it would require no power input from the battery.

Aluminum/Air Technology

Responsibility for the development of the aluminum/air battery was transferred from the TBR project to the ETD project in August 1987. Because this project was just initiated at SNL, only Technology Development was performed in 1987. The aluminum/air development program consists of two major tasks:

- Cell Design and Optimization
- Auxiliary Support System Design.

In addition to establishing the development program, the following work was carried out on the above two tasks:

- Equipment for battery evaluation was procured.
- A boundary-layer analysis was developed to describe cell behavior.
- A basic algorithm was developed to allow modeling of the motion of spherical particles in the hydrargillite/electrolyte separator.
- A system to characterize the above separator was developed, constructed, and operated.
- A system was designed to simulate heat transfer for a 10-cell battery, and equipment for this simulator was ordered.

Chapter 2. Aqueous Battery Development

Introduction

During 1987, the Exploratory Battery Technology Development and Testing (ETD) Project continued to support the zinc/bromine and nickel/hydrogen advanced secondary-battery systems. In addition, ETD initiated a program to further the development of the aluminum/air system. In all cases, these developmental activities are carried out by industrial organizations through cost-shared contracts.

The following development programs were supported in 1987:

- Zinc/Bromine Battery Development at Energy Research Corporation (ERC) (Danbury, CT)
- Development of a Zinc/Bromine Load Management Battery at Johnson Controls, Inc. (JCI) (Milwaukee, WI)
- Nickel/Hydrogen Battery Development at JCI (Milwaukee, WI)
- Aluminum/Air Battery Development at Eltech (Fairport Harbor, OH).

The largest program in this element is the Zinc/Bromine Battery Development with ERC. This $5.1M program was initiated in September 1985. The objectives were to continue the development of ERC's zinc/bromine core technology, which was acquired from Gould in 1982, and demonstrate a proof-of-concept 50-kWh stationary battery during the final contract year. The conclusion of the 1987 activities represented the half-way point of this four-year contract.

In February 1987 JCI was contracted to fabricate and qualify a 20-kWh proof-of-concept zinc/bromine load management battery. The battery stacks were fabricated from residual Exxon piece-parts, and the battery system was evaluated at the JCI Load Management Facility located at their Keefe Avenue Plant. The unit had completed 97 cycles by the end of the year.

During 1987, nickel/hydrogen battery development continued at JCI. The work originated at Communications Satellite Corporation (COMSAT) but was transferred to JCI, a COMSAT subcontractor, in 1986. The main emphasis of the nickel/hydrogen program was the reduction of costs of terrestrial battery systems without compromising the demonstrated performance of nickel/hydrogen batteries developed for satellite applications. The major accomplishment in 1987 was the design of a 7-kWh nickel/hydrogen battery system.

Responsibility for the development of the aluminum/air battery system was transferred from the Technology Base Research (TBR) project to the ETD project in 1987. A $2.2M, 2.5-year contract was placed with Eltech in August 1987. The major tasks were the optimization of the air cathode, development of aluminum alloy materials, and development of system ancillaries.

Zinc/Bromine Battery Development - ERC

Energy Research Corporation (ERC) is involved in a program to develop the zinc/bromine battery system for stationary energy storage applications. Two projects are currently underway:

- Technology development work is being done under a project supported by the U.S. Department of Energy through SNL.
- A smaller project supported by the Electric Power Research Institute (EPRI) examines design and commercialization issues specific to utility load leveling.

A discussion of the work conducted in the SNL-supported technology development project follows.

The SNL project, which began in September 1985, will run through September 1989, with the final year focused on the fabrication and testing of 50-kWh proof-of-concept systems. The work during 1987 involved component and subsystem optimization, with emphasis on the development of a new generation of stack and flow-system hardware.

Specifically, progess was made in 1987 in the following four tasks:

- **Component and Subsystem Development.** The designs of the bromine electrode, zinc electrode, and separator were improved. In addition, a bromine storage subsystem was developed that eliminated the need for a third (polybromide) recirculation loop.

- **Hardware Development.** An improved end electrode was incorporated into the 1986 stack-clamping design, and a new flow frame with 1500 cm^2 active cell area was developed to replace the 872-cm^2 flow frame.

- **System Development.** Pump performance was improved by eliminating the polybromide recirculation loop and adopting variable-speed control. An automatic electrolyte level-sensing system was designed to permit automatic level control. Three five-cell stacks and one 30-cell stack underwent extended cycle testing to evaluate new design features such as the two-loop flow system, the new stack-clamping design, level sensing, and electrolyte purification.

- **Material Stability Studies.** Immersion and cell-cycling tests were carried out on cell and hardware materials that are to be used in the 50-kWh prototype batteries.

The progress made in 1987 on the ERC zinc/bromine technology development supported by SNL is discussed below. Specific accomplishments are summarized in Table 2-1.

Component and Subsystem Development

Bromine Electrode Development

The ERC zinc/bromine battery utilizes a high-surface-area carbon-felt flow-through electrode to support the bromine/bromide reaction. The current baseline electrode is an ERC material developed during 1986.

In 1987, bromine electrodes using the following types of felts were studied:

- Baseline felt, which was produced by carbonizing a polymer felt precursor. This felt was made at ERC.

- Catalyzed felt, which was produced by applying RuO_2 (ruthenia) catalyst on the baseline felt. This felt was made at ERC.

- Activated felt, which was produced by modifying the carbonization environment. Two types of activated felt were studied, one made at ERC and one supplied by Kynol Corporation.

Electrode performance was evaluated using single cells with 20 cm^2 active electrode area. Half-cell potentials were measured against a silver/silver bromide reference electrode.

Catalyzed Electrode. Figure 2-1 compares the discharge polarization characteristics of the baseline electrode with an electrode catalyzed with 0.017 mg/cm^2 RuO_2. The data were obtained with a 13 g/l catholyte bromine concentration, corresponding to 100% state-of-charge. As the figure shows, discharge polarization was significantly lowered by the catalyst.

In order to determine if the performance enhancement could be attributed to the catalyst (and not the air heat treatment), cells were also tested with felt electrodes that had been heated in air or treated with hydrochloric acid, a by-product of the catalyzation process. No significant performance improvement was observed, so the ruthenia catalyst appears to be the component that is lowering electrode polarizations.

Table 2-1. Summary of Zinc/Bromine Battery Development - ERC

Component and Subsystem Development	
Bromine Electrode Development	
Catalyzed Electrode	RuO_2 catalyst lowers discharge polarization significantly (30 mV at 30 mA/cm^2 versus 74 mV at 30 mA/cm^2 for the baseline electrode).
	Cost of RuO_2 is low: less than $1/kWh because of the low loading.
Activated-Felt Electrode	Activated electrodes also achieve low discharge polarization (Kynol felt: 40 mV at 30 mAh/cm^2).
Final Selection	Final selection will be based on ongoing stability tests.
Zinc Electrode Development	
Kinetic Studies	Modeling shows that dense zinc deposition is enhanced by electrolytes with high chloride content.
	Tests in 75-cm^2 cells on high-chloride electrolytes show improvement in coulombic efficiency; however, improvement is not statistically significant.
Electrolyte Purification	Electrolyte production method improved: iron concentration reduced from as high as 5 ppm to 1 ppm.
Status	Tests on high-chloride electrolytes to be conducted in 1500-cm^2 cells.
Separator Development	
Thickness Optimization	35-mil Daramic yields better efficiency than 25-mil Daramic; however, this efficiency improvement decreases with extended cycling.
Modification of Transport Properties	Initial evaluations show that fluoropolymer treatment of Daramic reduces bromine permeability by up to a factor of four.
	Further testing required because of inherent variability of Daramic.
Gasket Filler	Tests show that a fluoroelastomer gasket filler provides more effective sealing than the baseline silicone material.

Table 2-1. Summary of Zinc/Bromine Battery Development - ERC (Continued)

Status	Greater than 70% energy efficiency possible with treated Daramic separator. Greater than 70% energy efficiency possible with untreated Daramic separator if polybromide buildup can be reduced.
Bromine Storage Subsystem	
Elimination of Polybromide Loop	New catholyte tank designed and tested that allows mixing and separation of the catholyte and polybromide fluids within the tank, thus eliminating the third recirculation loop.
Reduction of Polybromide Buildup	Studies underway to find bromination level that minimizes polybromide buildup in the stack.
Hardware Development	
Stack Clamping Assembly	Stack-clamping assembly developed in 1986 redesigned to prevent cracking of the end flow frames in the stack.
Flow Frame Design	New stack hardware with 1500 cm^2 active area designed, which features: • deeper flow channels (which reduces clogging and pumping pressure) • less cracking • improved sealing technique • increased flow velocity because of narrow cell geometry (which enhances dense zinc deposition). Two 52-cell stacks will be required for each prototype 50-kWh system. Six percent consumption of rated capacity by shunt current and pumping losses projected for 52-cell stacks of 1500-cm^2 frames.
System Development	
Electrolyte Circulation Pumps	Pump reliability improved by • elimination of polybromide circulation system • incorporation of variable-speed motor drives in the pump design.
Electrolyte Level Measurement	LVDT chosen to monitor electrolyte level.

Table 2-1. Summary of Zinc/Bromine Battery Development - ERC (Continued)

	Because LVDT is somewhat sensitive to changes in the specific gravity of the electrolyte, it is also possible that LVDT could be used to determine battery state-of-charge.
System Control	All testing in 1987 conducted with manual system control.
	LVDT has been incorporated into an automatic electrolyte level control system; testing to be carried out in 1988.
Battery Design and Testing	
Stack SNL-5-2	Design: five-cell stack; three-loop flow system; leaf-spring stack-clamping assembly; 25-mil Daramic separators.
	Electrolyte cleaning after 54 cycles improves performance.
	Coulombic and voltaic efficiencies decline after 146 cycles.
	Disassembly after 170 cycles shows that flow channels clogged by plastic debris and a gasket; redesign should take care of these problems.
Stack SNL-5-3	Initial design: five-cell stack; three-loop flow system; new ribbed end-plate stack-compression hardware; 25-mil Daramic separators.
	Electrolyte cleaning after 11 cycles improves performance.
	Stack disassembled after 40 cycles because of erratic coulombic efficiency; end frame cracked.
	Stack rebuilt with two-loop flow system, new end plates, and 35-mil Daramic separators; performance stable since rebuild.
Stack SNL-5-4	Design: five-cell stack; two-loop flow system; LVDT level sensor; new ribbed end-plate stack-compression hardware; 25-mil Daramic separators.
	Electrolyte cleaning required to achieve acceptable performance.
	New end-plate design installed at 109 cycles.
	Performance stable after more than 115 cycles.
Stack SNL-30-2	Design: 30-cell stack; two-loop flow system; LVDT level sensor; new ribbed end-plate stack-compression hardware; 35-mil Daramic separators.

Table 2-1. Summary of Zinc/Bromine Battery Development - ERC (Continued)

	Electrolyte from improved cleaning process used; no further cleaning of electrolyte required to achieve acceptable performance. Lower discharge rate improves energy efficiency, but not enough to compensate the higher cost incurred from using more cells in the battery system.
Material Stability Studies	
Immersion Tests	Immersion tests on candidate materials for flow system and stack hardware (polyolefins, PVC, and CPVC) show that PVC and CPVC are stable, but that CPVC leaches significant amounts of tin. PVC materials identified that are more stable than the types of PVC presently used. Immersion tests on carbon/plastic bipolar plate material show • negligible dimensional changes • 1% to 5% weight gain • 20% to 40% decrease in flexural strength. Most of the decrease in flexural strength is early; flexural strength projected to remain above 4000 psi for ten years.
Cell Tests	More than 2000 cycles achieved in small cells with no degradation of bipolar electrode material. Separator material has exhibited surface roughening and loss of silicone gasket filler during testing in small cells; however, no decline in performance observed.
Status	Testing has shown current components are sufficiently stable for the prototype 50-kWh batteries.

Several cells were tested with the baseline and catalyzed electrodes at 30 mA/cm^2 discharge current density. As is seen in Table 2-2, the baseline electrodes exhibited 74 ± 9 mV polarization, while the catalyzed electrodes exhibited 30 ± 8 mV polarization (using catholyte with only 5 g/l Br_2 concentration).

Activated-Felt Electrode. The baseline felt material has a specific surface area of about 0.5 m^2/g, and the catalyzed felt has a surface area of about 1 m^2/g (both determined by BET analysis). Carbon felt can be made with significantly higher surface area by modifying the carbonization conditions, producing an activated

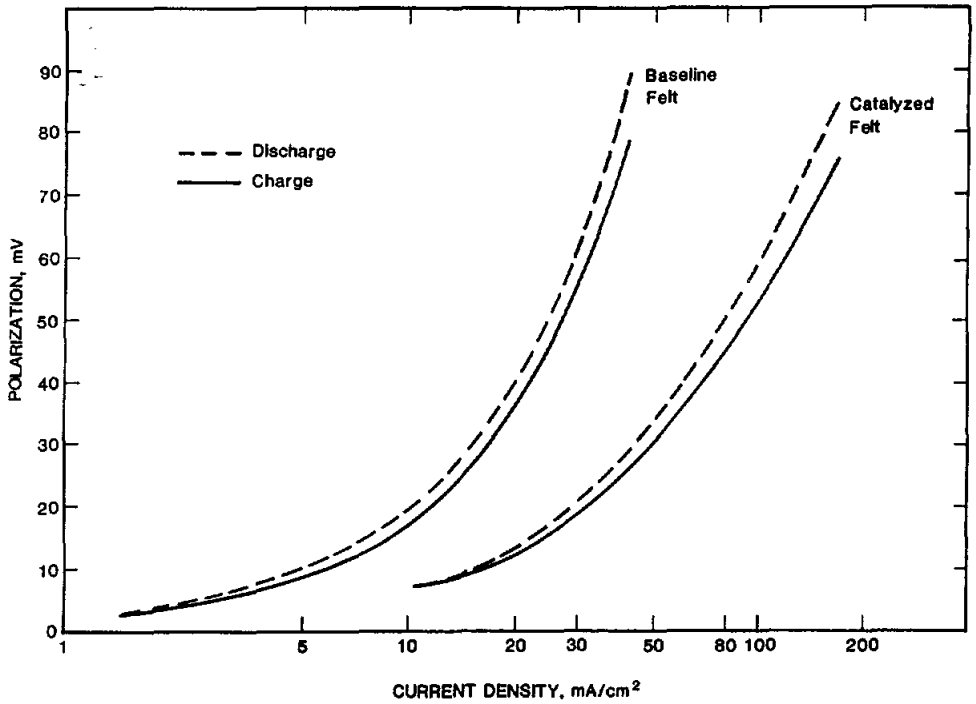

Figure 2-1. Bromine Electrode Polarization (Baseline Felt Versus Catalyzed Felt)

carbon felt. Two activated felt materials were evaluated, one made at ERC and one from Kynol Corporation.

Table 2-2. Bromine Electrode Discharge Performance in 20-cm² Cells

Electrode	Discharge Polarization at 30 mA/cm² Current Density
Baseline Felt	74 ± 9 mV
Catalyzed Felt	30 ± 8 mV
Kynol Activated Felt	40 ± 5 mV
ERC Activated Felt	55 ± 5 mV

The ERC material has a surface area of 160 m^2/g. The Kynol material has a specified surface area of 2000 $m^2/$, but ERC measured 1250 m^2/g. Even if the lower value is correct, the Kynol material has a much higher surface area than the ERC activated felt.

Two cells were tested with bromine electrodes made of Kynol felt. As is seen in Table 2-2, discharge polarizations of 35 to 45 mV were observed at 30 mA/cm^2 current density, while cells with in-house activated felt electrodes exhibited 50 to 60 mV polarization under the same conditions.

Status of Bromine Electrode Development. The Bromine Electrode Development subtask of the project has been completed. The catalyst appears to be a cost-effective design improvement, since the performance enhancement is significant and the cost of the catalyst is low (less than $1/kWh because of the low loading used). While less testing has been conducted on the activated materials, these electrodes also appear to offer improved voltaic performance.

In short, all four of the electrodes (the baseline, catalyzed, and two activated bromine electrodes) exhibit acceptable performance for the 50-kWh proof-of-concept batteries. Final selection of the electrode design for the 50-kWh systems will be based on ongoing stability tests. (See the discussion on the Material Stability Studies task.)

Zinc Electrode Development

The amount of zinc that can be plated on a given electrode determines the number of stacks needed in a battery system, which has a significant impact on system cost. A major objective of the project has therefore been to obtain dense, high-capacity zinc deposits. During 1986 it was demonstrated that capacity densities in excess of 200 mAh/cm^2 could be achieved in large single cells, but greater cell-to-cell uniformity was required to operate multicell stacks at this level.

During 1987 a series of electrochemical kinetic studies was completed on several experimental electrolyte and additive formulations. Evaluation of the most promising formulations was conducted in single cells with 75 cm^2 active area. Development work was also conducted to optimize the electrolyte production process, since electrolyte purity is one of the most significant factors in determining zinc deposit quality.

Kinetic Studies. The electrochemical studies involved potentiostatic step experiments using the various electrolytes and followed a series of galvanostatic step experiments conducted the previous year. The major variables in the electrolyte formulations were zinc ion concentration (to simulate various states-of-charge) and chloride ion concentration.

The galvanostatic step studies described in the last annual report (*ETD Report for 1986*, pages 15 and 16) showed that the chloride salts affected the activation kinetics of deposition, resulting in a lower exchange current density and higher nucleation overpotential. The potentiostatic step experiments done in 1987 examined deposition mechanism and morphology. The results were fitted to a number of mechanistic models, with the best fit being obtained with an instantaneous nucleation model, with lattice incorporation as the rate-determining step.

The instantaneous nucleation model generates two factors that indicate the relative direction of the deposit growth. One factor is proportional to the rate of growth perpendicular to the substrate while the other is proportional to growth parallel to the surface, with parallel growth being preferred for dense deposits. The analysis showed a greater proportion of growth parallel to the substrate in electrolytes with high chloride content.

After the electrochemical studies were completed, a series of 75-cm^2 cell tests were conducted on the baseline electrolyte and two formulations that the kinetic studies showed to be promising. These electrolytes, designated Q and R, were high-chloride electrolytes (as was the baseline) that exhibited lower overpotential at end-of-charge conditions. While zinc-electrode polarization is not a significant energy loss in the battery, lower zinc-deposition polarization could indicate more efficient zinc deposition (less hydrogen evolution) toward the end of charge.

The 75-cm^2 cells were cycled with charge input levels of 245 mAh/cm^2 at 35 mA/cm^2 current density. Eight cycles were run, with the deposit inspected after each charge. All three electrolyte formulations produced dense, uniform deposits at this high loading level. The cells using electrolytes Q and R had slightly higher average coulombic efficiency than the baseline electrolyte, but not enough to be statistically significant. Any efficiency improvement from these electrolytes would show up as reduced hydrogen evolution toward the end of charge, and this could only be detected by monitoring electrolyte pH over hundreds of cycles.

Electrolyte Purification. The above tests were run with electrolytes made in small batches using the purest salts available. Commercial zinc/bromine battery systems will use lower-cost raw materials, with cleaning processes required to obtain the required purity. Very low levels of impurities such as iron are essential for efficient zinc deposition. Iron is the most prevalent of a class of impurities that deposit with or before zinc and catalyze hydrogen evolution.

The procedure for making large electrolyte batches was improved during 1987, lowering iron levels from 2 to 5 ppm to less than 1 ppm. The

improvement was made by adjusting the pH at stages in the cleaning process to facilitate removal of oxides of the impurities. The technique can be used to produce sufficiently pure electrolytes in commercial volumes at a cost of about $10/kWh.

Status of Zinc Electrode Development. The only zinc deposition work remaining before an electrolyte for the 50-kWh system is to be specified is evaluation of the three formulations (baseline, Q, and R) in cells using the new, 1500-cm^2 flow frame hardware. As mentioned above, the primary problem presently limiting capacity densities in multicell stacks is cell-to-cell flow uniformity in the current 872-cm^2 hardware. Since the 1500-cm^2 hardware has been designed to address this problem, it is believed that the larger stacks will be capable of operating with a capacity density of 200 mAh/cm^2.

Separator Development

The separator presently used in the ERC zinc/bromine batteries is a porous, silica-filled polyethylene material from W. R. Grace with the trade name Daramic. The separator material is cut to the size of the flow frames and the area outside the active cell area is filled with a silicone elastomer. The filled area acts as a gasket to seal flow channels and manifolds.

The bromine permeability of Daramic is such that bromine diffusion into the anolyte causes a self-discharge rate equivalent to about 2 mA/cm^2. This, combined with the voltaic resistance of the separator (about 1 $\Omega \cdot cm^2$ for the 25-mil-thick material) makes the separator one of the significant sources of energy loss in the battery.

Work during 1987 on separator development included

- optimization of the Daramic thickness
- evaluation of treatments to modify the transport properties of Daramic
- continued development of a fluoropolymer-based gasket filler to replace the presently used silicone material.

Thickness Optimization. Separator modeling studies indicated that an improvement in energy efficiency could be achieved by using a Daramic separator thicker than 25 mils. As separator thickness is increased, coulombic losses decrease (because of reduced bromine diffusion), while voltaic losses increase (because of increased resistivity). The modeling studies indicated that up to a thickness of about 40 mils the coulombic efficiency gain would be greater than the voltaic loss, resulting in a net gain in energy efficiency.

Cycle test results for two 872-cm^2 single cells with 25- and 35-mil separators are shown in Table 2-3. The thicker separator achieved energy efficiencies from 70% to 77% over a wide range of operating capacity (charge input) densities. The 35-mil Daramic has since been tested in five-cell and 30-cell stacks, described in the discussion on the Battery Design and Testing subtask of the System Development task. With extended cycling, however, the efficiency improvement of the thicker separator decreases because the material is wetted with the organic complexing agent, which increases bromine permeability.

Modification of Transport Properties. Another area of development involves modifying transport properties by changing the separator pore structure with a solvent-based fluoropolymer filler. A treatment has been developed that appears to significantly reduce the bromine diffusion rate without an excessive voltaic loss.

Initial evaluations in bromine diffusion cells indicated that the fluoropolymer treatment reduced bromine permeability by up to a factor of four. Further testing is required to verify the effect because of the inherent variability of Daramic. Testing also will be conducted with the organic complexing agent to determine if the diffusion enhancement caused by the bromine complex significantly affects the treated separators.

Gasket Filler. The last annual report described initial studies with a new gasket filler that was being evaluated as a more stable alternative to the baseline silicone gasket filler (*ETD Report for 1986*, page 16). The filler is based on a fluoroelastomer from 3M Corporation with the trade name of Fluorel, which is applied in a solvent base to the separator outside the

Table 2-3. 872-cm^2 Single-Cell Test Data on 25- and 35-mil Daramic Separators

Cell Number	Separator	Cycle Number	Charge Input (mAh/cm^2)	Efficiencies (%)		
				Coulombic	Voltaic	Energy
SNL-1-8	0.025-inch Daramic	1	240.8	83.1	81.5	67.7
		2	240.8	81.0	81.6	66.1
		3	240.8	83.3	81.0	67.5
		4	240.8	79.8	81.0	64.6
		5	240.8	88.3	82.0	72.4
		6	240.8	85.7	82.4	70.6
SNL-1-9	0.035-inch Daramic	1	34.4	95.6	81.3	77.7
		2	240.8	89.3	82.6	73.7
		3	200.0	90.3	79.5	71.8
		4	240.8	90.3	80.1	72.3
		5	240.8	90.8	80.1	72.7
		6	320.0	87.8	80.2	70.4
		7	172.0	93.3	79.7	74.4

active cell area. The filler has been tested in 20- and 75-cm^2 cells and was found to provide effective sealing. A series of 20-cm^2 cells has been built using the new gasket and placed on long-term stability test. Fluorel has also been tested with the first 1500-cm^2 prototype flow frames and has been found to seal more effectively than the silicone-based gasket.

Status of Separator Development. In summary, separator development work currently underway is limited to continued evaluation of the treated and untreated Daramic materials. If the performance improvement suggested by initial evaluations of the treated separator is verified, then energy efficiencies in excess of 70% can be expected in the 50-kWh proof-of-concept systems. The untreated separator could achieve these performance levels if a means of reducing polybromide buildup in the separator is developed, which is the one of the objectives of the Bromine Storage subtask, discussed below.

Bromine Storage Subsystem

Elimination of the Polybromide Loop. One drawback to the polybromide/bromine storage system had been the need for a third flow loop in the battery. In the system design used prior to 1987, the polybromide and catholyte fluids were mixed in a static mixer as the catholyte returned from the stacks back to the storage tank (Figure 2-2a). The heavier polybromide would settle to the bottom of the tank and from there it would be pumped back to the static mixer.

A new catholyte tank was designed to allow mixing and separation of the catholyte and polybromide fluids within the tank. Catholyte leaving the stack is returned to the bottom of the tank and then circulates up through a column of polybromide (Figure 2-2b). Subsequent settling zones in the tank separate the two phases before the electrolyte reaches the pump suction port. This design eliminates the need for a third recirculation loop in the system.

The new system design has been tested in two five-cell batteries and one 30-cell system (see the discussion on the Battery Design and Testing subtask of the System Development task). The system has worked very well, and has been especially beneficial because the polybromide pump had always been extremely unreliable. The polybromide is very viscous and is also the most corrosive fluid in the battery. Both of these characteristics led to poor reliability in the

shown that the complex can significantly increase the self-discharge rate once it has been absorbed by the separators.

The polybromide buildup was reduced in 1986 with the development of the current bromine electrode. The improved flow uniformity in this electrode helps to expel some of the polybromide formed during charge; however, enough buildup occurs to affect cell performance. Alternate storage materials have been studied as one approach to this problem, but none has proven acceptable.

Another approach is to limit the amount of the monobromide dissolved in the electrolyte. Studies have shown that as the bromine content of the monobromide complexing agent increases, the level of dissolved monobromide in the aqueous phase (and the resulting precipitation of polybromide in the cell channels) decreases.

Quantifying this effect is important to specifying the optimum working bromination level of the complexing agent. Previously it was believed that the optimum bromination level was the lowest level that would allow operation of the bromine electrodes. But because low bromination levels enhance polybromide formation in the cells, it now appears that higher levels may be optimum. Tests on this design variable in five-cell stacks are currently planned.

Hardware Development

Stack Clamping Assembly

The zinc/bromine battery stack consists of a bipolar pile of electrode/flow-frame assemblies. The stack is held together by a compressive force that is applied by tie-bolts. Clamping hardware at each end of the stack distributes tie-bolt tension evenly over the flow-frame area. Originally, stacks built using the 872-cm² frame hardware utilized a clamping assembly consisting of thick plastic end plates, steel strongbacks, and leaf springs to distribute the tie-bolt tension.

The last annual report described development work conducted on an improved stack clamping system (*ETD Report for 1986*, page 17). In the initial version of this design, insufficient support was built into the felt contact area. The hydraulic pressure of the electrolyte on the other side of the working electrode led to cracking of the end flow frames in the stack. The end contact system was redesigned, and the system has operated properly in subsequent stack tests.

Flow Frame Design

The major focus of the hardware development work centered on the design of a new generation of stack hardware with 1500 cm² active area. The new flow frame was designed to address problems that have been encountered with the 872-cm² flow frame presently used. The major problems experienced with this hardware have been

- flow channel clogging, caused by debris or bowing of the separator into the channel
- frame cracking, caused by misalignment of stacked frames
- electrolyte leakage
- high pumping pressure requirements
- poor cell-to-cell flow uniformity in multicell stacks.

The flow channels in the 1500-cm² frame are much deeper than those in the 872-cm² frame, which should eliminate separator clogging and reduce debris clogging. The deep channels also significantly reduce required pumping pressure.

The new frame has been designed to take into account piece-to-piece variations that will occur in injection molding, thus avoiding interference of raised sections on the frame that would cause cracking as the parts were stacked. Additional structural support has been built into areas that had been common locations of cracks in the 872-cm² frames.

The sealing technique used in both frame designs uses ridges outside of the channel areas. These ridges are impressed into the separator gasket material, creating the required seals. The 1500-cm² frame uses multiple sealing ridges while the 872-cm² frame has only single ridges.

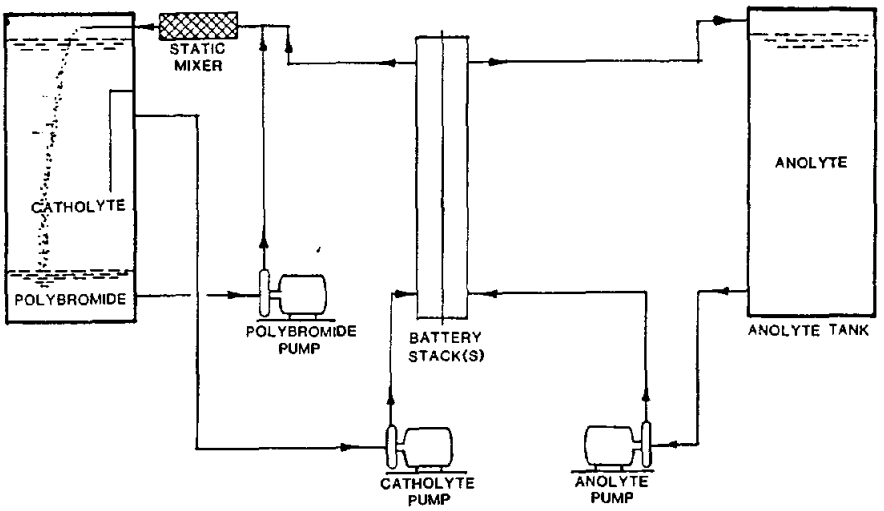

(a) Former System Configuration, with Three Recirculation Loops

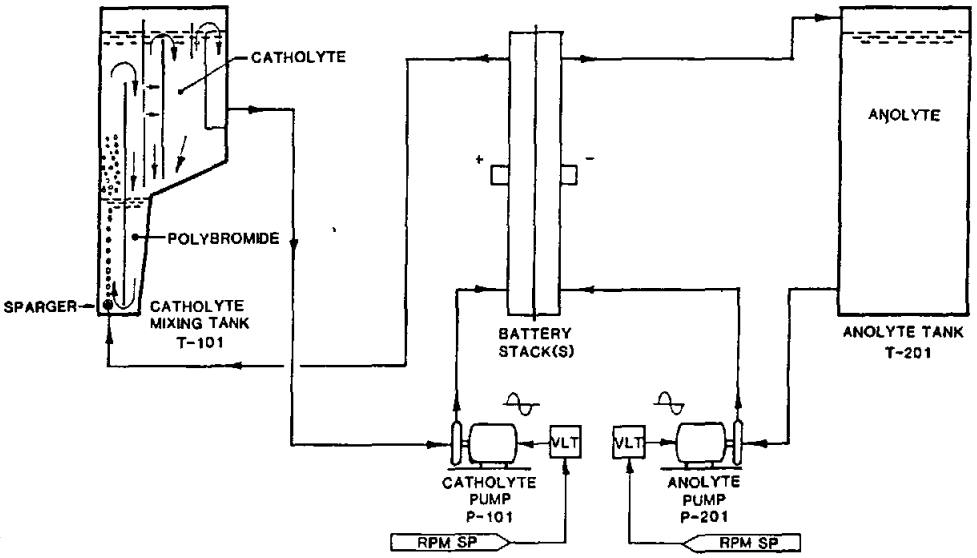

(b) Two-Loop System Configuration, with Catholyte/Polybromide Mixing/Settling Tank

Figure 2-2. Comparison of Zinc/Bromine Flow System Designs

magnetically driven centrifugal pumps used in the system.

The new system also offers inherent safety advantages over the previous design. Almost all of the bromine in the battery is stored in the polybromide, and because the complex is not circulated in any flow lines, the risk of a spill of this hazardous material is greatly decreased.

Reduction of Polybromide Buildup. Another objective of the development studies on bromine storage is to reduce the buildup of polybromide in the stack. The organic monobromide complexing agent is soluble in the electrolyte until it complexes with bromine, at which point it precipitates as a polybromide in a separate phase. The agent is complexed with bromine before use in a battery to ensure that the second phase is fully formed. However, there is always some uncomplexed monobromide dissolved in the electrolyte. As the battery is charged, this material forms a complex with evolved bromine and precipitates in the cell channels. It has been

The larger frame has also been designed to run at lower electrolyte pressures, which should also reduce the likelihood of electrolyte leakage.

The two frames are illustrated in Figure 2-3. The most apparent design change in the new frame is the narrow, high cell geometry. This design was chosen to enhance zinc deposition. In the range of flow rates used in ERC zinc/bromine batteries, flow velocity is more important than volumetric flow rate in achieving dense zinc deposits. A flow velocity of at least 2 cm/s is required to deposit zinc at the desired capacity densities. The narrow cell geometry achieves this flow velocity at a lower volumetric flow rate than a wider cell would, which reduces pumping losses in the long flow channels and ancillary piping.

The flow channels and manifolds were designed using a flow model that predicted shunt current losses, pumping power losses, and flow distribution among stacked cells. This model showed that the long, thin channels that run from the manifold holes to the flow plenum area reduce stack shunt currents by creating a high resistance to current flow. It also showed that this geometry increased electrolyte pumping power requirements. Therefore, the design criterion was to minimize the sum of shunt losses and pumping power losses. In 52-cell stacks built with the 1500-cm^2 frame, shunt current and pumping losses are expected to consume approximately 6% of the rated capacity.

The large manifold ports at the top and bottom of the frames are designed to ensure good flow uniformity among cells in a stack by limiting pressure drop in the manifolds. In theory this also increases shunt currents, but the contribution of the manifolds to shunt resistance is minimal compared to the cell flow channels.

Prototypes of the 1500-cm^2 frame have been machined and tested for uniformity of electrolyte flow velocity in the active cell area. After modifying the frame plenum design, a uniform flow profile was achieved. Testing has started on the first working cell prototypes, which exhibit uniform zinc plating over the entire electrode area at high capacity density levels. The desired zinc deposit is being achieved and current density is uniform over the plate.

All of the cell testing has been done with the Fluorel-based gasket filler, and no leakage has occurred. The decision to use the Fluorel gasket instead of the silicone was made after the flow distribution tests indicated that the Fluorel gasket provided superior sealing (see discussion on Separator Development subtask of Component and Subsystem Development task).

Additional frame prototypes are being fabricated for five-cell stack tests, and an injection mold is being made to produce the frames in large quantities. When operated with 200 mAh/cm^2 capacity density, each frame will store 480 Wh of energy. Two 52-cell stacks will be used in each 50-kWh system.

System Development

Electrolyte Circulation Pumps

The electrolyte circulation pumps used in the flow system of the ERC zinc/bromine battery are magnetically coupled centrifugal pumps. These pumps have historically been among the least reliable components in the system. The magnetic drive isolates the motor components from the corrosive electrolyte, but it can decouple if line power irregularities occur or if the starting torque is too high.

The most severe pump reliability problem was resolved with the elimination of the polybromide circulation system, described in the discussion in the Bromine Storage Subsystem subtask (Component and Subsystem Development task). Additional reliability and efficiency improvements were obtained by incorporating variable-frequency motor drives in the pump design. Initially, the circulation pumps were driven by single-speed synchronous motors with throttle valves used to control flow rates. The use of variable-frequency motor drives provides flow rate and pump pressure control by electronically adjusting the pump motor speed. This can be done manually or automatically by the system controller. The alternative to this approach in an automatically controlled system would be to use motor-driven throttle valves, which reduce pumping efficiency and overall system reliability.

Electrolyte Level Measurement

The electrolyte flow rates must be controlled to prevent bulk electrolyte crossover in the stack.

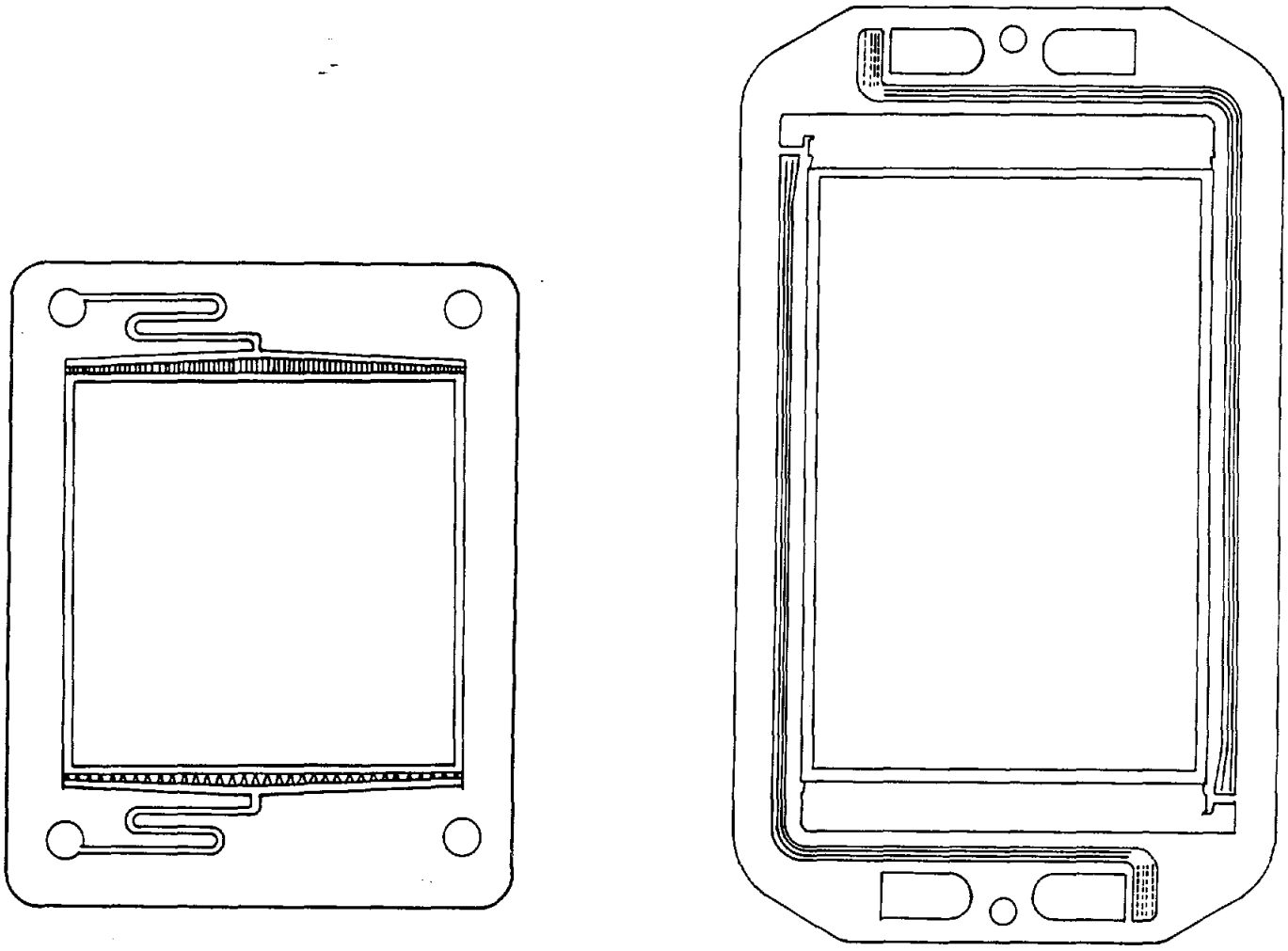

Figure 2-3. Zinc/Bromine Flow Frame Designs

Because the pressures of anolyte and catholyte fluids in the cells cannot be exactly matched, electrolyte flows through the porous separator from one recirculation system to the other. If left uncorrected, overflow of one of the tanks could result. In manually operated battery systems, the fluid levels are checked and the flow rates are adjusted when crossover is observed. For automatically controlled systems, a method of measuring tank liquid levels is needed.

After various approaches were evaluated, a technique was chosen that involves using a linear variable differential transformer (LVDT) in a float arrangement. A metallic core is sealed into a glass ampule that floats in the electrolyte in an extension fitted to the side of the tank. The LVDT consists of transformer coils embedded in a collar around the level arm extension. The position of the float affects the characteristics of the transformer, resulting in a signal that is proportional to the electrolyte level.

The signal is also slightly affected by changes in specific gravity of the electrolyte during cycling. This characteristic is currently being investigated as a technique for determining battery state-of-charge.

System Control

All of the staek testing during 1987 was conducted with manual system control. Work was done on the development of an automatic control system to allow unattended stack cycling.

The first area of development involved using the electrolyte-level signal to control electrolyte crossover. The LVDT signal was used to adjust the speed-control signal to the anolyte pump. For example, if the anolyte level was rising, the anolyte pump speed would be increased. This would increase anolyte pressure in the cell channels, thus balancing crossflow through the separators. Using this approach the catholyte pump was run at a constant speed, and based on the anolyte level, slight adjustments were made in the anolyte pump speed.

Overall system control, including start-up and shut-down sequences will be achieved using a ladder-logic programmable controller. Development of the control logic is underway, and the first battery tests with the controller will be carried out in 1988. The electrolyte level control subsystem has been evaluated in stack tests (SNL-5-4 and SNL-30-2), which are described below.

Battery Design and Testing

System and component designs were evaluated in three five-cell batteries and one 30-cell battery during 1987, using hardware with 872 cm^2 active cell area. SNL also evaluated ERC five-cell zinc/bromine stacks of the same design as SNL-5-2, SNL-5-3, and SNL-5-4. These stacks, designated SNL-5-2D, SNL-5-3D, and SNL-5-4D, are discussed in Testing of Flowing Electrolyte Batteries at SNL (Chapter 4).

The standard cycle test consisted of a 5-h charge at 30 A followed by a 30-A discharge to a voltage cutoff of 1.2 V/cell. After each discharge a brief low-rate discharge was usually conducted, followed by an open-circuit stand to remove residual zinc.

Stack SNL-5-2. Testing was completed on five-cell stack SNL-5-2, which used the leaf-spring stack-clamping assembly, the 0.025-inch-thick Daramic separators, and the three-loop flow system. Efficiency data for the cycle tests are shown in Figure 2-4. During cycles 20 through 24 the residual zinc stripping procedure was not conducted on the stack. Coulombic efficiency declined as a result, but recovered after the stripping procedure was resumed.

After 54 cycles the anolyte was filtered through activated carbon cartridges, and as a result coulombic efficiency increased to about 87% and remained at that level until cycle 117. During cycles 118 to 146 coulombic efficiency decreased to the 80% to 85% level. After cycle 146, coulombic and voltaic efficiency began to decline significantly. As shown in Figure 2-4, acceptable performance could be obtained by operating at lower charge input levels or discharging below the normal voltage cutoff. But energy efficiency was below 60% on the standard cycle test with 5-h charge input (172 mAh/cm^2).

After 170 cycles the stack was taken apart and inspected. Two anolyte flow channels were found to have been clogged by a buildup of plastic debris, which prevented delivery of proper electrolyte flow to the cells. One of the catholyte channels had been clogged by a gasket that had swelled and bent into the channel area. The gasket was redesigned to prevent recurrence of the problem, and basket filters were used on subsequent batteries to collect debris.

Stack SNL-5-3. The next five-cell system tested was SNL-5-3, which used the same flow system design as SNL-5-2 (three-loop design). The stack compression hardware featured the new ribbed end-plate design.

Efficiency data for the SNL-5-3 cycle tests are shown in Figure 2-5. As with SNL-5-2, an electrolyte cleaning was required to achieve acceptable performance, and this was done after 11 cycles. While performance improved, coulombic efficiency was erratic in subsequent tests, and after 40 cycles the stack was taken apart for inspection. The end frame was found to have cracked because of insufficient support in the contact area. The end electrode was redesigned and the stack was rebuilt with new end plates.

Two other design changes were made when the stack was rebuilt. The flow system was replaced with the two-loop design, and the 0.025-inch-thick Daramic separators were replaced with 0.035-inch-thick separators. Testing was resumed and performance has remained stable since the rebuild.

Stack SNL-5-4. Stack SNL-5-4 was built and put on test at the same time as SNL-5-3, and it also contained 0.025-inch-thick Daramic separators and the ribbed end-plate hardware design. The battery was the first to incorporate the two-loop flow system design and variable frequency pump motors. The system also included the first LVDT electrolyte level sensor, and the battery has been used to evaluate automatic pump speed control techniques. These investigations involved determining how to condition the level signal to provide an effective pump speed control signal. A proportional gain factor was found to be sufficient for pump speed control.

Efficiency data for the cycle tests are shown in Figure 2-6. SNL-5-4 has logged more cycles than stack SNL-5-3 because of down time associated with rebuilding the flow system in SNL-5-3.

As with the stacks discussed previously, SNL-5-4 required an electrolyte cleaning before exhibiting acceptable performance. After 109 cycles the stack was modified to include the newer end-plate design, but all other design features were left unchanged and cycle testing is continuing.

Stack SNL-30-2. Testing was also conducted on a 30-cell stack, SNL-30-2. This battery used the two-loop system. The battery is equipped with an electrolyte level sensor and variable speed pumps. The stack uses the ribbed end-plate compression hardware and 0.035-inch-thick Daramic separators.

Efficiency data for the stack are shown in Figure 2-7. The battery was built after the electrolyte production process had been optimized for improved electrolyte purity, and the electrolyte has not required cleaning. Anolyte pH is monitored continuously with a probe built into the flow loop, and it has remained stable throughout the duration of the test.

Energy efficiency was initially as high as 72%, but declined in early cycling. Performance has been stable at the 60% to 65% efficiency level during continued testing. The initial drop in performance is believed to have been caused by the cracking of the end electrode frame. The impaired end-cell performance lowers efficiency, but does not cause the erratic performance seen in five-cell stacks because the end electrodes comprise a smaller fraction of the total number of cells in the stack.

As with the five-cell stacks, the baseline cycle consisted of a 5-h, 30-A charge and a 30-A discharge. On cycle 47 a low-rate cycle was run in which the battery was charged at 13 A (15 mA/cm^2) for 8 h and then discharged at 13 A. Coulombic efficiency was lower than normal, since the operating current was closer to the self-discharge rate. The lower operating current led to higher voltaic efficiency, which more than compensated for the coulombic loss. Energy efficiency rose to 70%, which is typical of batteries tested at low capacity densities. Operating at this level would lower the operating cost of commercial batteries (because of the lower cost of charging energy at higher efficiency), but not enough to compensate for the higher capital cost associated with using more stacks in the battery system.

Status of Battery Design and Testing. Testing is continuing on SNL-30-2, SNL-5-3 and SNL-5-4. The level control system has been demonstrated to work well, and continuous unattended cycling will begin in 1988. Further stack testing will be done using the 1500-cm^2 cell hardware.

Material Stability Studies

The material stability work conducted during 1987 included immersion tests on cell and hardware materials as well as small-cell cycle tests. A discussion of these tests follows.

Immersion Tests

Immersion tests were done on several plastic materials that were candidates for flow-system and stack hardware. The tests were done at room temperature and at 60°C. The immersion solution was the battery electrolyte with 100 g/l bromine concentration, about ten times the bromine level normally used in the battery.

Parameters evaluated during the immersion tests included sample dimensions and weight, the presence of leachants in the immersion solutions, and sample molecular weight. Plastic materials studied included polyolefins, polyvinylchloride

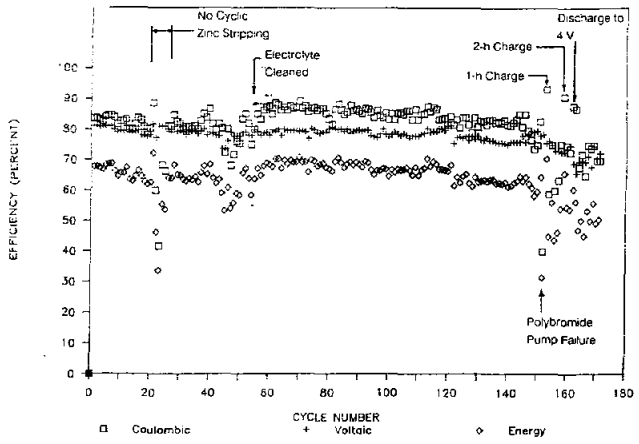

Figure 2-4. Cycle Performance of Five-Cell Stack SNL-5-2

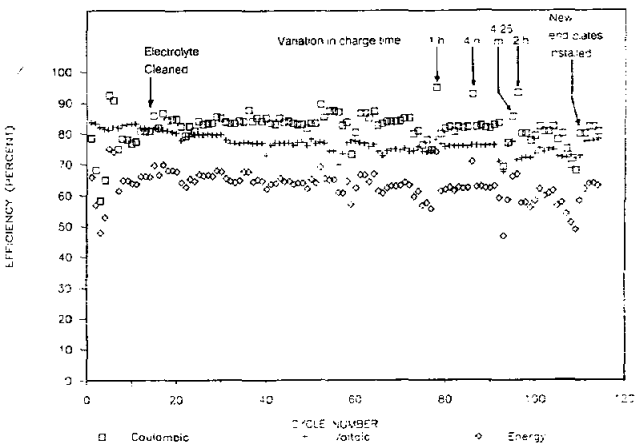

Figure 2-6. Cycle Performance of Five-Cell Stack SNL-5-4

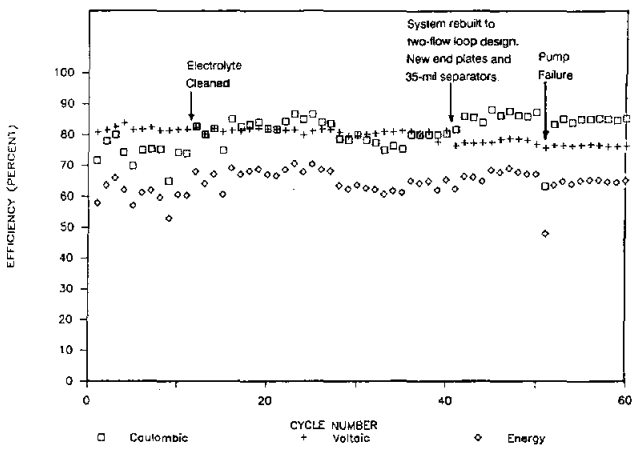

Figure 2-5. Cycle Performance of Five-Cell Stack SNL-5-3

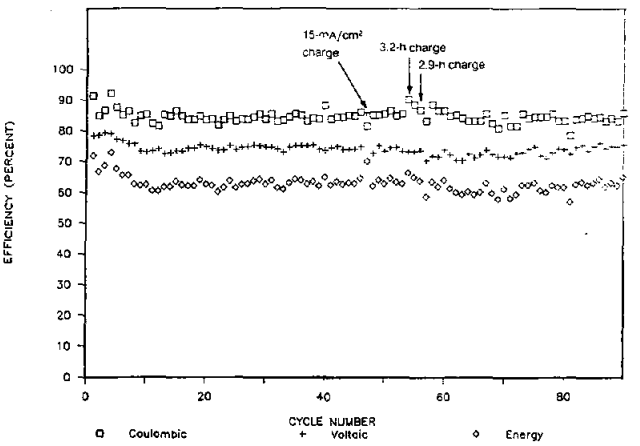

Figure 2-7. Cycle Performance of 30-Cell Stack SNL-30-2

(PVC), and chlorinated polyvinylchloride (CPVC). The PVC and CPVC materials were the most stable. However, high levels of tin were found to have leached out of the CPVC materials, ruling out their use in the system. The most stable grades of PVC have been selected for evaluation in an expanded stability test program. The test matrix includes three immersion temperatures, three immersion solutions, and a plurality of samples of each type of material. All immersed samples are fabricated as tensile test bars for evaluation of tensile strength throughout the test.

Based on the screening tests conducted to date, PVC materials have been identified that are more stable than the PVC grade presently used in flow frames. The expanded stability tests will focus on these materials and allow estimation of component lifetimes.

Immersion tests have also been conducted on the carbon/plastic bipolar plate material. After one year of immersion in bromine electrolyte solutions at 30°C to 60°C, dimensional changes have been negligible. Weight gain has ranged from 1% to 5% and flexural strength has decreased from 40% to 20%, depending on test conditions. Most of the strength decrease is seen early in the test, after which the rate of change decreases. Using a logarithmic fit to extrapolate the data beyond the test duration indicates that

flexural strength will remain well above 4000 psi over the ten-year life of the component.

Cell Tests

Cell component stability is also being studied in 10- and 20-cm^2 cells. These tests are run using a one-hour charge time to log cycles quickly. The cells are taken off test periodically for evaluation of component stability, which includes visual and microscopic inspection. Porosimetry and surface area tests are conducted on the separator and bipolar plate components. Cells have been cycled for over 2000 cycles with no degradation of the bipolar electrode material. One sample of purchased carbon felt material (the earlier baseline bromine electrode) exhibited fiber breakage and shedding. However, other electrodes made with this material did not degrade. None of the electrodes made with the current baseline felt have exhibited this type of breakdown.

The most significant degradation has been observed in the separator material, which has exhibited surface roughening and loss of the silicone gasket filler. While this has not led to impaired cell performance, it is being studied further to assess the impact on long-term battery operation.

Cells are currently on test with the candidate bromine electrodes described above (see discussion on the Bromine Electrode subtask of the Component and Subsystem Development task). However, not enough testing has been done to date to make a selection. Cells have also been placed on test with the fluorocarbon gasket filler and a comparison will be made with the silicone filler with respect to stability and long-term sealing capability.

Status of Material Stability Studies

The immersion and cell tests conducted to date have indicated that the components currently incorporated into the cell design are sufficiently stable for use in the 50-kWh prototype batteries. Continued testing will provide selection criteria for optimizing the bromine electrode, separator gasket, and materials of construction specifications for long-term commercial applications.

Future Work

The major advances made in the project during 1987 were the development of the catholyte/polybromide mixing tank and the design of the 1500-cm^2 flow frames. These design improvements are expected to significantly improve the reliability of the battery system.

Continued evaluation of the catholyte/polybromide mixing tank will be done in ongoing five-cell and 30-cell battery tests and in tests done using the 1500-cm^2 frame hardware. The new frame has been evaluated in die-injection flow tests and in single-cell tests. Future studies will include five-cell tests using machined frame prototypes and 52-cell tests using molded frames.

Ongoing material stability studies will be the basis for selecting the bromine electrode design. Selection of the electrolyte design will be done based on zinc deposition tests in 1500-cm^2 cells. Work will be continued on treated Daramic separator materials and on techniques to limit polybromide buildup in the separator.

The design of cell, stack and system components will be frozen in the fall of 1988, when detailed design work on the 50-kWh proof-of-concept systems begins. One 50-kWh system will begin testing at ERC in early 1989. A second system will be built and delivered for testing at a facility outside of ERC (either SNL or ANL).

Development of a Zinc/Bromine Load Management Battery - JCI

In March of 1987, the Advanced Battery Business Unit of Johnson Controls, Inc. (JCI) began work on a $25K fixed-fee zinc/bromine load management contract. (This work was also sponsored in part by Department of Energy contracts.) The contract scope included the fabrication and ten-cycle qualification of a proof-of-concept 120-V, 20-kWh zinc/bromine

load management battery in JCI's Load Management Test Facility. In addition, 97 charge/discharge cycles were completed in 1987.

Installation of the Load Management Test Facility itself was completed early in 1987. The bulk of the system is presently equipped with 300 lead-acid stationary batteries modified for load management requirements. The 600-kWh/600-V capability provides enough energy storage to operate a typical home for 30 days or 300 homes for two hours. Energy is stored at night when demand is low and is released to the manufacturing plant during the day to reduce peak demands.

The JCI advanced digital control system ensures safe and automatic operation of the Load Management Facility. This system consists of a JC/85 energy management system and a DSC-8500 digital controller. A MicroVAX-based data collection system monitors 300 cell voltages, 50 module voltages, 50 cell temperatures, string voltages and currents, and system power levels. The demonstration is a cooperative venture with the Wisconsin Electric Power Company and is the first of its kind in the U.S.

Progress on the JCI load management battery is discussed below. Specific accomplishments are summarized in Table 2-4.

Battery Description

The two 78-cell stacks for the 20-kWh zinc/bromine battery were fabricated from old Z-design components: coextruded polypropylene-based electrodes and framed submicroporous polyethylene (Daramic) separators. Stack components were held together by a bolt-and-adhesive sealing technique. The electrolyte was composed of 2.0M zinc bromide and 1.0M mixture of two quaternary ammonium complexing agents. This composition was chosen after limited testing of electrolytes used previously in load management batteries. The known shortcomings of the materials and design (stack leakage, adhesive blockage of electrolyte flow, and electrode warpage) led to energy efficiency expectations of 60% and an anticipated life of 90 to 100 cycles.

Table 2-4. Summary of Zinc/Bromine Load Management Battery Development - JCI

Battery Description	
	120-V, 20-kWh zinc/bromine load management battery consisting of two 78-cell stacks fabricated from old Z-design components.
	Expected problems: stack leakage, adhesive blockage of electrolyte flow, and electrode warpage.
	Expected energy efficiency: 60%; anticipated life: 90 to 100 cycles.
Cycle Tests	
	Testing carried out to obtain data for future system development and design.
	Performance better than expected: after 97 cycles, coulombic efficiency 80%; energy efficiency 62%.

The battery is intended for collection of critical cycling, control, and performance information for future system development and design. The modular design facilitates stack replacement as improved stack designs become available. The heart of the system is the load management test pod, which provides the electrolyte reservoir and flow subsystem and the thermal management subsystem.

Cycle Tests

After assembly, the battery stacks completed eight cycles on a laboratory test station to check for potential problems and to provide a performance baseline. Although overall performance was as expected, one cell group in the second stack showed some signs of low capacity, suggesting some flow maldistribution. Performance uniformity between all other cell groups and between the two battery stacks was good. The current draw for the shunt-current-protection system closely matched the theoretical requirement.

Subsequently, the battery stacks were installed in the load management test pod and cycled three more times to check the auxiliaries. The battery and subsystems performed well. Steady energy efficiencies of 62% were obtained. The electrolyte was drained from the test pod and the battery was shipped to the JCI Load Management Test Facility.

Cycling was initiated at the Load Management Facility in August of 1987. A total of 97 C/3 rate discharge cycles were completed by the end of 1987 (Figure 2-8). Initial energy efficiencies were as high as 65% and averaged 64%, about 4% higher than originally anticipated for the design and materials used. Coulombic

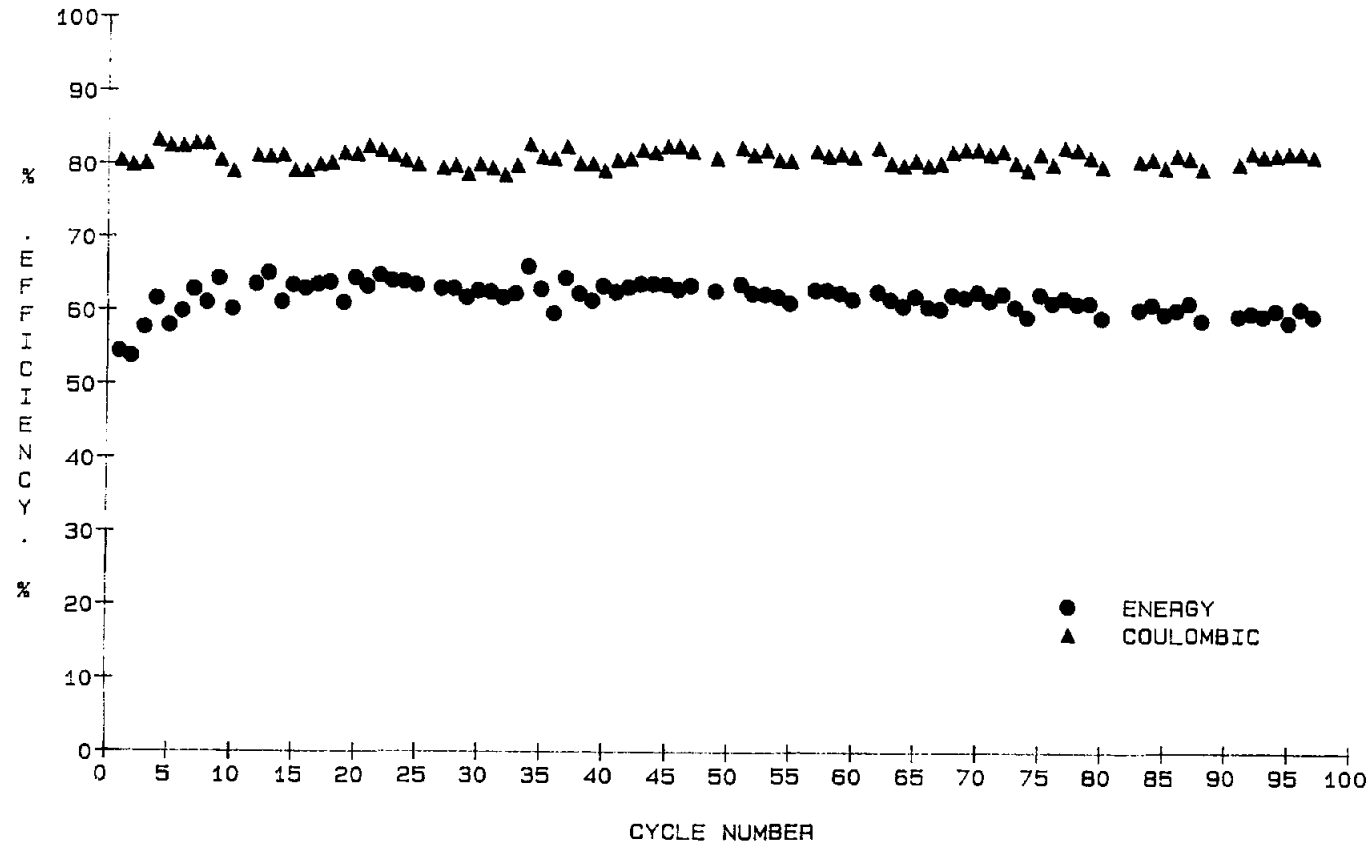

Figure 2-8. Cycle Efficiencies of the JCI Zinc/Bromine Load Management Battery

efficiencies have been steady in the 80% to 82% range, but a gradual decline in voltaic performance had reduced energy efficiencies to 62% by cycle 97.

The goals of the Load Management Contract have been achieved. Battery performance and life have already exceeded expectations. The data collected and the experience gained have been applied to new designs that are being considered for various applications.

Short-term plans are to continue cycling the existing stacks until they fail or are made obsolete by new designs expected to become available in July of 1988. Although initial expectations for the original stacks were lower, the completion of 97 cycles with no significant problems has raised the life expectation of this battery to 150 cycles or more.

Nickel/Hydrogen Battery Development - JCI

A program to design and develop a multikilowatt-hour nickel/hydrogen battery for storing electricity from photovoltaic or other power sources is continuing under a cost-sharing contract with SNL. The nickel/hydrogen battery has been successfully used for more than a dozen years in aerospace photovoltaic systems. The challenge was to dramatically reduce the first-cost of the battery to make it economically competitive, on a life-cycle cost basis, with other energy storage batteries used in terrestrial applications, without compromising the characteristics that make the nickel/hydrogen battery so useful in aerospace photovoltaic systems.

The advantages offered by nickel/hydrogen batteries include a significantly longer cycle life than any other battery system, no maintenance, and a high tolerance to abuse. This last characteristic is possibly the most important. It means that there may be no need for a charge controller between the solar array and the battery. Because the controller is the least reliable component in a photovoltaic system, its removal will have a beneficial effect on long-term reliability and cost. This is especially true in remote areas, where photovoltaics can play an important role but where skilled maintenance is often unavailable. Also, one can take full advantage of the maximum output of the solar array, in contrast to many other battery systems, where the controller isolates the battery during times of maximum insolation. This, coupled with the battery's excellent energy efficiency, reduces the required size of the array.

In 1987 JCI designed, built, and tested a 7-kWh nickel/hydrogen battery. JCI has also continued its cost analysis of the nickel/hydrogen battery system. Progress in 1987 is summarized in Table 2-5 and is discussed below.

Cell and Battery Design

JCI extended the manufacturing technology of the low-cost, mass-produced lead-acid automotive battery to the assembly of the nickel/hydrogen battery. Component technology and new design configurations were studied in an effort to reduce material, process, and assembly costs. Performance data on single cells and multicell batteries delivered to SNL were used to establish a baseline design.

The prismatic configuration of the cells and batteries developed for terrestrial applications in this program is a departure from the aerospace design. The batteries consist of a number of individual cells contained within one pressure vessel. The cells may be connected in series or parallel to meet the required voltage and capacity. If desired, bypass protection of individual cells can be provided. Better thermal management and greater design flexibility are the major advantages this new approach has over monolithic battery containers.

The primary objective in 1987 was to design, build, and test a 300-Ah, 24-V, 7-kWh nickel/hydrogen battery that operates at ambient temperatures of up to 30°C without active cooling. The battery, shown in Figure 2-9, consists of four 12-V, 150-Ah battery modules in a series/parallel configuration. Each battery module is contained in a boilerplate pressure vessel. The four vessels are connected with a common gas manifold. The battery is shown at JCI's Load Management Test Facility, where it was tested prior to being shipped to SNL. This prototype battery, which demonstrates the potential for lower manufacturing cost and

Table 2-5. Summary of Nickel/Hydrogen Battery Development - JCI

Cell and Battery Design	
	7-kWh battery consisting of four 12-V, 150-Ah battery modules delivered to SNL; can be configured in 12-V multiples up to 48 V with a capacity of 150 to 600 Ah.
	Better thermal management and greater design flexibility achieved through use of individual cells contained within one pressure vessel.
Cell Characteristics	Ten cells per battery module; cell design features: • injection-molded cell cases • leak-free penetrations for terminal posts • exterior ribs that separate cells and provide convective heat transfer • hydrophobic plug for hydrogen circulation without loss of electrolyte.
Cell-Module Characteristics	Nine cell modules per cell; the cell module consists of • two back-to-back nickel positive electrodes (sintered and electrochemically impregnated) • electrolyte absorber (between the positive electrodes) • two separators • two negative electrodes • two outside diffusion screens.
Design Changes From Aerospace Technology	Thicker electrodes lowers number of cell components and increases specific energy.
	Electrolyte absorber/wick increases cycle life.
	Peripheral seal enhances oxygen recombination.
	Electrolyte additives and changes in electrolyte concentration improve high-temperature performance.
	Employs common pressure vessel.

improved performance over aerospace technology, was delivered to SNL in 1987 for incorporation into an experimental field-scale photovoltaic system. Electrical connections were provided on the front panel to allow testing in 12-V multiples up to 48 V with a capacity of 150 to 600 Ah.

Each battery module contains ten cells as shown in Figure 2-10. The cells comprising the battery module are bonded together and restrained between spring-loaded end plates. A view of one of the cells is shown in Figure 2-11.

Table 2-5. Summary of Nickel/Hydrogen Battery Development - JCI (Continued)

Battery Conditioning	
	50 psig precharge of hydrogen gas.
	Battery modules individually subjected to 15 conditioning cycles.
	Pressure transducers were installed on each of the four pressure vessels.
	After conditioning cycles, pressure vessels connected to a common manifold; initial test results: 7.85 kWh and 84% energy efficiency; highest temperature during discharge was 33°C.
Cost Study	
	Additional 12% reduction in cost at lowest production level can be attributed to 1987 research and development.
	Important contributors to lower costs: 90-mil positive electrode and reduction of the platinum loading on the negative electrode.
	Cost study predicts that the $375/kWh goal can be achieved after cumulative sales of 11,000 units.
	The cost study shows that the nickel/hydrogen battery is competitive with other 15-kWh batteries in an autonomous photovoltaic system over a 30-year life; further cost reductions if a charge controller is not needed.
Technical Challenges Remaining	
	High processing costs of the nickel electrode.
	High materials costs of the negative electrode.
	Development of a field-deployable battery-containment vessel.
	Smaller 2-kWh battery proposed as a building block for larger systems.

The cell cases were injection-molded, and the covers were heat-sealed on. A crimp seal ensures leak-free penetrations of the terminal posts through the covers. Exterior ribs keep the cells apart and provide space for convective heat transfer, which represents an improvement in thermal management. The cap on each cell contains a porous, hydrophobic plug that allows the hydrogen gas to move freely in or out of the cell case while retaining the electrolyte. Tests

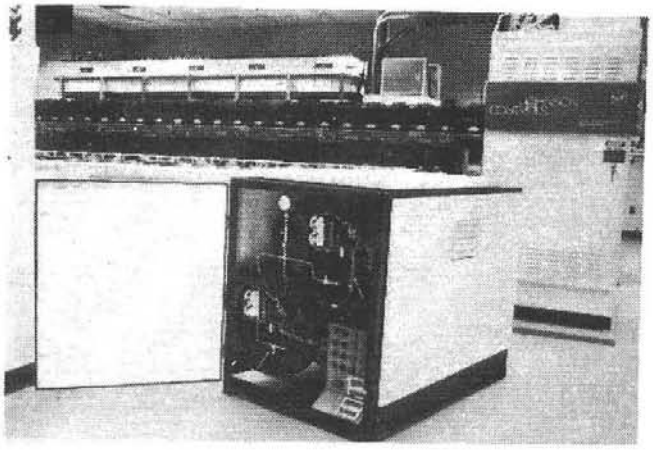

Figure 2-9. Terrestrial 7-kWh Nickel/Hydrogen Battery. Side panel is open.

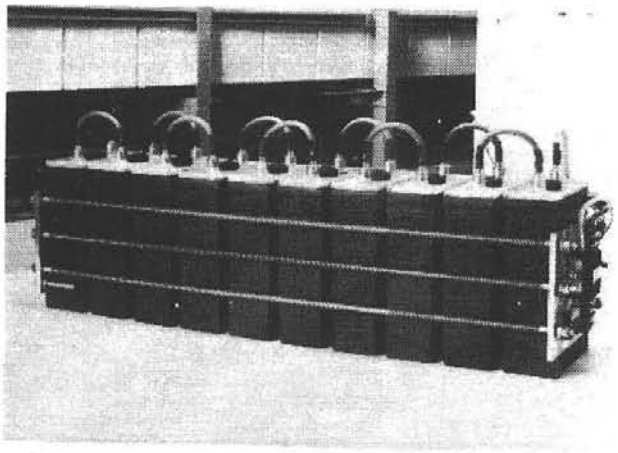

Figure 2-10. A 12-V 150-Ah Nickel/Hydrogen Battery Module

have shown that even at high rates of discharge the cells do not become starved of hydrogen gas, nor is there any loss of electrolyte at high charge rates.

Each cell contains nine cell modules. The cell module, the building block of the prismatic cell, consists of two sintered and electrochemically impregnated nickel positive electrodes configured back-to-back with an electrolyte absorber between them, two separators, and two negative electrodes. The components of the cell module are bound together by two outside diffusion screens.

The 7-kWh battery incorporates a number of design changes from aerospace technology that enhance the performance of the nickel/hydrogen system for terrestrial service. The use of thicker electrodes lowers the cost by reducing the number of cell components per cell module, as well as increasing specific energy. The absorber/wick improves electrolyte management, thus increasing cycle life, and the peripheral seal, used as an aid in assembly, enhances oxygen recombination. Also, the use of additives, along with a change in electrolyte concentration, improves high-temperature performance.

Battery Conditioning

Upon adding electrolyte to each cell and inserting the ten-cell pack into the boilerplate pressure vessel, the vessel was sealed and given a precharge of 50 psig of hydrogen gas. Each battery module was activated independently to determine how well the cells were balanced. Instead of using a common manifold, pressure transducers were installed on each of the four pressure vessels. The battery modules were then charged at the 10-h rate for 16 h and discharged at the 5-h rate to 10 V per module. The average capacity on the first discharge was 160 Ah at a mid-discharge voltage of 12.3 V. The highest recorded temperature on charge was 40°C. The battery modules were given 15 conditioning cycles to distribute the electrolyte properly within the cell components without overheating. Each conditioning cycle consisted of a charge of 25 A for 5 h and a discharge of 25 A to 10 V per module.

At this point the pressure vessels were connected to a common manifold and the battery was treated as one 24-V, 300-Ah unit. It was charged at 50 A for 6.4 h and discharged at 50 A to 20 V. The battery delivered 7.85 kWh on discharge with an energy efficiency of 84%. The highest cell temperature recorded was 33°C during discharge. As many as 24 temperature readings can be monitored during testing at SNL to assist in thermal modeling.

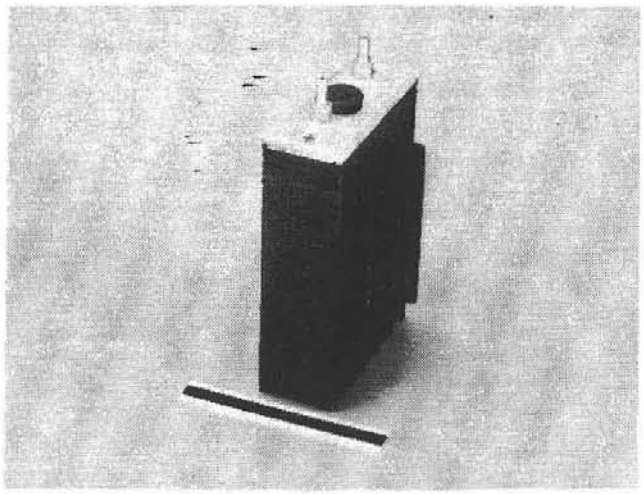

Figure 2-11. A Single 150-Ah Nickel/Hydrogen Cell

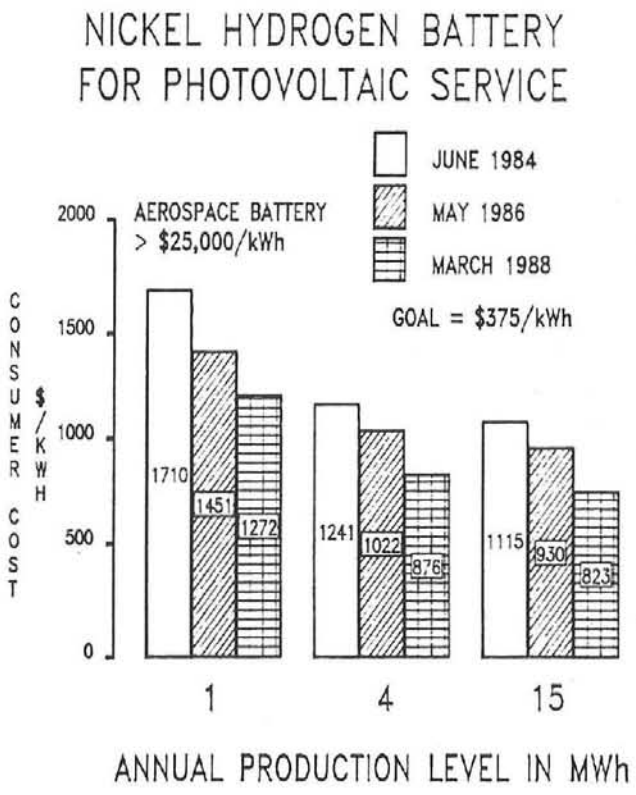

Figure 2-12. Relative Costs of a 15-kWh Terrestrial Nickel/Hydrogen Battery

Cost Study

Preliminary cost studies, which have been a significant part of the JCI program activity, indicate that this nickel/hydrogen battery system is approaching a position of economic superiority based on total life-cycle cost. The multikilowatt-hour system selected for the cost study is sized at 15 kWh. Costs to the consumer, in dollars per kilowatt-hour, were determined for production levels of 1, 4, and 15 MWh per year. The results of this study are presented in Figure 2-12. These production levels were fixed by the rates of three different bottleneck operations in the manufacturing process. The results of the current cost study, reflecting 1987 research and developmental efforts, show an additional 12% reduction in cost when compared to May 1986 results at the lowest production level.

The most important contributions to lower costs were the development of a 90-mil thick positive electrode and the reduction of the platinum loading on the negative electrode. These changes had no detrimental effect on performance.

An attempt to determine the likelihood of reaching the programmatic goal of $375 per kWh is difficult. The strong influence of fixed overhead makes cost dependent on production volume. An improvement curve was constructed based on the results of the 1987 cost study and an accumulated sales volume. It was assumed that each year the number of units sold increases to meet the increased production. All of these units are sold at the price determined in the cost study. The cost of the first 15-kWh unit is $5166 per kWh. Extrapolation shows that the $375 cost goal would be reached after cumulative sales of 11,000 units. The estimate in 1986 was 14,000 units to achieve the cost goal.

The results of the cost study can be used to form a basis of comparison with other 15-kWh batteries in an autonomous photovoltaic system with a 30-year life. When the discounted value of the required replacement units and the maintenance costs over the life of the system are taken into consideration, the nickel/hydrogen battery is shown to be competitive with other battery systems that might be used. In addition, if an elaborate charge controller between the solar array and the battery is not needed, further cost savings would accrue.

Technical Challenges Remaining

The cost study identifies a number of areas where further research and development will lead to additional cost reductions which, when coupled with a higher but reasonable production rate, will allow us to meet the programmatic life-cycle goal of 3.9 cents per kWh-cycle. Specifically, these areas include the high processing costs of the nickel electrode, the high materials cost of the negative electrode, and the development of a field-deployable battery-containment vessel. Hydrogen containment must be explored to develop an inexpensive and lightweight pressure vessel. One such approach is the use of hydrogen-storage alloys to reduce the demands on the pressure vessel and to improve safety.

The need to obtain data on real-life applications, along with the determination of unforeseen system limitations, is extremely important at this stage of development. The future objective is to design, develop, and build a multikilowatt-hour nickel/hydrogen battery incorporating a method of hydrogen storage suitable for field deployment. The proposed concept is to build a smaller, 2-kWh battery, to be used as a building block for the larger systems. Higher voltage can be achieved by connecting these batteries in series; more capacity can be achieved by connecting them in parallel. Likewise, the cost study should continue in an attempt to identify materials and components that are cost drivers and manufacturing processes that are bottleneck operations. It is important to continue the evaluation of status cells, representing the improved state-of-the-art technology, to ensure that the performance of the nickel/hydrogen system is not compromised.

Aluminum/Air Battery Development - Eltech

The SNL contract for development of aluminum/air batteries for electric vehicle applications was awarded to Eltech Research Corporation on 21 August 1987. Work began at Eltech and at the two subcontractors, Case Western Reserve University (Professor R. F. Savinell) and Helipump Corporation, on 1 September 1987.

Theory

Aluminum has attracted attention as a potential battery anode because of its high theoretical capacity: 2980 Ah/kg of aluminum. The energy obtained from the aluminum/air battery is derived from the reaction of the metal with water and atmospheric oxygen. For alkaline electrolytes the reactions are:

Anode Reaction:

$$4Al + 12OH^- \rightarrow 4Al(OH)_3 + 12e^- \qquad E = 2.34\ V$$

Cathode Reaction:

$$3O_2 + 6H_2O + 12e^- \rightarrow 12OH^- \qquad E = 0.4\ V$$

Overall Reaction:

$$4Al + 3O_2 + 6H_2O \rightarrow 4Al(OH)_3 \qquad E = 2.74\ V$$

Although the theoretical specific energy of the aluminum/air battery is high, the useful energy depends on several factors. The electrochemistry of both the aluminum anode and the air cathode critically affect energy efficiency. The $Al(OH)_3$ (aluminum hydroxide) product reacts with excess alkali to form a soluble aluminate ($Al(OH_4)^-$). The aluminate must then be decomposed to the crystalline hydrargillite ($Al_2O_3 \cdot 3H_2O$), and it may be necessary to separate this solid material from the electrolyte.

A true secondary battery requires that the metal be electrodeposited in the charging cycle. With aluminum, electrodeposition can only be achieved in aprotic solvents or molten salts. Both approaches represent significant technical hurdles to the development of a viable battery. An alternative approach, which Eltech has chosen, is to physically replace the aluminum anode to obtain the secondary (mechanically rechargeable) battery.

A diagram of an alkaline aluminum/air battery system is shown in Figure 2-13. The cell typically operates from 60 to 70°C with circulation of electrolyte and air (to the cathode).

The air is treated to reduce its carbon dioxide content. Hydrogen is generated by a parasitic corrosion reaction between aluminum and water, and safe disposal of this gas is necessary. A heat exchanger may be required to maintain the optimum temperature of the electrolyte in the battery during operation. A crystallizer and separator unit precipitates the hydrargillite (thereby regenerating sodium or potassium hydroxide in the electrolyte), and the solid product is then removed.

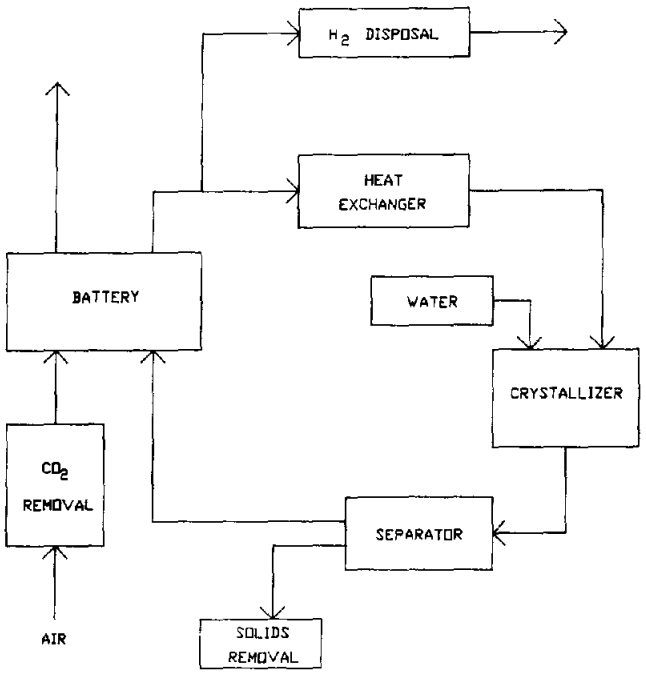

Figure 2-13. Alkaline Aluminum/Air Battery System

Current Status of Aluminum/Air Technology

Eltech Research Corporation has conducted research and development on aluminum/air batteries since 1980, focusing on

- development of improved air cathodes
- identification and development of aluminum alloys for the anode material
- computer modeling of the aluminum/air battery system
- development of improved battery designs.

The transition from component testing to battery and system evaluation occurred in 1985 with the transfer of the wedge-cell technology from Lawrence Livermore National Laboratories. Substantial modifications to this cell design led to acceptable performance and demonstrated refuelability in both a single cell and a five-cell battery. However, the volume and mass of the wedge cell precluded achieving target performance. Eltech independently continued the development of alternate designs, focusing on reduction of the weight and volume but without sacrificing the required rapid refuelability. The first phase of that effort has been completed and a new cell design, the B-300, has been identified. The components of this battery are shown in Figure 2-14.

Eltech also identified a separation method based on ceramic powder processing that promises to efficiently separate fine particles (5 to 10 μm). This approach may be preferred to the use of either a lamella settler or a tube settler, although the lamella settler has been successfully operated in a battery system. It is also possible that the separation device, the Helipump separator, will reduce the energy requirements for pumping the electrolyte in the battery system.

Research and Development Program

Program Description

The Eltech aluminum/air R&D program is divided into two phases:

- Phase I - Cell Design and Optimization
- Phase II - Auxiliary Support System Design

Cell Design and Optimization. The Phase I objective is to optimize the performance of the B-300 cell by characterizing its performance as a function of several independent operating

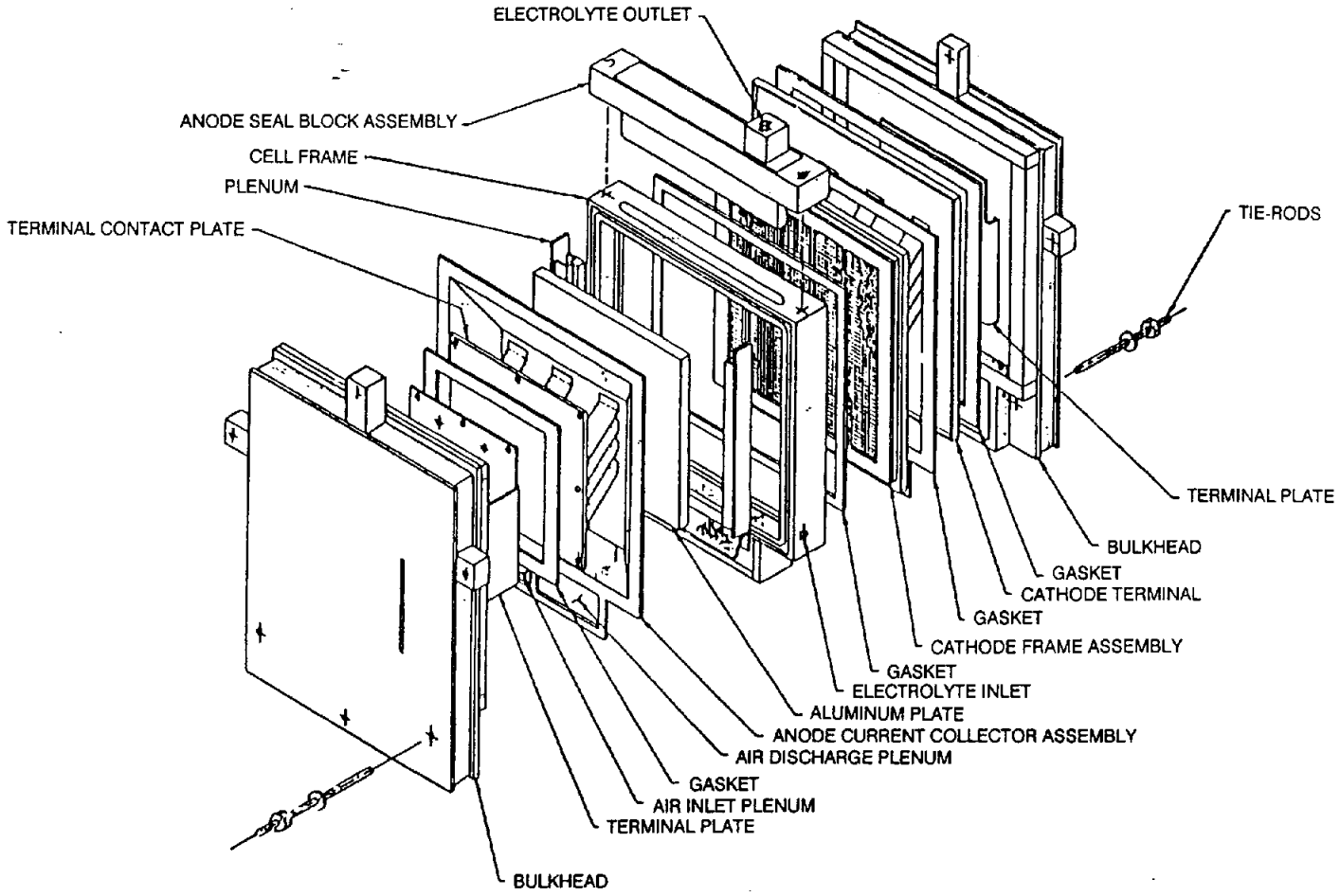

Figure 2-14. Components of the B-300 Battery

variables. The tasks combine both empirical studies and computer modeling. These tasks are:

- Task 1 - Fluid-Flow Characterization
- Task 2 - Steady-State Electrolyte Characterization
- Task 3 - Fundamental Modeling (to corroborate the empirical studies in Tasks 1 and 2)
- Task 4 - Data Acquisition for Cell Optimization
- Task 5 - Performance Characterization of the B-300 Cell
- Task 6 - Design Modification and Optimization
- Task 7 - Mathematical Analysis of Transient System Performance

Auxiliary Support System Design. The major Phase II objective is to develop technology to separate solid product from the circulating electrolyte. The Helipump separator will be characterized, and its design and performance will be optimized for the efficient removal of fine hydrargillite particles from the electrolyte. This part of the program will be supported by a mathematical analysis and computer modeling of the spatial distribution of particles in the

separator. The tasks associated with this portion of Phase II are:

- Task 8 - Computer Modeling of Particle Spatial Distribution
- Task 9 - Characterization of the Helipump Separator
- Task 10 - Alternate Vessel and Impeller Geometry
- Task 11 - Investigation of Separation-Enhancing Techniques
- Task 12 - Design of Prototype Separator
- Task 13 - Velocity Profile Studies

Additional tasks in Phase II deal with the selection and design of a heat exchanger, removal of carbon dioxide from the air stream to the cathode, and safe disposal of hydrogen gas:

- Task 14 - Heat Exchanger Design
- Task 15 - Carbon Dioxide Removal
- Task 16 - Hydrogen Safety and Disposal

Program Status

The tasks in which progress has been in 1987 are described below. Progress is also summarized in Table 2-6.

Task 1 - Fluid-Flow Characterization. Laboratory renovation and equipment procure-

Table 2-6. Summary of Aluminum/Air Battery Development - Eltech

Fluid-Flow Characterization	Laboratory renovated and equipment procured for construction of test system.
Cell Model	Boundary-layer analysis used to describe cell behavior.
Particle Distribution Model	Basic algorithm developed; modifications required.
Separator Characterization	Test system designed, constructed, and operated successfully, though some problems encountered with sampling procedures.
Heat Exchanger	System to simulate heat transfer for a 10-cell battery designed; equipment ordered.

ment was completed to allow construction of the test system. Flow sensors and conductivity meters were calibrated.

Task 3 - Fundamental Model of an Aluminum/Air Cell (Case Western Reserve University). Initially a model was selected, and a solution procedure using Fortran on an IBM AT computer was outlined. However, this rigorous, finite-difference approach proved very time consuming, and a simpler, boundary-layer analysis was used to describe cell behavior. This simpler model will be used to corroborate the data obtained from Task 1.

Task 8 - Modeling of Particle Spatial Distribution (Helipump). A basic algorithm was developed to allow modeling of the motion of spherical particles in the separator. The initial model determined the motion of a single particle; it indicated that future work should include simplifying the representation of the fluid-flow field.

Task 9 - Characterization of the Helipump Separator (Helipump). An experimental design to determine the effects of several variables (particle size, electrolyte flow rates, ratio of length to diameter of the separator unit, and impeller speed) upon separation efficiencies was developed. A test system was designed, constructed, and operated successfully. However, some problems were encountered with sampling procedures for Sedigraph particle-size analyses, and there appeared to be indications of physical instability of the alumina particles used.

Task 14 - Heat Exchanger (Eltech). A 3.3-kW system was designed to study heat transfer of a 10-cell B-300 battery. The equipment to construct the system was ordered prior to the year end.

Chapter 3. Nonaqueous Battery Development

Introduction

In 1987, the Nonaqueous Battery Development element of the ETD project focused exclusively on the sodium/sulfur technology. Sodium/sulfur is considered to be a leading candidate to satisfy the requirements of mobile and stationary energy storage applications. Programs were supported through development contracts with industrial participants and another national laboratory. The industrial contracts were cost-shared.

The following programs were supported in 1987:

- Sodium/Sulfur Core Technology Development at Chloride Silent Power, Ltd., (CSPL) (Runcorn, England) with Science Applications International Corporation (SAIC) (San Diego, CA) as a subcontractor
- Beta"-Alumina Electrolyte Development at Ceramatec (Salt Lake City, UT)
- Posttest Analysis of Sodium/Sulfur Cells at Argonne National Laboratory (ANL) (Argonne, Illinois).

The four-year contract with CSPL was placed in September 1985. CSPL is cost-sharing 35% of this $8.5M program. The program was directed to the continued research and development of the core sodium/sulfur technology needed to support both stationary and electric vehicle battery development. The key objectives were to enhance the understanding of sodium/sulfur cell and battery technology and to deliver a subscale battery module based on an approach appropriate for stationary applications. SAIC has been a significant subcontractor to CSPL, particularly in the areas of analysis and modeling.

A contract was initiated with Ceramatec in June 1986 to evaluate beta"-alumina electrolyte improvements, which were developed under previous ETD contracts, in sodium/sulfur cells. Electrolytes that were evaluated during this reporting period included: the Ceramatec Zeta process; the seeded, slurry-solution spray dried (S^4D) process; the unstablized zirconia-toughened process; and the yttria-stabilized zirconia-toughened process. Cells were periodically removed for posttest analysis and electrolyte characterization. The technical effort on this program is scheduled to conclude early in 1988.

The ANL posttest analysis effort focused exclusively on CSPL cells. The first group from CSPL were baseline cells that were terminated at different states of charge for morphological studies of the sulfur electrode. Analysis of cells delivered later in the year placed a greater emphasis on corrosion of container materials, degradation of seals, the beta"-alumina electrolyte, and gas compositions.

Sodium/Sulfur Battery Development - CSPL

This program, sponsored by the Department of Energy (DOE), commenced on 16 September 1985 at Chloride Silent Power, Ltd., Runcorn, England. The Core Technology and Battery Engineering Program was intended to be executed in parallel to a program sponsored by the Electric Power Research Institute (EPRI). The EPRI contract, to develop and construct a 500-kWh sodium/sulfur battery for the Battery Energy Storage Test (BEST) facility commenced in December 1985, but was substantially reduced in content on 14 February 1986. Plans to construct a 500-kWh battery were deferred.

At the request of Sandia National Laboratories, the Core Technology and Battery Engineering Program was extended in November 1987 by one year to reduce the annual program costs. This was achieved by deferring the construction of the main contract deliverable, a battery tentatively sized at 100 cells, into a fourth year, while maintaining the three-year time frame for the Core Technology Task 1

activities. An 18-kWh EV module was removed from the deliverable schedule to complete the cost adjustments. At the time of the cost adjustment, the opportunity was taken to redefine the work statement in line with developments in technology achieved between submission of and agreement on the proposal.

The objective of the program is to advance the state of the art of sodium/sulfur technology in components, cells, and small batteries. The program is divided into two tasks:

- Task 1 - Core Technology Research and Development
- Task 2 - Battery Engineering and Testing

Task 1 is devoted to research and development in the areas generic to both stationary and electric-vehicle applications of sodium/sulfur batteries. Major emphases of the program are performance, reliability, safety, and cost.

The following subtasks are part of Task 1:

- Subtask 1.1 - Electrolyte Research and Development
- Subtask 1.2 - Materials Development and Qualification
- Subtask 1.3 - Cell Development
- Subtask 1.4 - Cell Testing and Posttest Analysis
- Subtask 1.5 - Module Development and Testing

Work on Task 2, design and building of batteries for stationary applications, was not due to commence during the first year of the contract. In 1987 preliminary design and conceptual work was carried out. A substantial part of the program is subcontracted to Science Applications International Corporation (SAIC). The SAIC contribution to the Task 2 effort is discussed later in this report (Sodium/Sulfur Battery Development - SAIC, Chapter 3).

The CSPL Core Technology R&D progress is discussed below. Specific accomplishments are summarized in Table 3-1.

Background

The CSPL sodium/sulfur cell design strategy is based on a family of cells designated PB cells. Two specific sizes are currently being tested: a 45-mm-diameter by 45-mm-high cell called PB and a 45-mm-diameter by 110-mm-high cell called the Extended PB (XPB). The cells have central-sodium electrodes and are based on identical components as far as possible, particularly the seal designs.

The XPB has been proposed for stationary applications and the PB for electric vehicle (EV) applications, although it is intended to develop a generic technology. This generic technology will enable the commercialization of optimized cell designs, which are close in size to those for which a data base has been established. Selection of cell size is a complex issue that interacts with battery voltage, battery capacity, cell reliability, vertical dimensions of the battery bay, and costs.

CSPL has a long-term technology data base from the central sulfur 150-Ah NaS7 and 30-Ah technology demonstration (TD) cells. These designs have now been tested for up to 5450 deep-discharge cycles and eleven such cells have exceeded 4000 cycles. The longest-lived cell, still operating at the time of writing (February 1988), has completed more than 44,500 h on test. The longest-lived PB cell has completed 1800 cycles, and the longest-lived XPB cell has completed 1400 cycles.

During 1987 the production facility at CSPL was scaled up to produce cells at a maximum rate of 350 PB cells per week. This was a strategic objective of CSPL's UK-funded EV program, which enabled the construction and testing of a PB-cell battery in the 3.5-ton Bedford CF delivery van. This vehicle achieved a range of 100 miles on its second run. Much of the core technology related work was devoted to the study and implementation of technology for producing cells at higher rates and testing them. The cumulative production of PB cells is shown in Figure 3-1.

Core Technology Research and Development

The objective of Task 1 is to carry out the basic research, cell development, cell testing,

Table 3-1. Summary of Sodium/Sulfur Battery Development - CSPL

Electrolyte R&D	
Production Scale-Up	Grade I (zero-defect) ceramic production was 14,910 (up from 3600 in 1986), without zirconia toughening. Alcohol reclamation rate at 200 l/day; reclaimed alcohol higher in quality than supplied material. Ceramics made with recovered powder successfully fabricated. Multiple-sourcing has made lower-cost materials available. Pilot studies on rotary calcining carried out. Batch-sintering capacity increased; batch-sintering techniques improved. High PB- and XPB-ceramic yields: • 37% average annual yield for PB ceramics, with three monthly yields near or over 50%; • best XPB yield: 42% from a batch of 360 deposits.
Minimum-Grind Electrolyte	Lower resistances achieved by grinding a minimum of material from open end of electrolyte.
Zirconia Toughening	Tests on cells containing optimal levels of zirconia show dramatic increases in cycle life: 47,000 cumulative cell cycles without a single failure. Fifty PB cells with electrolytes containing optimal levels of zirconia constructed for further testing. Zirconia-toughened ceramics now considered worthy of further development, despite problems with moisture sensitivity.
Materials Development and Qualification	
Alpha-Alumina-to-Beta"-Alumina Glass Seals	Cell with a barium aluminoborate glass (no longer used) has completed 5454 deep-discharge cycles. Cell with an aluminoborosilicate glass (now used in all production cells) has completed 4900 cycles.

Table 3-1. Summary of Sodium/Sulfur Battery Development - CSPL (Continued)

	Testing of a CABAL-12 glass shows that its chemical resistance is superior to the aluminoborosilicate glass, but its thermal expansion does not match that of beta"-alumina and alpha-alumina.
Metal-to-Alpha-Alumina Seals	MkIII design improved by selecting optimal sealing conditions to overcome variable cell performance.
Sodium Electrode	Testing on automatic sodium-filling machine shows that it lowers initial cell resistance. Initial trials carried out on a safety container that totally encloses the electrolyte and seal subassembly. Problems with welding operation that seals the sodium electrode overcome.
Sulfur Electrode	The following analyses of the sulfur electrode carried out: • real-time hot radiography • AC impedance spectroscopy • parametric study of manufacturing conditions • cost analysis.
Containment	Duplex chromized steel container user for all production containers in 1987; other coatings being developed.
Cell Development	
Reliability Development	
PB Cell	Shown capable of yielding high Weibull shape parameters both as a single cell and in stationary batteries. Cell life shown to be dependent on the rate of electrical cycling (number of cycles per day). Over 1575 cells tested (516,500 cumulative cycles); 282 cells have completed over 500 cycles. Sixteen-fold improvement achieved in cycle time required to fail 1% of the cells.

Table 3-1. Summary of Sodium/Sulfur Battery Development - CSPL (Continued)

XPB Cell	361 cells constructed, of which 235 have been electrically tested. Twelve cells have exceeded 500 cycles; maximum cell life: 1400 cycles. 60-cell repeatability trial does not achieve benchmark characteristic life of 1300 cycles because of mechanical and design imperfections; actual XPB concept is sound, and improvements have been developed.
Performance	PB-cell performance remains at 1986 level in terms of capacity and discharge resistance; some improvements in initial resistance.
Freeze/Thaw	Automatic freeze/thaw facilities installed. Testing shows that freeze/thaw cycling has minimal impact on single-cell failure.
Cell Fabrication and Termination	10,000 welds made with a single set of welding electrodes.
XPB Cell Development	Rise in resistance, which was attributed to sodium current collector, resolved by using a spout for filling sodium; however, spout was difficult to construct and sodium filling can only be achieved with hand-filling equipment.
Safety	Testing carried out on PB cells, PB modules, and XPB cells. Tests on open-topped safety cans prompts work on totally enclosed safety containment.
Quality Control	QC effort strengthened: • drawings brought up to date; • drawing control and issue system implemented; • material and process specifications completed; • QC procedures being brought under control of the British Standards Institute.
Cell Test and Posttest Analysis	
	New testing rigs installed to support XPB testing. Test support provided for other subtasks.

Table 3-1. Summary of Sodium/Sulfur Battery Development - CSPL (Continued)

Module Testing	
	Tests on all modules built in 1986 continued, except for the • 24-PB-cell module on the 1-h discharge/2-h charge regime, which was removed from testing after 1000 cycles • 120-PB-cell battery (see below).
	Seven 128-PB-cell modules (submodules for the Bedford EV battery) tested for safety and freeze/thaw analysis; two cells failed during freeze/thaw testing.
	One 120-MkIII-PB cell module constructed; testing began in early 1988.
120-PB-Cell Battery	Capacity decline matched the SAIC computer predictions.
	Removed from testing after 630 cycles; 52 Ah of original 120-Ah capacity.
	Eight cell failures, plus two cell failures during cool down; posttest analysis in process.
XPB Modules	Module consisting of four XPB cells constructed; 55 SFUDS cycles completed.
	16-cell XPB module constructed with air-over facilities and air-flow instrumentation.

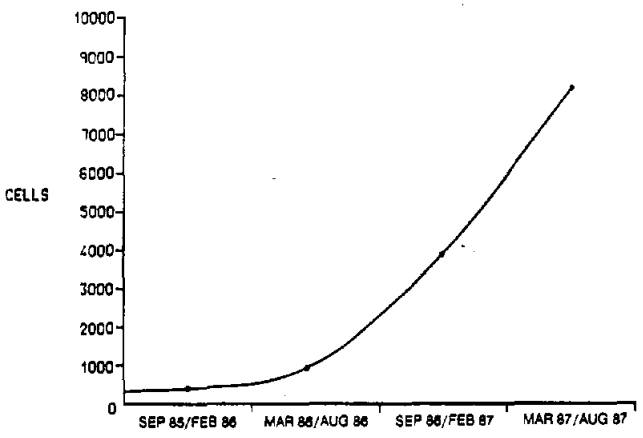

Figure 3-1. Cumulative Production of PB Cells

materials studies, quality control, and computer modeling required to support a battery program directed to the fabrication of the final deliverable, a battery consisting of at least 100 XPB cells, and also to advance generic sodium/sulfur technology for both utility and EV applications. The issues of performance, reliability, safety, and cost are specifically addressed.

There was extensive transition in Core Technology Research and Development during 1987:

- Manufacture of PB cells was scaled up. During 1987 more than 8000 PB cells and 361 XPB cells were manufactured for all

CSPL programs. The electrolyte department produced almost 15,000 first-grade PB ceramics at an overall yield of 37%.

- The core technology developed on PB cells was transferred to the XPB program and work commenced on XPB modules in preparation for the start of design work on the final contract deliverable: an XPB module tentatively consisting of 100 cells.

- Towards the end of 1987 the CSPL direct-metal-bonded seal (the MkIIA) was replaced by the MkIII seal, which has been developed under the SNL/DOE contract. The MkIII seal was selected after analysis of PB-cell performance in the Bedford Battery, a favorable independent cost analysis, and resolution of the performance problems previously experienced with the MkIII design.

Progress was made on all the subtasks of Task 1. A battery consisting of 120 PB cells completed testing after 630 electrical cycles in 11,600 hours. Using data from a reliability trial on 36 PB cells, the computed performance of the 120-cell battery was close to predictions, which included a capacity decline towards its end of life. During posttest analysis of the battery it was possible to determine exactly which cells had failed. This capability, combined with electrical data, made accurate life analysis possible, which showed that there is no significant difference in electrical cycle life between the battery cells and those tested singly. However, the data imply that chronological life is dependent upon rate of cycling (i.e., number of cycles per day).

Once the baseline had been established on the MkIIA cell design via the 120-cell battery and the 36-cell repeatability experiment, work on the analysis of cell freeze/thaw cycling was carried out. Four single cells were subjected to 147 thermal cycles without any failures, and a module consisting of 128 PB cells was subjected to five freeze/thaw cycles during 84 electrical cycles. Two cell failures were discovered during posttest analysis of the module.

During 1987, collaborative freeze/thaw work was conducted between CSPL and SNL, ANL, and SAIC. Both SNL and ANL tested PB cells, and ANL conducted posttest analysis work. SNL and ANL testing is discussed in Sodium/Sulfur Testing at SNL (Chapter 4) and Testing and Analysis at ANL (Chapter 4), respectively. ANL posttest analysis is discussed in Posttest Analysis of CSPL Sodium/Sulfur Cells - ANL (Chapter 3). The SAIC freeze/thaw work is found in Sodium/Sulfur Battery Development - SAIC (Cell Freeze/Thaw Modeling and Testing), Chapter 3.

A major objective of the contract was to establish quality control within the more production-oriented environment at CSPL. More formal quality-control procedures, process-control manuals, materials specifications, and engineering drawings were implemented during 1987, although such methodologies will need to be continuously updated as the technology develops further.

Electrolyte Research and Development

During 1987 all aspects of electrolyte fabrication were further developed with an emphasis on improved productivity, cost reduction, and quality improvement. All of these objectives were achieved without zirconia additions for microstructural improvement, although the life data accrued during the year suggest that further benefits can be derived from zirconia. However, if zirconia is to be used, solutions that accommodate its increased moisture sensitivity must first be found.

A discussion of the scale-up in electrolyte production and evaluations of minimum-grind electrolyte and zirconia toughening follows.

Production Scale-Up. CSPL has continued developing the electrophoretic deposition (EPD) process during 1987. The output of Grade I (zero-defect) ceramics has risen from 390 in 1985 to 14,910 in 1987. (3600 zero-defect electrolytes were produced in 1986.) The capital equipment was purchased by CSPL under its UK-funded contract, but the underlying technology was funded by the SNL Core Technology Program.

The alcohol that makes up the beta"-alumina suspension is expensive, and its reclamation was an objective for economic production. This was achieved during the year: the alcohol was routinely recovered at a rate of 200 l/day. Tests showed that the quality of the reclaimed product

exceeded that of the supplied material, and substantial improvements in the life of molecular sieves used to dry the alcohol were therefore achieved.

Recovery of the unused powder from the EPD slurry is a beneficial objective, and ceramics made with a proportion of recovered powder were successfully fabricated. Further developments on a 12-chamber EPD rig, which was commissioned in late 1986, improved the yield from the process. Parametric studies of voltage, flow rate, and chamber design were employed to significantly reduce the number of reject flaws in the finished product.

Multiple sourcing of raw materials is a strategic objective. This was achieved with significantly lower-cost materials from a variety of sources. Blending and calcining of the materials was investigated for the 1987 rate of production (≈15,000 electrolytes per year) and for a potential rate of at least 5000 ceramics per week.

Because batch processing is unattractive in comparison to continuous processing, rotary calcining was studied and piloted through small-scale production runs. Purchase of in-house rotary calcining equipment has been proposed for 1988 so that more detailed investigations can be carried out.

Changes were made to the way ceramics were batch-sintered. The furnace charge was increased so that up to 420 PB shapes could be fired at one time. Changes in method obviated the need for beta"-alumina support bisques. These modifications improved dimensional control and reduced losses (caused by out-of-specification open ends) from 27% to 6%.

High yields were achieved with both PB and XPB ceramics. The best weekly yield of PB ceramics was 76%. The high monthly PB yields in 1987 were as follows: May (56%) and December (49%); the January 1988 yield was 49%. Low yields in 1987 were recorded in June and August, for reasons that are understood. These reduced the overall yearly yield to 37%. There is a strong expectation that yields in excess of 50% are maintainable with current technology, although a higher figure is sought. Cost analysis during 1987 has shown that battery marginal manufacturing cost is relatively insensitive to ceramic yield and that a 50% yield is considered commercially viable. Yield of XPB ceramics was also good. The best yield during 1987 was 42% from a batch size of 360 deposits. A total of 1330 XPB ceramics were deposited in 1987.

Minimum-Grind Electrolyte. As part of an investigation into reducing the amount of grinding carried out on the electrolyte (and thus the time and money associated with grinding), a group of ceramics was made in which only a minimum of material was removed from the open end. A consequence of this procedure was that the ceramics had to be made with thin walls, (1.3 to 1.4 mm compared to a specification of 1.2 to 1.8 mm) to accommodate the alumina header. The cell performance and cycle data of cells made from the ceramics is shown in Table 3-2. The resistance of PB cells averages 36 to 37 mΩ, depending on which group is used to calculate the data.

Zirconia Toughening. No experimental work was carried out during 1987 on the fabrication of electrolytes containing significant amounts of zirconia. However, cell testing of zirconia-bearing ceramics continued in both PB and technology demonstration (TD) cells. A group of eight TD cells commenced testing before the start of the contract. A single cell failure, which occurred at 949 cycles, was reported in the *ETD Report for 1986*, page 47. This cell contained a nonoptimum zirconia addition. No further failures occurred in 1987, and as of February 1988, four cells had completed 3104 cycles, and three cells had completed 3164 cycles. (Ceramatec also tested sodium/sulfur cells with zirconia-containing electrolytes. See Development of Beta"-Alumina Ceramic Electrolyte - Ceramatec, Chapter 3.)

In a program coordinated with a parallel EPRI program (EPRI 128-13), the sensitivity of beta"-alumina to moisture was investigated. The EPRI investigations involved a nontoughened (low-zirconia) beta"-alumina; the SNL investigations involved beta"-alumina containing optimized zirconia additions. The cells were constructed during the first year of the contract and have continued cycling since that time. The storage conditions and cycle status are shown in Table 3-3. Storage in both the ambient laboratory atmosphere (average relative humidity 55%) or 100% relative humidity resulted in disintegration of the ceramic tubes.

Table 3-2. Minimum Grind Electrolyte (PB Cells)

Cell No.	Cycle	Resistance (mΩ)	Resistance Rise (mΩ)	Status
8575	573	28.8	0.0096	Failed
8574	1103	31.0	0.0058	Cycling
8576	1103	30.5	0.0050	Cycling
8577	1103	26.5	0.0068	Cycling
8578	1103	30.6	0.0081	Cycling
Mean ± 1 Std. Dev.		29.48 ± 1.87	0.007 ± 0.0019	

The combined data in Table 3-3 represent more than 47,000 cell cycles without a single failure. Although it is impossible to make life predictions using Weibull statistics, it can be inferred that, in terms of cycle life, these two populations are the best cells ever made. A similar group of TD cells containing non-zirconia-toughened ceramic has been tested (partly under EPRI contract 128-13). This population has Weibull parameters of 3300 cycles (characteristic) and 0.88 (modulus). From these data it might be expected that ten of the zirconia-toughened population would have failed by February 1988. However, based on Weibull parameters of 3300/0.88, the probability of experiencing zero failures by the cycle lives achieved is 4×10^{-7}, and the probability of observing one failure is 9×10^{-6}.

Additional batches of electrolyte containing optimum quantities of zirconia were made at the end of 1987, and 50 PB cells were constructed and are awaiting test. Experiments with small numbers of PB cells containing zirconia-toughened ceramic gave some encouraging results, and the ceramic was judged worthy of further development, in spite of difficulties with moisture sensitivity.

Materials Development and Qualification

The major objective of this subtask is to qualify cost-effective candidate materials for cell and system design. The subtask includes the following activities:

- alpha-alumina-to-beta"-alumina glass seal
- metal-to-alpha-alumina seals
- sulfur- and sodium-electrode design
- sulfur-electrode containment.

A materials-durability data base had been established before the start of the Core Technology program. This was based on CSPL's NaS7 and TD cell designs, which contain materials and materials combinations pertinent to the present PB family of cells. The increased maturity of the data base is shown in Table 3-4.

Alpha-Alumina-to-Beta"-Alumina Glass Seal. A glass joint hermetically seals the alpha-alumina seal header to the beta"-alumina. The longest-lived cell contains a 668 formulation glass (barium aluminoborate modified with silica). This cell, which is an NaS7 cell, contains two glass seals, one at each end of the electrolyte. The cell had completed 5454 deep-discharge cycles to 1.76 OCV (open circuit voltage) in 44,520 h (5 years 1 month). The present composition, employed in all standard production cells, is 2112 formulation glass (an aluminoborosilicate). This has been tested for 4900 cycles in 40,932 h.

Table 3-3. Cycle Status of TD Cells Containing Optimized Zirconia Additions

Cell Number	Storage Conditions	Days Stored	Resistance (mΩ)	Capacity (% theoretical)	Cycles
6013	50% RH	50	11.3	81.5	2016
6014	in	50	12.0	81.3	2149
6025	Glass	50	11.5	79.8	2079
6047		100	11.0	81.8	2079
6012	0% RH	50	12.7	81.5	2149
6015	Over	50	12.4	79.2	2149
6024	Silica	50	11.8	81.0	2079
6038	Gel	100	11.5	79.4	2079
6016	0% RH	50	20.0	79.0	2149
6048	in N_2	100	11.0	74.7	2079
6011	25% RH	50	11.0	80.8	2149
6039	in N_2	100	11.8	79.8	2079

Table 3-4. Component/Materials Durability Data Base

	10/10/85		12/31/86		3/15/88	
	Cycles	Hours	Cycles	Hours	Cycles	Hours
Electrolyte Comp.	2603	21,834	3960	32,328	4900	40,932
Glass Comp.	2603	21,834	3690	32,328	4900	40,932
Thermocompression Seal Materials	3278	27,024	4646	37,968	5454	44,520
Sodium Electr. Design	2603	21,384	3960	32,328	5454	44,520
Sulfur Electr. Design	2987	24,696	4336	35,640	5454	44,520
Secondary Protection	2987	24,696	4336	35,640	5454	44,520

In response to concerns over the freeze/thaw properties of glass joints exposed to cell-cycling conditions, work on these aspects was increased during 1987. Three cells from a 36-cell reliability experiment (which commenced in 1986) were subjected to freeze/thaw cycles. One of these cells underwent freeze/thaw after 700 charge/discharge cycles; the other two underwent freeze/thaw after 1100 charge/discharge cycles. All three cells survived and continued cycling for a further 200 cycles.

Despite these encouraging results, greater resistance to sodium and sodium polysulfide attack was sought during 1987. A CABAL-12 glass, supplied by SNL, was tested for sodium resistance and freeze/thaw survivability. This glass was also tested in electrically cycled cells. Chemical resistance was shown to be superior to the 2112 formulation glass, although some concerns were raised in regard to the thermal expansion mismatch of CABAL-12 and beta"-alumina/alpha-alumina. However, the results were sufficiently encouraging for further work to be planned with glass specialists from SNL on the CABAL class of materials.

Metal-to-Alpha-Alumina Seals. The ceramic-to-metal seal is of critical importance to the satisfactory life and performance of the sodium/sulfur cell. Two concepts have been studied at CSPL: a direct metal-to-ceramic bonded seal (funded by CSPL) and one employing an aluminum interstrate between the chromized steel and the ceramic header. The former concept was employed on cell designs designated MkII and MkIIA; the latter was known as the MkI seal. In 1986 a hybrid of the two seal concepts was selected for further development and was designated MkIII. This seal contains a direct metal-bonded sodium-electrode closure and a sulfur-electrode closure employing chromized mild steel and an aluminum interstrate.

The MkIII design was refined during 1987. An independent design and cost study carried out by a team of consultants in Advanced Manufacturing Technology favored the MkIII design over the MkIIA design. Their report, combined with continuing problems of corrosion resistance of the MkIIA design, led to an increased emphasis on the MkIII seal during the latter part of 1987. Problems of variable cell performance had been encountered with the early MkIII seal cells, but following a parametric study, an optimized set of sealing conditions was established. Data from an early MkIII cell group and from two groups of MkIII cells made in early 1988 are shown in Table 3-5.

Table 3-5. Resistances of MkIII Cells

Cell Group	No. of Cells	Average Resistance at 20 Cycles ± 1 Std. Dev. (mΩ)	Average Minimum Resistance ± 1 Std. Dev. (mΩ)
Nonoptimized Conditions (7518 to 7525) (7819 to 7821)	10	44.1 ± 3.83	35.7 ± 4.46
Nonoptimized Conditions (9569 to 9582)	11	59.5 ± 23	55.0 ± 21
Optimized Conditions (9640 to 9749) (non inclusive)	13	36.9 ± 1.9	36.4 ± 1.9

The last group of cells, made under optimized sealing conditions, does not exhibit the high and variable resistance problems associated with the other two groups. Sodium-sodium cycling, AC impedance spectroscopy and real-time hot X-ray radiography were employed in defining the problem and solving it. The radiography was carried out at SAIC on a MkIII cell made under nonoptimum conditions (Sodium/Sulfur Battery Development - SAIC (Cell Freeze/Thaw Modeling and Testing), Chapter 3). The middle group of cells (made in early 1988 under nonoptimum conditions) also suffered from drastically reduced cycle life. Its Weibull parameters are shown below (95% confidence intervals).

Weibull Characteristic Life (cycles)	${}_{75}117^{182}$
Weibull Modulus	${}_{0.8}1.4^{2.5}$

The reduced life and increased resistance is thought to be associated with poor electrode wetting following ceramic contamination under nonoptimum sealing conditions.

Sodium Electrode. The design of the sodium electrode strongly affects the cell performance under failure conditions. Improved sodium electrode performance was achieved in both PB and XPB designs during 1987.

The automatic sodium-filling machine was commissioned in the first quarter of 1987. An immediate benefit was the lowering of the initial cell resistance. Table 3-6 compares the initial resistances of the 36-cell reliability experiment (hand-filled), the automatically filled cells, and a control group that was hand-filled at the same time. The improvement in resistance is both in the absolute value and the variability. The sodium-filling equipment is shown in Figure 3-2.

During 1987 a greater synergy was achieved between the sodium electrode safety features of the PB and XPB designs. The use of a totally enclosed safety containment within the electrolyte/seal subassembly progressed, and initial trials were conducted. The new design has prospects for multi-orientation safety performance, a criterion of greater significance for mobile applications. Some development was required to enable the new design to be filled on the automatic-filling machine, and solutions were proposed by the end of 1987. Patent applications were made for several features of the sodium electrode.

Table 3-6. Initial Resistance of PB Cells on Automatic-Filling Machine

Cell Group	Mean (mΩ)	Std. Dev. (mΩ)
36-Cell Experiment	81.82	58.26*
Auto-Filled	38.89	1.58
Glove-Box Filled (Control Group)	83.64	65.48*

* Non-normal distribution

Prior to the commissioning of the sodium-filling machine, problems had occurred in the final welding operation, which seals the sodium electrode by means of a central metal current collector. This particular weld was responsible for many of the problems associated with the early PB-cell work and was partly solved by the time the 120-cell-battery and the 36-cell reliability experiments were constructed. Extensive parametric studies were conducted during 1987 to establish a reliable set of welding conditions. This was achieved, and process specifications and quality control procedures were established, and over 5000 successful welds were made with one set of electrodes. The increased understanding of this critical welding process enabled a smooth electrode change to be effected with a rapid re-establishment of baseline quality.

Sulfur Electrode. Fundamental studies of the sulfur electrode made during 1987 included the study of operation in sodium/sulfur cells by means of real-time hot X-ray radiography. AC impedance spectroscopy was used to characterize

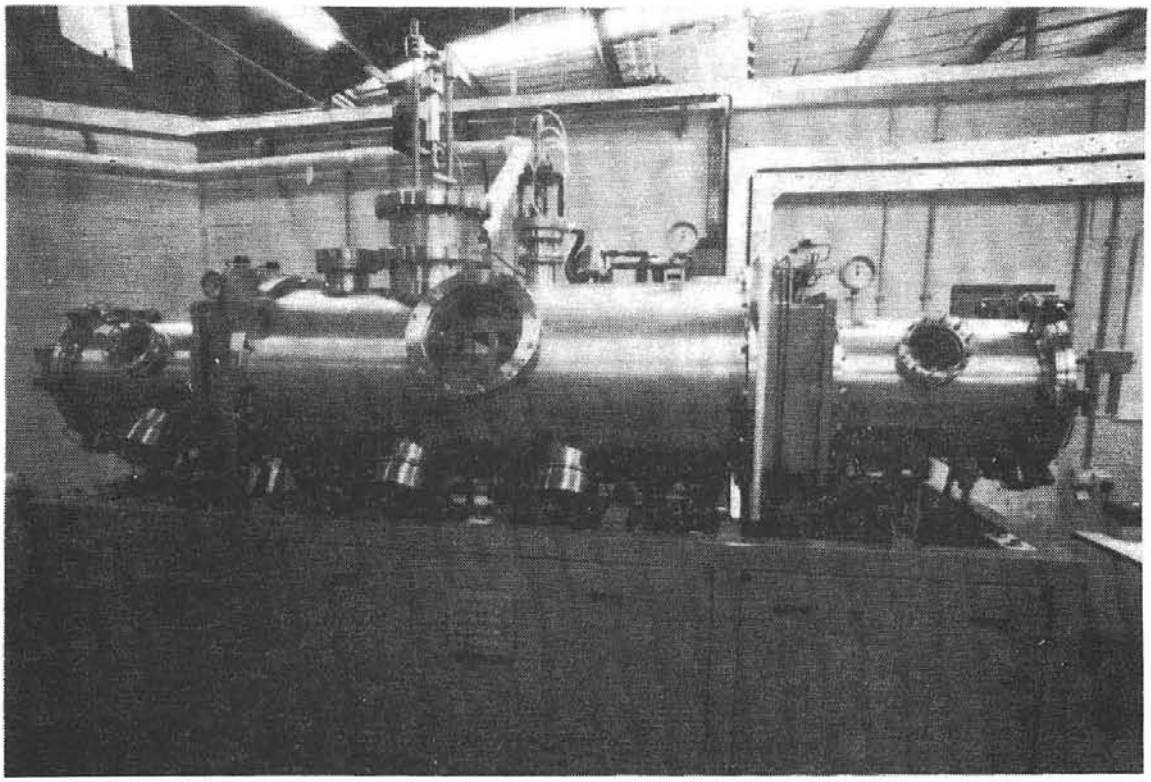

Figure 3-2. Automatic Sodium-Filling Machine

electrodes. Parametric studies of manufacturing conditions were employed to define the sulfur electrode more closely in terms of both materials and processing conditions. An independently conducted cost analysis showed the cell cost to be sensitive to the method of sulfur electrode manufacture, and other methods were proposed and tested in cells. These activities were anticipated to require further development during 1988, but the ground work on characterization, which was being concluded by the end of 1987, was expected to provide a useful diagnostic tool.

Containment. Long-term corrosion-resistant containment is one of the major challenges of the Core Technology program. The presently preferred approach is the use of a duplex chromized steel container; this type of container was employed on all the production cells made in 1987. Other coatings were developed during 1987 at CSPL and in collaboration with Sandia Laboratories, Livermore (see Improved Chromium Plating of Sodium/Sulfur Cell Containers, Chapter 5).

Cell Development

The objective of this subtask is to develop cell designs for both stationary and motive power applications, and to establish cell performance, reliability, safety, cost, and freeze/thaw survivability. Progress in cell development is discussed below.

Reliability Development. In 1986 a group of 204 PB cells was being tested, and Weibull parameters were predicted from the five cell failures that had occurred during 1986. All of the experiments were concluded during 1987, and the final statistics were computed.

The two major groups of cells were tested in

- a 36-cell reliability experiment

- a module consisting of 120 cells arranged in two 60-cell, 8-V banks arranged in four-cell strings.

A single cell from the 36-cell experiment remains on test as of February 1988. It has completed 1800 cycles. The summarized data for the two tests is shown in Table 3-7.

The data demonstrate the ability of the PB cell to give high Weibull shape parameters in both single cells and stationary batteries. A relationship is also implied between electrical cycling and life as can be seen in the performance difference between the 36 cells, tested at 3 cycles per day, and the 120 cells, tested at 2 cycles per day. The test regime of the 120-cell battery is described in more detail under subtask 1.5 (Module Development and Testing).

By the end of 1987, 282 PB cells had exceeded 500 cycles. The improvement in life statistics is shown in Figure 3-3, which reflects a sixteen-fold improvement in the cycle time required to fail 1% of cells. Including all programs, a total of 5165 PB cells were tested up to the end of 1987. Over 1575 PB cells were tested in stationary modules and small batteries, and these completed 516,500 cumulative cell cycles.

Extended PB (XPB) cells were in the early stages of development at the start of 1987. During the year the maximum life achieved in an XPB cell exceeded 1400 cycles in 12,700 h.

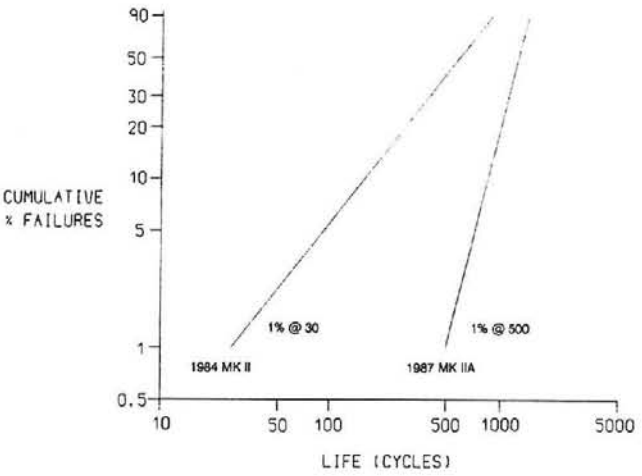

Figure 3-3. Reliability Improvement of PB Cells (1984 to 1987)

Twelve XPB cells exceeded 500 cycles. The total number of XPB cells constructed was 361 for all aspects of development; of these, 235 were electrically tested.

Two major XPB trials were conducted in 1987: (1) a scoping trial aimed at defining (2) a subsequent matrixed, 60-cell repeatability trial, in which performance parameters were predicted prior to cell test. A benchmark characteristic life of 1300 cycles was established prior to the 60-cell repeatability trial. The results from the 60-cell trial indicate that the original reliability

Table 3-7. Summary of Weibull Statistics for the 36 PB Cell Experiment and the 120 PB Cell Battery

	Cycles		Hours	
Experiment	Weibull Characteristic	Weibull Modulus	Weibull Characteristic	Weibull Modulus
36-Cell Population	$_{1183}1314^{1459}$	$_{3.2}4.7^{7.0}$	$_{10000}11,174^{12459}$	$_{3.1}4.6^{8.7}$
120-Cell Battery	$_{750}1225^{2001}$	$_{2.0}4.0^{8.0}$	$_{14872}29,867^{59983}$	$_{1.4}2.8^{5.6}$

benchmark was not achieved by any of the three groups of cells. Problems with the building of the cells implicate mechanical and design imperfections rather than the actual concept, and improvements had been developed but not tested at the end of 1987. The performance of XPB cells from the 60-cell experiment and the pretest predictions are shown in Table 3-8.

Performance. The performance of PB cells manufactured in 1987 remained at the 1986 level in terms of capacity and discharge resistance. Some improvement in initial resistance was achieved in the group of cells described in subtask 1.2 (Materials Development and Qualification - Sodium Electrode).

Freeze/Thaw. During 1986, automatic freeze/thaw facilities were installed at CSPL. Table 3-9 is a summary of the freeze/thaw tests carried out on single cells by the end of 1987. All of the cells were intact after the tests. In addition to these tests, a prequalification freeze/thaw procedure was employed during the building of part of the Bedford Vehicle Battery in CSPL's UK program. A total of 2172 cells were subjected to two freeze/thaw cycles. The failure rate for this procedure was less than 0.2%.

Cells were also subjected to freeze/thaw cycles during long-term testing. Figure 3-4 shows that there was no perceptible change in performance after the freeze/thaw cycles.

Cell Fabrication and Termination. This section of the program subtask was ongoing during 1987 and mainly consisted of monitoring the progress of production scale-up and providing core technology support where needed. An independent assessment of termination welding was made on subcontract by the UK Welding Institute. In this work 10,000 welds were made with a single set of welding electrodes.

XPB Cell Development. A major objective of the contract is to develop the family concept of PB cells based on generic core technology. A variety of cell designs had been constructed by the end of 1987. While much of the PB technology was transferred directly into the XPB designs, a number of specific problems required solutions.

In particular, a rise in resistance caused by an increasing contribution from the sodium current collector was observed. Attempts were made to electrically couple the current collector and the sodium electrode safety container. This was eventually resolved by the use of a spout attached to a totally enclosed container as described in subtask 1.2 (Materials Development and Qualification - Sodium Electrode). The design is shown in Figure 3-5. Although this

Table 3-8. Predictions and Performance of XPB Cells at 150 to 250 Cycles

Cell Type	Cell Resistance (mΩ)		Cell Capacity (Ah)	
	Predicted	Actual Mean ± 1 Std. Dev.	Predicted	Actual Mean ± 1 Std. Dev.
Composite	13.0 to 16.0	13.6 ± 1.37	25.0 to 28.0	29.6 ± 1.0
Infilled	13.0 to 16.0	15.9 ± 3.1	25.5 to 29.6	27.5 ± 0.9
Segmented	10.0 to 15.0	16.4 ± 2.0	25.5 to 29.6	27.6 ± 0.5

Table 3-9. Summary of Single-Cell Freeze/Thaw Data

State of Disch. (OCV)	Cell Test Population	Number of F/T Cycles
0% (2.076V)	4	147
	12	6
	2	4
	4	1
80% (1.90V)	2	2
	9	1
100% (1.76V)	2	4
	1	3
	4	2
	11	1

design was used for the repeatability experiment with the 60 XPB cells, it was difficult to construct, and these difficulties were reflected in the poor reliability achieved. An additional complication was that sodium filling of the spout design could only be achieved on hand-filling equipment.

A further concept was developed that appears to overcome the problems described above. The idea was transferred back into PB cells for initial construction trials and as of February 1988 was under consideration for the next build of XPB cells.

Safety. Safety testing was carried out during 1987 on PB cells, PB modules, and XPB cells. The most effective concept, designated "composite," was tested both in single PB cells and in modules of PB cells. No loss of reactants occurred in any of the failures. However, occasional leakages occurred during the testing of large numbers of cells in vehicle batteries. To address this, work was carried out on the totally enclosed safety features described above (Materials Development and Qualification - Sodium Electrode).

As of February 1988, the protection afforded by the composite safety feature was insufficient

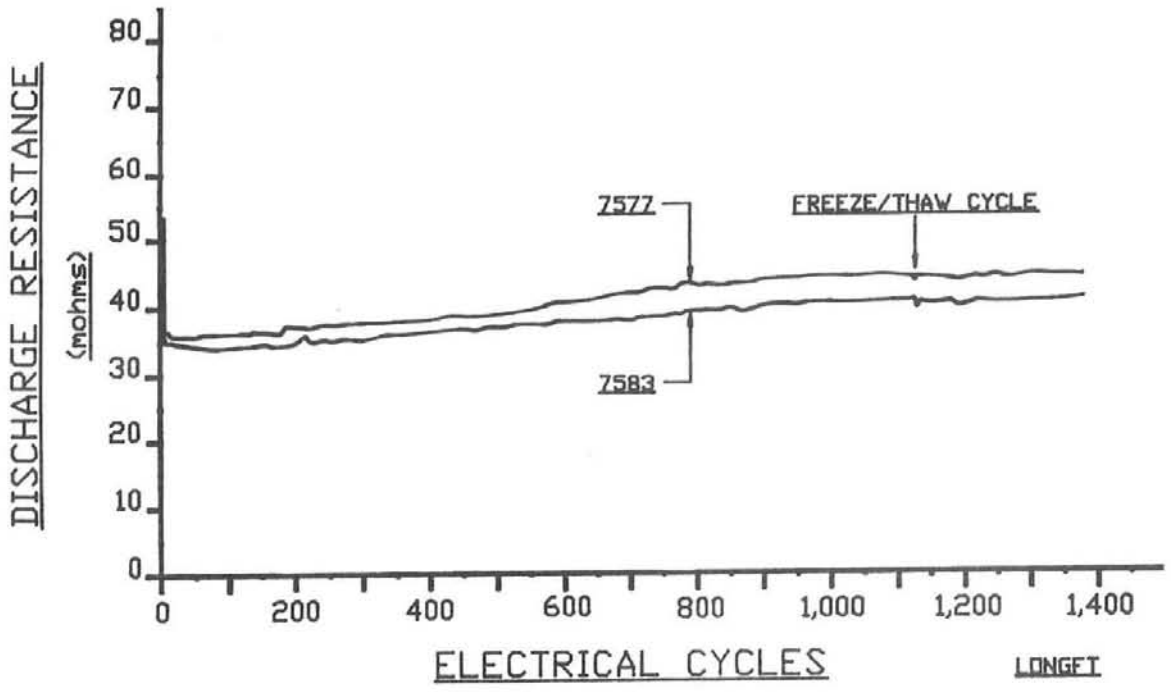

Figure 3-4. Freeze/Thaw of Long-Lived PB Cells

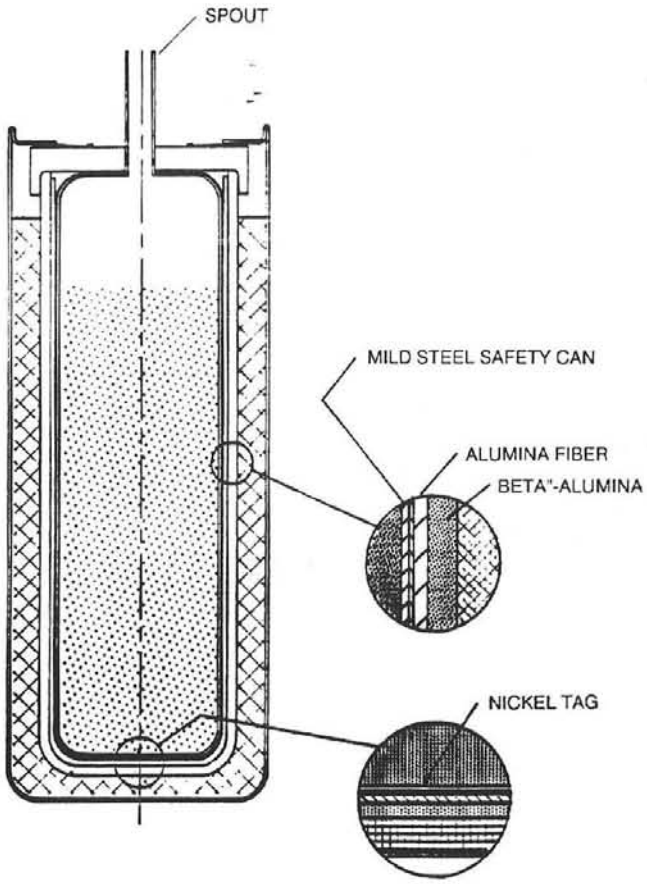

Figure 3-5. Composite XPB Cell Design

in the XPB design. This was because of compromises in the clearance between the sodium electrode can and the electrolyte. However, for the later generations of cells, closer tolerances were being achieved and benefits were anticipated.

Quality Control. It has always been recognized that, as the production of sodium/sulfur cells moved away from the laboratory to pilot-production levels, the need for more closely defined control would arise. To meet this demand the quality control (QC) effort was strengthened in 1987. When the cell design for manufacture at the rate of 350 units/week was fixed, the drawings were brought up to date and a system for controlling and issuing drawings was implemented. Materials and process specifications were completed for many of the manufacturing operations, and change procedures that require executive-level authorization were implemented. Outside supplier control was also implemented for key purchased items.

By the end of 1987 the QC procedures were being brought under a system controlled by the British Standards Institute (BSI). In this scheme (designated BS 5750), a set of defined methodologies have to be installed at the participating organization and their operation is overseen by third-party external examiners. Continued participation and accreditation by the BSI depends upon satisfactory reports that follow unannounced visits by the external examiners.

Cell Test and Posttest Analysis

The objective of this subtask mainly consists of providing test support and posttest analysis for other subtasks, and as such the effort is reported elsewhere. New testing rigs installed during 1987 include additional facilities to support the increasing number of XPB cells being tested. One of the new rigs is shown in Figure 3-6.

Module Testing

The primary objective of this subtask is to develop and test submodules of larger battery designs in order to explore the interactions of cell-connection strategy and to test groups of cells against application-specific requirements. Other objectives are to study the effect of cell failure interactions and the effect that varying cell performance has in an interconnected group of cells.

Tests on a number of modules were reported in last year's annual report (*ETD Report for 1986*, pages 57 and 59 through 61), and these continued to be tested during 1987. The module consisting of 24 PB cells, which operated on a 1-h discharge/2-h recharge regime was cycled for 1000 cycles before removal from test. The module consisting of 120 PB cells completed its testing as described below. In 1987, two modules consisting of 128 PB cells each were tested. These 8-V submodules of the Bedford EV battery were constructed to test the electrical performance of new safety features and for freeze/thaw analysis. The freeze/thaw module completed 84 electrical cycles interrupted by five deliberate thermal cycles. Two cell failures occurred during this experiment. A further five modules were tested to investigate the effect of

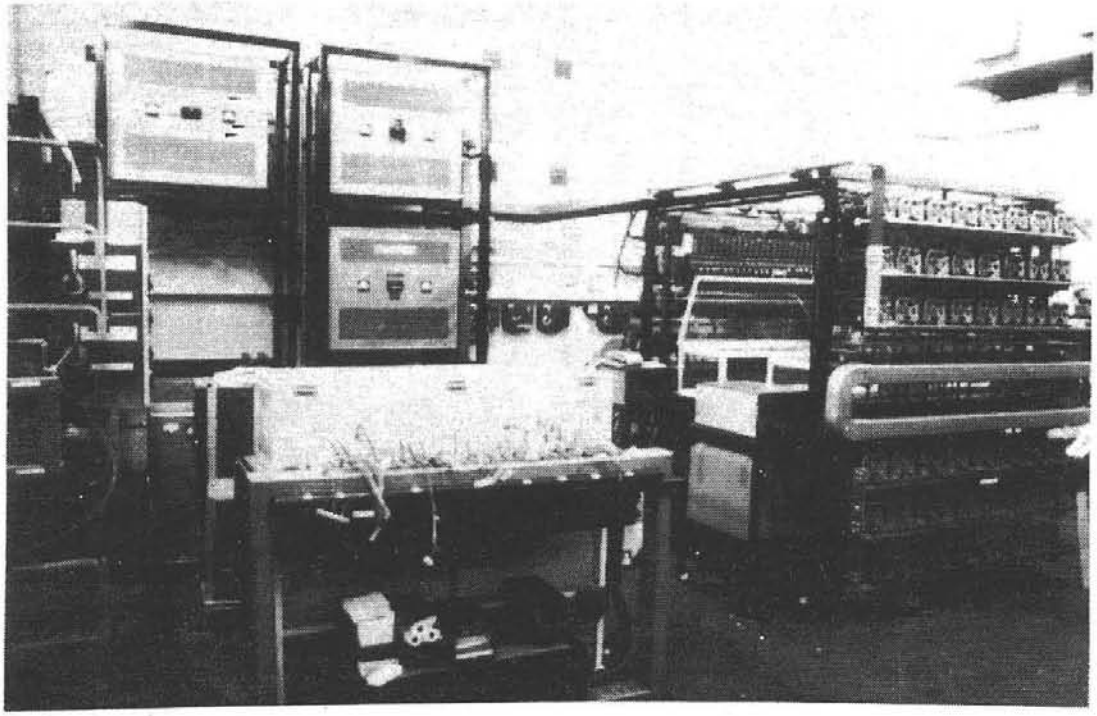

Figure 3-6. XPB Test Rig

module/battery hardware on the interaction of failing cells with neighboring cells. These experiments were used to define the hardware for the Bedford CF battery for CSPL's EV program.

The final module constructed in 1987 consisted of 120 MkIII PB cells. This module, the first to be constructed from MkIII cells, commenced test early in 1988 and is shown in Figure 3-7.

120-PB-Cell Battery. This battery had operated for 250 cycles (4.5-h discharge/7-h recharge) with no cell failures by the end of 1986. Cycling was continued during 1987 and once-weekly testing to the Simplified Federal Urban Driving Schedule (SFUDS) was introduced after 300 conventional cycles. The capacity of the battery began to decline towards the middle of 1987 and matched the computer predictions of life performance generated by SAIC as shown in Figure 3-8. (Further discussion of the SAIC model is found in Sodium/Sulfur Battery Development - SAIC (Cell/Battery Statistical Analysis), Chapter 3.) The battery was taken off test after 630 electrical cycles in 11,500 hours when the capacity had declined from the nominal 120 Ah to 52 Ah. Eight cell failures had occurred at that time and the high loss of capacity resulted from six of these being on one of the banks of 15 four-cell strings. Two further cell failures occurred on cool down. An analysis of the cell data was presented in Table 3-7. The battery was removed from test in November 1987, and as of February 1988 the posttest analysis (PTA) was proceeding. A photograph of the battery, after test, is shown in Figure 3-9.

XPB Modules. Construction and testing of XPB modules commenced during 1987. Initially a four-cell module, utilizing EV module hardware, was constructed and tested under an SFUDS regime. Fifty-five SFUDS cycles were completed.

The final contract deliverable, an XPB module consisting tentatively of 100 PB cells is conceived with blown-air cooling and temperature control, in line with studies made under EPRI Contract 2123-4 and the original proposal for the core technology contract. As a stepping stone to the deliverable battery design, a 16-cell XPB module was constructed with air-over facilities and air-flow instrumentation. This unit, shown in Figure 3-10, was constructed in late 1987 but had not commenced testing.

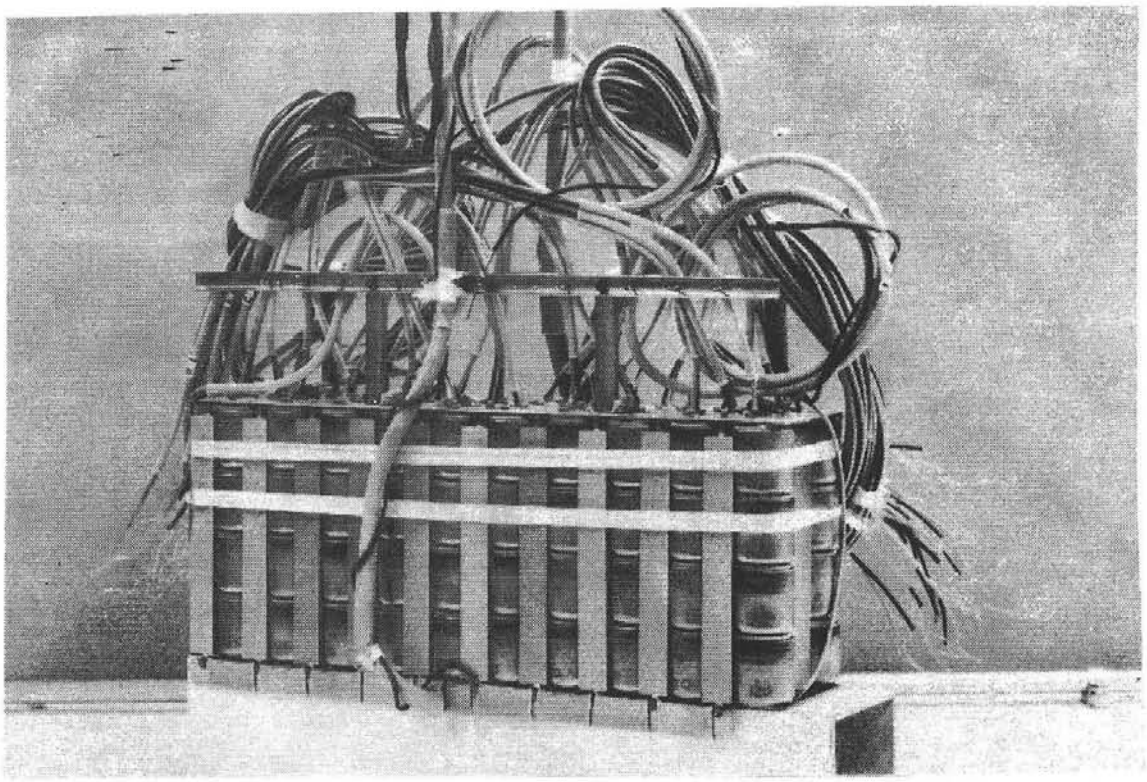

Figure 3-7. 120-MkIII-PB-Cell Module

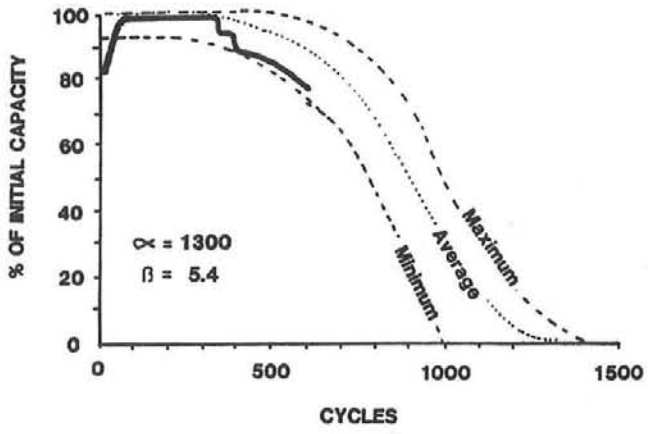

Figure 3-8. Computer Prediction and Actual Capacity of 120-PB-Cell Battery

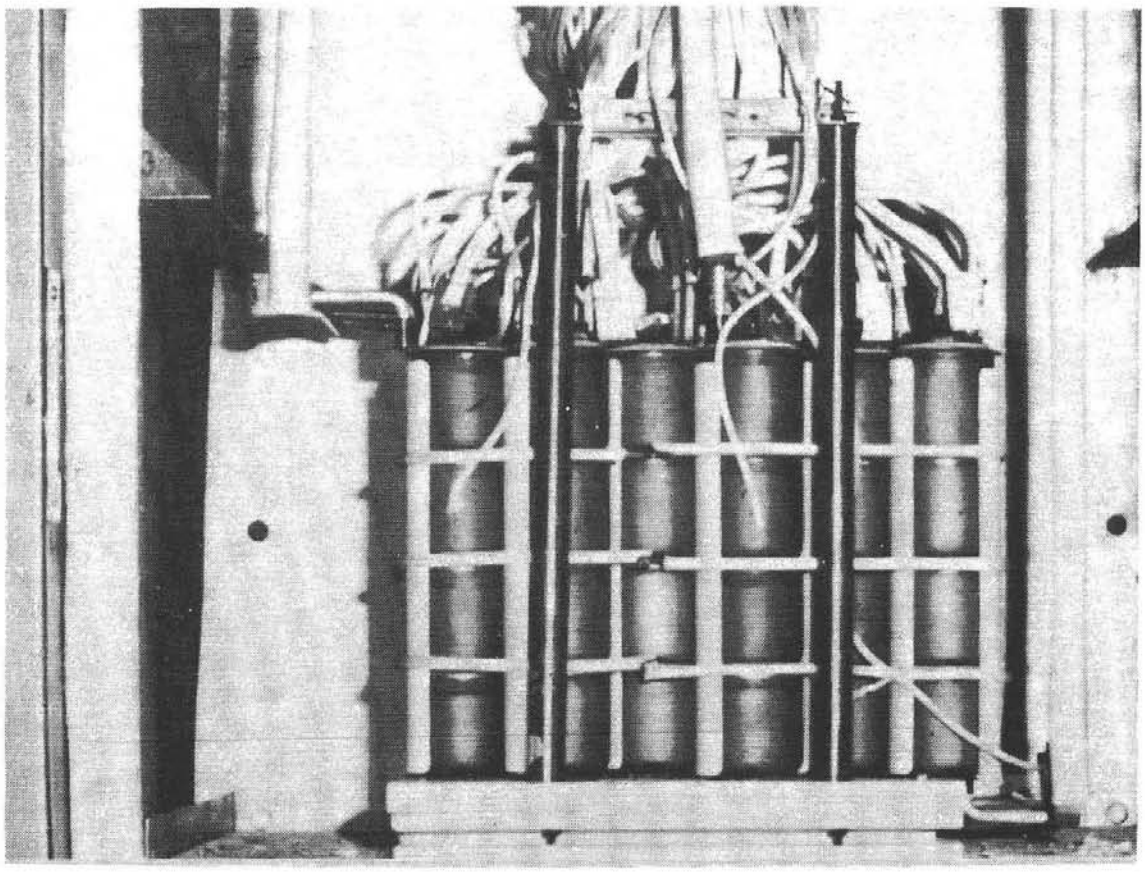

Figure 3-9. 120-PB-Cell Battery After Test

Battery Engineering and Testing

The preliminary design and conceptual work was carried out partly by SAIC. The SAIC work is discussed in the next section, Sodium/Sulfur Battery Development - SAIC. Close liaison was maintained between the EPRI 2123-4 design team and personnel working on Task 2, so that maximum synergy of concepts could be achieved. One outcome of this approach was a move toward increasing the size of the contract deliverable from the nominal 100 cells to more than 200 cells, so that a complete tray subunit of the design proposed in the EPRI 2123-4 program could be employed. This tray contains 26 rows of 10 XPB cells.

Sodium/Sulfur Battery Development - SAIC

Science Applications International Corporation (SAIC) is a subcontractor to CSPL on the Battery Engineering and Testing Program, the second task in a two-task sodium/sulfur battery development program sponsored by SNL. (The CSPL program is presented in the previous section, Sodium/Sulfur Battery Development - CSPL.) The objective of the SAIC effort is to support CSPL in the design of electric vehicle and utility load-leveling battery systems using PB and XPB cells. The SAIC program consists of seven tasks:

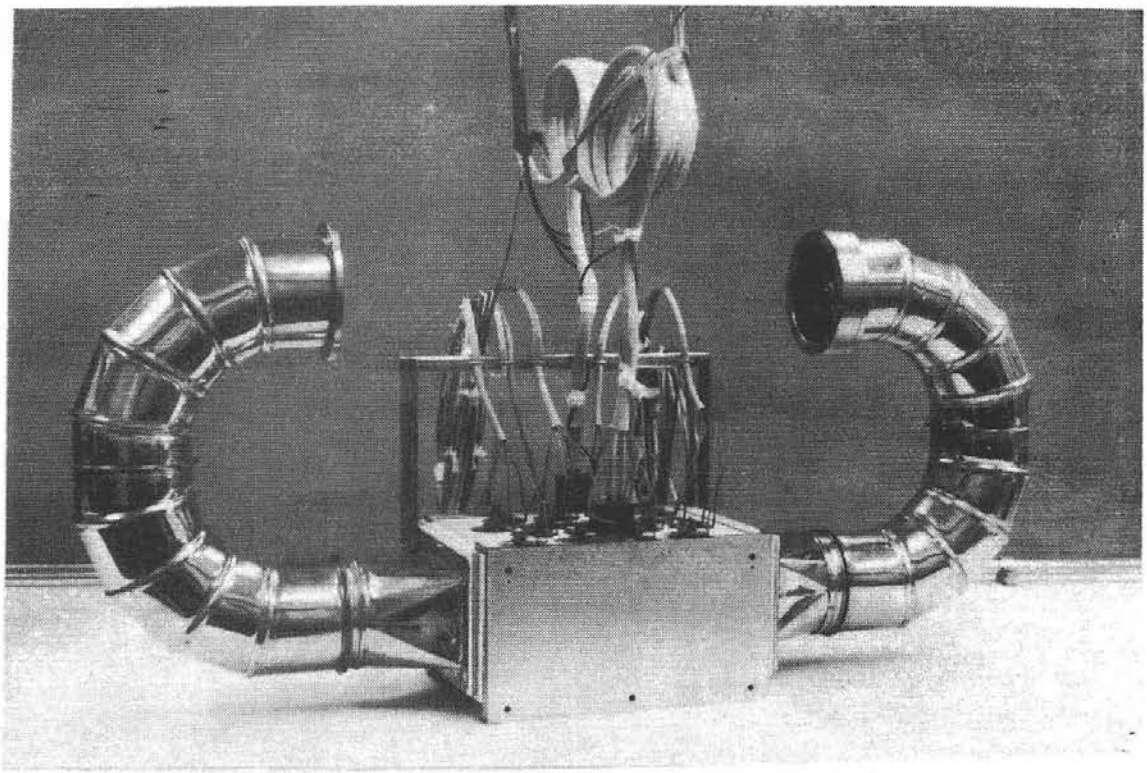

Figure 3-10. 16-Cell XPB Module with Air-Over Facilities

- Cell/Battery Statistical Analysis
- Cell Freeze/Thaw Modeling and Testing
- Cell Performance Modeling
- Cell Component Materials Support
- Battery Module Simulator
- Battery Engineering Design
- Testing Support.

Significant progress has been made in each task. The progress on these tasks is discussed below and is summarized in Table 3-10.

Cell/Battery Statistical Analysis

Cell-Failure Analysis

A methodology for cell-failure analysis was developed to determine the effects of cell load and environment on the failure of sodium/sulfur cells. This statistical model correlates the failure probability of sodium/sulfur cells with their discharge rate, depth of discharge, temperature, and the number of freeze/thaw cycles.

Although this methodology has been defined, it has not been included in the reliability analysis because sufficient data are not available to test the hypothesis and to perform the correlations. If the CSPL test data indicate that the effect is significant, this methodology can be incorporated into the computer models.

Table 3-10. Summary of Sodium/Sulfur Battery Development - SAIC

Cell/Battery Statistical Analysis	Methodology defined to allow investigation of load and environment on cell failure. Calculated performance of the CSPL 120-PB-cell battery achieved acceptable agreement with test results.
Cell Freeze/Thaw Modeling and Testing	Void formation in the sulfur electrode identified as a possible source of electrolyte stress. Freeze/thaw cycling, cell break-in, and electrical cycling observed by real-time X-ray radiography revealed: • gas generation • irreversible net movement of material • changes in density of sulfur electrode • selective nonwetting of the electrolyte.
Cell Performance Modeling	Cell performance model used to simulate electrical cycling of PB cells at various charge/discharge rates and various temperatures; results used to improve test procedures.

120-PB-Cell Battery

The reliability simulation program was run on a configuration matching the 120-PB-cell battery that was tested at CSPL. The purpose of the simulation was to determine the reliability parameters required to duplicate the test results.

The battery experienced a cell failure at 329 cycles, which reduced capacity to 95% of the maximum, and another cell failure at 390 cycles, which reduced capacity to 89% of the maximum. After 630 cycles, eight cells had failed, and the battery was removed from test.

The results predicted by the computer analysis for a Weibull lifetime of 1304 cycles and a Weibull shape factor of 5.37 were presented in the CSPL discussion on the 120-PB-cell battery and in Figure 3-8. The Weibull lifetime (α) and shape (β) values of 1304 and 5.37 are the current best values for single-cell reliability parameters.

To generate the average degradation curve, the results of 100 separate simulations were performed. As is seen in Figure 3-8, the battery performed within the bounds of the simulation results, but deviated significantly from the average of the simulation results. This may indicate that the α and the β for the battery are not represented well by 1304 and 5.37, or that random effects are modifying battery performance. Drawing conclusions from the data is difficult because, at this small size (the battery consists of strings of only 15 cells in parallel), random effects can cause large variations in the

Table 3-10. Summary of Sodium/Sulfur Battery Development - SAIC (Continued)

Cell Component Materials Support	
	A bad-cell-detection device was demonstrated.
	Investigations into a thermal fuse to be used with the bad-cell sensor initiated.
	Significant levels of iron detected in the chromium coating of the cell container, which may be a source of corrosion.
Battery Module Simulator	
	Cell performance model incorporated.
	Simulated performance of 10 x 10 cell battery highlights the need for bad-cell detection and removal.
Battery Engineering Design	
	Baseline conceptual design for SNL-deliverable battery defined to consist of six single-level 40-cell segments that are reconfigurable.
Testing Support	
	Utilities contacted to determine load profiles for testing the SNL-deliverable battery.

capacity of a particular battery, which can mask the effects of α and β.

The modeling results predicted a rapid decrease in battery capacity between 400 and 600 cycles. This prediction was confirmed when the battery suffered a drastic capacity loss as it continued cycling.

Cell Freeze/Thaw Modeling and Testing

Freeze/Thaw Modeling

Comparison of SNL modeling results (J. W. Braithwaite, S. R. Subia, and W. F. Hammetter, "Determination of Electrolyte Stress During Freeze/Thaw Cycling," *Sodium-Sulfur Batteries*, Electrochemical Society, Pennington, NJ, pp. 200-213, 1987) and X-ray radiographs of cells electrically cycled and cooled at SAIC suggested a possible link between voids in the sulfur electrode and freeze/thaw stress on the electrolyte. Although the SNL analysis was performed on an FACC cell, which has a different cell geometry than the CSPL cells, it showed that voids in the positive electrode next to the electrolyte can lead to high electrolyte tensile stresses caused by bending when the cell freezes.

X-ray radiography at SAIC of electrically cycled PB cells cooled to room temperature showed voids in the sulfur electrode in the vicinity of where the bottom and side pre-forms meet (Figure 3-11). It is hypothesized that the

pre-formed positive-electrode pieces behave as fiber-reinforced blocks that move independently of one another and that block movement upon cooling leads to formation of voids where the blocks meet. These voids may lead to tensile stresses in a manner similar to the SNL predictions for the FACC cell. This hypothesis has not yet been substantiated or disproved by X-ray radiography.

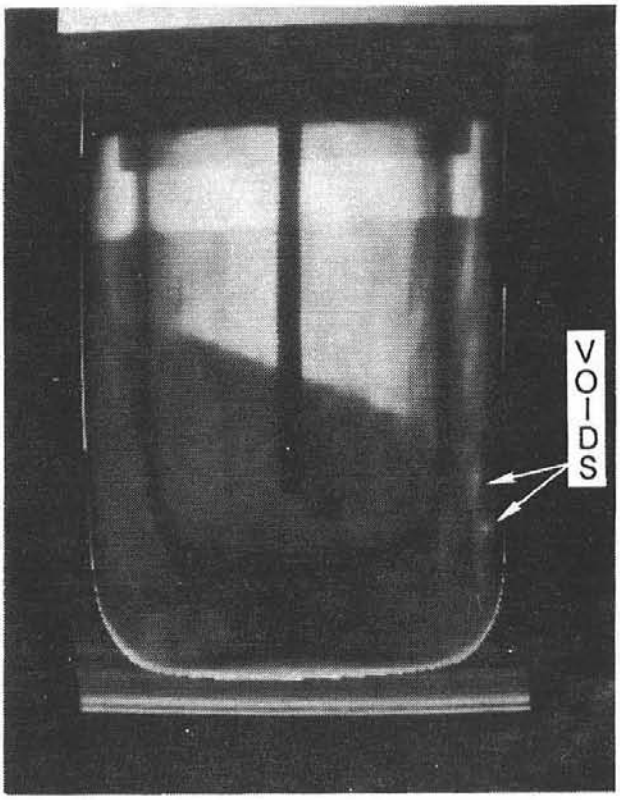

Figure 3-11. X-Ray Radiograph Showing Void Areas Near Positive Electrode Block Joints

Freeze/Thaw Testing

The data acquisition and control apparatus for the electrical cycling of cells during real-time X-ray radiography was assembled into a complete system (Figure 3-12). Software to automatically control electrical cycling and to acquire data was also developed. Experiments were run on a previously cycled sodium/sulfur cell and a virgin sodium/sulfur cell. Both cells were from CSPL.

Previously Cycled Cell. This cell was thawed, electrically cycled, and refrozen. The following phenomena were observed:

- Changes in density of the polysulfide areas during electrical cycling. Some areas showed large changes in density as the cell was electrically cycled.

- An irreversible net movement of material from one charge/discharge cycle to the next. This redistribution, expected in virgin cells, apparently continues even after many cycles. Continued segregation may be a mechanism of cell degradation or failure.

- A general increase in density in the sulfur electrode during the discharge cycles accompanied by a decrease in density in some areas within the same electrode. It is not known whether previously formed polysulfide is dissociating and moving elsewhere to be reformed or if voids are being created within the graphite felt.

Virgin Cell. This cell was broken-in, frozen in the fully charged state, rethawed, electrically discharged, and finally frozen in a nearly fully discharged state. Observations made at these different states confirmed the need for further X-ray radiography experiments.

The following phenomena were observed during cell break-in:

- Gas generation during discharge in the sodium electrode and during charge in the sulfur electrode. It is not clear if this gas is reabsorbed or if there is a continual build-up. After testing, the cell was shipped to ANL for gas analysis.

- Selective nonwetting of the electrolyte, which affects internal resistance. This behavior, which may persist throughout the lifetime of the cell, may be controlled by a sodium-filling process during assembly or by improved cell break-in procedures.

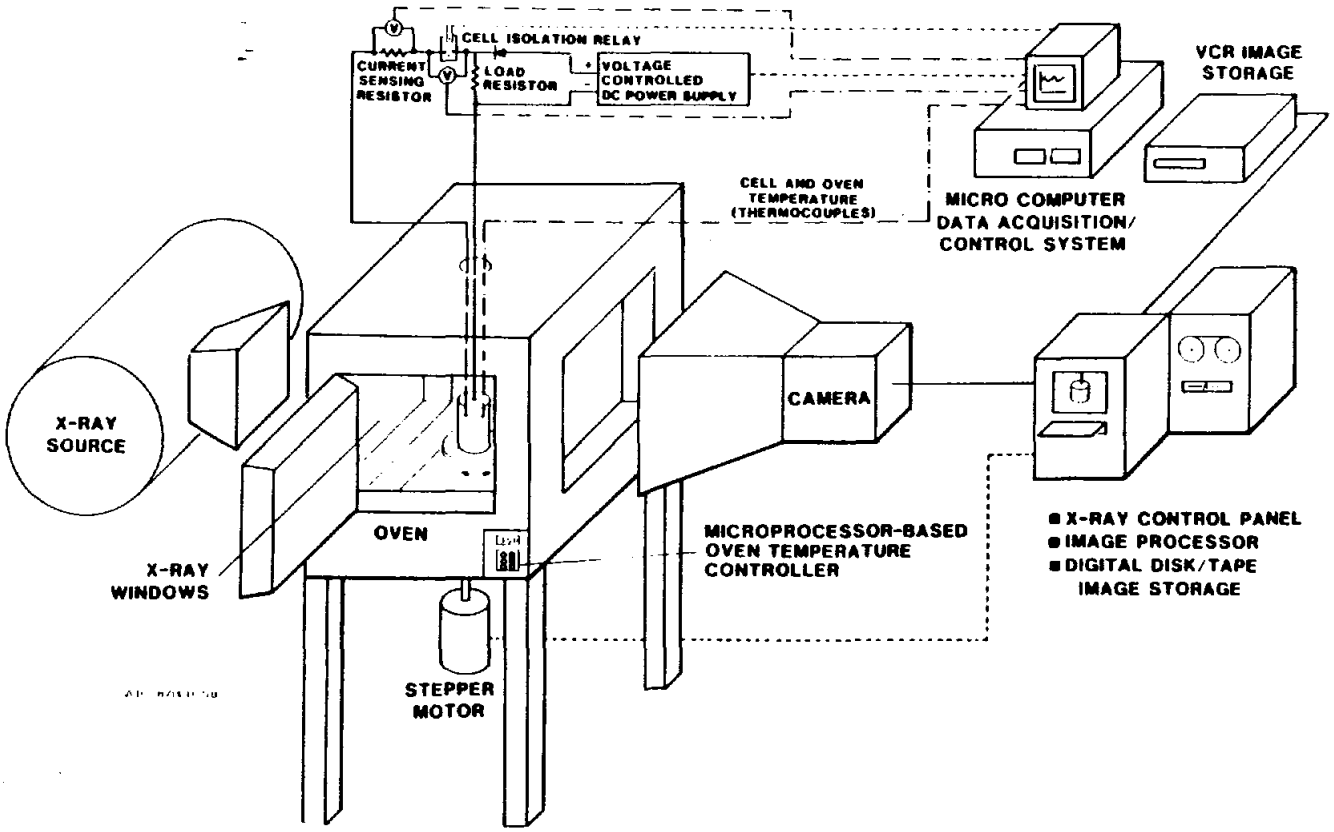

Figure 3-12. Freeze/Thaw Data Acquisition and Control Device

- Sudden sulfur melting, which filled the gaps between the pre-forms.
- Spotty formation and dissociation of polysulfides during charge/discharge accompanied by a net movement of material. This is expected during break-in, though it was also observed in the previously cycled cell (see above).

Observations on subsequent freeze/thaw cycles did not provide any new insights. No indications of sulfur or polysulfide void formation on freezing was observed.

Cell Performance Modeling

The integration of the sodium/sulfur cell performance model into the module simulator was completed, and the cell model is now considered to be finished. Figure 3-13, a comparison of the cell performance model results with test data for a PB cell, shows excellent agreement for cell voltage and temperature.

To assist in sodium/sulfur testing at SNL and ANL, this model was run with varying charge and discharge currents at four different temperatures to demonstrate how temperature affects cell behavior. The results were used to predict appropriate cut-off voltages for charging and discharging cells at different temperatures.

Cell Component Materials Support

Bad Cell Sense-and-Remove Device

A device for detecting bad cells in a sodium/sulfur battery was demonstrated on a laboratory scale. This device measures current passing through each cell at top of charge.

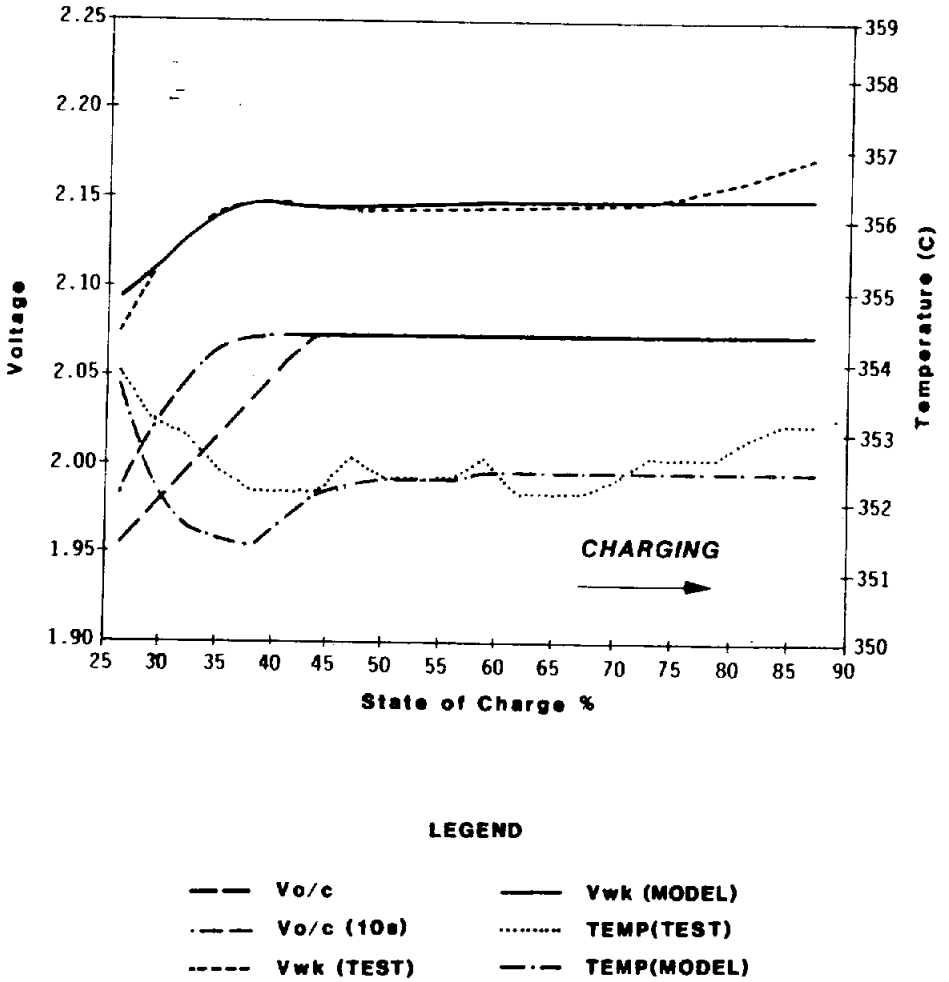

Figure 3-13. Cell Performance Model Versus Test Data for XPB Cell 8032

Suspect cells show a negative current that is larger than the residual charging current. The bad-cell detector requires no direct contact with the current-carrying wire and can therefore be used in a matrix fashion, which reduces wiring requirements and minimizes the risk of creating a short circuit.

Investigations into a thermal fuse that would be used with the bad-cell sensor were initiated. This device would also be wired to each cell in a matrix fashion. Once a bad cell had been detected, it would be pulsed with a large current, which would cause the fuse device to short-circuit the bad cell, removing it from the battery circuit.

Cell Container Examination

A metallurgical examination of an empty cell container was performed. Microscopic analysis showed the chromium coating on the base steel to be continuous, despite significant surface roughness and porosity, with a thickness of about 30 μm. The coating on the inner portion of the container was found to be in tension, and the coating on the outer container was in compression. X-ray energy spectrometry showed a significant amount of iron diffusion into the surface of the coating. This iron could cause corrosion problems if it is available to react with the sulfur.

Battery Module Simulator

The module simulator, which has now incorporated the cell performance model, was used to model the performance of a battery consisting of a 10 x 10 array of cells. With no failed cells, the capacity remained constant as the module cycled. However, the presence of even one failed cell caused one parallel bank of the module to become depleted within a few cycles. These results emphasize the need for a bad-cell sensing and removal device in a parallel array.

Battery Engineering Design

Preliminary requirements and options for the SNL-deliverable, XPB-cell battery were forwarded to CSPL in September 1987. The basis for the initial unit design was as follows:

- 6 V (optionally 8 V)
- approximately 105 XPB cells
- three- or four-cell strings
- 26 to 35 parallel strings.

Other design requirements are as follows. Output could not be tied to an inverter because inverters require 12 V or more to operate, which would reduce the number of parallel strings. Minimum discharge time was two hours; minimum charge time was five hours. Instrumentation requirements included sensors for bank/cell voltages and currents and temperature sensors.

Two initial battery concepts were developed:

- a single-level reconfigurable battery
- a multilevel battery.

After discussion with CSPL, it was decided to pursue the reconfigurable battery design as a baseline. Further design iterations led to a baseline conceptual design consisting of six 40-cell, single-level battery segments. The baseline design is shown in Figure 3-14 and is described in Table 3-11.

Testing Support

Several activities were undertaken this year in support of testing the SNL deliverable battery, the most significant of which was determination of an appropriate load profile. For customer-side-of-the-meter applications, peaks were found to range from in the order of minutes to five or six hours, and utility load profiles seem to be rather uniform at a substation level. Opportunities therefore appear to exist even for batteries with relatively long discharge periods.

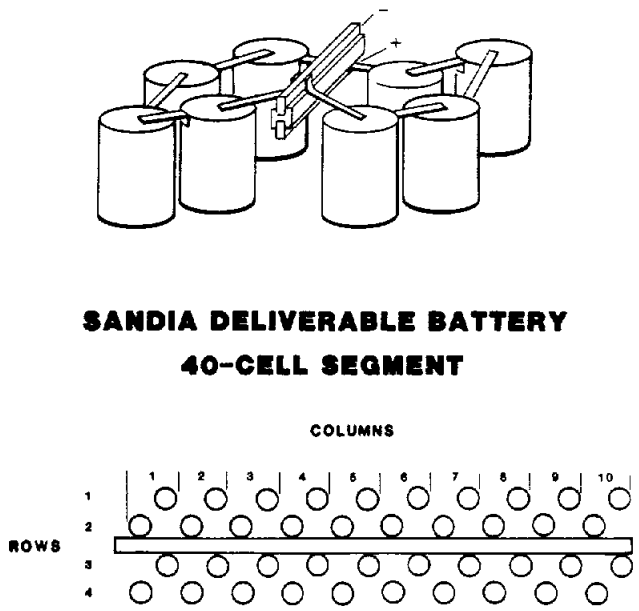

Figure 3-14. Baseline Design of SNL-Deliverable Battery

Table 3-11. Baseline Concept for SNL-Deliverable Battery

Battery

Levels	1
Cells/String	4
Total Cells	240
Battery Segments	6

Electrical Configurations

	Baseline	Options A	Options B	Options C
Volts	8	16	24	48
Amps	600	300	200	100
Parallel Strings	60	30	20	10

Cell-Array Dimensions

	Width (m)	Length (m)	Height (m)
Full Width	1.36	0.60	0.13
Half Width	0.68	1.20	0.13

Enclosure Dimensions

Full Width	1.66	1.10	0.43
Half Width	0.98	1.70	0.43

Thermal Management System

- Cell Temperature Range: 345°C to 365°C
- Flowing Heated Air at 0.126 g/s/cell
- Fresh-Air Venting and Mixing (Air Temperature: 340°C to 360°C)
- Minimum Thermal Mass Outside of Cell Tray
- Guard Heaters on Top, Bottom, and Sides

Segments

Cell Type	XPB
Cells/Segment	40
Parallel Strings	10
Voltage	8 Vdc nominal per segment
Current	100 A nominal per segment
Height	130 mm (between top and bottom plates)
Intercell Spacing	10 mm
Width	226.5 mm
Length	600.00 mm

Development of Beta"-Alumina Ceramic Electrolyte - Ceramatec

The focus of this project has been on the comparative testing in sodium/sulfur cells of four types of beta"-alumina electrolytes: standard Zeta process; seeded, slurry-solution spray dried (S^4D); unstabilized zirconia-toughened; and partially stabilized zirconia-toughened. The objectives of the project were to compare the characteristics of the four electrolyte types before and after cycling in cells (but prior to cell or electrolyte failure) to determine whether any subcritical electrolyte degradation occurred during cell cycling and to compare the performance of cells in which the only variable was the electrolyte type. Progress made on this project, summarized in Table 3-12, is discussed below.

Experimental Methods

Electrolyte Fabrication

During the first year of the project, electrolytes of the four types were fabricated and characterized. Wet-bag isostatic pressing was used in all cases as the method of forming the green electrolytes. The electrolytes were fired in platinum-lined alumina carriers under conditions optimized for the particular electrolyte type. For the toughened electrolytes, zirconia was incorporated by adding it to the slurry before spray drying. Prior studies showed that a much more uniform distribution of zirconia in the green body could be obtained by incorporating it into the S^4D process than by incorporating it into the Zeta process.

Following fabrication, the electrolytes were characterized for mass density, ionic resistivity, burst-strength characteristics (on tube sections), visual characteristics, and dimensional characteristics. These data formed the basis for comparison with properties of the electrolytes that had been cycled.

Sodium/Sulfur Cell Assembly

After being characterized, the electrolytes were assembled into sodium/sulfur cells. The cell design used was essentially that of the FACC EH-2A electric vehicle cell, which was one of six designs transferred to Ceramatec during 1986. However, two aspects of the FACC cell design were modified: E-Brite was used as the sulfur container material rather than the 410 stainless steel, and cells were operated vertically rather than horizontally for improved freeze/thaw durability. Handling of electrolytes and assembly of cells was in accordance with the standard procedures developed and specified by FACC.

During cell assembly, a number of electrolytes fractured. These failures were attributed to several factors, which in all cases included an insufficiently tight tolerance on the alignment between the insulating alumina header and the electrolyte. In the case of the unstabilized zirconia-toughened materials, moisture degradation was believed to be a major factor as well, as only two of eight electrolytes survived assembly. The outside diameter of the S^4D electrolytes was larger than the design specification by an average of 0.5 mm (because of lower shrinkage of the material during firing), which further aggravated the header-to-electrolyte misalignment.

Sodium/Sulfur Cell Testing

The cells were installed into individual furnaces, heated to 350°C, and given several conditioning cycles at low currents. After conditioning, the cells were cycled according to the following regime: discharge at 28 A constant current to a depth of discharge of 35 Ah or a voltage under load of 1.49 V and charge at 7 A constant current to a voltage of 2.3 V. After charge and discharge, the cell was allowed to stand at open circuit for 15 minutes. The discharge current was twice the design current specified by FACC. This current level was chosen on the basis of qualification testing on similar cells as being a current level sufficient to provide for some acceleration of the test but which would not cause severe degradation of cell life and performance. Attempts to charge the cells at higher rates than the specification and thus further accelerate the testing resulted in loss of cell capacity. During testing, the cell voltages, currents, temperatures, and times for charge and discharge were monitored. From these raw

Table 3-12. Summary of the Development of Beta"-Alumina Ceramic Electrolyte - Ceramatec

Experimental Methods	
Electrolyte Fabrication	Fabrication process: • green shapes formed by wet-bag isostatic pressing; • electrolytes fired in platinum-lined alumina carriers; • zirconia added to slurry before spray drying.
Sodium/Sulfur Cell Assembly	Cell design essentially the same as that of the FACC EH-2A EV cell. Electrolyte fracture problems caused by misalignment between the insulating alumina header and the electrolyte and moisture degradation of unstabilized zirconia-toughened electrolytes.
Sodium/Sulfur Cell Testing	Cells discharged at twice the FACC-specified rate to accelerate testing. Two cells removed from each of the four groups after 277, 345, and 763 cycles. Electrolytes visually inspected and burst-tested.
Results and Discussion	
Cell Test Results	Both of the remaining unstabilized zirconia-toughened electrolytes failed during initial cell heat-up. Two S^4D electrolytes failed during cell heat-up; three failed during cell testing. No cell failures with partially stabilized zirconia-toughened electrolytes or the Zeta electrolytes. Electrical performance in agreement with FACC data. Resistance rise lowest in Zeta and partially stabilized zirconia-toughened electrolytes; highest in S^4D electrolytes. Low resistance rise in partially stabilized zirconia-toughened electrolytes attributed to gettering capability of zirconia.
Burst-Test Results	Burst-test results inconclusive; testing of larger populations of electrolytes and of complete (uncut) electrolytes required.

data, the cycle-average cell resistances, energy efficiencies, capacities, and energies were computed and stored for later retrieval.

Two cells from each electrolyte group were removed from test after 277, 345, and 763 cycles. The cells were cut apart, the reactants were removed by reacting with alcohol, and the electrolytes were removed, intact, from the cells for further testing and analysis. During the cell teardown, care was taken to minimize the amount of time the electrolytes were exposed to alcohol, though at least 48 hours were generally required to remove all of the reactants from the cells.

The electrolytes were first examined visually for any evidence of degradation and then cut into sections for burst testing. The ends of the samples were ground and polished to minimize the effects of damage (microcracking) caused by cutting, which would reduce the strength of the samples. The burst tests were conducted by loading the sample with uniform internal pressurization until the hoop stress in the section was sufficiently great to cause the electrolyte to fail. The Weibull statistics for the sample populations were then computed.

Results and Discussion

Cell Test Results

The two cells containing unstabilized zirconia-toughened electrolytes that survived assembly failed during the initial heat-up. These failures were attributed to the moisture degradation that unstabilized zirconia-toughened electrolytes appear to undergo during handling prior to cell assembly. The exact mechanism by which unstabilized zirconia-toughened electrolytes degrade has not been determined. However, on the basis of prior data and the experiences of others working in the field, the rate of degradation is dependent on the zirconia content. The material used on this project contained 15 wt.% zirconia, and therefore the degradation was relatively rapid.

Two S^{4}D electrolytes failed during initial heating of the cells, and three of these electrolytes failed during testing. A contributing factor in these failures was the out-of-specification outer diameter of these electrolytes combined with the loose tolerance on the alignment between the header and the electrolyte. It is believed that these dimensional problems caused excessive stresses on the electrolytes, eventually resulting in failure.

No failures occurred in either the partially stabilized zirconia-toughened electrolytes or the Zeta electrolytes during initial heating or during test.

The electrical performance of the cells was in relatively good agreement with data obtained at FACC during their work on this cell. A typical plot of voltage as a function of depth of discharge during both charge and discharge is shown in Figure 3-15. Some slump in voltage at the beginning of discharge was observed in most cells as a result of the high current level and the very high rechargeability. Typical plots of cycle average cell resistance and capacity for one of the cells are shown as functions of cycle number in Figures 3-16 and 3-17, respectively. This cell contained a Zeta-process electrolyte and at the end of the year had accumulated over 1000 cycles. The step change in cell resistance at cycle 760 shown in Figure 3-16 is an artifact of reducing the charging current from 7 to 5 A without reducing the charge voltage cutoff limit.

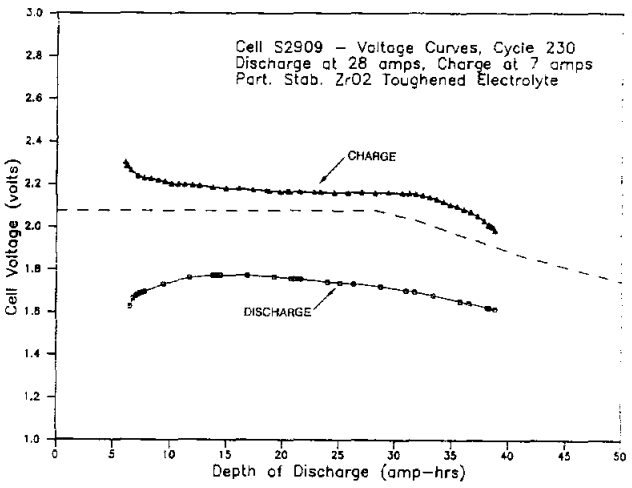

Figure 3-15. Typical Cell Voltage

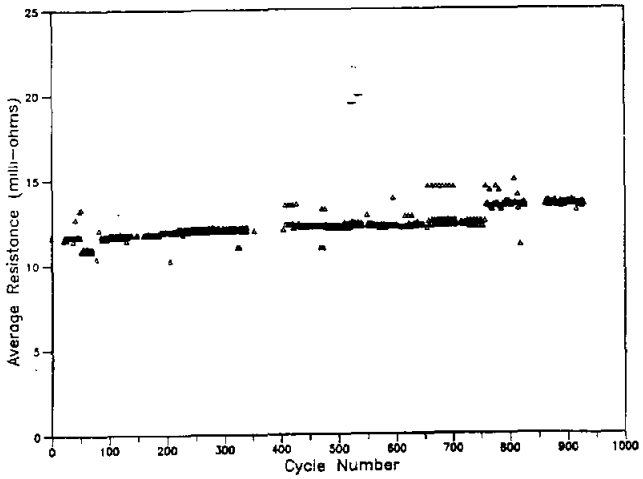

Figure 3-16. Average Resistance Versus Cycle Number of a Cell Containing a Zeta-Process Electrolyte

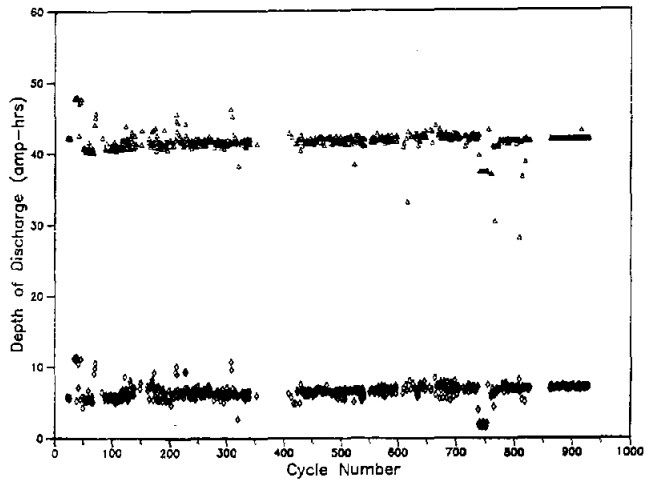

Figure 3-17. Cell Capacity Versus Cycle Number of a Cell Containing a Zeta-Process Electrolyte

The resistance of all cells increased with cycling, which is considered to be typical for sodium/sulfur cells. However, the initial resistance and the rate of resistance rise were different for cells with different types of electrolytes. The average initial resistance and average resistance rise for the three groups of cells tested is shown in Table 3-13. The Zeta materials showed the lowest initial resistance as well as the lowest rate of increase, with the partially stabilized zirconia-toughened material being a very close second. The S⁴D electrolytes exhibited the highest resistance initially and the highest rate of increase.

Both the S⁴D and the toughened electrolytes utilized Reynolds RCHPS alumina as the starting material, which has a lower purity than the Baikowski used as the starting material in the Zeta process. It has been shown by other workers that calcium impurities in the beta"-alumina may "leach" out of the ceramic during cycling, causing part the observed rise in resistance. This could explain the difference in the resistance rise between cells with Zeta process electrolytes and those with S⁴D electrolytes. The addition of zirconia to beta"-alumina may reduce the level of "leachable" calcium by chemically "gettering" calcium, thus reducing the rate of resistance change.

Table 3-13. Cycle Average Cell Resistance

Electrolyte Type	Initial Resistance (mΩ)	Rate of In Increase (μΩ/cycle)
Zeta Process	11.7	1.8
S⁴D	13.3	4.0
Part. Stab. Zirc. Toughened S⁴D	12.0	2.1

Burst-Test Results

The results of the burst-testing of electrolytes after being cycled in cells were disappointing. There was considerable scatter in the data, though most of the characteristic strengths and shape factors after cycling were lower than before cycling for the various electrolyte types. However, there was no clear trend evident. As all of the burst tests were conducted on tube sections rather than complete tubes, much of the reduction in strength may have been because of flaws introduced in the sections during sample

preparation, in spite of the extreme care taken to avoid such damage.

In order to make a fully valid evaluation of any subcritical electrolyte degradation during cell cycling, it would be necessary to test a much larger population of cells and to burst-test complete electrolytes without cutting. This applies not only to electrolytes after cycling, but also to electrolytes before cycling.

Conclusions

On the basis of the data obtained from this project to date, several conclusions can be drawn:

- Unstabilized zirconia-toughened electrolytes with high zirconia levels possess insufficient resistance to moisture degradation to enable practical cell manufacture.
- Additions of partially stabilized zirconia contributes to reduced resistance aging of cells apparently by gettering leachable impurities in addition to any mechanical benefit that may be obtained as a result of toughened effects.
- Continued development and evaluation of S^4D electrolytes is warranted.
- More extensive, more carefully controlled experiments are required in which greater attention is given to proper electrolyte size and in which burst testing is conducted on complete electrolytes in order to fully assess the extent of subcritical electrolyte degradation.

Posttest Analysis of CSPL Sodium/Sulfur Cells - ANL

Selected sodium/sulfur cells fabricated by Chloride Silent Power, Ltd., (CSPL) were given detailed examinations using specialized facilities maintained at Argonne National Laboratory. The posttest examinations served to characterize morphological changes in the sulfur electrode, to assess the performance of hardware components, and to identify potential failure mechanisms. In 1987, capabilities were expanded to include quantitative measurements of the gases present in sulfur electrodes. The information gathered from these analyses was reported to CSPL in support of its efforts to improve performance, cycle life, and reliability.

Nine CSPL MkIII cells were processed this year. Seven of these cells were voluntarily terminated after less than 65 cycles. Each of these seven baseline cells were cooled either slowly or rapidly from one of three different states-of-charge (2.076 V, 1.90 V, or 1.76 V). The other two cells were also voluntarily terminated but after extended cycling (242 and 520 cycles). Table 3-14 presents the key posttest findings for each of the nine cells. The electrode and hardware studies are discussed below.

Electrode Morphology Studies

Charged Cells

Four of the cycled cells (7521, 7820, 7822, and 7833) were terminated in the charged state with an open-circuit voltage of 2.076 V. Their positive electrodes shared a number of compositional and morphological features:

- The volumetric quantities of sulfur and sodium pentasulfide (Na_2S_5) averaged about 55% and 10%, respectively.
- Most of the Na_2S_5 was dispersed throughout the electrode interior in discrete globules of about 1 mm in length along their major axis.
- Na_2S_5 also preferentially wetted the ceramic surfaces, forming a 5- to 15-μm film on the electrolyte.
- Voids were concentrated in the internal regions of the felt structure and along the base radius of the electrolyte where the felt failed to conform to the curvature of the electrolyte.

Distribution of Active Materials. The charged sulfur electrodes did vary in the way that the

Table 3-14. Key Posttest Findings for CSPL Cells

Cell	Condition at Termination		Major Findings
	Cycles	Voltage (V)	
7521	520	2.076	Thickness of the chromized coating reduced in half by accelerated corrosion at the base. No migration of corrosion products to the electrolyte.
7820	242	2.076	H_2S and CO_2 gases in sulfur electrode.
7822	63	2.076	Off-centered electrolyte promoted greater retention of active material in cylindrical section of electrode.
7833	60	2.076	Slumping of active material into base section of sulfur electrode.
7823	63	1.90	≈2.1 at.% Ca level found for the interior electrolyte surface. Partial separation in the seal of the aluminum ring to the top cap.
7827	60	1.90	Composition of polysulfide melt dependent on location. Poor fusion of the sodium terminal weld.
7824	63	1.76	2 at.% sodium gradient in slowly cooled sulfur electrode. Porosity in case-to-cap weld.
7826	60	1.76	7 at.% sodium gradient in rapidly cooled sulfur electrode. Interior surface of electrolyte has a fibrous structure.
7834	0	2.076	Nitrogen and argon are major gases in this uncycled sulfur electrode.

active materials were distributed between the cylindrical and base sections. The variation appeared to be attributable to the alignment of the electrolyte within the cell case. This point was best illustrated by cells 7822 and 7833. Both of these cells were rapidly cooled by transferring them to an unheated furnace to minimize movement of active materials during cooling. In cell 7833, the electrolyte was centered, and the sulfur content averaged 40 vol.% in the cylindrical sections and 75 vol.% in the base sections. In cell 7822, the electrolyte was off-center by 0.5 mm, and higher volume percentages of sulfur content were noted for cylindrical sections, particularly in the thinner cross sections where greater felt compression had occurred. These findings suggested that the slumping of active materials can occur in charged cells, but this condition can be counteracted, if desired, by using higher-density felts in cylindrical sections. The distribution of active materials in cells 7820 and 7521 was comparable to the distribution for cell 7833. Both of these cells received standard cool downs but also had centered electrolytes.

Corrosion. The sulfur electrodes from cells 7521 and 7820 were also carefully studied for evidence of corrosion products since these cells had been in operation for 520 and 242 cycles, respectively. For cell 7521, the cell case was definitely corroded, but no corrosion products were detected within the electrode or adjacent to the electrolyte. A barrier material used between the case and the electrode prevented the transport of corrosion products into the electrode. For cell 7820, both nickel disulfide (NiS_2) and iron disulfide (FeS_2) were found. Deposits of these compounds were present on the electrolyte surface, especially at the base. The source of nickel and iron for these compounds was not the cell case but two corrosion coupons of a nickel-iron alloy. Both coupons were located on the outer perimeter of the electrode but within the barrier material.

Discharged Cells

Energy dispersive spectroscopy was used to measure compositional changes in sulfur electrodes from cells discharged into the single-phase polysulfide melt region (cells 7827, 7824, and 7826). The electrodes were scanned radially across the bottom quarter of the cylindrical portion. For cell 7827, a second scan was made diagonally across the bottom portion of the electrode from the base radius of the electrolyte to the base radius of the cell case. Approximately 20 spectra were collected for each full scan. The findings for all three cells are presented graphically in Figure 3-18.

Cells 7824 and 7826. The scans for cells 7824 and 7826 illustrated the effect cooling rate has on the information retained in the solidified electrodes. Both cells were deeply discharged (1.76 OCV) prior to termination; however, cell 7824 received a standard cool-down while cell 7826 was rapidly cooled. The relatively flat slope of the regression line through the cell 7824 data (Figure 3-18a) indicated that the radial gradient in sodium distribution was virtually dissipated during standard cooling. The data for the rapidly cooled cell 7826 (Figure 3-18b) provided a more accurate representation of the sodium distribution at the end of discharge and indicated that the radial gradient across the electrode thickness was at least 7 at.% Na. The average sodium content in these uncharged electrodes was also estimated and found to be about 35.5 at.% Na. This value is well below 40 at.% Na, the melt composition expected under equilibrium conditions for a potential of 1.76 V.

Cell 7827. Polarization was found to be location-dependent for the electrode from cell 7827 (Figure 3-18c). This cell was rapidly cooled after termination at 1.90 OCV. For the radial scan, the measured value of 34.5 at.% sodium near the electrolyte agreed well with the 35 at.% sodium value expected from thermodynamic considerations. The 1 at.% sodium gradient corresponded to a potential difference of no more than 40 mV. The scan between the base radii, however, revealed greater polarization for this localized area. The composition near the electrolyte was nearly 2 at.% lower than that found for the radial scan. This suggested that sodium transport through the base radius of the electrolyte lagged behind transport elsewhere. For the corner scan, the gradient in sodium content was about four times greater, and the electrode composition at the case approached stoichiometric Na_2S_5. The compositional difference was equivalent to at least a 140 mV difference in potential between the corner of the

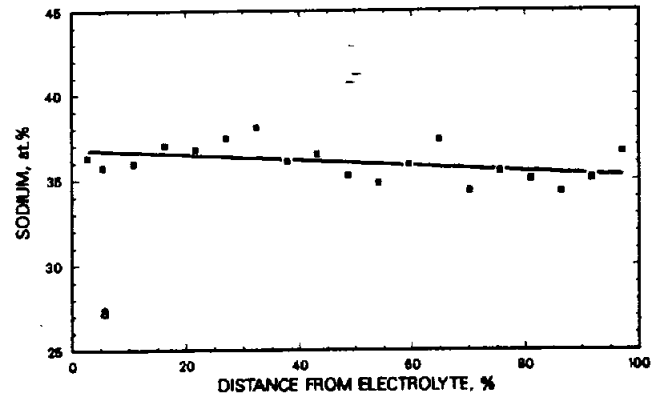

(a) Cell 7824: Discharged to 1.76 V and Slowly Cooled

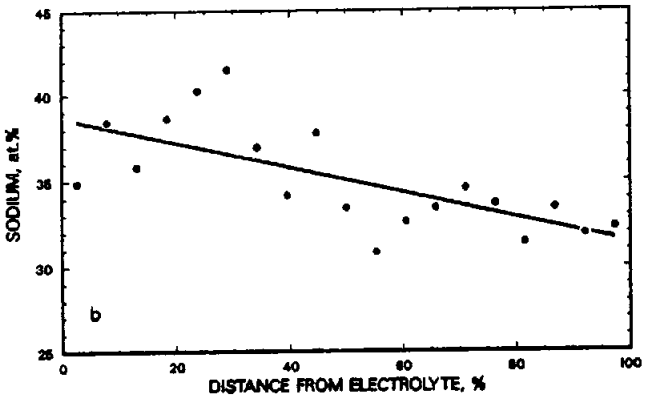

(b) Cell 7826: Discharged to 1.76 V and Rapidly Cooled

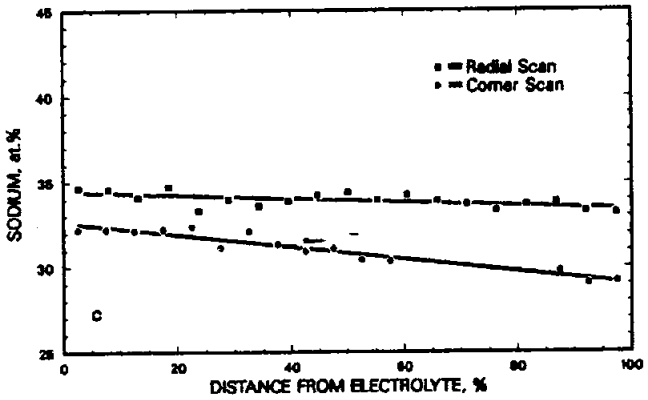

(c) Cell 7827: Discharged to 1.90 V and Rapidly Cooled

Figure 3-18. Sodium Profiles for Three Discharged Electrodes

cell case and a typical section near the electrolyte. The degree of polarization that could be attributed to differences in electrode thickness was small because the scan between base radii covered only 25% more distance.

Voids in the electrode may have been a major cause of polarization. This electrode, like the other ones, contained voids at the base radius of the electrolyte. In addition, other voids were also present near the base radius of the case.

Data Scatter. The divergence of data points from their respective regression lines varied from electrode to electrode. The source of this variability was the different phase compositions and phase separations that occurred during solidification of the electrode melt.

The data for the two 7827 scans deviated from the regression lines by 1 at.% sodium or less. The 7827 electrode was primarily composed of sodium tetrasulfide (Na_2S_4), with small quantities of Na_2S_5. These two compounds differ in sodium content by less than 5 at.%.

The scatter in the data was as much as 5 at.% sodium for scans across the electrodes from cells 7824 and 7826. These electrodes contained about two parts Na_2S_4 for each part sodium disulfide (Na_2S_2). (These electrodes also contained sizeable quantities of metastable polysulfides.) The difference in sodium content for Na_2S_2 and Na_2S_4 is more than 16 at.%. Furthermore, the coarse eutectic structures formed in these two electrodes during cooling produced local compositions that varied widely over a 0.1 mm^2 area, the scale at which these scans were done.

Sulfur Electrode Gas Analyses

Quantitative determinations were made of the ambient-temperature gases present in the sulfur electrodes of cells 7834 and 7820. Cell 7834, which was heated and held at 350°C for 94 days but was not cycled, was analyzed to characterize the initial mixture of electrode gases. Cell 7820, which was cycled 242 times, was analyzed to identify the changes in gas composition caused by extended cycling. The gases were collected by drilling through the cell case in the gas space above the sulfur electrode. The electrode gases were directed into an evacuated cylinder and analyzed with a mass spectrometer.

Table 3-15 summarizes the findings for both cells. For uncycled cell 7834, the primary constituents were argon (Ar) and nitrogen (N_2). Low or trace amounts of methane (CH_4), helium (He), hydrogen (H_2), oxygen (O_2), and carbon dioxide (CO_2) were also detectable.

Table 3-15. Sulfur Electrode Gas Analyses

Gas	Volume Percent	
	Cell 7834	Cell 7820
Ar	92.6 ± 0.5	0.03 ± 0.01
He	0.05 ± 0.01	≤ 0.02
N_2	6.9 ± 0.2	2.0 ± 0.1
H_2	≤ 0.5	0.5 ± 0.2
O_2	≤ 0.02	n.d.
CH_4	0.40 ± 0.02	n.d.
CO_2	0.014 ± 0.005	32.5 ± 0.8
COS	n.d.	2.2 ± 0.1
SO_2	n.d.	0.05 ± 0.02
H_2S	n.d.	62.7 ± 1.2

n.d. = not detected.

For cycled cell 7820, the total gas content increased by approximately a factor of five, and the electrode gas composition was radically different. The major constituents were hydrogen sulfide (H_2S) and CO_2. Low levels of other gases, such as carbon oxysulfide (COS) and sulfur dioxide (SO_2), were also generated. The H_2 content was slightly greater, but O_2 and CH_4 were undetectable. Ar, N_2, and He were present in reduced percentages.

A reasonable explanation for the dramatic change in electrode gas composition would be the presence of water. The atomic ratio of hydrogen to oxygen for the gases found in the cycled cell was 1.9, and a value of 2 fell within the limits of experimental error. For the uncycled cell, an absorbed film of H_2O on a high surface-area component, such as the graphite felt, would be difficult to detect with the sampling method employed. However, in a cycled cell, the adsorbed H_2O would readily react with sodium polysulfides to form H_2S. At the cell operating temperature, subsequent reaction with the graphite would consume the oxygen liberated by the polysulfide.

Gas analyses will be performed on the sodium electrode as well as the sulfur electrode in future studies.

Cell Hardware Observations

Cell Case

A duplex chromized layer is used to impart corrosion resistance to the cell case and the top cap, both of which are fabricated from low-carbon steel. The protective coating was free of cracks and pinholes in all of the examined cells.

Corrosion was minimal after 60 to 63 cycles. The outer layer of the chromized coating was essentially unchanged in thickness and only a 2- to 4-mm layer of sodium thiochromide ($NaCrS_2$) was present.

After 242 cycles (cell 7820), corrosion reduced the average thickness of the high chromium layer to less than one-half of the initial thickness. The attack was nonuniform, however, and was most severe for the base portion of the cell case. The chromium layer was under 2 μm in thickness for this section, and localized attack of the inner ferrochromium layer had begun.

Figure 3-19 illustrates the condition of the ferrochromium layer at the base of cell 7521 after 520 cycles. The thickness of this layer, which was about five times greater than the high-chromium layer, was reduced in half for the entire base section of the cell case. Corrosion was significantly less along the walls of the cell case. The high chromium layer was still present, although reduced in thickness. The coating on the top cap of this cell also fared well and showed only minor scale formation.

Figure 3-19. Corrosion of the Chromized Layer (Top) at the Base Section of Case for Cell 7521 (Etched)

Other factors need to be considered in assessing the severity of corrosion at the base of the cell case:

- The concentrated attack of the base section was probably the result of preferential formation and retention of sodium polysulfides in the base of the sulfur electrode during cycling. Refinements in electrode design could lessen corrosion by effecting more uniform reaction throughout the cell.

- The corrosion noted for cell 7521 generated a thick band (70 to 100 μm) of reaction products, primarily $NaCrS_2$, at the bottom of the cell. The barrier material, however, effectively contained these products between the case and the electrode and prevented transport to the electrolyte. The corrosion products represented a source of lost capacity but not an impedance to sodium transfer at the electrolyte interface.

- The chromizing process used for these cells also produced an equivalent duplex coating on the exterior of the cell case. The exterior coating can be expected to be equally resistant to corrosion.

- A minimum lifetime of 1500 cycles can be conservatively projected before the case would be breached on the basis of the penetration rates found for cells 7820 and 7521. The progressive loss in capacity from corrosion would, in all likelihood, necessitate termination of operation before a breached condition could develop.

Seals

The various intercomponent seals were also examined for evidence of potential or existing degradation mechanisms.

Sulfur Seal. For the sulfur seal, the aluminum ring maintained good adherence to both the top cap and the insulator cap for all of the cells except cell 7827. A partial separation existed between the ring and the top cap that extended from the outer diameter of the ring to a depth of 270 μm in one radial cross section through this seal. The only evidence of corrosion of the aluminum ring was found in cell 7824. Intergranular attack extended one to two grains deep for the outer perimeter of the ring, which is exposed to sulfur-electrode gases.

Sodium Seal. For the sodium seal, the thermocompression process formed secure bonds among the two metal components and the insulator cap. Only in cell 7824 was there a partial separation between the metal shim and the insulator.

Glass Seal. For the glass seal, the adherence of the glass to both the electrolyte and the insulator was excellent for all of the cells. The quantity of glass sealant within the joint did vary from cell to cell. Typically, the glass filled all of the horizontal joint section and most of the vertical joint section in one continuous bead, as shown in Figure 3-20. For several cells, however, there was a complete or partial absence of glass in the horizontal joint section in one or more of

the examined cross sections. Large voids were found in the joint corners of cell 7521. In cells 7820 and 7827, the lack of glass in the horizontal joint section appeared to be attributable to incomplete filling when the seal was formed. In none of these cases did the missing glass appear to be related to reaction of sodium with the sealing glass.

Electrolyte

Although no cell had its operation terminated because of electrolyte failure, this critical component was examined for evidence of degradation. Scanning electron microscopy of the cleaned electrolyte samples found one anomaly for the electrolytes from cells 7826 and 7827. As shown in Figure 3-21, a fibrous network was present over extended sections of the interior surface. All of the other interior and exterior surfaces had the expected granular appearance. The fibrous topography probably developed during the electrolyte fabrication process because energy-dispersive spectroscopy detected no significant variation in electrolyte composition between fibrous and granular regions.

Spectroscopy did reveal measurable levels of calcium on the interior surfaces of all of the electrolytes. The calcium peaks were small, but estimates were derived for the electrolytes from cells 7521, 7820, 7823, and 7827 by collecting multiple spectra. The average calcium levels were placed at 2.1, 3.6, 5, 9, and 6.2 at.% for the cells with 63, 60, 242, and 520 cycles, respectively. The variation from these averages was as high as ±1.2 at.%. The general trend appeared to be that the calcium levels rose rapidly during initial cycling but soon reached a plateau value. However, it should be noted that operation of these cells was terminated at different states of charge, and this variable could also influence the

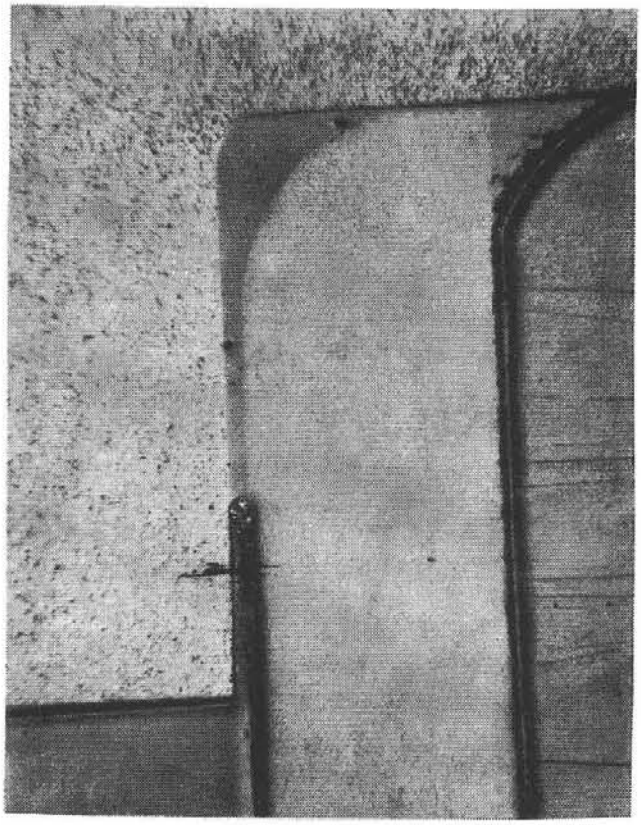

Figure 3-20. Typical Glass Seal Between the Insulator Cap (Top and Left) and the Electrolyte (Center)

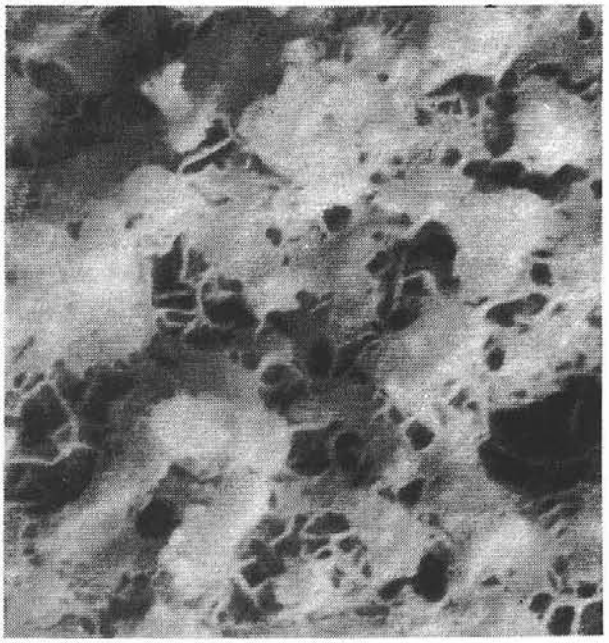

Figure 3-21. A Fibrous Network of Beta"-Alumina Found on the Interior Surface of the Electrolyte from Cell 7826

surface concentrations of calcium. The source of calcium was undoubtedly ceramic components associated with the sodium-electrode. References in the literature state that high levels of calcium impede sodium transport through the electrolyte.

Similar studies of the exterior surfaces of the electrolyte revealed no measurable levels of calcium. In fact, the exterior surfaces were remarkably free of contaminants with the sole exception of cell 7820, the cell with two corrosion coupons in the sulfur electrode.

Chapter 4. Battery Technology Evaluation

Introduction

Rechargeable cell and battery testing was performed within the Battery Technology Evaluation element. Work was carried out at Argonne National Laboratory (ANL), SNL, and at a field site in Hawaii. Evaluation tasks consisted of cell and battery laboratory testing at ANL, specialized cell and battery testing at SNL, and wind-turbine generator/battery system testing at the field site.

The objective of these activities was to provide independent prototype testing. The majority of units tested were deliverable units from the major DOE Office of Energy Storage and Distribution (OESD) battery development projects. Cells and batteries were evaluated from CSPL, ERC, Exxon, FACC, JCI, and Powerplex during the year. The results of these tests were used in part to verify developer claims and predictions. Additional tests were conducted in order to fully characterize each prototype. These tests assisted in identifying the strengths and weaknesses of each technology. In some cases, problem areas were identified for additional research and development tasks, either by the developer or at a national lab. These evaluations provided essential information for critically judging the technical progress of each development project. In virtually all cases, the evaluation activities provided new performance and design information that was previously unknown to the developers.

A wide variety of test methods were utilized in these experiments. At ANL, tests were performed to determine peak-power capability, specific energy (as a function of specific power), self-discharge rate, and life. At SNL, evaluation techniques included capacity measurements, parametric and factorial tests to determine performance prediction equations, and special electrical, chemical, and mechanical studies. In all cases, data were collected that described cell or battery voltage, current, temperature, and other parameters determined by the technology under test.

These data and results were distributed to DOE and national laboratory program managers for use in judging the progress of the development projects. The tests were conducted with the close cooperation of the respective developers, and the results were shared on a timely and open basis to provide the maximum benefit to each project.

In 1987, evaluation work at ANL was conducted within the Analysis and Diagnostic Laboratory (ADL). Two activities were part of this project:

- **Experimental Evaluations of Advanced Battery Technologies.** Testing was completed on an Exxon 30-kWh zinc/bromine battery. New tests were started on several CSPL sodium/sulfur PB cells. Data on life, peak power, and range (from driving-profile tests) were collected. Tests of several other technologies that were funded by other organizations at the ADL are reported for completeness.

- **Sodium/Sulfur Cell Posttest Examination.** This posttest analysis task is reported on elsewhere in this report (Posttest Analysis of CSPL Sodium/Sulfur Cells - ANL, Chapter 3).

SNL battery evaluation activities were divided into two categories:

- **Prototype Battery Evaluation.** Flowing electrolyte batteries, sodium/sulfur cells, and nickel/hydrogen cells and batteries were tested under specialized parametric evaluation regimes. Computer-controlled test facilities were used to perform these activities.

- **Systems Evaluation.** A wind/battery utility system experiment by the Hawaii Natural Energy Institute (HNEI) was in progress on

the island of Hawaii, and a battery/solar energy system experiment was completed at SNL's Photovoltaic Advanced Systems Test Facility (PASTF). SNL-designed, computer-controlled data acquisition systems were used in the PASTF experiments.

Several significant events occurred in SNL Prototype Battery Evaluation.

- An Exxon zinc/bromine battery, which completed 2030 electrical cycles, was disassembled and the cause of performance degradation was determined. Current-collector corrosion was the cause of a significant decline in efficiency at the end of the test, while electrode warpage caused gradual degradation during the life of the battery. This test has provided valuable new insight regarding the longevity of zinc/bromine batteries.

- In other zinc/bromine tests, several engineering-related problems were identified with ERC prototypes tested at SNL. ERC had proposed solutions for resolving these problems by year's end.

- Evaluation of FACC and CSPL sodium/sulfur cells continued. By year's end, one CSPL cell had completed 1125 cycles with stable performance. Other CSPL cells failed after fewer than 200 cycles, primarily because of seal problems. Parametric test results indicated a strong dependence of cell capacity on temperature.

- Several nickel/hydrogen cells and batteries were evaluated during the year. Experiments were performed that characterized battery performance with PV arrays.

SNL battery field tests with solar and wind electric generators provided valuable data for the advanced lead-acid and zinc/bromine technologies. A 20-kWh Exxon zinc/bromine battery was removed from test after almost 200 charge/discharge cycles. It will be disassembled early next year to determine the cause of failure. A gel-cell lead-acid battery was evaluated with a wind turbine array in Hawaii and performance data were collected.

Testing and Analysis at ANL

During 1987, technology evaluations were performed at the ANL Analysis Diagnostics Laboratory (ADL) for the DOE Office of Energy Storage and Distribution (OESD) and Office of Transportation Systems (OTS), and others. The results of the OESD technology evaluations are primarily discussed here, but selected results from the Electric Hybrid Propulsion Division of OTS (OTS/EHP) are also presented to provide a more complete picture. The ADL conducted performance and life characterization tests on 298 cells in 1987, which included nine single cells, ten modules, and two batteries from the sodium/sulfur, zinc/bromine, lead-acid, and nickel/iron technologies. The status and performance of these units are listed in Table 4-1. A discussion of the ADL evaluations on these battery technologies, summarized in Table 4-2, follows.

Sodium/Sulfur Technology (PB) - CSPL

As part of the sodium/sulfur battery development program sponsored by DOE/OESD, the ADL conducted experimental evaluations on eight individual CSPL sodium/sulfur PB cells rated by ANL at 10 Ah and 20 Wh. Four of the cells underwent performance characterization tests followed by life-cycle testing. The other four cells were only life tested.

Performance Testing

Performance testing included verification of capacity and determination of

- specific energy (as a function of specific power)

- peak power

Table 4-1. Status and Performance of Modules Under Test at the ADL During 1987

Test Program	ID No.	Maximum[1] Sp. Energy (Wh/kg)	Maximum PPSD[2] 50%/30 s (W/kg)	Accumulated Cycles[3]
(a) CSPL Sodium/Sulfur Cells				
Performance & Life	7495	132	200[4]	743
Performance & Life	7494	131	220[4]	630
Performance & Life	7467	137	231[4]	(388)[5]
Performance & Life	7464	125	207[4]	538
Life	7472	135	--	807
Life	7438	139	--	524
Life	7440	127	--	577
Life	7437	128	--	529
(b) Zinc/Bromine EV Battery (Exxon)				
Performance & Life	2	50.2	78	(75)
(c) Flow-Through Lead-Acid Cell (JCI)[6]				
Performance & Life	2	47.0	--	(82)[7]
(d) Nickel/Iron EV Modules (EPI)[6]				
Performance & Life	29	49.8	107[4]	(57)
Performance & Life	30	53.2	121[4]	(213)
Performance & Life	31	52.3	111[4]	(167)
Performance & Life	32	47.0	96[4]	227
Performance & Life	33	53.0	88[4]	(220)
Performance & Life	34	47.9	96[4]	153
Performance & Life	35	49.8	92[4]	155
Performance & Life	36	54.0	92.5[4]	50
(e) Nickel/Iron EV Battery and Modules (Eaton)[6]				
Performance & Life	1	35.9	--	502
Performance	2	44.2	118	(217)
Performance	3	45.5	115	(212)

1 Maximum specific energy for CSPL cells measured at 3.3-A rate using discharge cutoff algorithm.
2 PPSD=Peak power sustained for 30 s at 50% depth of discharge
3 All evaluations are on-going except those in parentheses, which indicate evaluation completion during the year.
4 Derived from SAE J227aD/IETV-1 driving schedule.
5 Cell seal failure on cycle 388 (11/13/87).
6 Testing supported by the EHP Division.
7 Includes 14 cycles at JCI before delivery.

Table 4-2. Summary of Experimental Evaluations at ANL

Sodium/Sulfur Technology (PB) - CSPL	
	Eight cells tested: four underwent performance characterization and life-cycle testing; four underwent solely life-cycle testing.
Performance Testing	
Capacity Verification	Three cells required extra conditioning cycles to achieve acceptable performance.
	All cells achieved 8.2 ± 0.5 Ah capacity with resistance of 33 to 40 mΩ.
Specific Energy Versus Specific Power	CSPL PB cells exceeded FACC EV cells by 18%.
Peak Power	CSPL PB cells exceeded FACC EV cells by 19%.
Self-Discharge Rate	No measurable loss in capacity after a one-week stand.
	No capacity loss when cells recharged after discharge to 50% DOD.
Driving Simulation Results	An average of 258 miles range was measured with the SFUDS test.
Life-Cycle Testing	Seven of the eight cells continue life-cycle testing; 524 to 807 cycles accrued.
	Average capacity degradation: 0.1 Ah/100 cycles; however, degradation usually occurs in increments of 0.2 to 0.3 Ah.

- self-discharge rate
- estimated range (using simulated driving profiles).

Capacity Verification. Initially, two of the CSPL cells required extra conditioning cycles to obtain a cell resistance of less than 80 mΩ. A third cell required conditioning for about 30 cycles to eliminate an erratic capacity behavior. After their conditioning periods, all of the cells operated in a reproducible manner and achieved capacities of 8.2 ± 0.5 Ah (15.7 ± 1.0 Wh), resistances of 33 to 40 mΩ, coulombic efficiencies of about 100%, and energy efficiencies ranging from 86% to 89%.

Specific Energy Versus Specific Power. The results of the performance characterization tests showed that the specific energy of the CSPL cells as a function of specific power was about 18%

Table 4-2. Summary of Experimental Evaluations at ANL (Continued)

Zinc/Bromine Technology (EV) - Exxon	Tests show that the Exxon 30-kWh battery undergoes increased self-discharge at elevated operating temperatures. Component failures and electrolyte leakage continue to be significant problems with this technology.
Flow-Through Lead-Acid Technology (EV) - JCI	75-Ah lead-acid cell shows improved performance: 70 cycles accrued before capacity dropped below 80% of the rated value; driving range estimated at 78.4 miles.
Advanced Nickel/Iron Technology	Seven modules featuring a matrix of improved nickel-electrode designs (plate type, plate thickness, and loading of active material) evaluated. Module 33 peak power and capacity declined by 12% and 10%, respectively, over 185 cycles.
Eaton/DSEP Nickel/Iron Battery Technology (EV) - EPI	Two five-cell modules and one 140-cell battery pack evaluated. Power capability of the pack decreased at a faster rate than capacity. Testing suspended after 502 cycles.

greater than that of previously tested FACC EV cells. A Ragone plot (which maps specific energy versus specific discharge power level) for each technology is given in Figure 4-1. The measurements were based on

- a naked weight of 120 g and discharge cutoff voltage (V_{co}) algorithm of:
  $V_{co} = 1.9 - 0.034 \times I$, where I is the discharge current in amperes (CSPL technology).
- a naked weight of 750 g and a discharge cutoff voltage algorithm of:
  $V_{co} = 1.76 - 0.008 \times I$ (FACC technology).

Peak Power. The peak-power capability of the CSPL cells was found to be about 19% greater than that of the FACC cells. A plot of peak power versus DOD for each technology is given in Figure 4-2. The specific peak power for both systems was derived from cell data acquired during an SAE J227aD/IETV-1 discharge. The

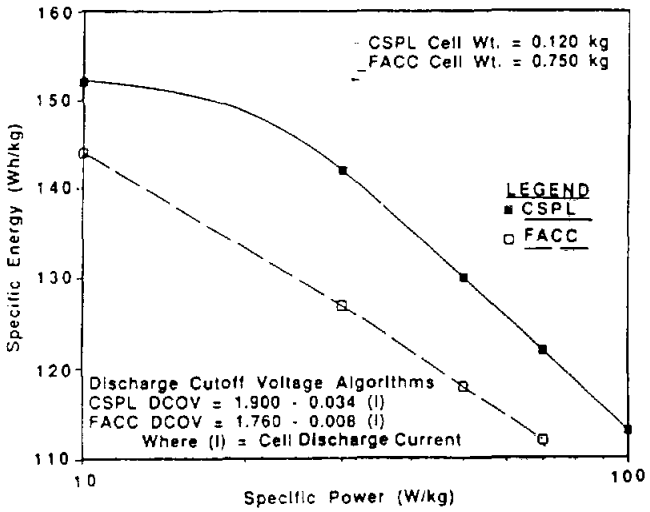

Figure 4-1. Ragone Plot for CSPL and FACC Sodium/Sulfur Cells Tested at the ADL

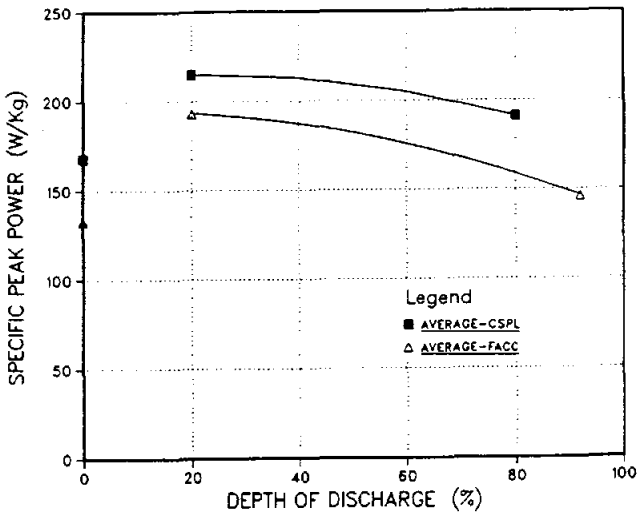

Figure 4-2. Specific Peak Power Versus Depth of Discharge for CSPL and FACC Sodium/Sulfur Cells Tested at the ADL

reduced peak power at 0% DOD for both technologies is caused by the voltage depression that results from the characteristically high initial resistance of sodium/sulfur cells in the fully charged condition.

Self-Discharge Rate. A self-discharge test was also conducted, and it confirmed that the CSPL cells had no measurable loss in capacity after a stand period of one week. There was also no change measured in cell-available 100% DOD capacity after a series of partial discharges to 50% DOD. It was noted that during the recharges after these partial discharges, the charge-voltage curve of the CSPL cells tracked the 100% DOD charge-voltage curve starting at the 50% recharge point. Coulombic efficiencies of 100% and energy efficiencies of about 87% were obtained throughout these tests.

Driving Simulation Results. The results of the driving-profile, peak-power, and sustained hill-climbing tests are summarized in Table 4-3. The sustained hill-climbing test shows that the cells were capable of delivering a power level of 45 W/kg for 6 minutes to a DOD level of ≈93% with no burden and ≈82% with a 100% burden. After performing a peak-power test, one of the cells (number 7467) started to loose capacity at a rate of 0.1 Ah/cycle. The charge-current taper limit was reduced from 1.0 A to 0.1 A during this period to furnish additional charge, but this had no significant effect on the rate of decline in cell capacity. After completing 388 cycles and 80 h in a fully charged open-circuit condition, the cell shorted, which was apparently caused by a breach of its top seal.

Life-Cycle Testing

The seven remaining cells are undergoing life-cycle testing (100% capacity discharges at a constant-current 3-h rate) and have accrued from 524 to 807 cycles. No sudden changes have been noted in their capacities as determined using the algorithm for discharge cutoff voltage. The present values of cell capacity and resistance are listed in Table 4-4. A comparison of initial and present capacities indicates an average degradation of about 0.1 Ah/100 cycles for the seven cells under test. However, the decline in capacity usually occurs in discrete steps of 0.2 to 0.3 Ah with life-cycling.

Table 4-4. CSPL Cell Resistance and Capacity Data at the End of 1987

Cell Number	Cell Resistance (mΩ)	Accum. Cycles	Available Capacity at 3.3-A Rate (Ah)	(Wh)	% of Original Capacity
7495	39.5	743	7.5	14.4	94
7494	38.4	630	7.6	14.6	95
7472	39.6	807	7.5	14.4	94
7438	38.8	524	7.7	14.8	89
7464	40.6	538	7.1	13.4	90
7440	38.8	577	7.4	14.1	96
7437	40.0	529	7.8	15.0	91

Zinc/Bromine Technology (EV) - Exxon

For a number of years, SNL has been developing zinc/bromine battery systems for the DOE through contracts with Exxon, ERC, and JCI. Performance characterization testing of an Exxon 30-kWh, 124-cell zinc/bromine battery was initiated at the ADL in 1986 and was completed during the first quarter of 1987. Early test results showed that the specific energy of this battery (50 Wh/kg) at operating temperatures of 10 and 20°C was comparable to that of the nickel/iron technology but was power-limited at discharge rates greater than 25 W/kg. The specific energy of the Exxon battery was also reduced by about 20% at an elevated operating temperature of 40°C. The energy loss at high temperature was believed to be the result of increased self-discharge. This was verified, and the measured energy loss was plotted as a function of stand time for three temperatures (Figure 4-3). As compared to the available energy with no open-circuit period, a one-hour stand time with the pumps operating caused an energy loss of ≈14% at 40°C, ≈7% at 20°C, and ≈5% at 10°C. The ADL tests also indicated that component failures and electrolyte leakage are significant problems with this technology.

Testing was voluntarily terminated at the conclusion of the performance characterization test plan. Battery performance was still nominal after 75 cycles. However, because of manpower limitations and test results of duplicate batteries evaluated elsewhere, life testing was not conducted.

Flow-Through Lead-Acid Technology (EV) - JCI

DOE/OTS/EHP has sponsored a cost-shared program with JCI to develop a flow-through lead-acid battery for electric vehicles. As part of this program, a second JCI flow-through 75-Ah lead-acid cell was delivered to the ADL for testing in 1987. The performance and life of this cell was much improved over that of the first, which is discussed in the previous annual report (*ETD Report for 1986*, page 97). A capacity of 88 Ah (175 Wh) at the C3/3-h rate and a specific energy of 47 Wh/kg (assumed cell weight of 3.72 kg) was achieved prior to the initiation of 80% DOD life cycling at a 3-h discharge rate. Cell capacity remained relatively stable throughout most of the life test, but adjustments and repairs had to be made to the pumping system and the electrolyte specific gravity during its life. A total of 70 cycles were accrued (including 14 at JCI) before the available capacity declined to less than 80% of the rated

Table 4-3. Results of Driving-Profile-Range, Peak-Power, and Hill-Climbing Tests on CSPL Sodium/Sulfur Cells

Test	% Burden 0%[1]	50%	100%[2]
Average Cell Wt. (kg)	0.12	0.18	0.24
Driving Profile Range			
SAE J227aD/IETV-1[3] (Miles) (with regenerative braking)			
Cell 7494	313	195	136
Cell 7495	342	202	142
Cell 7467	301	188	136
Cell 7464	306	186	130
4-Cell Average	316	193	136
SFUDS79/IDSEP[3,4] (Miles) (with regenerative braking)			
Cell 7494	257	159	112
Cell 7495	271	167	115
Cell 7464	247	150	98
3-Cell Average	258	159	108
Peak Power (W/kg) at 50% DOD[5]			
Cell 7494	220	147 (139)[6]	110
Cell 7495	200	134 (133)[6]	101
Cell 7467	231	158 (153)[6]	118
Cell 7464	207	137 (133)[6]	103
4-Cell Average	215	144	108
Sustained Hill-Climbing (% DOD) Tests			
Cell 7495	91	91	80
Cell 7494	93	87.5	82
Cell 7467	95	91	85
Cell 7464	92	85.5	81
4-Cell Average	93	89	82

1 Cell weight of 120 g=0% burden.
2 Assumed cell weight of 240 g=100% burden.
3 Normalized to 8.0-Ah capacity.
4 Based on a battery weight of 695 kg.
5 Derived from SAE J227aD/IETV-1 profile data at 50% DOD.
6 Measured 30-s peak power at 50% DOD and assumed 50% burden for a cell weight of 180 g.

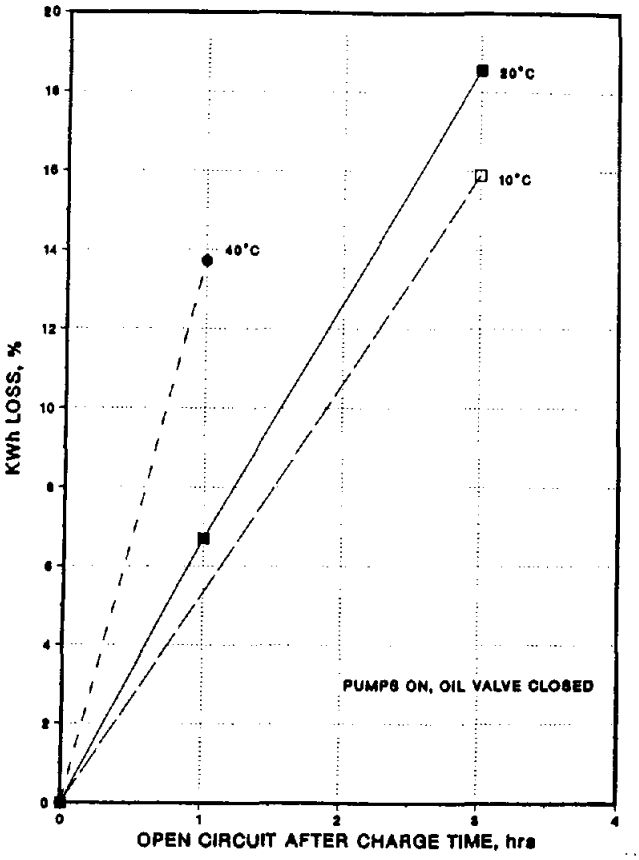

Figure 4-3. Exxon 30-kWh Zinc/Bromine Battery Energy Loss as a Function of Stand Time After Charge

value. At the end of life, an 8% reduction in cell capacity resulted during a discharge with no electrolyte flow in the cell. The cell also achieved a derived peak power was 101 W/kg at 50% DOD and an estimated range of 78.4 miles for a SAE J227aD/IETV-1 driving profile when normalized to 75 Ah.

Advanced Nickel/Iron Technology (EV) - Eagle Picher Industries

A cost-shared DOE/OTS/EHP contract was initiated with EPI in January 1986 to improve the performance and reduce the cost of nickel/iron EV batteries. The R&D effort is focused on the development of low-cost nickel electrodes up to twice as thick as that of the prior technology. Some designs incorporate electrodes fabricated from a metal-fiber substrate instead of the conventional sintered-powder nickel electrode. As part of this contract, the ADL provides independent testing and evaluation of the hardware resulting from the development efforts.

In 1987, the ADL conducted experimental evaluations on seven modules involving a matrix of improved cell designs listed in Table 4-5. The evaluation of each module included capacity verification at two discharge rates, and determination of estimated range and available acceleration power using simulated driving profiles. This was followed by an abbreviated life test wherein the module was discharged at a 120-A rate for about 200 cycles. All modules were maintained in a water bath to enhance cooling. A summary of results from the ADL performance evaluation tests is listed in Table 4-6.

An important factor to the operational life of a battery is its ability to maintain its initial peak-power capability. EPI module 33 was discharged using a J227aD/IETV-1 driving profile on cycles 26, 133, and 211 to derive and evaluate its peak power as a function of cycle life. The measured and derived data from these cycles are given in Table 4-7. The results show that module peak power and capacity declined by about 12% and 10%, respectively, over the 185-cycle period. However, the reduction in capacity occurred in the first 133 cycles of module life while the decline in peak power occurred after that point. This study is continuing.

Eaton/DSEP Nickel/Iron Battery Technology (EV) - EPI

As part of a cost-shared DOE/OTS/EHP contract with Eaton Corporation to develop an advanced electric vehicle, several nickel/iron batteries were designed and procured from EPI for evaluation and vehicle use. In March 1986, two individual 170-Ah nickel/iron five-cell modules and the 140-cell (28-module) battery pack were delivered to the ADL for evaluation. Performance characterization tests were conducted on the two modules and life testing

Table 4-5. Design Characteristics of Improved Eagle-Picher Nickel/Iron Modules

Module No.	Delivery	Type Positive Plate	Plate Thick (in)	Loading (g/cm^3)
29	9/86	Powder	0.059	1.6
30	9/86	Powder	0.059	1.6
31	1/87	Powder	0.114	1.5
32	3/87	Fiber	0.115	1.3
33	4/87	Powder	0.114	1.6
34	5/87	Fiber	0.110	1.3
35	8/87	Powder	0.112	1.45
36	9/87	Fiber	0.055	1.59

Table 4-6. Results of Performance Evaluation Tests on EPI Nickel/Iron Modules

Module Number	Type Pos. Plate	Initial Capacity 75-A (Ah)	Range for Specified Driving Cycle (Miles) J227aD /IETV-1	FUDS /DSEP	SFUDS79 /IDSEP	Derived Peak Power @ 50% DOD (W/kg)
29	Powder	222	92	46.0	46.6	107
30	Powder	227	99	66	62.3	121
31	Powder	223	106	68	68.2	111
32	Fiber	184[1]	92	--	62.3	96
33	Powder	224	102	68	60.4	88
34	Fiber	186	85.5	60.7	66.2	96
35	Powder	216	99	68	74	92
36	Fiber	206	102	76.2	70.2	92.5

1 Discharged at 65-A rate.

Table 4-7. Capacity and Driving Profile Peak Power Versus Cycle-Life Data for EPI Module 33

Cycle No.	Module Capacity @ 75-A Rate (Ah)	Module Capacity % Decline	Module Peak Power @ 50% DOD (W/kg)	Module Peak Power % Decline	J227aD /IETV-1 (Miles)
26	212	--	88	--	102
133	191	10	85	3	88.4
211	190	10	77.5	12	83.6

was performed on the battery pack. Module performance testing was completed in early 1987 and each module maintained a capacity of ≈163 Ah (970 Wh) after about 215 cycles of operation.

The life characterization test for the battery pack originally consisted of applying a 1377-s driving profile having a 56-kW maximum power and an average velocity of 19.6 mi/h until the battery reached a specified minimum voltage level. After operating the battery for 150 cycles, the driving profile was modified to have a 52-kW maximum power and a concluding 52-kW, 20-s power pulse after completing 49.5 miles. Test results indicate that the power capability of the pack decreased at a faster rate than its capacity loss. After about 250 cycles, the pack had difficulty completing the concluding 52-kW power pulse without reaching the discharge cutoff voltage (DCOV) limit. The cooling pattern within the pack enclosure was found to cause thermal gradients that contributed to the power capability problem. Thermal management was improved but, soon after, the power problem returned. Various parameters (DCOV, time of open-circuit stand following charge, and overcharge) were altered, which temporarily allowed the battery to successfully complete the final 20-s power pulse. Although its peak-power capability is decreasing faster than its capacity and may be a limiting factor, overall pack operation has been good.

Testing of the Eaton/EPI/DSEP battery pack was suspended in October 1987 after accumulating a total of 502 cycles (209 cycles in 1986). At that time, the battery was exhibiting a C2/2-h capacity of 153 Ah and 25.6 kWh (90% of rated) with a 220 Ah charge and 1-h open-circuit period after charge. The battery was placed on a constant-current trickle charge of about 3 A and testing is expected to be resumed in January 1988 pending a DOE review.

Testing of Flowing-Electrolyte Batteries at SNL

Five flowing-electrolyte batteries were tested electrically, chemically, and mechanically during 1987 at SNL. These units were built by two developers: Exxon and Energy Research Corporation (ERC). All five batteries completed electrical evaluation and were disassembled during the year.

In addition to the above units, one eight-cell JCI zinc/bromine battery and two single cells built by SNL were tested as part of the EV-ABS program. These evaluations, however, are not discussed in this report.

Table 4-8 describes the Exxon and ERC batteries, and a summary of their test results is presented in Table 4-9. These two tables contain the following information on each battery:

- the manufacturer ID number and the SNL ID number (In this discussion all batteries are identified by their SNL ID numbers.)
- the technology (This year all flowing-electrolyte batteries evaluated at SNL were zinc/bromine.)
- the developer
- when testing started and ended
- number of cells per battery
- rated capacity (at a specified C rate)
- total battery weight
- mean coulombic, voltaic, and energy efficiencies (based on the life of the battery during testing at SNL)
- total cycles completed and cycles completed in 1987
- status.

A discussion of the SNL evaluation of these flowing-electrolyte batteries, summarized in Table 4-10, follows.

Evaluation Procedures

The evaluation procedures used on the Exxon and ERC zinc/bromine batteries consisted of electrical charge and discharge at various rates and charge levels. In addition, chemical analyses of several battery electrolytes were conducted. These were considered necessary for system maintenance and for evaluation of system problems. Data were collected on pump and plumbing longevity and maintenance requirements. Failure analyses were conducted on all batteries that failed during the year.

A typical electrical cycle for these systems consisted of a timed, constant-current charge related to a theoretical zinc loading. After a one- to five-minute open-circuit wait following charge, a constant-current discharge was imposed until the cell or battery voltage fell below a predetermined cutoff level, typically 1.0 or 1.2 V per cell.

Periodically, it was necessary to discharge these units to the completely discharged condition (0 V). This is a maintenance requirement of the zinc flow technology. The frequency of this deep discharge, which is an operating variable that depends on the cell design, varies from every one to every forty cycles.

The measured parameters of these tests included cell or battery voltages, currents, temperatures, and electrolyte pressures or flow rates. Several data items were calculated from these parameters, including

- ampere-hours and watt-hours in and out of the battery
- coulombic, voltaic, and energy efficiencies for each charge/discharge cycle.

The efficiency values reported in Table 4-9 represent averages over the life of each unit while at SNL. One of the goals of these investigations was to evaluate these batteries using meaningful and comparable test regimes. Individual design limitations were considered during test planning. Test regimes for each battery were different and involved various charge and discharge rates, zinc loading, and temperatures. Thus, individual test conditions must be considered when interpreting these data.

Baseline cycles were defined for each of the units tested. The cycles were based on developer guidelines and design information. These regimes and corresponding battery electrolyte characteristics are specified in Tables 4-11 and 4-12, respectively.

Other electrical tests were conducted in addition to baseline cycles. Self-discharge rate and internal resistance were determined. The failure criterion for these tests was battery performance of less than 40% average energy efficiency for five consecutive cycles using the baseline test. Failure was also declared if the cell or battery became unserviceable because of leakage or component failures.

The Exxon battery was tested using "standard" electrolyte consisting of 3M zinc

Table 4-8. Flowing-Electrolyte Batteries Tested at SNL in 1987

SNL ID No.	Technology	Developer (ID No.)	Start/End Test Date	No. of Cells	Rated Capacity (Ah)	Wt. (kg)
301	Zinc/Bromine	Exxon (S8-2)	10-82/1-87	8	40 @ C/3	46
430	Zinc/Bromine	ERC (SNL-5-1D)	10-86/12-86	5	125 @ C/3	200
442	Zinc/Bromine	ERC (SNL-5-2D)	2-87/5-87	5	125 @ C/3	200
447	Zinc/Bromine	ERC (SNL-5-3D)	7-87/10-87	5	125 @ C/3	200
448	Zinc/Bromine	ERC (SNL-5-4D)	7-87/11-87	5	125 @ C/3	200

Table 4-9. Flowing-Electrolyte Battery Data Summary as of December 1987

SNL* ID No.	Mean Coulombic Efficiency**	Mean Voltaic Eff.**	Mean Energy Eff.**	Total No. of Cycles	No. of Cycles in 1987	Status
301	86.9 ± 0.2	77.3 ± 0.1	67.2 ± 0.2	2030	5	Off Test
430	37 ± 14	76 ± 2	28 ± 10	8	0	Failed
442	57 ± 7	77.0 ± 0.8	44 ± 6	23	23	Failed
447	77 ± 2	73 ± 2	56 ± 2	59	59	Failed
448	78 ± 5	72 ± 1	56 ± 4	39	39	Failed

* See Table 4-8 for battery identification.
** Uncertainties are expressed at 95% confidence limits.

Table 4-10. Summary of Testing of Flowing-Electrolyte Batteries at SNL

Evaluation Procedures

Cycle regime: charge/discharge at various rates and charge levels, with periodic zinc stripping.

Capacity and energy efficiency measurements.

Chemical analysis of electrolytes.

Data collection on pump/plumbing longevity and maintenance requirements.

Baseline cycles defined for each battery.

Failure criterion: less than 40% average energy efficiency for five consecutive baseline cycles, or if battery unserviceable because of leakage or component failures.

Evaluation Results

Exxon 500-Wh Zinc/Bromine Battery (SNL ID No. 301)

Five additional cycles after voluntary suspension from testing in 1986 at 2025 cycles; performance during these last cycles significantly lower.

Observations during disassembly:

- current-collector screen severely corroded;
- interior electrodes warped (but warpage confined to bottom and top of electrodes);
- unidentified coating on zinc side of several electrodes near the positive and negative ends of the stack.

Conclusions:

- final performance degradation attributed to current-collector corrosion;
- gradual degradation caused by warpage and coatings;
- pattern of electrode warpage permitted uniform electrolyte distribution (which is the main reason why the battery exceeded 2000 cycles).

Further analysis of this battery's electrodes, separators, and electrolyte planned.

Table 4-10. Summary of Testing of Flowing-Electrolyte Batteries at SNL (Continued)

ERC Zinc/Bromine Battery (SNL ID No. 430)	Featured three-loop flow system. Failure after eight cycles. Poor and inconsistent efficiency and uncontrollable electrolyte crossover. Disassembly attributed early failure to loose pipe-thread bits and small pieces of teflon tape that blocked the electrolyte flow channels.
ERC Zinc/Bromine Battery (SNL ID No. 442)	Used same flow system as battery 430. Same results as with battery 430, though battery 442 completed 23 cycles before failure.
ERC Zinc/Bromine Battery (SNL ID No. 447)	Used same flow system as battery 430 and 442. 59 cycles completed before failure; performance more consistent than that of batteries 430 and 442. Electrolyte crossover not a problem, but there was a significant decline in coulombic and voltaic efficiencies. Disassembly attributed failure to a hairline crack in the flow channel of the postive end electrode; ERC is redesigning end electrodes to overcome this problem.
ERC Zinc/Bromine Battery (SNL ID No. 448)	Featured improved (two-loop instead of three-loop) flow system and clamping hardware. Electrolyte leak at positive end terminal eventually sealed by salt crystallization. Electrolyte overflow problems encountered. 39 cycles completed before failure. Cause of failure same as that of battery 447.

Table 4-11. Baseline Cycle Regimes for Flowing-Electrolyte Batteries

SNL* ID No.	Electrode Area (cm^2)	Current Density		Zinc Loading (mAh/cm^2)	Electrolyte Temperature (°C)
		Charge (mA/cm^2)	Discharge (mA/cm^2)		
301	600	20	20	60	20
430	872	34	34	138	30
442	872	34	34	138	30
447	872	43	43	170	30
448	872	34	34	138	30

* See Table 4-8 for battery identification.

Table 4-12. Electrolyte Characteristics of Baseline Cycles for Flowing-Electrolyte Batteries

SNL* ID No.	Anolyte Pressure (psi)	Catholyte Pressure (psi)	Total Volume (l)	Electrolyte Utilization (%)
301	3	3	4	50
430	13	10	15	37
442	13	10	15	37
447	13	10	15	47
448	13	10	15	37

* See Table 4-8 for battery identification.

bromide (discharged state) and 1M quaternary ammonium compounds (bromine complexing agents). Two ammonium compounds were used, in equal ratios: N-ethyl, N-methyl morpholinium bromide and N-ethyl, N-methyl pyrollidinium bromide.

The ERC zinc/bromine batteries used a similar electrolyte composition. However, only one bromine complexing agent was used, and potassium chloride was added to the electrolyte to improve its conductivity.

Battery electrolytes were chemically analyzed using traditional wet methods and instrumental techniques. Bromine and trace metal concentrations were determined. Electrolyte pH was monitored and adjusted with hydrobromic acid to maintain a value of less than 3.0 pH. These analyses were used to evaluate chemical changes during electrical tests.

Required and preventive maintenance was carried out on each unit. Problems with plumbing components, electrolyte pumps, thermal management systems, and cell-case leaks were identified, documented, and resolved.

Evaluation Results

Exxon 500-Wh Zinc/Bromine Battery (SNL ID No. 301)

Evaluation of an Exxon eight-cell battery was completed in 1987. A qualified life-cycle test, begun in 1984, was terminated after 2030 cycles, with only five cycles run in 1987. An additional 20 cycles had been run on this battery at Exxon prior to its delivery to SNL in 1982. Performance declined gradually over the life of the battery until cycling was voluntarily suspended in November 1986, after 2025 cycles had been completed. A complete summary of the life data for this battery appeared in last year's annual report (*ETD Report for 1986*, pages 107 and 108). During the last five cycles run in 1987, performance dropped significantly. The average efficiency performance observed at SNL during the last five cycles (cycles 2026 through 2030) was:

Coulombic	73 ± 3%
Voltaic	68 ± 2%
Energy	50 ± 4%

These efficiencies can be compared with overall life data shown in Table 4-9. Coulombic efficiency declined 14% and voltaic efficiency dropped 9% during these last five cycles. The battery had been idle for about two months between cycle 2025 and cycle 2026, and it was disassembled immediately after cycle 2030.

On 16 January 1987, the battery stack was disassembled. In addition to SNL personnel, Pat Grimes of Exxon and Mike Eskra and Jeff Zagrodnik of JCI participated in the disassembly. The battery was prepared by discharging it completely. The electrolyte was drained from the stack. It was then flushed once with 1M potassium chloride and once with acidified distilled water. The stack was drained, placed in a fume hood, and all assembly hardware were removed. The subsequent disassembly was videotaped.

Before the stack was opened, the resistance of the current collectors was measured. This stack was constructed with silver mesh wire embedded in the bromine and zinc end electrodes for current collection. The mesh was soldered to copper bus bars in the front and back of the stack. These bus bars were wired in parallel to the positive and negative battery terminals. After 2030 cycles, the mesh from the edge of the electrodes to the copper bus bars had severely corroded, and in some places it had totally separated from the electrode. The measured resistance through the mesh screen in the positive end electrode was 50 mΩ; the negative end electrode registered 100 mΩ resistance.

The stack was opened from the positive end. The end current-collector electrodes were flat, but all interior electrodes were warped. Figures 4-4 and 4-5 are photographs of representative zinc and bromine interior electrodes, respectively. The bright white areas in both figures are artifacts of the photographs.

As is seen in the figures, the warpage was confined to the top and bottom of each electrode

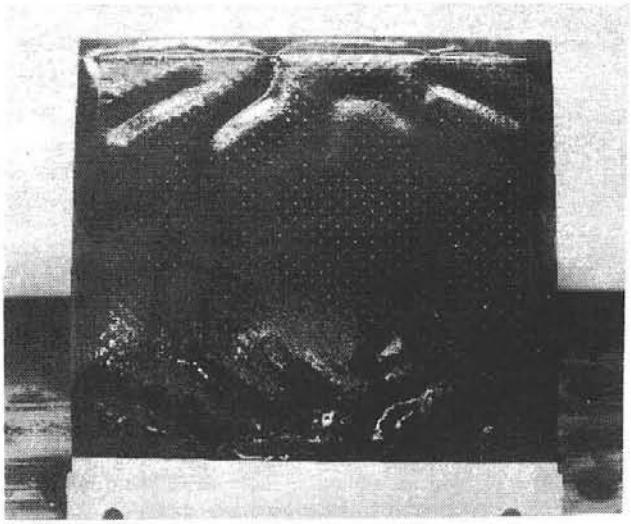

Figure 4-4. Zinc Electrode from Exxon Zinc/Bromine Battery 301 after 2030 cycles

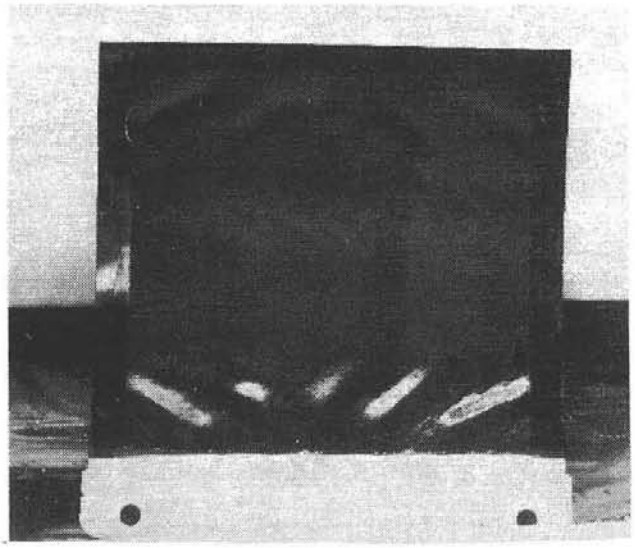

Figure 4-5. Bromine Electrode from Exxon Zinc/Bromine Battery 301 after 2030 cycles

type and was primarily parallel to the electrolyte flow path. The first three separators contained a coating adjacent to the warped electrodes. Also, the zinc side of several electrodes nearest the positive end of the battery had an unknown material coating most of its surface. The activation layer on the positive electrodes appeared to be in good condition. The electrodes in the middle of the stack were clean and showed very little of the unknown coatings. These coatings reappeared near the negative end of the stack. All flow channels inside the stack were clear and open.

In summary, the cause of the final, significant performance degradation in this Exxon zinc/bromine battery was corrosion of the current-collector screens, which resulted in high battery resistance. The gradual degradation observed over the life of the battery was probably caused by electrode warpage and the coatings on the electrodes. In general, most of the materials used in the battery appeared to be in good condition.

The main reason that this battery operated for over 2000 cycles was that the pattern of electrode warpage permitted uniform electrolyte distribution in the cell stack. Thus, the warpage did not cause significant nonuniform current distribution. These results have been shared with JCI for use in battery development. The current-collector design has been modified to avoid the problem observed with this battery.

All plastic stack components were saved in distilled water. The positive end electrode and electrodes 3 and 4, with separators, were shipped to JCI for analysis. Other pieces were retained at SNL for chemical and physical analyses.

Representative parts of the stack were photographed. Pieces were cut from electrodes and separators and the following analyses were planned on these battery components:

- resistivity
- determination of surface area and porosity
- thermal gravimetric analysis
- differential thermal analysis
- scanning electron microscopy
- electron microprobe analysis
- metal and sulfur concentrations
- special studies of the degraded areas on both the zinc electrodes and separators.

Electrolyte conductivity and metals concentrations analyses of the electrolyte were also planned. Results of these analyses will be available in the near future.

ERC Zinc/Bromine Battery (SNL ID No. 430)

The first ERC prototype zinc/bromine battery was delivered to SNL in late June 1986. It consisted of a five-cell stack, three electrolyte pumps, and associated plumbing. Battery performance data and the operational problems associated with this unit were described in last year's annual report (*ETD Report for 1986*, pages 109 and 110). In summary, the battery was operated eight cycles; its efficiency performance was poor and inconsistent, and electrolyte crossover made operation extremely difficult. No electrical cycles were conducted in 1987, but the stack was disassembled and the cause of the unusual performance determined.

On 22 January 1987, the cell stack was disassembled with the help of ERC personnel. The cause of the poor performance and electrolyte crossover was found to be blocked electrolyte flow channels to all zinc electrodes. The blockage led to poor electrolyte flow uniformity, localized high current densities, and high pressure gradients across the separators. The particles causing the obstruction were pipe thread bits and small pieces of teflon tape, which can be seen in Figure 4-6. When the stack was assembled, one or more of the threaded

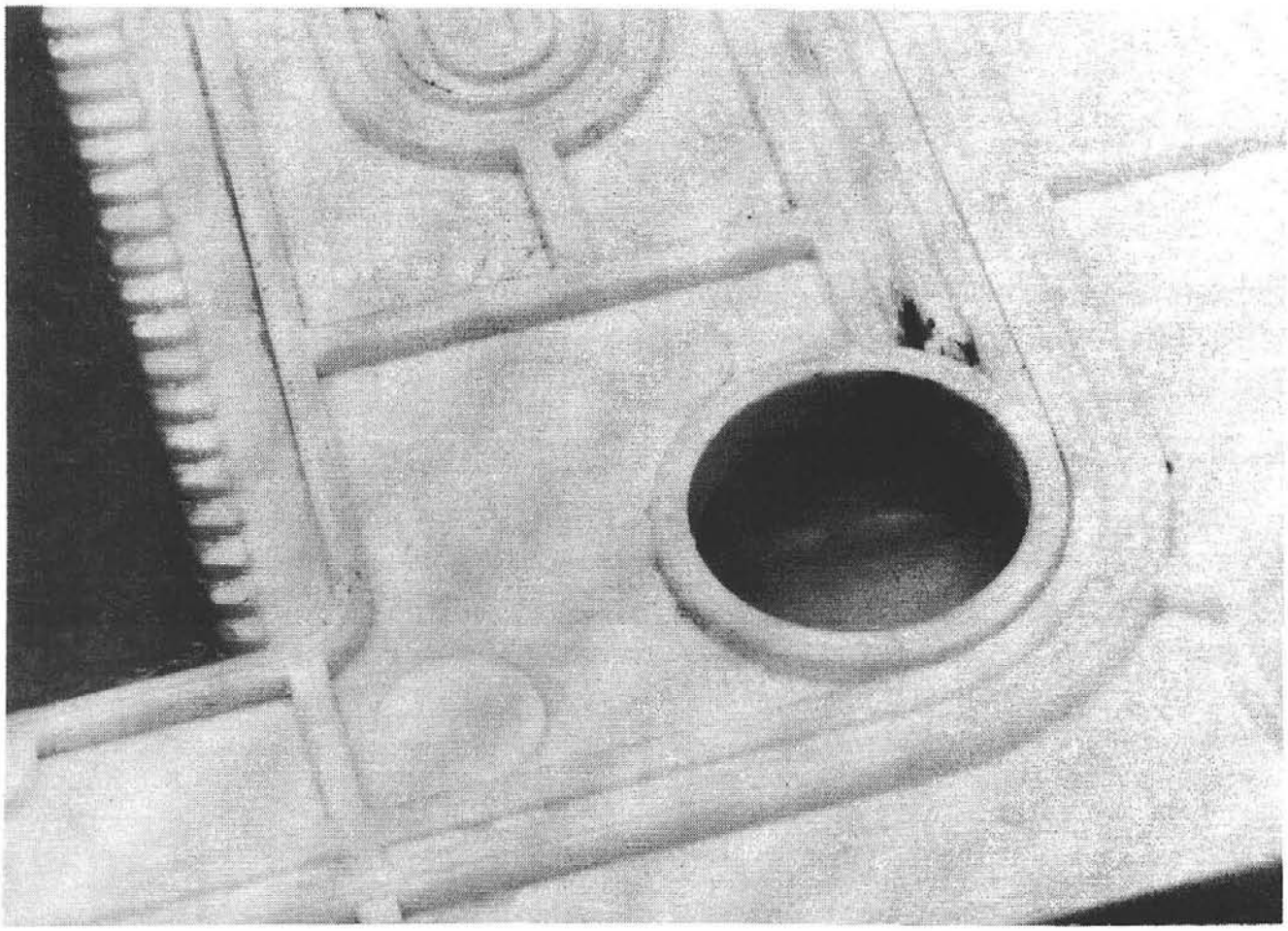

Figure 4-6. Blocked Flow Channels From ERC Zinc/Bromine Battery 430

connections apparently contained loose plastic material that eventually entered the flow system.

The cell-stack parts were saved for future analysis. The battery flow system was flushed with distilled water to remove any additional loose particles. A new cell stack was installed with the flow system from this battery. A discussion on this battery follows.

ERC Zinc/Bromine Battery (SNL ID No. 442)

The second ERC cell stack was operated from February 1987 until May 1987. Its construction characteristics were identical to battery 430. It was tested using the same flow system as battery 430. This cell stack also demonstrated poor and inconsistent performance and uncontrollable electrolyte crossover. Coulombic and voltaic efficiency are plotted in Figure 4-7 over the 23 cycles this stack operated. The observed performance was similar to that of battery 430.

The stack was removed from evaluation because of the observed performance. On 16 July 1987, the cell stack was disassembled. The cause of the failure was the same as that of ERC battery 430: blockage of the zinc flow channel by small plastic particles. The source was apparently the same as before. All threaded pipe fittings were examined and cleaned following the failure. Several fittings were found to release small particles when a pipe was threaded into them. All fittings on the zinc flow system were scraped and threaded in and out several times until no additional particles were released. A new cell stack was installed on this flow system.

ERC Zinc/Bromine Battery (SNL ID No. 447)

On 17 July 1987, a new cell stack was placed on test using the same flow system as the previous ERC batteries. It was constructed with ERC felt on the bromine electrodes, 40-mil-thick Kynar electrodes, and 35-mil-thick Daramic separators. This battery operated for 59 cycles before it was removed from test in October 1987. Figure 4-8 illustrates efficiency performance over the life of this battery.

As shown in the figure, compared to the previous ERC batteries the performance improved greatly in consistency, and the initial efficiency levels were closer to the expected values. Electrolyte crossover, which had been a significant problem in the previous tests, was manageable. Pump output was manually adjusted about twice a cycle to maintain proper electrolyte levels. The polybromide and anolyte pumps were replaced near the end of the test because of inconsistent operation.

Voltaic efficiency declined steadily during the tests. Coulombic efficiency dropped significantly during the last ten cycles. There was no noticeable effect on efficiency when zinc loading on charge was increased from

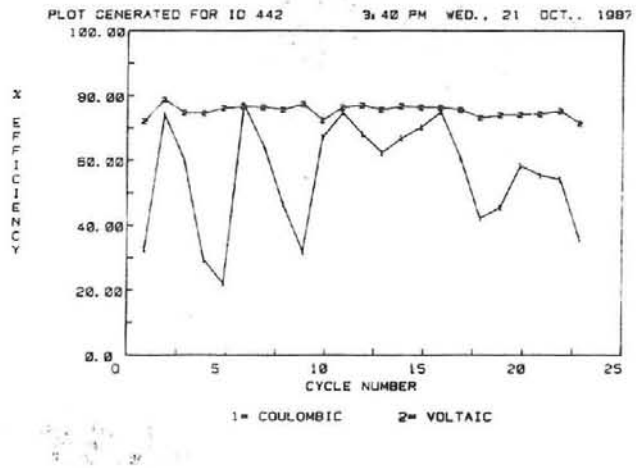

Figure 4-7. Cycle Data for ERC Zinc/Bromine Battery 442 at SNL

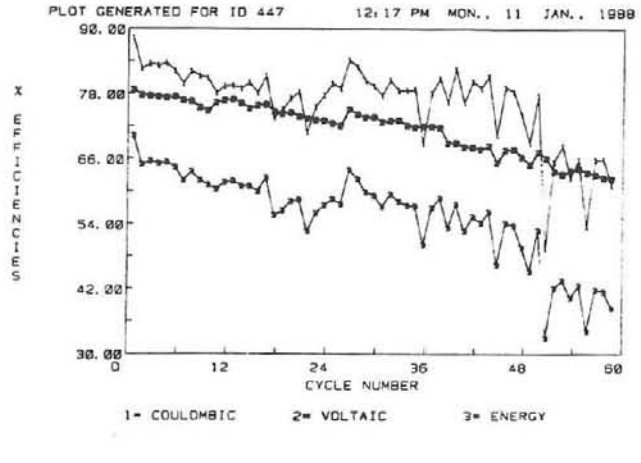

Figure 4-8. Cycle Performance of ERC Zinc/Bromine Battery 447 at SNL

137 to 170 mAh/cm² and the charge and discharge rates were increased from 34 to 43 mA/cm² at cycle 39. Battery resistance was measured using polarization techniques at 100% and 66% state-of-charge (SOC) near the end of the test. Resistance was 40 mΩ at 100% SOC and 50 mΩ at 66% SOC. Because the battery performance was declining while these measurements were made, there may be a significant error in the result.

Because of the declining performance, the battery was removed from test and disassembled. All of the flow channels were open and clear of obstructions. The only damage inside the stack was a hairline crack in the flow channel of the positive end electrode, which is shown in Figure 4-9. The crack allowed electrolyte to enter the normally dry positive current-collector chamber. The titanium current collector was coated with a resistive film of electrolyte over about 50% of its area. This led to high current densities on the remaining active area and subsequently poor electrode performance.

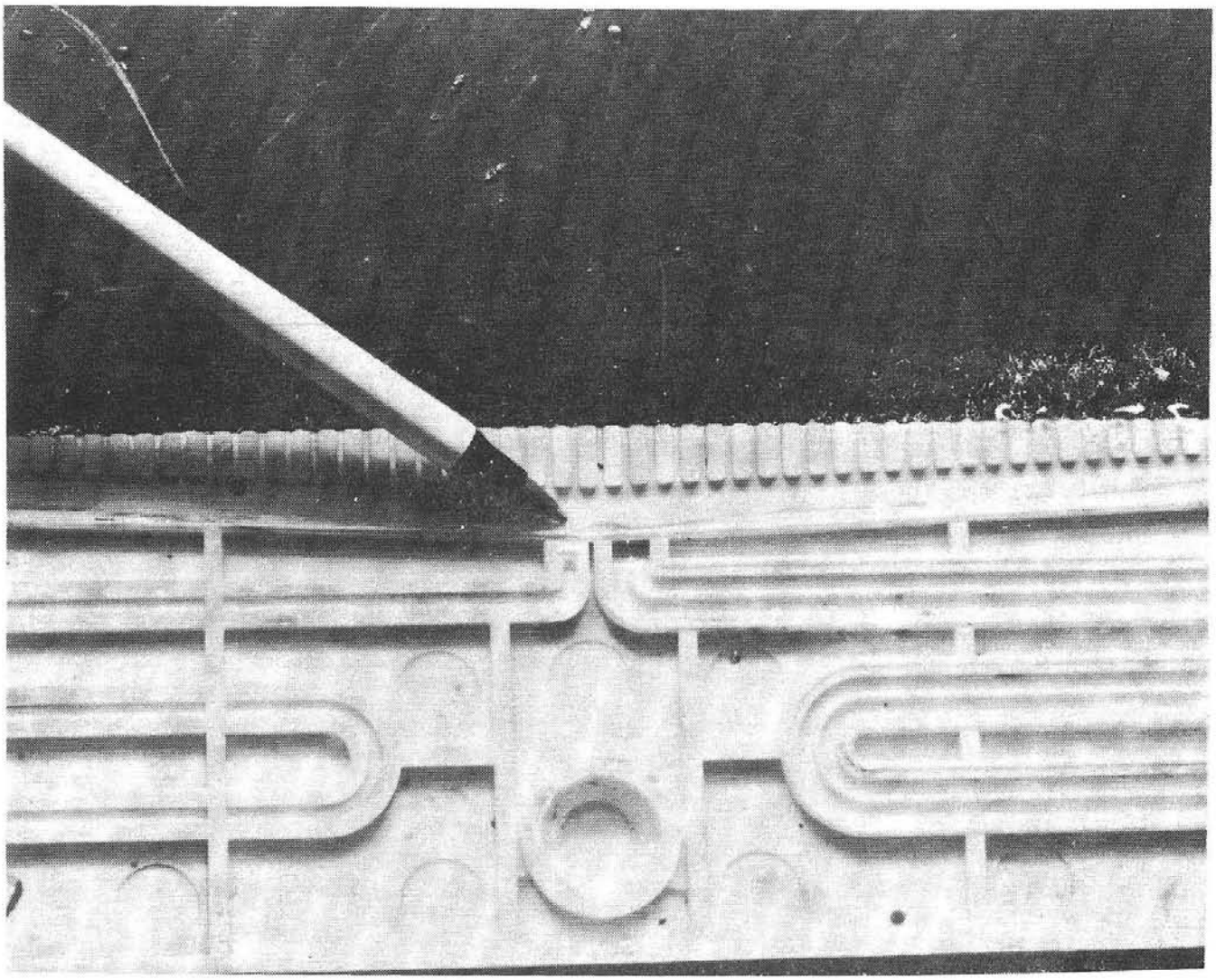

Figure 4-9. Positive End-Electrode Flow Frame From ERC Zinc/Bromine Battery 447. Note crack in flow channel (at tip of pen).

The crack in the flow frame was probably caused by insufficient mechanical support of the flow frame against the pressure exerted by the electrolyte. ERC had observed this condition previously and is in the process of redesigning the structural support of the end electrodes. No further evaluations were planned with this cell stack or flow system.

ERC Zinc/Bromine Battery (SNL ID No. 448)

One ERC zinc/bromine battery featuring an improved flow system was evaluated during 1987. A photograph of this unit is provided in Figure 4-10. This battery consisted of two pumps and flow systems (instead of three), in-line electrolyte filters, and an electrolyte-level sensor

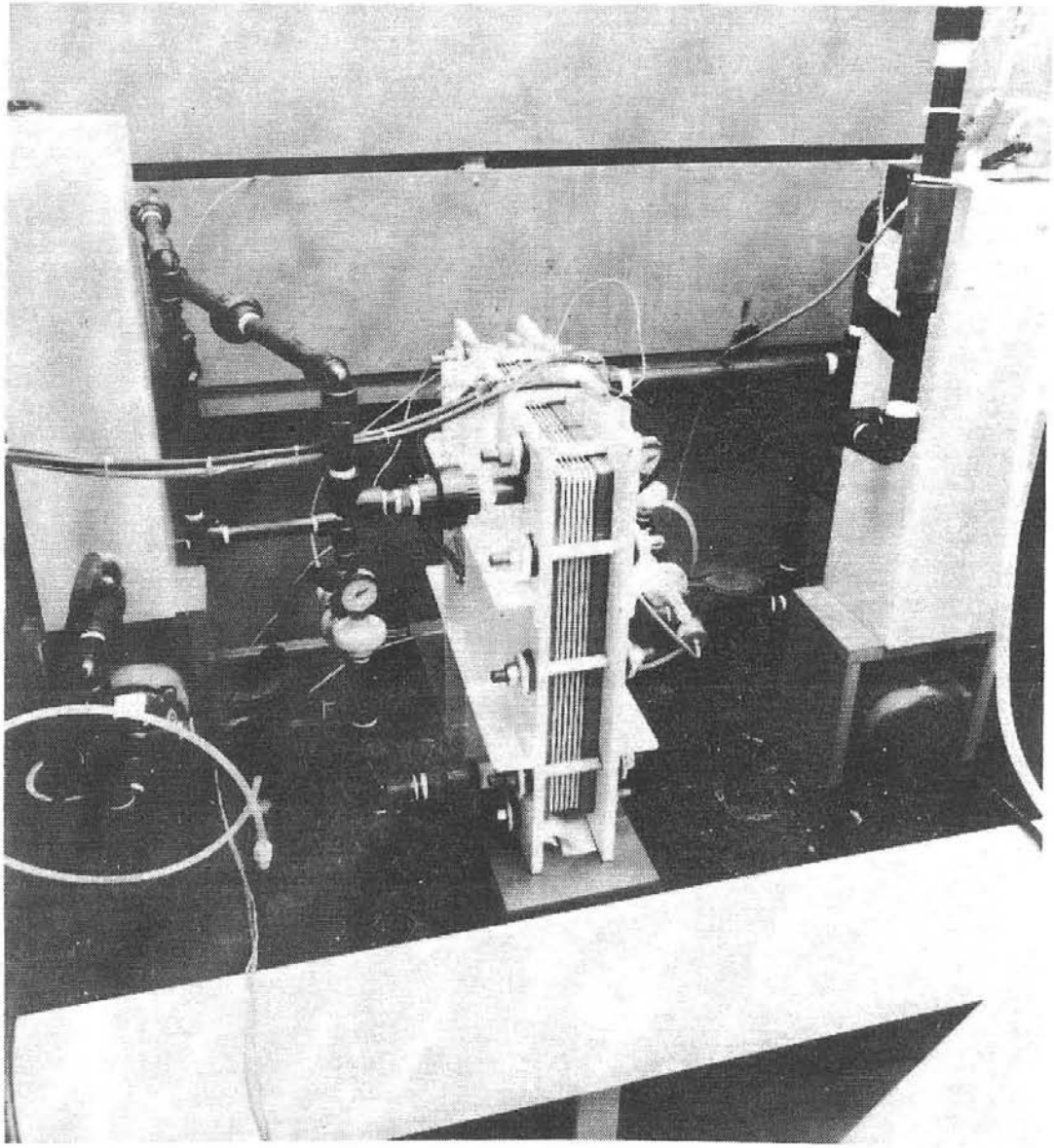

Figure 4-10. ERC Zinc/Bromine Battery 448 at SNL

in the zinc-electrolyte reservoir. The cell-stack clamping hardware was also modified to more evenly distribute the compressive forces and reduce leakage. The cell stack design and materials were identical to battery 447 described above.

The battery operated for 39 cycles at SNL. Efficiency performance is plotted in Figure 4-11. Coulombic efficiency was inconsistent during most of the tests, and significantly dropped after cycle 37. Electrolyte crossover was controlled with manual adjustments about twice a cycle. Limited headspace in the bromine reservoir resulted in overflow on several occasions. An electrolyte leak was observed at the positive end terminal of the battery at cycle 10. The leak gradually increased in severity until the leak rate was about 30 ml/h. Then, salt crystals gradually sealed the opening and the leak stopped at cycle 22.

Testing was terminated after the rapid drop in coulombic efficiency was observed. The cell stack was disassembled and the cause of the performance was determined to be the same problem as for battery 447. A hairline crack in the positive end-electrode flow channel allowed electrolyte to enter the current-collector chamber. This caused the leak at the positive battery terminal and led to reduced efficiency in the same way as described for battery 447.

No further tests were run with battery 448. A new cell stack was installed on the flow system. It will be evaluated during 1988.

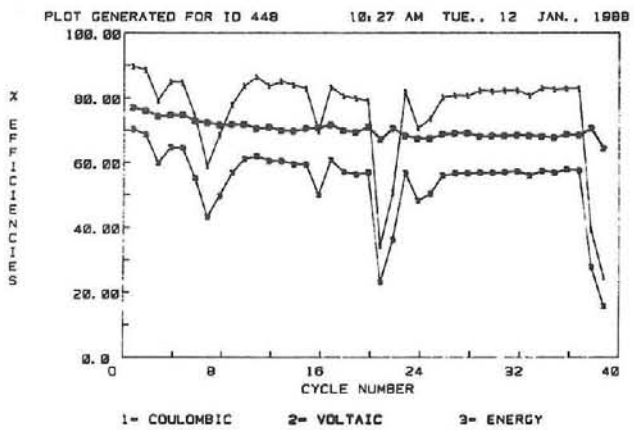

Figure 4-11. Efficiency Performance of ERC Zinc/Bromine Battery 448 at SNL

Sodium/Sulfur Testing at SNL

SNL continued testing sodium/sulfur cells during 1987. In addition to testing Chloride Silent Power, Ltd., (CSPL) and Ford Aerospace and Communication (FACC) cells, tests were initiated on two Powerplex electric vehicle (EV) cells. The testing activities on the FACC cells were suspended in June 1987 and will resume when equipment can be installed to handle the higher power requirements of future tests.

Table 4-13 summarizes the status of the sodium/sulfur cells that remained on test at the end of 1987. This table shows the following information on each cell:

- manufacturer ID number and the SNL ID number (In this discussion all cells are identified by their SNL ID numbers.)
- cell type, which can be LL (load-leveling), EV (for electrical vehicles), or PB (the standard CSPL cell)
- number of cycles completed
- test regime, which can consist of capacity, FUDS (Federal Urban Driving Schedule), parametric, or peak-power tests
- present capacity, expressed as a percent of initial capacity at a specified C rate.

The status of *all* sodium/sulfur cells (both those on test and those that have completed testing), along with parametric tests performed on the CSPL and FACC cells, is summarized in Table 4-14 and is discussed below.

FACC and CSPL Cells

FACC Cells

At the beginning of 1987, only three FACC sodium/sulfur cells were still on test at SNL. These cells consisted of one 155-Ah Mark IID

Table 4-13. Sodium/Sulfur Cells on Test at SNL, December 1987

ID No. (Manufac./ SNL)	Type	Rated Capacity (Ah)	Initial Capacity (Ah)	No. of Cycles	Test Regime	Present Capacity (% of Initial)
(a) FACC						
LL972/390	LL	155[1]	160	798	Off Test	100 @ C/5
VB007/407	EV	55[1]	60	393	Off Test	97 @ C/3
VB003/410	EV	55[1]	60	423	Off Test	97 @ C/3
(b) CSPL						
7503/437	PB	8.8[2]	8.7	1140	Capacity/FUDS/Peak Power	86 @ C/3
7435/438	PB	8.8[2]	9.1	781	Capacity/Para-metric/FUDS	84 @ C/3
(c) Powerplex						
P090-040/452	EV	38[3]	38[4]	31	Break-In/Capacity	82 @ C/8
P090-015/453	EV	38[3]	37[4]	31	Break-In/Capacity	86 @ C/8

1 FACC rated capacity: C/5 (LL) or C/3 (EV) to 1.8 VOC @ 350°C.
2 CSPL rated capacity: C/3 to 1.9 VOC @ 350°C.
3 Powerplex rated capacity: C/2.4 to 1.8 VOC @ 350°C.
4 Poweplex initial capacity: C/8 to 1.8 VOC @ 350°C.

load-leveling cell and two 55-Ah ETX electric vehicle cells. All three cells were taken off test in June 1987. They are being maintained at operating temperature awaiting the installation of equipment that can handle the higher power requirements of the simplified FUDS and peak-power tests.

Load-Leveling Cell. Prior to being removed from test, the load-leveling cell (cell 390) was being life-cycle capacity tested. This test consisted of a 30-A discharge rate to 1.8 V open circuit and 18-A charge rate to 2.5 V. This cell had completed 798 cycles and its capacity was 160 Ah, 100% of its operating capacity.

Table 4-14. Summary of Testing of Sodium/Sulfur Cells at SNL

FACC and CSPL Cells	
FACC Cells	Tests suspended until installation of equipment that can accommodate higher power requirements.
LL Cell	Was being life-cycle tested before test suspension; at 100% of initial capacity after 798 cycles.
EV Cells	Were also being life-cycle tested before test suspension; at 97% of initial capacity after completing ≈400 cycles.
CSPL Cells	
Cell 427	Failed in 1986 and underwent failure analysis discussed in Chapter 5.
Cell 434	Failed at 265 cycles, four cycles after its first cycler failed; capacity decline after electrical cycling at C/1 rate; sulfur seal failed.
Cell 435	Failure at 34 cycles preceded by drastic decrease in coulombic efficiency; spalled electrolyte attributed to large grain growth; sulfur seal failed; underwent failure analysis discussed in Chapter 5.
Cell 436	Failed at 152 cycles while on open-circuit stand; sodium- and sulfur-seal failures detected.
Cell 437	At 86% of original capacity after 1140 cycles; simplified FUDS and peak-power tests planned.

EV Cells. The EV cells (cells 407 and 410) were also being capacity life-cycle tested before they were removed from test. They had completed 393 and 423 cycles, respectively. Their capacities were both 97% of the 60-Ah initial capacity. The capacity test consisted of an 18-A discharge (C/3 rate) to 1.8 V open circuit and a two-step charge of 9-A and 3-A to a 2.3-V cutoff.

CSPL Cells

Ten CSPL cells were sent to SNL in mid-1986 to be tested under various conditions. Nine of these cells underwent cycle testing and one was used solely for freeze/thaw testing by the Battery Technology Improvement element. (See Component Stress During Freeze/Thaw Cycling of Sodium/Sulfur Cells, Chapter 5, for a

Table 4-14. Summary of Testing of Sodium/Sulfur Cells at SNL (Continued)

Cell 438	At 84% of original capacity after 781 cycles.
Cell 439	Failure at 59 cycles attributed to crack in the sodium seal.
Cell 445	Over-discharge during simplified FUDS cycle caused cell failure.
Cell 446	Removed from cycle testing after 180 cycles for freeze/thaw testing discussed in Chapter 5.
Parametric Tests	
	Box-Behnken quadratic test matrix consisting of 15 sets of cycles; temperature, discharge rate, and charge rate varied.
FACC	Test results matched predicted results.
	Charge and discharge rate has little effect on predicted capacity.
CSPL	Test results do not match predicted results as well as they did in the FACC tests because • cells could not be held at constant temperature • there is no well-defined end-of-discharge criteria.
Powerplex Cells	
	Decrease in capacity after 31 cycles in both cells 452 and 453.
	Cell 453 has a high end-of-discharge resistance (over 31 mΩ).

discussion on the freeze/thaw testing of the tenth cell.)

The status of the nine cells is shown in Table 4-15. The table shows the cell ID numbers, the number of cycles run on each cell, the start- and end-of-test dates, and the cell resistances after ten cycles and just prior to failure. In addition, information on the failure of the cells and the posttest status of each cell is shown. A detailed discussion of these cells follows.

Cell 427. This was the first cell to be tested, and it experienced a failure early in cycle life (see *ETD Report for 1986*, pages 114 and 115). In 1987 the cell underwent failure analysis, which is discussed in Chapter 5 (Failure Analysis of the Beta"-Alumina Electrolyte).

Cell 434. This cell was placed on test in November 1986, and 261 cycles were run. The cell was moved to an adjacent test bench after its cycler had failed. Capacity tests were started on the new cycler. However, the cell completed only four more cycles when it failed. This cell did experience a decline in coulombic efficiency when it was moved to the new test location. The

Table 4-15. CSPL Cell Summary

ID No. (Manufac./ SNL)	No. of Cycles Run	Start/ End-of-Test Date	Cell Resis. at 10 Cycles and at Failure (mΩ)	Beta"-Al Fracture	Seal Leaked Na	Seal Leaked S	Coul. Eff. Decline	Cell Status
7436/427	23	9/18/86-10/17/86	150/283	Y	N	N	Y	T 4,5,6,7H,8
7466/434[1]	265	11/11/86-7/6/87	37/39	?	?	Y	Y	T 4,5
7498/435[2]	34	11/12/86-1/9/87	35/32	Y	?	Y	Y	4,5,7H,8
7497/436[2]	152	2/21/87-4/22/87	35/35	N	Y	Y	N	T 4,5,6
7503/437	1140	2/21/86-	43/--					
7435/438	781	12/9/86-	48/--					
7439/439[2]	59	12/18/86-3/10/87	126/54	Y	Y	N	Y	4,6,7V
7465/445[3]	459	3/24/87-10/20/87	42/38	?	?	Y	Y	T 4,7H
7461/446	180	5/26/87-8/8/87	36/--					

1 Cycler failed; cell moved to different cycler after cycle 261.
2 Over-fired electrolyte.
3 Cell over-discharged.
4 X-ray.
5 Photos.
6 Leak test.
7 Cell sectioned: H = horizontal section; V = vertical section.
8 Posttest analysis.
T Large temperature pulse when cell failed.

cell resistance at the beginning of cycle-life testing was 34 mΩ (normal for these cells) and was 37 mΩ close to end of life. On the final cycle, the cell resistance increased to 38.7 mΩ.

The majority of the cycles performed on this cell were capacity tests run under the standard discharge and charge rates. The capacity of the cell was near or in many cases above the rated 8.8 Ah. Short sets of three cycles each were also run at C/1, C/2, and C/3 rates. It appeared that cell capacity started to slowly decline after the C/1 cycles were performed. This loss in capacity was approximately 1 Ah.

Upon failure, the cell was cooled and removed from the furnace. X-rays and photographs of the cell were taken, but the cell was not sectioned. This cell will be returned to CSPL for posttest analysis. Though the X-rays did not show electrolyte fracture, they did indicate that the sulfur seal had failed.

Cell 435. This cell had achieved only 34 cycles when it failed. The end-of-discharge cell resistance was normal (35 mΩ after ten cycles and 32 mΩ prior to failure). Just before failure, the coulombic efficiency of the cell decreased drastically. X-rays and photographs were taken of the cell, and as with cell 434 the X-rays did not indicate an electrolyte fracture. However, if there was a small fracture in the electrolyte, the sodium could have filled the void, and the crack would be difficult to detect by X-ray. The cell did have a sulfur seal failure caused by corrosion. A photograph of this cell is shown in Figure 4-12 and illustrates what typically happens to the cell when a seal failure occurs.

Once the cell was sectioned and the sulfur/carbon material was removed from around the electrolyte, spalling of the electrolyte was observed. After consulting CSPL, it was noted that the electrolyte from cell 435 had

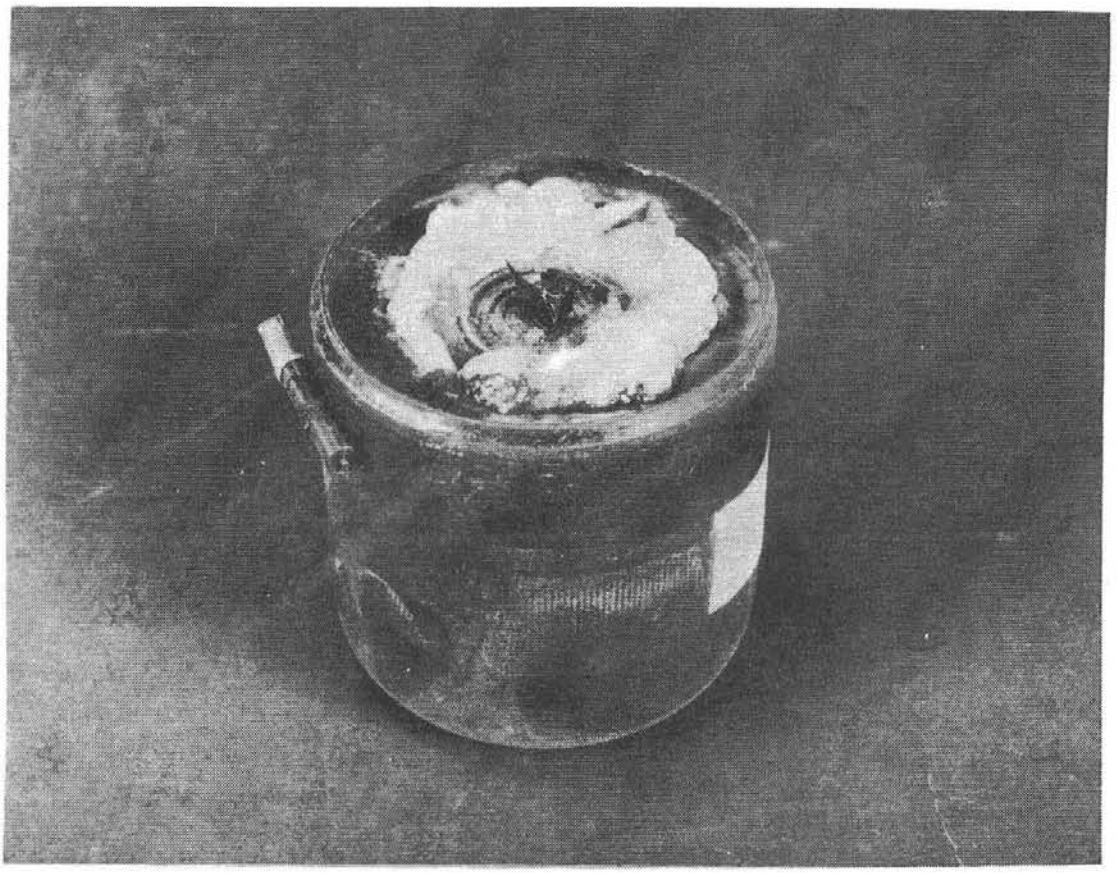

Figure 4-12. Sodium/Sulfur Cell with Sulfur Seal Failure

experienced a sintering problem caused by the electrolyte material being over-fired. This could have led to large grain growth of the material. The cell underwent posttest analysis and is discussed later in this report (Failure Analysis of the Beta"-Alumina Electrolyte, Chapter 5).

Cell 436. This cell was on test for approximately one year and had completed 152 cycles when it failed. Baseline capacity tests had just been completed and the cell was on open-circuit stand in the fully charged state when the failure occurred. The capacity of the cell was still 8.1 Ah, and no loss in coulombic efficiency was observed. The open-circuit voltage after the last cycle was 2.074 V, and thereafter the voltage gradually decreased to zero.

The standard posttest procedures were followed and no evidence of electrolyte fracture was detected. There was, however, a seal failure. With the beta"-aluminum tube and alpha-alumina cap intact, the unit was leak-tested by placing it in a heated oil bath. This caused the internal pressure of the vessel to rise, and air bubbles were observed at two locations on the top of the alpha-alumina cap.

Cell 437. This is one of the two CSPL cells remaining on test. It has been on a life-cycle test with a discharge current rate of 4 A to an open-circuit voltage of 1.9 V. The charge current rate is 3 A to an end-of-charge voltage of 2.4 V. The cell has completed 1140 cycles and the present capacity is 7.6 Ah, which is 86% of the 8.8-Ah rated capacity. Simplified FUDS and peak-power tests are planned for this cell in the near future.

Cell 438. A total of 781 cycles have been completed on this cell, the other CSPL cell remaining on test. These cycles have included capacity tests, parametric tests, and several simplified FUDS tests. The capacity of this cell started out at 9.1 Ah, above the 8.8-Ah rated capacity. After the parametric tests were completed, numerous capacity cycles were run, and the capacity of the cell was still over 8.7 Ah.

Next, simplified FUDS tests were started with several baseline capacity cycles run between each FUDS test. An average of 127 simplified FUDS cycle repetitions were achieved before the cell reached the end-of-discharge loaded voltage of 1.75 V. This number of repetitions is typical for the CSPL cells. It appeared that the capacity dropped approximately 0.5 Ah after one FUDS test was conducted. The capacity of this cell has decreased from 98% to 84% of the 8.8-Ah rated capacity after several FUDS cycles. This large drop in capacity could be attributed to the severity of the simplified FUDS cycle testing, cell aging, or both.

Cell 439. This cell, like CSPL cell 427, had a high end-of-discharge resistance after 10 cycles (126 mΩ). This cell failed after 59 cycles and the end-of-discharge resistance was still 54 mΩ. Only capacity tests were performed on the cell and the capacity of this cell appeared to be normal (8.8 Ah). Prior to failure, a decline in coulombic efficiency was observed. Upon failure, no increase in temperature was seen. The X-rays did not show any cracks in the electrolyte, but when the cell was leak tested, the results showed a failure in the sodium seal. This cell was sectioned in a vertical direction and nothing unusual was seen. The cell was given to the Failure Analysis of the Beta"-Alumina Electrolyte task of the Battery Technology Improvement element for further posttest analysis to be conducted in 1988.

Cell 445. This cell was the last CSPL cell to be tested to failure. Besides baseline capacity tests, parametric and simplified FUDS tests were conducted. The cell completed 459 cycles and failed because it was over-discharged during a simplified FUDS test. The resistance of the cell was normal (42 mΩ after ten cycles and 38 mΩ prior to failure). Prior to failure, a decline in coulombic efficiency was observed. Upon failure, there was a temperature increase. The cell was X-rayed and sectioned with no indication of electrolyte failure. However, the sulfur seal did fail.

Cell 446. This cell was placed on test in May 1987, and 180 cycles were completed before it was removed from cycle testing so that freeze/thaw tests could be performed (see Component Stress During Freeze/Thaw Cycling of Sodium/Sulfur Cells, Chapter 5). All of the cycles placed on this cell were capacity cycles at 350°C. The discharge rate was 3 A to an open-circuit cut-off voltage of 1.9 V. The cell was then charged at a 3-A rate to 2.4 V. The capacity of the cell under these conditions was 9.1 Ah, which is above the rated capacity of 8.8 Ah. The end-of-discharge cell resistance after 10 cycles as well as after 180 cycles was 36 mΩ. This is a typical resistance for these cells.

Parametric Tests

A parametric test plan was developed for the FACC and CSPL sodium/sulfur cells to characterize their performance. A Box-Behnken quadratic test matrix was utilized. The test plan consisted of 15 sets of cycles (five cycles per set) with three baseline capacity cycles run between each set. Within the test matrix, temperature, discharge rate, and charge rate were varied. All three parameters had center-point values, and this test was run at the beginning, middle, and end of the test matrix. Minimum and maximum values were also chosen for each parameter, and the other 12 sets of tests were randomly selected to complete the test matrix.

FACC Tests. This parametric test plan was conducted first on the FACC cells. Start-of-discharge temperature was varied between 300°C and 375°C with the center-point temperature at 337°C. The discharge current was varied between 9 A and 45 A with a center-point current of 27 A. The end-of-discharge open-circuit voltage was approximately 1.8 V for all the tests, as specified by the FACC-supplied discharge cutoff algorithm. The charge current varied from 9 A to 18 A with a center-point current of 13 A. The end-of-charge voltage was 2.3 V. Two FACC EV cells (cells 410 and 407) were chosen for these parametric tests, and the results were used to calculate a capacity-prediction equation.

Figures 4-13 and 4-14 compare the test results with the predicted results. The averaged data points taken from the test matrix are indicated as single points (#, *, and @). The prediction equation results are depicted as continuous curves. For the most part, the actual data agreed with the predicted curves.

Figure 4-13 indicates that charge rate had little effect on the predicted capacity of cell 410 when the discharge rate was held constant over a temperature range of 300°C to 375°C. However, the predicted capacity of cell 407 varied more than that of cell 410 over the same temperature range. This could be because there was very little temperature increase in cell 410 during the tests

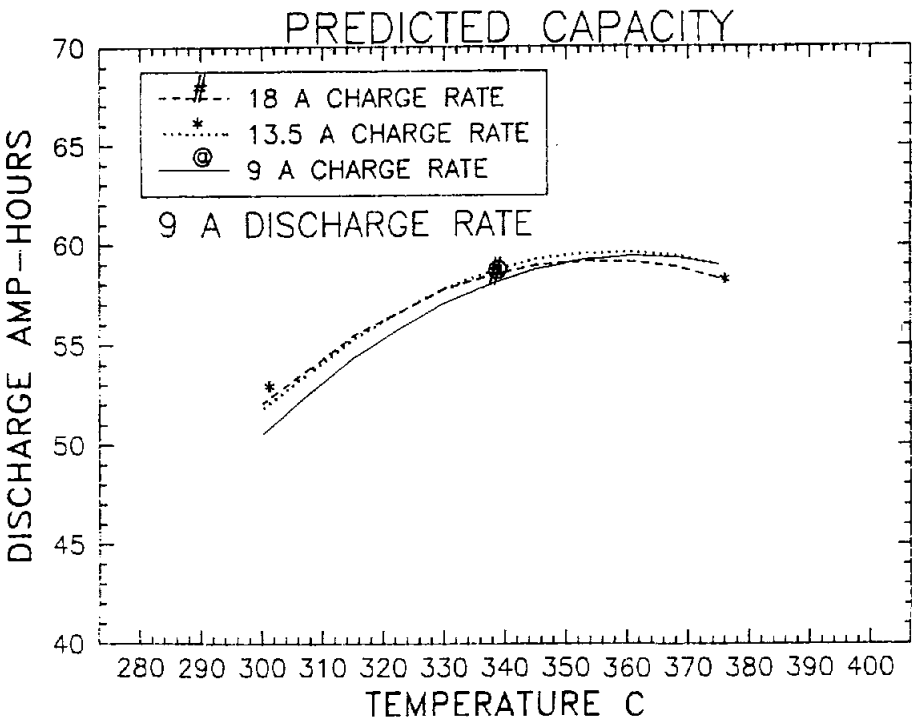

Figure 4-13. Predicted and Actual Capacity of FACC Sodium/Sulfur Cell 410 versus Temperature and Charge Rate

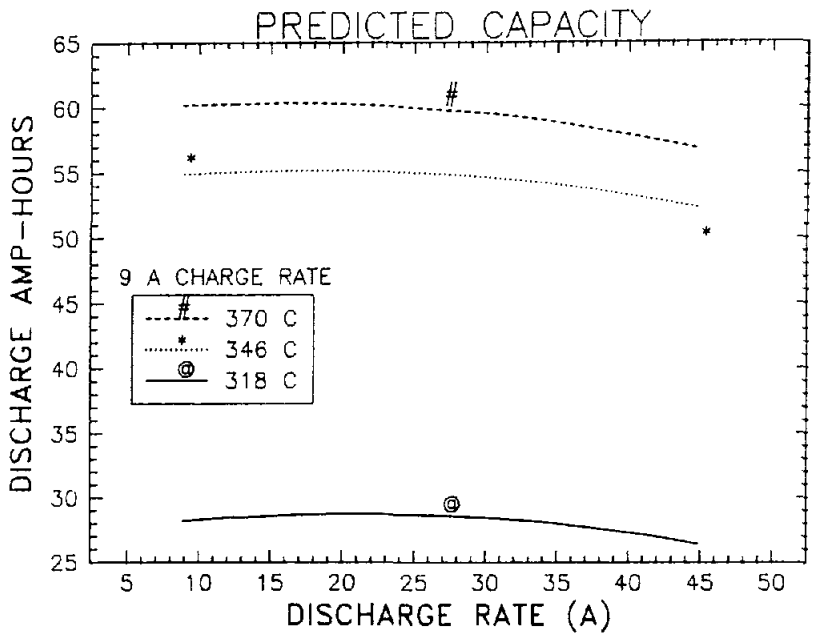

Figure 4-14. Predicted and Actual Capacity of FACC Sodium/Sulfur Cell 407 versus Discharge Rate and Temperature

while cell 407 experienced a significant temperature increase, which was related to the discharge current rate.

The predicted capacity for cell 407 is illustrated differently in Figure 4-14. Here, the discharge rate is varied over the three temperatures, and the results show a slight decrease in predicted capacity as the discharge rate is increased.

CSPL Tests. Two CSPL cells (438 and 445) were parametrically tested. This test matrix was similar to FACC's; however, the test values were different for the CSPL cells. The temperature was varied between 300°C and 365°C with a center-point temperature of 333°C. The discharge currents ranged from 2 A and 9 A with a center-point current of 4.5 A and the end-of-discharge open-circuit voltage was approximately 1.9 V for all the tests. The charge currents were varied between 2 A and 4.5 A with a center-point current of 3.25 A. The end-of-charge voltage was 2.4 V. These results were used to derive a prediction equation and plots were generated.

Plots chosen to demonstrate the results of these tests are shown in Figures 4-15 and 4-16. These figures compare the test results with the predicted results for CSPL cell 438. As with Figures 4-13 and 4-14, the averaged data points taken from the test matrix are indicated as single points (#, *, and @), and the prediction equation results are depicted as continuous curves.

In Figure 4-15, capacity as a function of temperature and charge rate is plotted for CSPL cell 438. There appears to be good correlation at the 3.25-A charge rate, as indicated by the location of the averaged data points and the predicted plot. On the other hand, for the 2-A charge rate, the actual averaged data falls above the predicted plot, and for the 4.5-A charge rate, the averaged data is below the predicted plot. In addition, the CSPL cells show a wider range of capacity as a function of charge rate and temperature than the FACC cells do, which may be attributable to the higher internal resistance of the CSPL cells.

In Figure 4-16, capacity as a function of discharge rate and temperature is plotted for

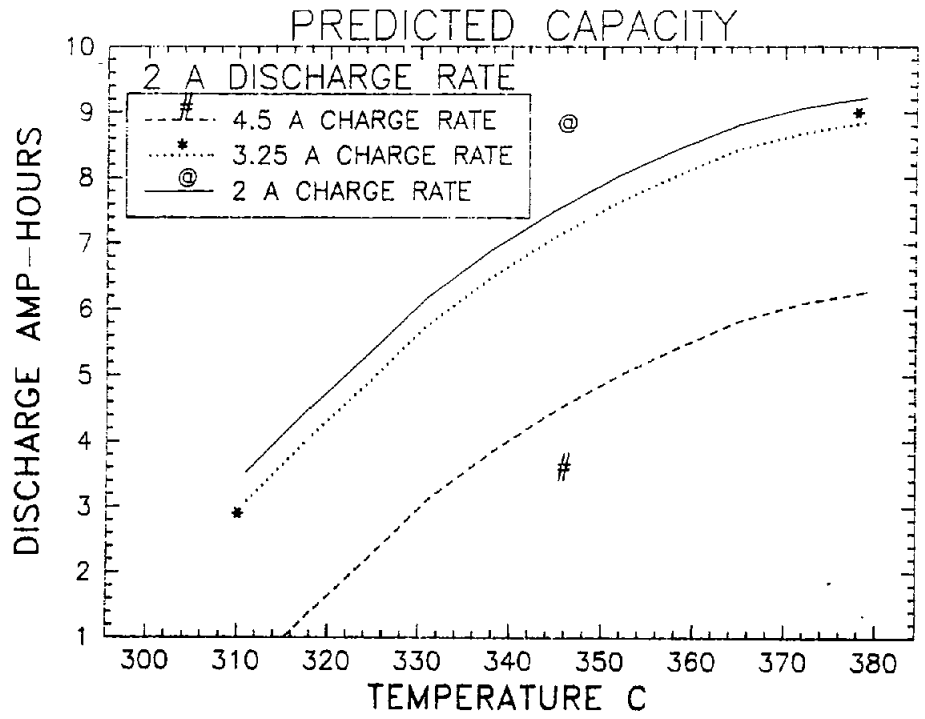

Figure 4-15. Predicted and Actual Capacity of CSPL Sodium/Sulfur Cell 438 versus Temperature and Charge Rate

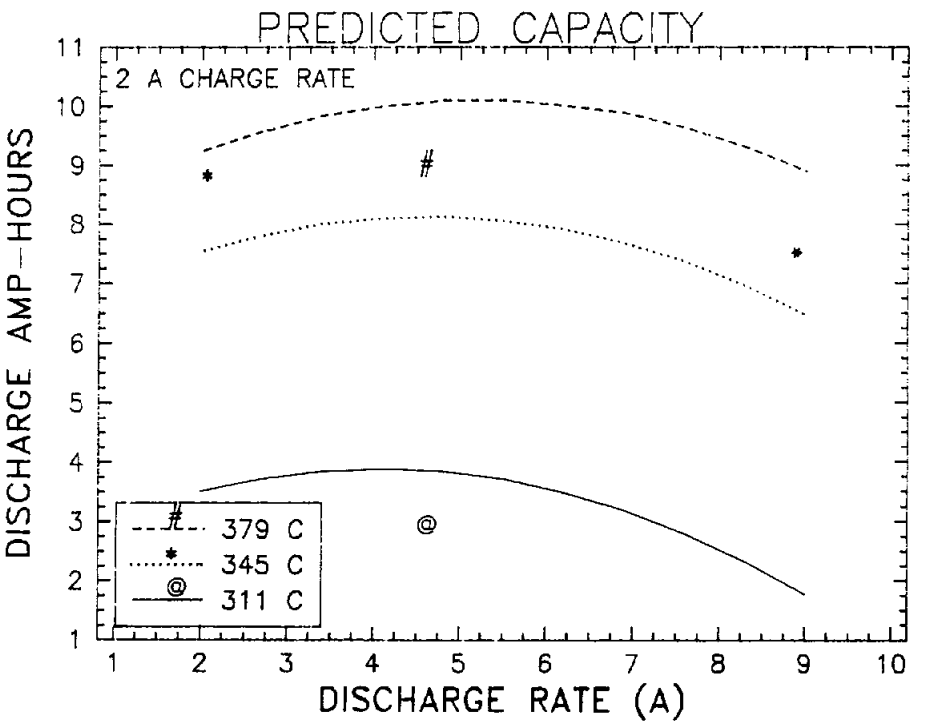

Figure 4-16. Predicted and Actual Capacity of CSPL Sodium/Sulfur Cell 438 versus Discharge Rate and Temperature

CSPL cell 438. The predicted decrease in capacity at low discharge rates is an artifact of the test conditions. The plot shows a strong dependence of capacity on cell temperature.

The prediction equation and data plots presented in this figure were affected by two significant test conditions. In three of the four cells tested, cell temperature could not be held constant during the various experiments. Thus, cell temperature tended to increase during discharge because of cell-resistance heating. The temperature increase was greater at higher discharge rates.

The other test condition that affected the results was the lack of a consistent and well-defined end-of-discharge criterion. FACC supplied an algorithm for discharge cutoff that was intended to be used for baseline capacity tests conducted close to 350°C. CSPL specified a cutoff criterion based on an open-circuit voltage measurement. Most conventional battery testing uses loaded voltage cutoff criterion. There presently is no standard method of terminating discharge for sodium/sulfur cells.

These test conditions are being studied at SNL. Constant-temperature mechanisms are being explored for cells in tube furnaces. A consistent end-of-discharge cutoff criterion will be developed. These parametric tests will be repeated using state-of-the-art CSPL cells. Cells from other developers will also be included in the test matrix.

Powerplex Cells

At the request of DOE/EHP, a contract agreement was placed with Powerplex to test their sodium/sulfur EV cells in a manner similar to which SNL tests other manufacturer's cells. The test plan consisted of capacity, parametric, simplified FUDS, and peak-power tests. The agreement with Powerplex was that SNL could report the results of the tests, but without X-raying, opening, or conducting posttest analysis on any of the cells. In addition, the cells would be returned to Powerplex upon completion of the tests.

The initial break-in cycles were placed on cells 452 and 453 at Powerplex prior to being shipped to SNL. Because of this, the cells had experienced a freeze/thaw cycle before they were tested. The cells were placed on test in November 1987 and several cycles were run at a 5-A discharge rate to 1.8 V open circuit. The cells were then charged at a 5-A rate to 2.4 V. All of these cycles were performed at 350°C.

The initial operating capacity for both cells was close to their rated capacity of 38 Ah. However, a resistance problem was experienced with both cells. This problem was initially traced to a wiring mistake by SNL, but when the error was corrected, the end-of-discharge resistances were still high:

- The resistance for cell 452 started out at 8 mΩ, which was close to Powerplex's measured value of 7.91 mΩ. After 30 cycles, the end-of-discharge resistance had increased to over 9 mΩ.

- The end-of-discharge resistance for cell 453 started out much higher: 13 mΩ versus 7.76 mΩ measured by Powerplex. The resistance of this cell steadily increased to over 31 mΩ after 30 cycles.

Both cells experienced a decrease in capacity exceeding 10% after only 31 cycles. The initial capacity and present capacity for these two cells is shown in Table 4-13. The plan is to continue to test the cells according to the test plan and to place an additional cell on test in the near future.

Nickel/Hydrogen Testing at SNL

A nickel/hydrogen battery is being developed for terrestrial applications such as remote solar, where the battery is interfaced to a load and a photovoltaic array. The main emphasis continues to be the reduction of battery cost compared with aerospace technology. The latest battery design consists of individual prismatic cells in a sealed common pressure vessel. The development work is being conducted at Johnson Controls, Inc., under a cost-sharing contract. Contract deliverables include cells and batteries for evaluation; six cells and two batteries are currently on test at SNL. Both cycling and solar tests are being conducted. Nickel/hydrogen testing at SNL, discussed below, is summarized in Table 4-16.

Table 4-16. Summary of Nickel/Hydrogen Testing at SNL

Test Conditions	
Test Equipment	An HP-85 desktop computer, an HP-3497A data acquisition/control unit, and an HP-82901M flexible disc drive.
Standard Cycle Test	Constant-current discharge to 1.0 V/cell followed by charge until increase in pressure decreases to 50% of linear slope.
Solar Test	Battery connected in parallel to a photovoltaic array and either a constant-current or resistive load.
Cycle Tests	
Status of Cells and Batteries	
Cell 12	This 1984 baseline cell is performing well after additional electrolyte added; continues cycling with capacity near original value of 100 Ah.
Cell 18	Longest-lived cell with 70-mil positive electrodes.
	Capacity at 1200 cycles is 117 Ah, 29 Ah less than last year.
Cell 19	Configured the same as cell 18, but without lithium additive in electrolyte.
	Capacity at 1153 cycles is 108 Ah, 27 Ah less than last year.
Cells 20 and 22	Configured the same as cell 18, but with no Gore-Tex backing on negative electrodes.
	Capacity decline after ≈500 cycles; posttest examination indicates removal of Gore-Tex backing inhibits the hydrogen reaction.
Cell 23	Configured the same as cell 18, but with reduced KOH concentration.
	Capacity remains above nominal capacity after more than 800 cycles.
Cell 144	New features: wider cell case that accommodates nine cell modules (instead of seven); reduced KOH concentration, which allows operation without active cooling at ambient temperatures up to 30°C.
	476 cycles accumulated; capacity gradually increasing.

Table 4-16. Summary of Nickel/Hydrogen Testing at SNL (Continued)

Cell 161	Has thicker (90-mil) positive electrodes.
	Actual capacity remains below theoretical capacity; problems encountered uniformly impregnating thicker plaques with active material.
Battery 2	Six-cell, 7.2-V battery with cells configured the same as cell 12 and assembled into a monoblock; used in the solar tests after accumulating 1150 cycles.
Battery 4	Consists of five individual cells, yielding a nominal 6-V, which is compatible with existing solar systems; cell design the same as cell 23.
	Capacity is 138 Ah at 515 cycles.
Test Conclusions	Thicker positive electrodes yield increased capacity in same-size cell case.
	Electrolyte management problems identified and design changes made.
	Hydrophobic backing on negative electrode found to be necessary for prolonged cycle life.
	Operation without active cooling possible when lithium added to an electrolyte with low KOH concentration.
Solar Tests	
Light Load	Battery fully charged for several consecutive days; overcharge accommodated by internal recombination of hydrogen and oxygen.
Intermediate Load	SOC cycled between 40% and 90%.
Heavy Load	SOC went below 0% with no adverse effects, demonstrating that the nickel/hydrogen battery is tolerant of overdischarge and cell reversal.
	Nickel/hydrogen battery plays a very active role, even though the net ampere-hour output from the battery is relatively small.
Test Conclusions	No need for a controller, since battery is tolerant to both overcharge and overdischarge.
	During discharge, it would be possible to shed load based on hydrogen pressure.

Test Conditions

Switching functions and data gathering are accomplished using an HP-85 desktop computer in conjunction with an HP-3497A data acquisition/control unit and an HP-82901M flexible disc drive. The sensor outputs are scanned every minute, calculations are performed, and the data are stored when there is a significant change in a selected parameter. One of the items calculated is the state-of-charge (SOC) of the battery, which is a function of the hydrogen pressure. The standard cycle test consists of a constant current discharge to 1.0 V/cell, followed by a charge until the pressure slope drops to 50% of the linear value. This is a relatively severe test with a 100% depth of discharge on each cycle. For the solar test, the battery is connected in parallel to a photovoltaic array and a load; the load can be either constant current or resistive.

The configuration of the cells and batteries on test during 1987 are given in Table 4-17, along with the test conditions. The most important design variations under test are:

- The number of cell modules, which is a function of the thickness of the positive electrode and the width of the cell case. Note that cell 144 had a wider case, which allows two additional cell modules.
- Lithium, which was added to the electrolyte of more recent cells to improve performance at and above room temperature.
- The lower concentration of potassium hydroxide, which permits operation at room temperature without active cooling.
- The hydrophobic backing on the negative electrode, which enhances the reaction of hydrogen on discharge.

A more thorough description of the cell components and configuration is given in Chapter 2 (Nickel/Hydrogen Battery Development - JCI).

Cycle Tests

The test results, including the total number of cycles to date, are summarized in Table 4-18. These results, reported in terms of capacity, ampere-hour efficiency, mid-point discharge voltage, and end-of-charge/discharge pressures, are averages of the last five cycles. Performance of the individual cells and batteries is discussed in detail below; the order is chronological rather than as listed in Tables 4-17 and 4-18.

Status of Cells and Batteries

Cell 12. This was the baseline cell at the end of 1984. It has the 30-mil positive electrodes and other design characteristics listed in Table 4-17. A significant capacity decline was noted after about 1200 cycles. The cell was shipped to JCI, and examination indicated that the cell was quite dry. Additional electrolyte was added, and an immediate improvement in performance was noted. Cell 12 was returned to SNL in April 1987, where it continues on test with capacity near the original 100 Ah. The experience with cell 12 has prompted reconfiguration of the cell module in recent cells to improve electrolyte management.

Battery 2. This battery has six cells in a monoblock case, yielding a nominal 7.2 V. These cells are configured the same as cell 12. Battery 2 has been on test since June 1984, and had accumulated about 1150 cycles when the solar tests discussed below were started in January 1987.

Cell 18. This cell has the 70-mil positive electrodes instead of the earlier 30-mil electrodes, which increased the theoretical capacity from 80 to 120 Ah for the same size of cell case. This increased energy density, along with the reduced number of required electrodes, had a very favorable impact on cost. Cell 18 has performed very well; it has accumulated over 1200 deep-discharge cycles since October 1985. There has, however, been a recent downward trend in capacity; the latest capacity is about 30 Ah less than a year ago.

Table 4-17. Configuration and Test Conditions for Nickel/Hydrogen Cells and Batteries

S/N	Number of Cell-Modules	Positive Thick. (in.)	Li Added	Gore-Tex on Neg.	KOH (%)	Coolant (°C)	Current Chrg./Dischrg. (A)
(a) Cells							
12	10.5	0.030	No	Yes	40	10	20/25
18	7	0.070	Yes	Yes	38	10	25/25
19	7	0.070	No	Yes	38	10	25/25
20	7	0.070	Yes	No	38	10	25/25
22	7	0.070	Yes	No	38	10	25/25
23	7	0.070	Yes	Yes	33	10	25/25
144	9	0.070	Yes	Yes	24	None	28/25
161	7	0.090	Yes	Yes	24	None	25/25
(b) Batteries							
02	10.5	0.030	No	Yes	40	10	20/20
04	7	0.070	Yes	Yes	33	10	20/20

Table 4-18. Summary of Nickel/Hydrogen Battery and Cell Test Results

S/N (ID)	Cycles	Capacity (Ah)	Ah Eff. (%)	Mid. Pt. (V/Cell)	Pressure (psig) EOC	Pressure (psig) EOD
(a) Cells						
12 (393)	1765	99.6	89.2	1.204	282	62
18 (414)	1234	116.7	86.6	1.210	281	109
19 (415)	1153	108.2	86.7	1.198	263	113
20 (416)[1]	852	103.9	88.8	1.183	238	99
22 (421)[2]	431	103.9	86.3	1.194	254	112
23 (422)	823	149.3	91.7	1.249	267	60
144 (441)	476	194.2	89.2	1.244	313	72
161	67	171.9	86.0	1.248	344	77
(b) Batteries						
02 (385)	1451	79.8	89.4	1.229	113	58
04 (433)	515	138.4	93.0	1.217	265	103

1 Removed from test July 1987.
2 Removed from test March 1987.

Cell 19. This cell is configured the same as cell 18, except there is no lithium additive in the electrolyte. Like cell 18, cell 19 has also experienced a gradual drop in capacity: 108 Ah from 135 Ah a year ago.

Cells 20 and 22. To reduce cost, these cells had negative electrodes without hydrophobic backing. However, capacity began to decline after about 500 cycles. Posttest examination revealed electrolyte on the back of the negative electrode, which inhibits the hydrogen reaction. The use of Gore-Tex has therefore been retained in the standard cell design.

Cell 23. This cell is configured the same as cell 18 with the exception that the electrolyte is 33 wt. % KOH rather than 38 wt. % KOH. It is performing very well with a capacity of 149 Ah after 823 cycles, well above the nominal capacity of 130 Ah.

Battery 4. This battery has five individual cells, yielding a nominal 6.0-V rating for better compatibility with existing solar systems. The cell design is the same as that of cell 23. There is a gap between the individual cells to improve thermal management. It is performing well with the latest capacity being 138 Ah.

Cell 144. This cell has a wider cell case to accommodate nine rather than seven cell modules, which increases the nominal capacity to 150 Ah. This was done to provide the capacity required for a 7-kWh battery. Also, the concentration of KOH in the electrolyte was reduced, which improves performance at and above room ambient temperature. Cell 144 is designed to operate passively up to ambient temperatures of 30°C, and all testing at SNL has been done without active cooling. It has now accumulated 476 cycles with capacity gradually increasing as shown in Figure 4-17, where capacity is plotted versus cycle number. With charging based on the pressure slope, the capacity is near the theoretical value of 190 Ah. The drop in capacity near cycle 140 was caused by a pressure leak at a pipe thread in the boilerplate pressure vessel, which was repaired. Other stray points are the result of computer hardware and software problems, rather than the cell.

Cell 161. This cell is the first cell with thicker, 90-mil positive electrodes. It was put on test in November 1987 and had accumulated 67 cycles by the end of the year. The capacity at that time was 172 Ah, somewhat less than 210 Ah, the theoretical capacity predicted by the amount of active material in the positive electrode. Uniformly impregnating the thicker plaques is a significant technical challenge that is being pursued at JCI.

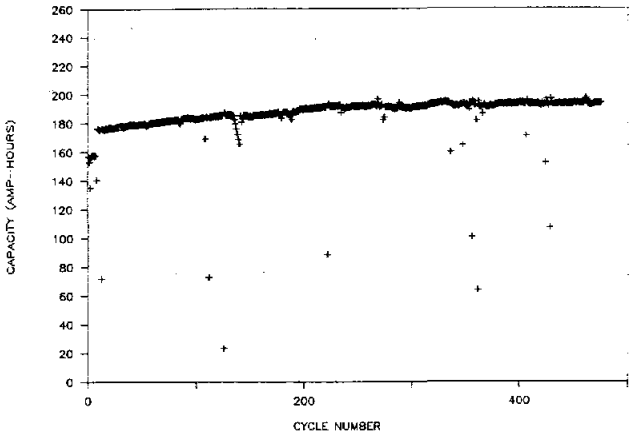

Figure 4-17. Capacity Versus Cycle Number for Cell 144

Test Conclusions

From the results of these cycling tests, it is observed that

- Increasing the thickness of the positive electrode results in a significant increase in capacity in the same size cell case.
- When a thicker cell case is used, the capacity is a linear function of the number of cell modules the case can accommodate.
- Drying out of early cells indicated a need for better electrolyte management.
- The use of a hydrophobic backing on the negative electrode appears necessary for long cycle life.
- Using a lithium additive in an electrolyte with low KOH concentration results in a cell that can operate at ambient temperature without active cooling.

Solar Tests

Tests have been run during the last year to investigate the interaction of a photovoltaic array, load, and a nickel/hydrogen battery in a solar system. One item to be determined was the need for a controller in such a system. Both constant-current and resistive electronic loads have been used. In the tests discussed below, the load consisted of emergency lamps.

Battery 2 was connected in parallel with a photovoltaic array and a resistive load. There were remotely controlled switches between the components, but no controller. Battery 2, described previously, is nominally rated at 7.2 V and 80 Ah. It had accumulated over 1100 cycles when the solar tests were begun in January 1987.

Flat-plate photovoltaic panels on the roof of the test facility in Albuquerque, NM, were configured to obtain sufficient voltage to charge the battery. The maximum current that this array is capable of producing is about 10 A, and from previous characterization tests it was known that the battery could accommodate this rate of overcharge.

The load consisted of two 6-Vdc emergency lights. The load was varied periodically by changing the length of time the lights were on each day, and the number of lights connected. Load variations for three different conditions are tabulated below:

Load	No. of Lamps	Hours/Day On	≈Ah/Day
Light	1	20	36
Intermediate	2	12	43
Heavy	2	20	70

In the results that follow, the SOC has been calculated from the pressure. Each test condition covered a seven-day period; the plots provided in Figures 4-18, 4-19, and 4-20 begin and end at midnight, with data points every hour.

Light Load

Battery current and SOC are plotted in Figure 4-18 for the "light" load condition over a period of seven days. As is seen in the current-versus-time plot (Figure 4-18a), the battery supplied the 2-A load at night when there there was no output from the array. As the output of the array increased each morning, the current would go positive, indicating that the battery was charging. A maximum current of ≈10 A was reached near noon of each day. Just prior to day 7, the second lamp was turned on for the intermediate condition (increased load current).

As is seen in the SOC-versus-time plot (Figure 4-18b), the battery was fully charged during portions of several consecutive days, with the overcharge accommodated by internal recombination of hydrogen and oxygen. Towards the end of the period, cloudy weather decreased the output of the array, and the SOC pressure trended down slightly.

Intermediate Load

For the "intermediate" condition, the current to the lamps was between 3 and 4 A (Figure 4-19a), with a decreasing trend at night since the battery voltage was dropping. The SOC cycled between about 40% and 90% (Figure 4-19b).

Heavy Load

With the "heavy" load, the lamps were on for a longer period of time; therefore there was less charging of the battery (Figure 4-20a). The SOC was less than 0% (Figure 4-20b), indicating that the hydrogen pressure had dropped below 60 psig, the value corresponding to a battery voltage of 6.0 V (1.0 V/cell).

Figure 4-21a is a bar chart for day 2 through day 7 with the "heavy" load showing the daily capacity flow. Current from the array is positive. Into the load it is negative, and the net output of the battery is positive. While the battery net is relatively small, Figure 4-21b, showing the daily amp-hour flow into and out of the battery, demonstrates that the battery played a very active role in the system.

Test Conclusions

Because the nickel/hydrogen battery is tolerant to both overcharge and overdischarge, it was not necessary to use a controller in the

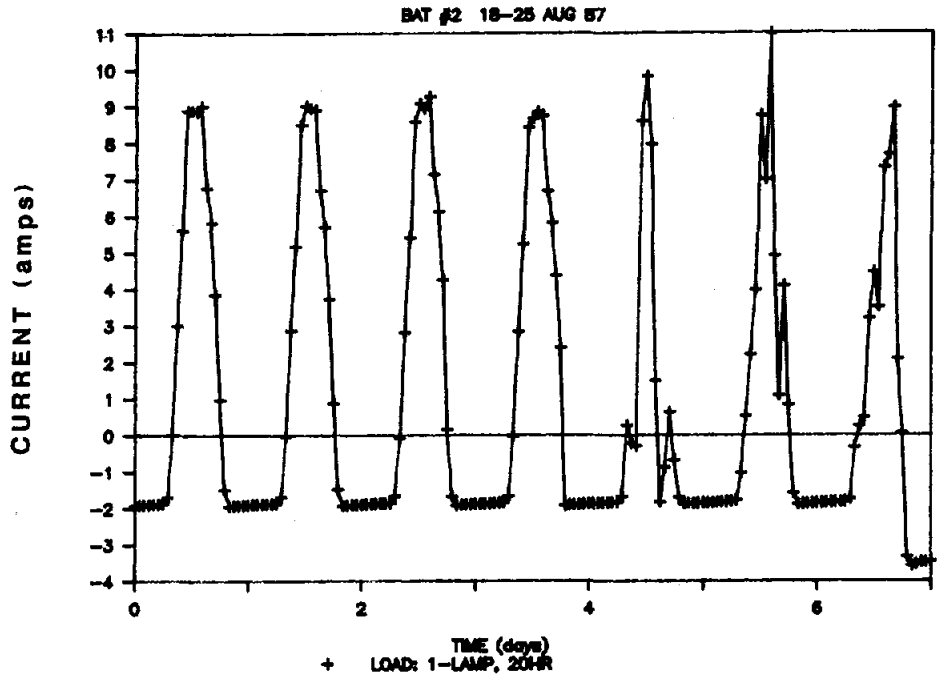

a. Current Versus Time

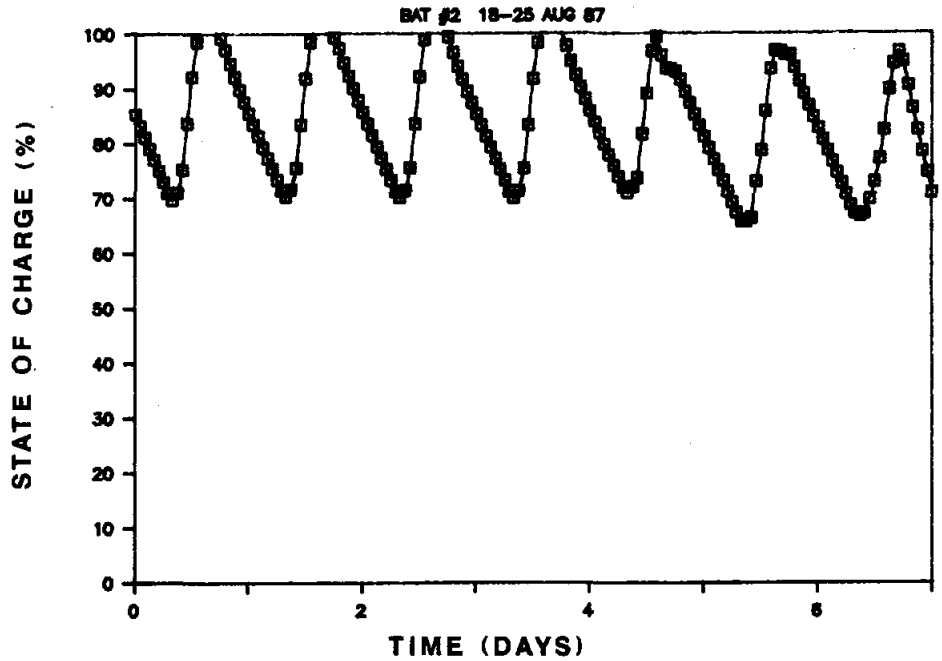

b. SOC Versus Time

Figure 4-18. Current and SOC Versus Time (Light Load)

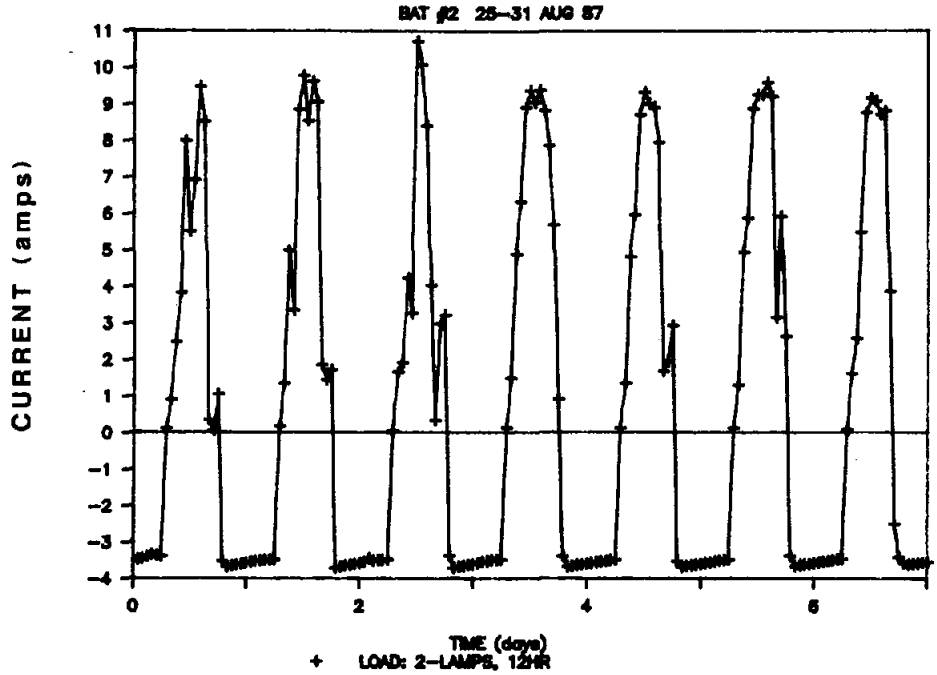

a. Current Versus Time

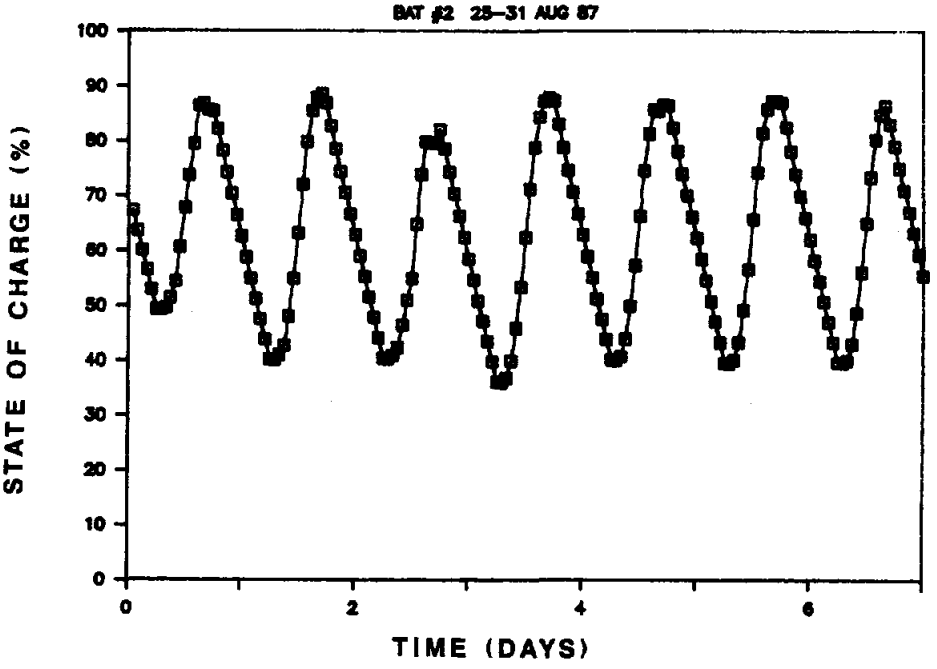

b. SOC Versus Time

Figure 4-19. Current and SOC Versus Time (Intermediate Load)

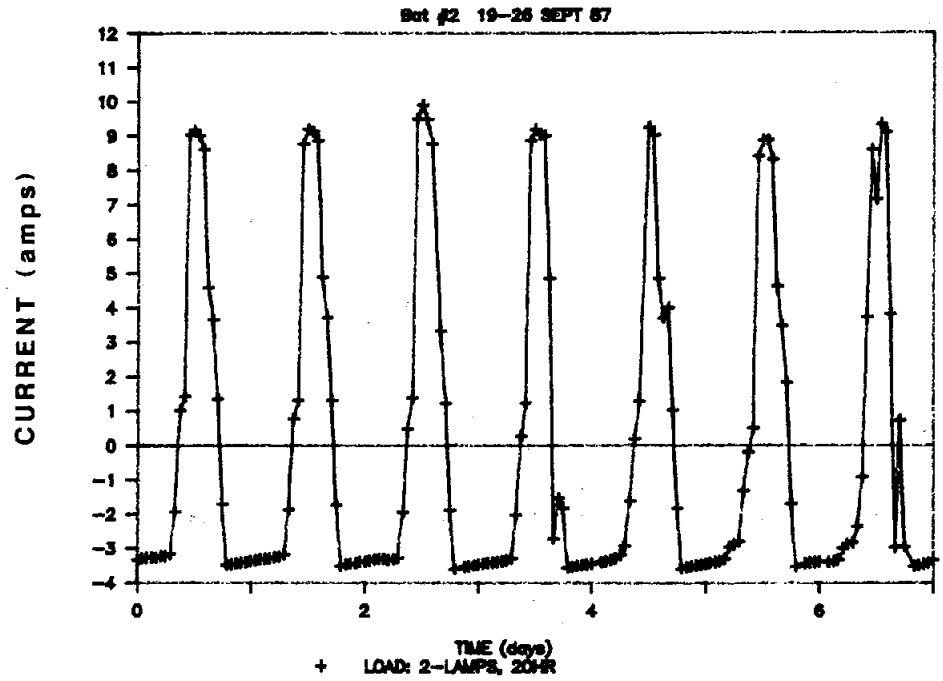

a. Current Versus Time

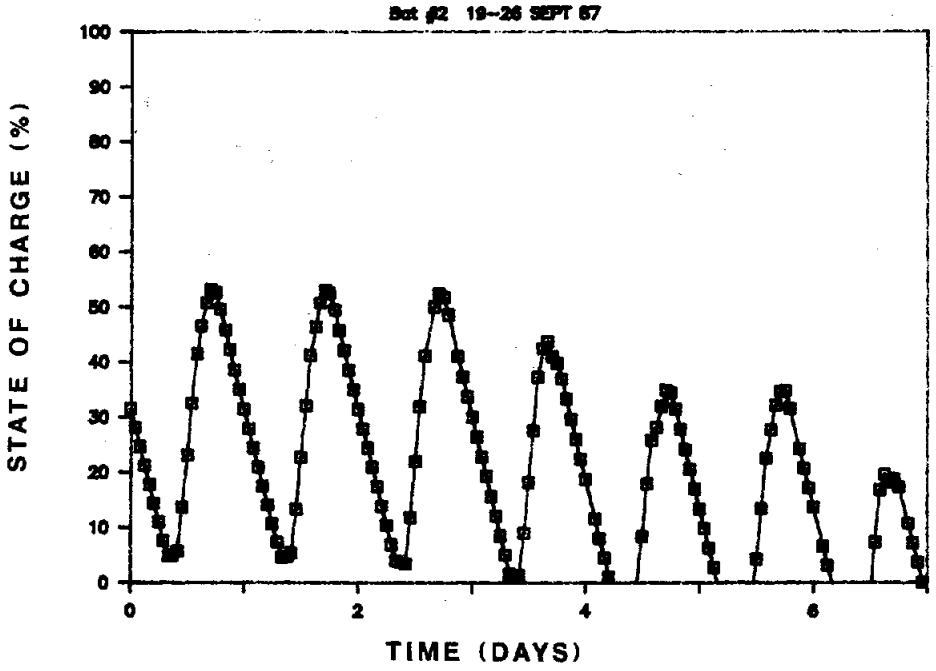

b. SOC Versus Time

Figure 4-20. Current and SOC Versus Time (Heavy Load)

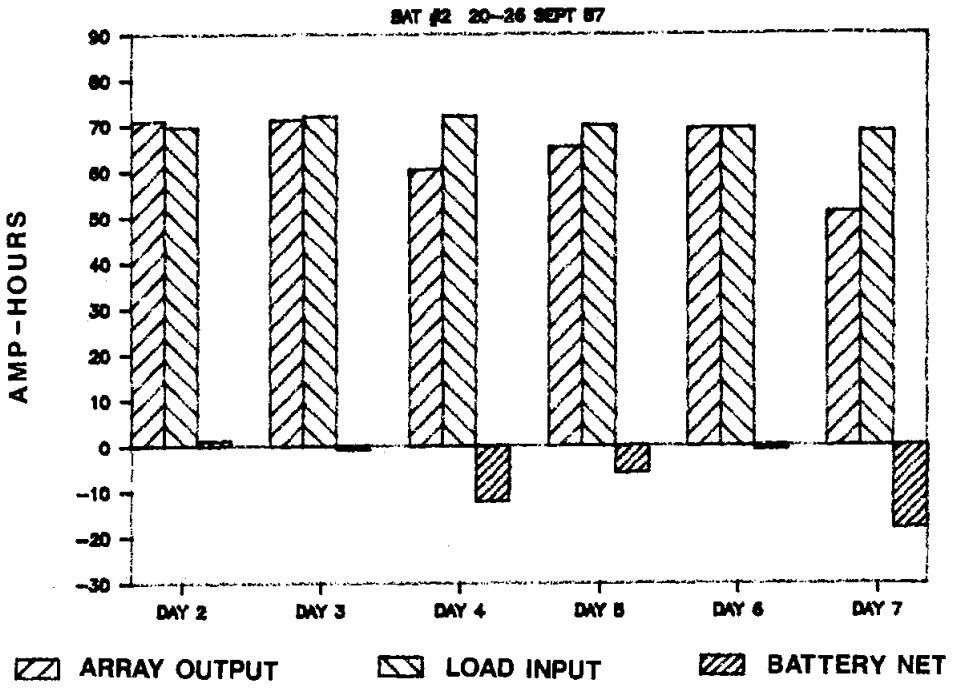

a. Array, Load, and Battery (Net)

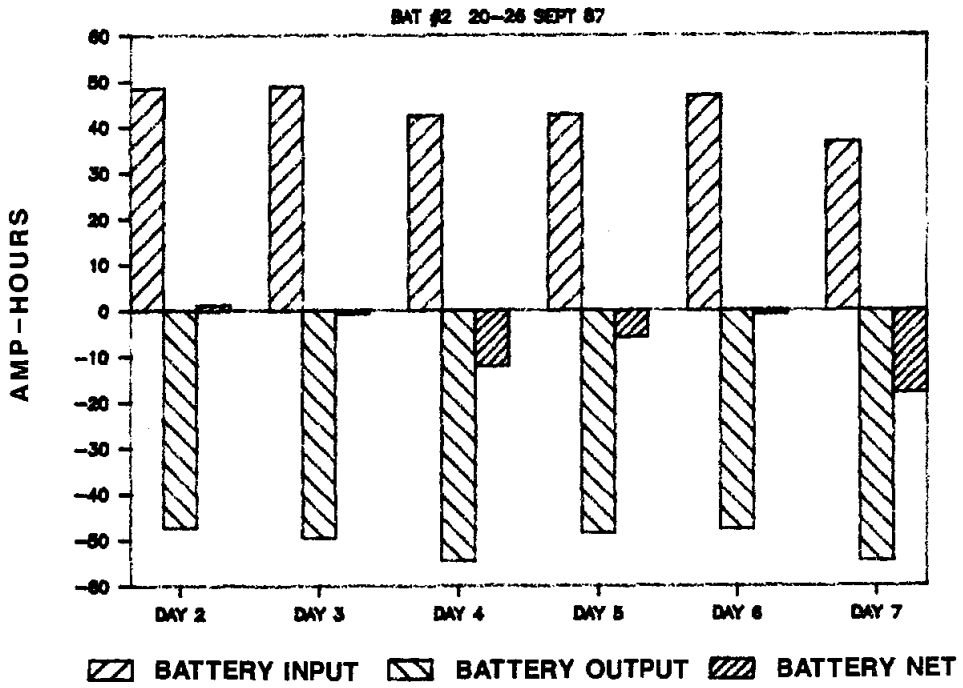

b. Battery 2 Input, Output, and Net

Figure 4-21. Daily Capacity Flow (Heavy Load)

system. Overcharge is accommodated by the internal recombination of oxygen and hydrogen. If it would be desirable to do so, the battery could be disconnected based on its SOC. In fact, the hydrogen pressure could be used for shedding the less critical loads.

Systems Evaluation at SNL

Two field test projects were conducted by SNL during 1987. The first involved Exxon's PV-20 (20-kWh) zinc/bromine battery located at the SNL Photovoltaic Advanced Systems Test Facility (PASTF). The second field test operation involved a wind/battery/utility system operated by Hawaii Natural Energy Institute (HNEI). The HNEI project, carried out on the island of Hawaii, is a cooperative effort between private industry, the State of Hawaii, the University of Hawaii, and SNL.

Progress made on the PASTF and HNEI projects is discussed below. A summary of this work is found in Table 4-19.

PASTF Tests

The goal of the PASTF project was to evaluate how the Exxon 20-kWh zinc/bromine battery (Figure 4-22) performs when it is interfaced to a photovoltaic array. In addition, various other experiments, shown in Table 4-20, were performed on the battery. The average efficiencies for each test are also displayed in this table. Parametric and stand-loss tests shown on this table were run in 1986, and the results were discussed at length in the previous annual report (*ETD Report for 1986*, pages 124 through 126). Because of safety issues at the test site, the battery was only operated during working hours,

Table 4-19. Summary of Systems Evaluation at SNL

PASTF Tests	Tests conducted on a 20-kWh zinc/bromine battery interfaced to a photovoltaic array: • no decline in performance when power-conditioning interface removed; • only slight decrease in coulombic efficiency when load varied on discharge; • efficiencies comparable to laboratory-scale zinc/bromine batteries. After 186 cycles (20 months), battery to be removed from test because of declining performance; posttest analysis to be performed.
HNEI Tests	Problems with voltage fluctuations and phase shifts caused by wind machines overcome. Disconnect capability from utility added. WEBS model adapted to Kahua Ranch; preliminary test run of the model performed.

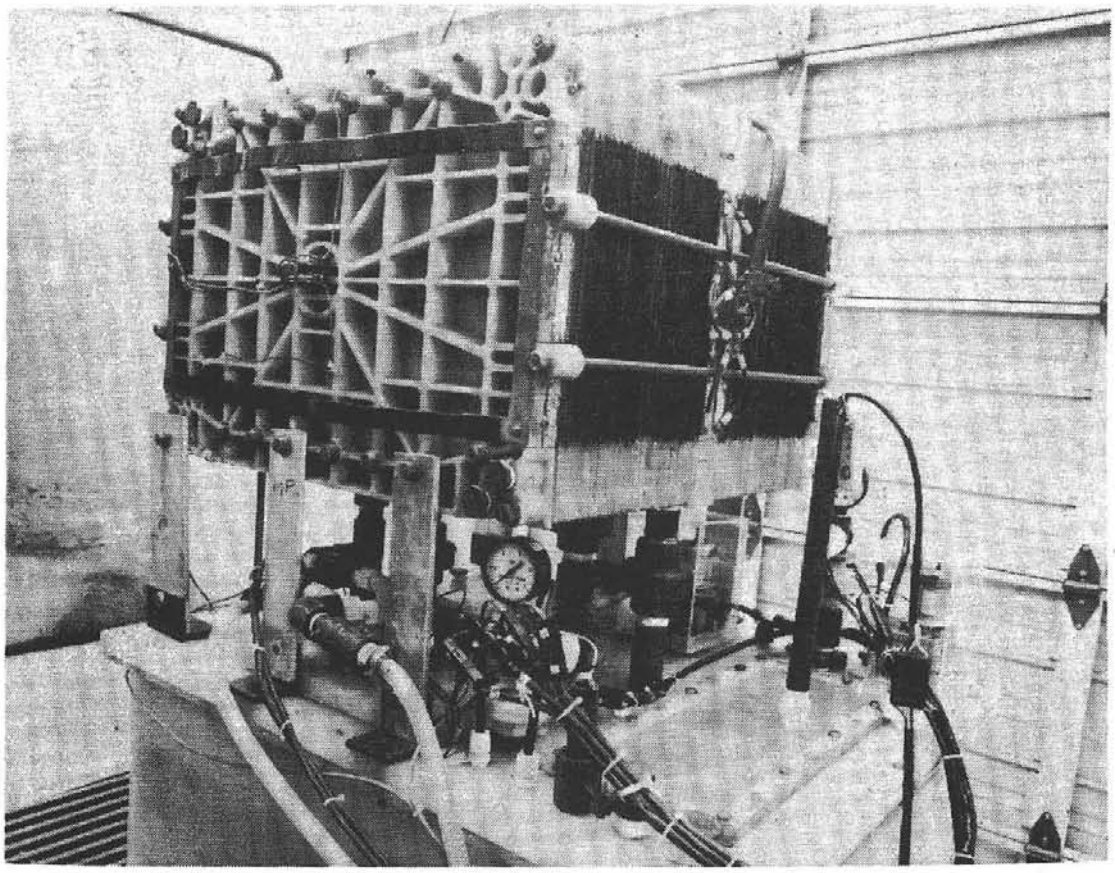

Figure 4-22. Exxon PV-20 Zinc/Bromine Battery

and thus only one cycle per day could be achieved.

The important tests run in 1987 consisted of interfacing the battery to the photovoltaic array with and without the power-conditioning Abacus interface. This interface was primarily used to keep the output of the array constant during cloudy periods when the array output fluctuated. The efficiencies with and without the interface are close to those of the baseline capacity cycles. This demonstrates that a zinc/bromine battery could be interfaced directly to a photovoltaic array, thus eliminating the expense of an interface.

Finally, one of the last sets of experiments run on the battery consisted of a constant charging regime in which the load was varied on discharge. There was only a slight decrease in coulombic efficiency when the battery was operated under these conditions.

At this point in battery life, the frequency at which acid was being added was steadily increasing, and the battery resistance was also increasing. From past experience, these observations indicated that the battery was nearing end-of-life. A few additional baseline capacity tests were performed, and the battery was finally removed from test. Figure 4-23 plots of the efficiencies and energy output of the zinc/bromine battery. A gradual decrease in the efficiencies over the life of the battery is evident.

In summary, the Exxon 20-kWh zinc/bromine battery was on test at SNL for 20 months, and during that time 186 cycles were run. This was the first advanced battery to be

Table 4-20. Test Regime for Exxon PV-20 Battery

Cycle Type	No. of Cycles	Average Efficiencies (%) Coulombic	Voltaic	Energy
Exxon Tests	35	68 ± 6	80 ± 3	55 ± 4
Baseline	87	77 ± 5	73 ± 4	57 ± 6
Baseline Without Zinc Stripping	11	76 ± 5	69 ± 6	52 ± 7
Stand-Loss With Cleanout	5	61 ± 17	70 ± 5	43 ± 13
Stand-Loss With Pumps On	3	70 ± 3	71 ± 1	50 ± 3
Parametric	8	81 ± 2	79 ± 2	64 ± 2
Parasitic Energy Consumption	4	76 ± 2	74 ± .3	56 ± 1
PV/Battery With Abacus Interface	18	77 ± 3	78 ± 2	60 ± 3
PV/Battery Without Abacus Interface	6	76 ± 2	75 ± 1	57 ± 2
Constant Charge/Variable Discharge	4	74 ± 3	73 ± 1	54 ± 3
Short Cycles	4	--	--	--

interfaced to a photovoltaic array, and the results were favorable. The efficiencies for PV-20 were comparable to those of the smaller laboratory zinc/bromine batteries and showed that scaling up in battery size was not a factor. This battery did, however, require extensive manpower to operate and maintain. A posttest analysis on this battery will be conducted in the near future.

HNEI Tests

At HNEI, a considerable amount of time was spent analyzing voltage waveforms from the utility grid. Kahua Ranch, where this project is located, experiences significant voltage fluctuations and phase shifts that occur when wind machines from a nearby wind farm come on line. This in turn caused problems with the inverter associated with the project. With the additional data acquisition equipment and the help of Hawaiian Electric Company, these problems were finally solved. A disconnect capability was also added to allow Kahua Ranch to operate independently of the utility grid.

Capacity tests were performed on the gel-cell lead-acid battery and the results were close to the manufacturer's specifications. Tests are planned early next year during low-wind, average-wind, and high-wind conditions to characterize the interaction of the wind-energy/battery-storage interface conditions.

The wind energy battery storage model (WEBS) was adapted to the Kahua Ranch site with the annual hourly wind data from Kahua Ranch (based on the best typical average monthly data from the Kahua site from five years of

wind data, 1982 through 1986). A typical hourly load was used from Kahua for a stand-alone or small-utility system example. Annualized hourly load data from Hawaiian Electric Company will also be added, using a typical weekday and weekend day for winter, summer, and fall/spring. The performance curve for a 10-kW and a 17-kW Jacobs wind turbine generator also was added.

A preliminary test run of the model that used strategy 1, which involved winds at the 30-ft level, was performed. The model also took into account the use of a 125-kWh battery storage system and three 20-kW Jacobs wind machines. The results indicate that the wind machines operate 77.5% of the year. Only 17.7% of the year is the wind speed below the cut-in speed of the turbine, and 4.75% of the time the wind speed is above the cut-out speed of the turbine.

The total energy demand of Kahua Ranch is approximately 215,000 kWh/y. Wind turbines provide 65% of the demand: 5% comes from batteries, and 30% is from the utility. The utility output to load is 67,815 kWh/y, and is used 100% for the load (no utility output for charging the batteries). Total energy supplied by the wind turbines annually is 289,677 kWh, with 53.4% going to the load and 7.2% to the batteries. The remaining 39.4% was exported. Total battery output is 15,076 kWh/y. The number of battery cycles is 133 (mid-capacity) and 150 (energy summation). Review of the drafts for the final reports on both the computer model and the field test project are forthcoming.

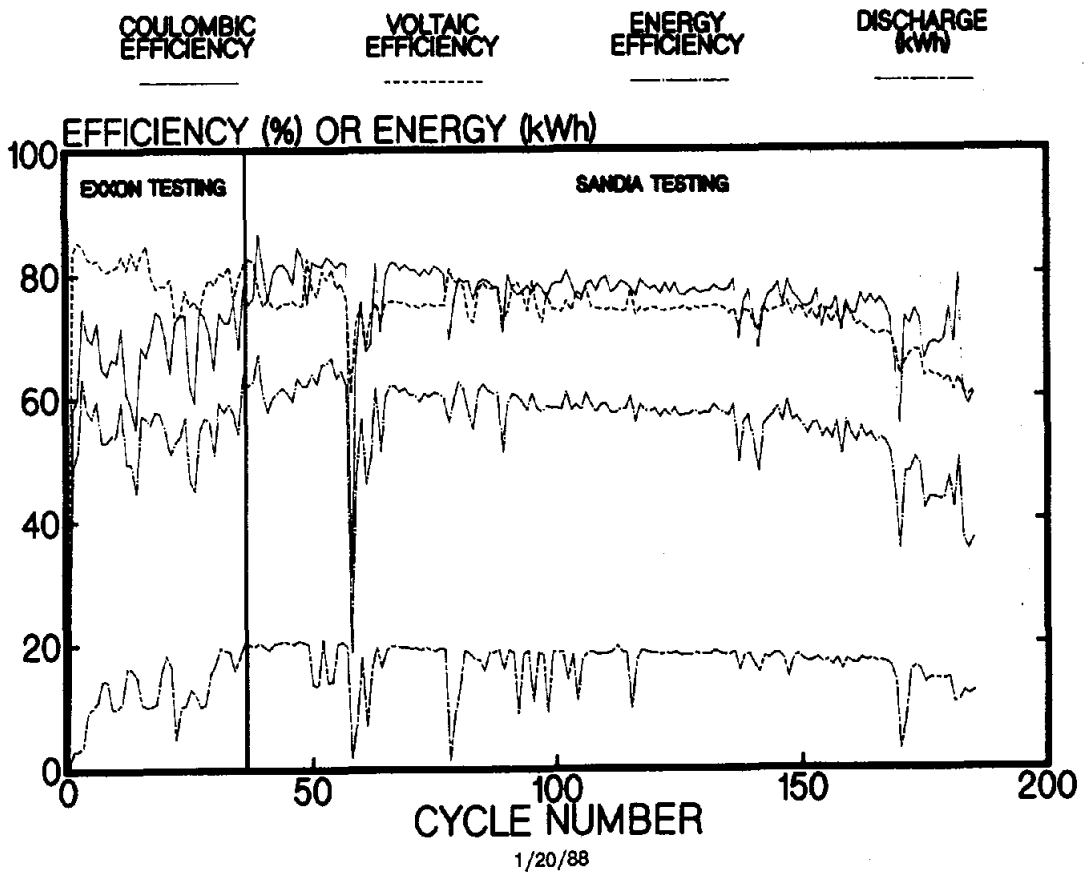

Figure 4-23. Efficiencies and Energy Output versus Cycle Number for the Exxon PV-20 Zinc/Bromine Battery

Chapter 5. Battery Technology Improvement

Introduction

The objective of the Technology Improvement element is to investigate and solve specific problems encountered during the development of advanced secondary batteries. The following three criteria are used to select and continue tasks associated with this element:

- the prime contractor does not have the resources to adequately address the problem;
- the solution to the problem must be important to the continued development of the technology, and therefore, useful to the prime contractor;
- adequate resources must be available to allow a timely contribution to be made.

The majority of the tasks under this element will be performed at SNL. As such, secondary benefits provided by this element to the ETD program include a better and more active understanding of the obstacles facing each technology. This in turn allows more effective program management, plus a means to utilize the wide range of excellent capabilities and resources at SNL directly in the technology development process. The number and size of these tasks is limited to ensure that proper perspective is maintained with respect to the primary technology-development goal of the ETD program. Finally, nonessential overlap with Technology Base Research (TBR) activities is minimized because a close relationship is maintained with the industrial partner.

This element was established as part of the ETD program in 1985. During 1987, the element had five active tasks: two supporting zinc/bromine battery development and three supporting the sodium/sulfur technology. These tasks are as follows:

- Advanced Membrane Development for Zinc/Bromine Batteries (previously for zinc/redox batteries--see below);
- Durability of Zinc/Bromine Materials (continued from 1986);
- Failure Analysis of the Beta"-Alumina Electrolyte (continued from 1986);
- Component Stress During Freeze/Thaw Cycling of Sodium/Sulfur Cells (continued from 1986);
- Improved Chromium Plating of Sodium/Sulfur Cell Containers (a new sodium/sulfur task).

The advanced membrane development activity supporting the zinc/redox program during 1986 was switched to zinc/bromine because of three factors:

- the zinc/redox program was canceled at the end of the year;
- the work was immediately applicable to the zinc/bromine technology;
- a need exists to significantly improve zinc/bromine membrane performance.

Advanced Membrane Development for Zinc/Bromine Batteries

The concentration of free bromine in the positive electrolyte of zinc/bromine batteries is reduced by addition of quaternary ammonium bromide salts. The resulting low free-bromine concentration in these batteries allows the use of relatively inexpensive microporous separators rather than the more expensive ionic membranes, which are permselective. Even though the concentration of bromine is quite low, sufficient quantities of bromine permeate through the separator and react with deposited zinc to adversely affect the coulombic efficiency of the system.

Furthermore, thermal management problems are created because of the heat generated by the exothermic reaction of bromine with the zinc electrode, which results in the need for auxiliary cooling.

The objective of this study was to improve the selectivity performance of microporous separators by impregnating and/or coating them with cationic polymers. Such treatments should bring about a reduction in the rate of bromine transport by two mechanisms:

- repulsion of the negatively charged bromine complexes by similarly charged groups in the polymer
- physical closure of some fraction of the pores.

If the ion exchange capacity (IEC) of the impregnant is sufficiently high, the detrimental increase in ionic resistivity should be minimal.

General requirements of the cationic impregnant are:

- stability in the electrolyte over long time periods
- solubility in solvents that are capable of wetting the separator
- insolubility in the supported zinc-bromide electrolyte.

Two cationic polymers have been studied. Sulfonated polysulfone resins (SPS), developed in earlier programs for use in the zinc/redox battery, satisfied the above requirements and were the chief impregnant that was investigated. Another impregnant that was evaluated was polyacrylic acid (PAA). The chief advantages of PAA is its ready availability and low cost. The current status of this technology-improvement effort is summarized in Table 5-1 and is discussed below.

Membrane Preparation and Evaluation

The microporous separators used in this study were 0.635-mm thick sheets of Daramic and SF-600 and several thin (0.033 to 0.051 mm) microporous polyolefin films designated PM-13E, PMP-15W, and PM-20E. Daramic is a silica-filled polyethylene-based separator available from W. R. Grace Co., and SF-600 is a competitive separator of the same type made by Asahi Company, a Japanese firm. The polyolefin films were obtained from RAI Research Corporation.

Impregnation of these separators by SPS resins was achieved by immersion in solutions of SPS in dimethylformamide (DMF) followed by drying to remove the DMF. The effects of multiple immersions, vacuuming, and heating during the immersion step and of the concentration of SPS in the impregnating solution on membrane properties were investigated.

Membranes were also prepared using polyacrylic acid (PAA) as the impregnant. These membranes were prepared by immersion techniques similar to those described above, except water was used as the immersion solvent instead of DMF. In addition, some PAA membranes were prepared by plasma polymerization of acrylic acid in the presence of the separator.

Both impregnated and unmodified separators were pretreated by successively soaking them in a synthetic, aqueous zinc-bromide electrolyte at 100% state-of-charge (SOC) and a 0%-SOC electrolyte for various time periods. These pretreatments served to wet the membrane or separator to simulate battery conditions. The area resistivity was measured using an RAI impedance meter (Model 2401) in 0%-SOC electrolyte.

To determine bromine transport rates, impregnated and unmodified separators were clamped into a diffusion cell consisting of two compartments. The catholyte, a two-phase mixture of a 100%-SOC ammonium-chloride-supported electrolyte containing 2M bromine, was added to one compartment and 100%-SOC ammonium chloride anolyte was added to the other compartment. The bromine permeation rates were calculated from the bromine concentration in the anolyte after four hours. Both the anolyte and catholyte were stirred during this test.

The stability of SPS was determined by monitoring the modulus and weight changes that occurred when films of SPS were exposed to the upper (aqueous) phase of a 100%-SOC catholyte for three weeks at 50°C.

Table 5-1. Summary of Advanced Membrane Development for Zinc/Bromine Batteries

Membrane Preparation and Evaluation	
	Separators studied: • 0.635-mm Daramic (silica-filled polyethylene-based separator, manufactured by W. R. Grace) • 0.635-mm SF-600 (silica-filled polyethylene-based separator, manufactured by Asahi) • 0.033 to 0.51-mm microporous polyolefin films manufactured by RAI Research Corporation.
	Membrane impregnation by exposure to sulfonated polysulfones (SPS) and polyacrylic acid (PAA).
Results	
SPS Impregnation	
Daramic and SF-600	Bromine permeation rate reduced by as much as 100 fold.
	Area resistivity increased by as much as 6 fold.
	Optimum balance of properties achieved with high-temperature vacuum impregnation of Daramic.
	Impregnation process affects the properties of Daramic more than those of SF-600.
Thin Microporous Separators	Very low resistivities (less than 1 $\Omega \cdot cm^2$), but bromine permeation unacceptably high.
	Further work planned to increase SPS content and optimize membrane thickness.
Membrane Stability	After three weeks in 50°C electrolyte, SPS membranes showed • no changes in weight or chemical structure • ≈15% increase in modulus.
PAA Impregnation	
	PAA-impregnated Daramic yields unacceptably high area resistivities, and PAA not completely insoluble in the electrolyte.
	Plasma polymerization of acrylic acid yields insoluble coatings, but not without loss of ion-exchange capacity.

Results

SPS-Impreganted Membranes

Daramic and SF-600. Typical data showing the effect of impregnating Daramic and SF-600 with various processes and a 20% DMF solution of SPS in the acid form on the important electrochemical parameters, area resistivity and bromine transport rate, are summarized in Table 5-2. It is apparent from these data that impregnating microporous separators with SPS reduced the bromine permeation rate by factors of up to 100 and increased the area resistivity by factors up to only six.

Processing differences had an effect on the resultant properties. When the separators were impregnated under vacuum at room temperature, the increase in area resistivity was less, but the reduction of the bromine permeation rates was also less. A somewhat better balance of properties was achieved when the vacuum impregnation was carried out at elevated temperatures. For example, at 90°C, the bromine transport rate decreased appreciably and there was no significant change in area resistivity.

In a study in which the concentration of SPS in the impregnating solution was varied from 5% to 20%, greater improvements in the electrochemical properties were realized with Daramic than with SF-600. Whereas only a 32% decrease in the bromine permeation rate was obtained with SF-600 when the concentration of SPS in the impregnating solution was increased from 5% to 20%, a 56% decrease was attained with Daramic under the same conditions. Furthermore, greater percentage increases in area resistivity were incurred with SF-600 as opposed to Daramic. The percentage increases in area resistivity for Daramic and SF-600 were 30% and 65%, respectively.

Thin Microporous Separators. Attempts were made to make membranes with lower area resistivities by the impregnation of thin (0.033-mm to 0.051-mm) microporous separators with SPS in a sodium form. The results of this effort are summarized in Table 5-3. Although the area resistivities of these impregnated separators were less than 1 $\Omega \cdot cm^2$, the bromine transport rates were unacceptably high. Further work along these lines is planned to (1) increase the SPS content; and (2) optimize membrane thickness. One possible problem with these very thin membranes might be that they were not mechanically robust.

Membrane Stability. All of the SPS membranes appeared to be quite stable toward the electrolyte used in the zinc/bromine battery.

Table 5-2. Weight Gain, Bromine Permeation, and Resistivities of Substrate Coated with a High IEC SPS Resin

Substrate	Impregnation Process	Weight Gain (%)	Bromine Permeation Rate (mole $Br_2/(s \cdot cm^2 \times 10^9)$)	Area Resistivity ($\Omega \cdot cm^2$)
W.R. Grace	Control	--	5.24	1.06
	3 x Dip	66.8	0.05	4.95
	Vacuum, RT	41.3	0.73	2.88
	Vacuum, 90°C	44.1	0.23	2.64
SF-600	Control	--	2.30	1.18
	3 x Dip	59.4	0.05	6.96
	Vacuum, RT	31.6	0.29	2.80
	Vacuum, 90°C	39.8	0.03	2.98

Table 5-3. Resistivities and Bromine Permeation Rates of Thin Microporous Separators (Impregnated* and Unimpregnated)

Separator/ Membrane	Percent Weight Gain	Thick-ness (mm)	Area Resistivity ($\Omega \cdot cm^2$)	Bromine Permeation Rate (mole $Br_2/(s \cdot cm^2 \times 10^9)$)
PM-13E (Control)	--	0.033	0.127	13.5
PM-13E (Impregnated)	27	0.033	0.664	5.6
PMP-15 (Control)	--	0.038	0.137	17.6
PMP-15 (Impregnated)	19	0.038	0.789	6.4
PM-20E (Control)	--	0.051	0.185	10.4
PM-20E (Impregnated)	31	0.051	0.517	11.9

* SPS (sodium form)

After exposure to the electrolyte at 50°C for three weeks, no changes in weight or chemical structure occurred. A slight, but significant (≈15%), increase in the modulus was observed. The film, however, was not embrittled by the aging treatment.

PAA-Impregnated Membranes

Membranes made by impregnating Daramic with polyacrylic acid (PAA) were unsatisfactory. Area resistivities were unacceptably high and PAA was not completely insoluble in the electrolyte. It was discovered that insoluble coatings could be made by plasma polymerization of acrylic acid; however, these coatings lost a considerable fraction of their ion-exchange capacity in the plasma. Future work using plasma polymerization will focus on more readily polymerizable monomers such as methacrylic acid.

Durability of Zinc/Bromine Materials

Flow frames for Energy Research Corporation's zinc/bromine battery are fabricated from polyvinyl chloride (PVC), a widely used thermoplastic that is inexpensive and easy to mold. The flow channels in these frames are in continuous contact with a bromine-containing electrolyte. Though it is well known that bromine

is chemically aggressive, its effect, as a component in an aqueous electrolyte, on PVC was not understood.

The purpose of the current study is to characterize the degradation processes that occur when PVC is exposed to the electrolyte used in zinc/bromine batteries. Ultimately, the obtained information should allow lifetime estimates to be made. Two B. F. Goodrich formulations, designated PVC-1 and PVC-4, were studied. PVC-1 is the baseline material, and PVC-4 is a new formulation developed specifically for battery applications.

A specific objective was to answer the following questions:

- Does oxidation or bromination, or both, take place?
- Does bromine penetrate into the sample and, if so, how far?
- How are the mechanical and morphological properties affected?
- Are there differences in stability between PVC-1 and PVC-4?

The 1987 results from this activity, summarized in Table 5-4, are discussed below.

Test Conditions

Compression-molded samples of PVC-1 and PVC-4 were exposed at 60°C for 18 weeks to an aqueous bromine-containing electrolyte consisting of 0.5M zinc bromide ($ZnBr_2$), 1.5M zinc chloride ($ZnCl_2$), 2M potassium bromide (KBr), and 100 g/l bromine. The elevated temperature was used to accelerate the aging process. In addition to monitoring the dimensional and weight changes of the aged and control samples of PVC-1 and PVC-4, these samples were characterized by the following analytical techniques:

- Fourier transform infrared analysis (FTIR)
- electron microprobe analysis (to measure bromine, zinc, and potassium concentrations as a function of depth)
- scanning electron microscopy (SEM)
- modulus profiling (tensile modulus as a function of depth)
- laser Raman spectroscopy
- emission spectroscopy
- energy dispersive X-ray analysis
- gel permeation chromatography (GPC) (to determine molecular weight).

Results

Sorption of Electrolyte

Exposure to the bromine-containing electrolyte significantly increased sample weight and thickness. PVC-1 was more severely affected than PVC-4: the weight gain of PVC-1 was 99% versus 36% for PVC-4, and the thickness of PVC-1 increased by 36% versus only 6% for PVC-4. One possible explanation for these physical changes is sorption of the electrolyte by the PVC.

The bromine profile for PVC-1 indicated that bromine permeated the entire sample and its sorption was high (22.5 wt.%). In contrast, the concentrations of zinc and potassium were relatively low, with zinc confined to the edges of the samples. These results indicate that sorption of zinc and potassium halides in the electrolyte contribute only slightly to the mass gain of PVC-1.

The bromine profile for PVC-4 was markedly different from that of PVC-1. Zinc and potassium profiles were similar. For PVC-4, bromine did not completely permeate through the sample; about one-fifth of the sample in the center region was practically bromine-free. The small amount of bromine in the center of aged PVC-4 was also present in unaged samples of PVC-4.

Table 5-4. Summary of Analyses of Durability of Zinc/Bromine Materials

Test Conditions	
	PVC-1 and PVC-4 aged for 18 weeks in a 60°C bromine-containing electrolyte.
Results	
Sorption of Electrolyte	Significant weight gains and increases in thickness (more pronounced in PVC-1 than in PVC-4) attributed to sorption of electrolyte.
	PVC-1: Significant bromine permeation throughout sample; $ZnBr_2$, $ZnCl_2$, and KBr permeation low.
	PVC-4: incomplete bromine permeation; center of sample practically bromine-free.
Inorganic Additives	PVC-1: calcium, barium, and lead.
	PVC-4: titanium.
Chemical Structure	Virtually no bromination, bromine addition, or dehydrochlorination in PVC-1.
	Loss of methylene groups and increase in carbonyl functionality and absorbed water.
	Lower molecular weight in reacted areas caused by chain cleavage.
	Some crosslinking observed in PVC-4.

Inorganic Additives

Though the reasons why PVC-1 and PVC-4 respond differently toward the electrolyte are not known, the variation in behavior may be related to minor differences in composition. Emission spectroscopy revealed differences in the ash contents of PVC-1 and PVC-4. The predominant elements present in PVC-1 were calcium, barium and lead. No barium or lead was detectable in PVC-4, but relatively large quantities of titanium were observed.

Chemical Structure

FTIR spectra of aged and unaged samples were measured to determine the effect of aging on the chemical structure of the polyvinyl chloride component of PVC-1 and PVC-4. Differences caused by degradation were observed. Aged samples suffered a loss of methylene groups (negative peaks at 2925, 2850, and 1460 cm^{-1}) and an increase in carbonyl functionality (positive peak at 1735 cm^{-1}). Oxidative degradation probably increased the

Table 5-4. Summary of Analyses of Durability of Zinc/Bromine Materials (Continued)

Morphology	1-μm to 10-μm voids and $PbBr_2$ and $BaSO_4$ crystals on fracture surface of aged PVC-1.
Mechanical Properties	90% decrease in tensile modulus over thickness dimension of aged PVC-1.
	Lower modulus in outer one-fifth of PVC-4; center of sample modulus higher than unaged sample.
Conclusions	
	Although degradation is accompanied by considerable loss of mechanical properties, integrity of samples maintained. Additionally, PVC is more stable than polyolefin thermoplastics toward bromine-containing electrolytes.
	PVC-4 is more stable than PVC-1; TiO_2 may have contributed to PVC-4's enhanced stability.
	Degradation processes that occur when PVC is exposed to bromine-containing electrolytes include: • oxidative chain cleavage • crosslinking (PVC-4 only) • void formation caused by bromine attack on lead additives (PVC-1 only).
	Bromination of PVC does not occur, possibly because of incorporation of antioxidants.

concentration of carbonyl groups. However, because carbonyl groups were present in the unaged samples, loss of other groups may have caused this concentration increase. The carbonyl groups present in the unaged samples are probably attributable to metal carboxylate salts, which are often added as thermal stabilizers.

Aged PVC contained considerable amounts of absorbed water that could not be removed by thermal-vacuum treatments. Absorbed water was manifested as positive peaks at 3440 and 1630 cm^{-1}. Alcohol groups, which could form via hydrolysis of the carbon-chlorine bonds in PVC, are masked by the presence of absorbed water.

Laser Raman data complement the elemental profiling data. Zinc bromide and zinc chloride were detected in the outer regions of PVC-1 (peaks at 163 and 293 cm^{-1}, respectively), and a band for absorbed bromine was apparent at 310 cm^{-1}. Somewhat surprisingly, peaks in the 500 to 600 cm^{-1} region of the spectrum for carbon-bromine bonds were not found in PVC-1. Also absent were peaks for conjugated double bonds

at 1123 and 1508 cm^{-1}. These results indicate that bromination, bromine addition, and dehydrochlorination did not take place to any appreciable extent. The Raman bands of interest in PVC-4 were at 237, 448 and 617 cm^{-1}. These bands are attributable to the rutile form of titanium oxide.

Both the number-average and weight-average molecular weights of PVC-1 decreased after aging, which indicates that chain cleavage accompanied degradation. Chain cleavage also occurred with PVC-4, but there was also a broadening of the molecular weight distribution. This indicates that some incipient crosslinking processes took place in PVC-4, leading to some components with higher molecular weights.

Morphology

The effect of aging on the morphology of PVC-1 is shown in Figure 5-1, a scanning electron photomicrograph of the fracture surface of the aged PVC-1. The fracture surface is covered with voids ranging from less than one micron to ten microns in diameter. No voids were present in unaged PVC-1. Lead bromide and barium sulfate crystals were detected on the fracture surface of other samples of PVC-1 by energy dispersive X-ray analysis. Morphological studies of PVC-4 will be performed in 1988.

Mechanical Properties

The effect of aging on the mechanical properties of PVC-1 and PVC-4 was determined by modulus profiling, a recently developed technique in which a modified thermomechanical analyzer is used to measure moduli at 0.1-mm intervals across the sample thickness. For the aged PVC-1, the modulus decreased by approximately 90% over the entire thickness dimension. The high scatter in the data (≈35 variation) was attributed to discrete additives of inorganic materials, such as barium sulfate.

The modulus profile for aged PVC-4 was quite different. The modulus of the aged material was low in the outer one-fifth of the sample on both sides. However, in the central core, the modulus of the aged sample was actually higher than that of the unaged sample. These data are consistent with the bromine profiling data that showed no bromine in the central core. Conceivably, the formation of voids caused the rather large decreases in moduli observed in PVC-1 and in the outer regions of PVC-4. Crosslinking may have caused a higher modulus in the central core of the PVC-4.

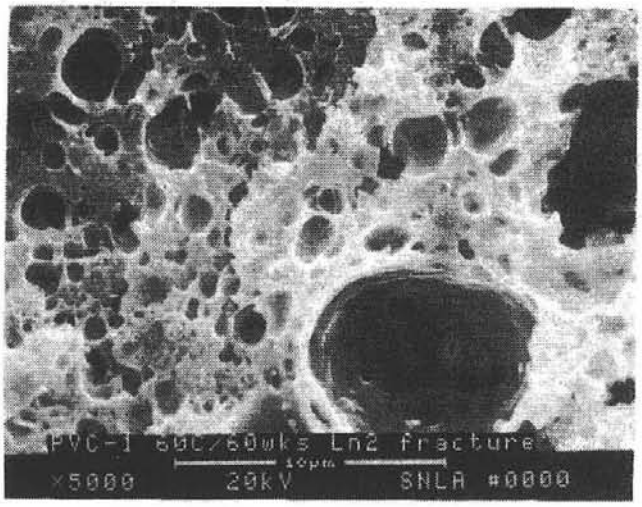

Figure 5-1. Scanning Electron Photomicrograph of the Fracture Surface of PVC-1 After Aging

Conclusions

Without complete knowledge of all the components in PVC-1 and PVC-4, firm conclusions on why the durability of PVC-4 was found to be superior to PVC-1 are not possible. It can only be said that the presence of titanium dioxide in PVC-4 may have contributed to the observed enhanced stability.

The absence of detectable bromination in these PVC formulations requires some explanation. It is well known that bromination occurs by a free radical chain reaction and that it is catalyzed by light. Although the aging experiments were not carried out in the dark, there was no exposure to light once bromine had permeated into the interior of the sample. In

addition, if the manufacturer incorporated antioxidants into these formulations, the active free radicals would be deactivated, which would inhibit bromination. The lack of detectable carbon-bromine bonds also suggests that dehydrochlorination did not occur to any appreciable extent. Otherwise, carbon-bromine bonds would have been formed by bromine addition.

The occurrence of oxidation leading to chain cleavage during aging can readily be rationalized:

- Bromine-oxidized water generated nascent oxygen that then oxidized the PVC. Oxidative degradation proceeded by well-established free-radical chain mechanisms.

- Bromine reacted with water to form hypobromous acid, which is a strong oxidizing agent that attacked PVC. The attacking species was the electronically deficient bromonium ion.

Lead bromide crystals, detected on the fracture surface of PVC-1, arose from direct attack by bromine on lead-containing additives. Lead bromide is partially soluble in the electrolyte and could have crystallized out during the degradation. The combined processes of bromine attack on the lead additive and leaching of lead bromide may be the primary cause of the voids.

Although the mechanical properties of these PVC formulations did deteriorate during aging, the overall mechanical integrity of the samples was maintained. This was not true of polypropylene based polymers that were aged under similar conditions in previous studies (*ETD Report for 1986*, pages 131 and 132). In this respect, PVC formulations appear to be superior to polyolefins.

Based on these degradation studies, the following conclusions can be made:

- PVC is inherently more stable to aqueous bromine electrolytes than polypropylene-based thermoplastics.

- Additives in PVC are attacked and leached during accelerated aging. This may account for the formation of voids and the deterioration of mechanical properties.

- Degradation of PVC is accompanied by chain cleavage. Some crosslinking was observed with PVC-4.

- PVC-4 is more stable that PVC-1.

- PVC is not brominated.

This activity is being continued with emphasis on aging under milder conditions, which will allow lifetime estimates to be made. In addition, studies that take into account the effect of stress on the degradation process have been initiated.

Failure Analysis of the Beta"-Alumina Electrolyte

The objective of this task is to identify mechanisms that cause beta"-alumina electrolyte failure in sodium/sulfur cells. Two subtasks are included:

- Fractographic analysis of electrolytes from actual cells. In this subtask, posttest analysis was performed on two CSPL cells with fractured electrolytes.

- Experimental evaluation of the electromechanical degradation of the beta"-alumina electrolyte. This study, performed by A. Virkar at the University of Utah, supplies fundamental information needed to determine potential mechanisms for electrolyte degradation.

The results obtained during the past year on these activities are presented below and are summarized in Table 5-5.

Electrolyte Fractographic Analyses

Several of the CSPL cells that were sent to SNL failed during testing (see Sodium/Sulfur Testing at SNL, Chapter 4). One of these, CSPL cell 7498, failed after 34 cycles; the other, CSPL cell 7436, failed after 23 cycles. Upon disassembly, both of these cells showed extensive fracturing of the beta"-alumina electrolyte. To

Table 5-5. Summary of Failure Analysis of the Beta"-Alumina Electrolyte

Electrolyte Fractographic Analyses	
Cell 7498 Findings	
	Inner surface was in a compressive state potentially because of sodium deposition.
	The electrolyte was overfired during production, leading to numerous large grains; cracking initiated at large grains on or near the interior surface.
	Sodium pressure caused cracks to propagate during charging.
	Outer surface contained spall fragments, probably caused by pressure in interior cracks that were parallel to surface.
Cell 7436 Findings	
	Crack growth in steps, indicating cracking during charging cycles.
	In regions of poor wetting, tensile stresses were produced and cracks were initiated.
	Cracks propagated because of increased current density and resulting sodium pressure.
Electromechanical Degradation	
	Critical current density to produce degradation is reduced by a factor of ten when compressive stress is applied.
	The electrochemical degradation experiments indicate that the electrolyte in the sodium/sulfur battery may have to be free of both tensile and compressive stresses and that transformation toughening may not be desirable.

identify the cause of the electrolyte failure, extensive examination of the fracture surfaces was performed.

To expose the interior of the cell for examination, a saw-cut was made through the cell perpendicular to its axis just below the beta"-alumina-to-alpha-alumina seal. A second, parallel cut was made to the electrolyte (but not through it) at the bottom of the electrolyte. This cut was annular, which permitted the bottom of the cell to be separated from the rest of the cell. The sodium polysulfide cathode was then dissolved in butyl alcohol. The cylindrical portion of the can came loose from the cathode quite easily, but prolonged soaking was necessary to remove the lower section.

Cell 7498 Findings

Exterior Surface Features. When the surface of the electrolyte in cell 7498 was exposed during removal of the cathode material, an array of cracks was observed in the electrolyte tube wall. During the last stages of removal, fragments of the electrolyte were loosened, and some of these separated from the tube wall. The fragments were roughly lenticular in shape, with a maximum thickness about half the tube-wall thickness. Their general character strongly suggested spall fracture produced by internal pressure in the tube wall.

Figure 5-2 shows the bottom and one side of the electrolyte tube at low magnification after removal of many of the fragments. Most of the fragments from the bottom of the electrolyte came from two cracks that ran across the bottom and intersected (Figure 5-2b). The two intersecting cracks extended through the tube wall with an opening that probably permitted easy egress of the sodium from the anode. Although it is not apparent in the figure, the bottoms of the concavities produced by spalling were darker than the rest of the spalled surface. The discoloration was produced by gray deposits on the surfaces. The spall features were associated with cracks that initiated at the inner surface of the tube and extended through the tube wall. Some of those cracks extended axially to the glass-bond region.

A scanning electron micrograph of the fracture surface of one of the fragments is shown in Figure 5-3. The fragment was the one that came from the spot to the left of arrow E in Figure 5-2b. From the fracture surface features, it is clear that the fracture initiated in or near the large crystal at the lower center of the micrograph (Figure 5-3a). One of the interesting details of this micrograph is the presence of bright spots on the surface of the large crystal and on the nearby surfaces. These spots decrease in size and concentration away from the large crystal and do not appear at all on surfaces of this fragment located closer to the outer surface of the tube. The spots are also clearly associated with the gray discoloration at the bottom of the spall concavities.

Interior Surface Features. To permit examination of the interior surface of the electrolyte tube, the alpha-alumina cap was sawed off at the tube rim. Subsequently, the flange of the cap, which remained attached to the tube after the major portion was sawed off, was split and separated from the tube. The tube was then easily split into two sections along existing cracks approximately on a diametral plane. These sections were very fragile because of cracks extending through them. In the handling during preparation of replicas of the fracture surfaces, they were easily broken into smaller fragments.

As Figure 5-4a shows, the interior surface of the tube showed a pattern of dark-colored, irregularly shaped, elongated features extending to within about 0.5 cm of the rim. In every case, the major cracks through the tube wall extended along these dark bands, and although not all features had a major crack associated with them, there was subsurface cracking along every feature.

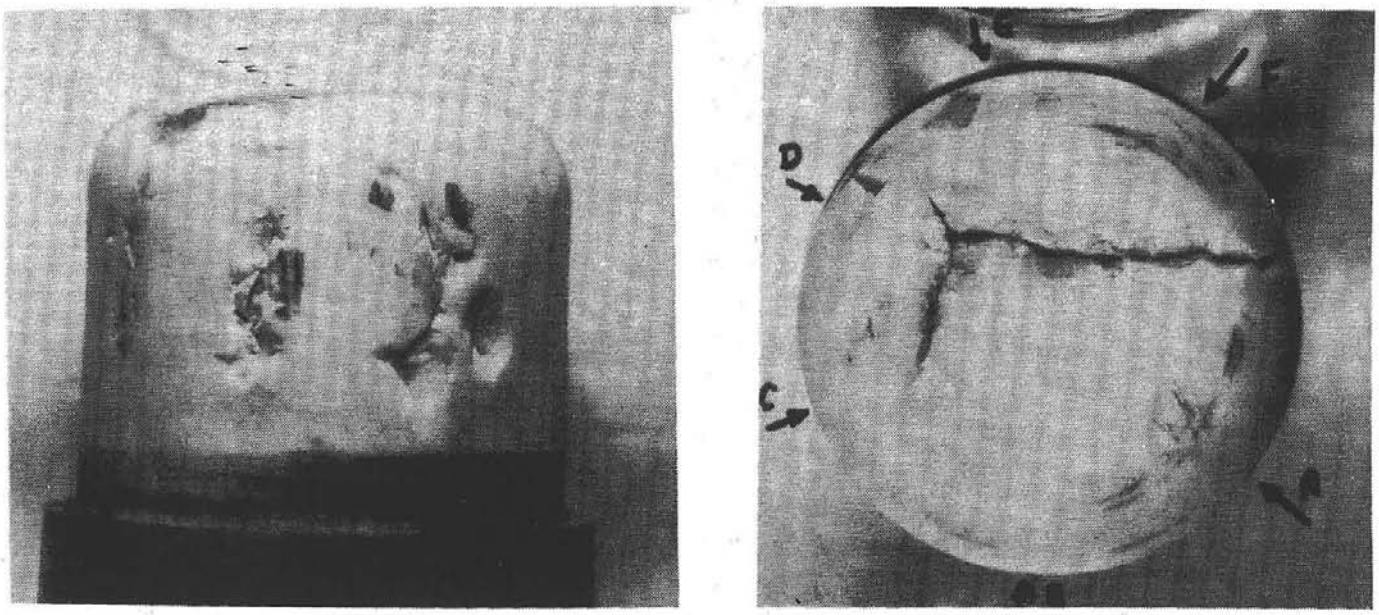

(a) Side View

(b) Bottom View

Figure 5-2. Electrolyte Tube from Sodium/Sulfur Cell 7498

When these dark features and the associated cracks were examined at higher magnification (optically, with light transmitted through the tube wall) it was observed that many of the cracks ran through very large grains that were located just below the tube surface (Figure 5-4b). In only very few cases, these grains actually intersected the surface. Often, the crack nearest a large grain formed a straight line running along the central plane of the long dimension of the grain. Irregular cracks in the fine-grained matrix connected many of these straight-line segments. However, in many instances, these straight crack segments at large grains remained isolated from the rest of the crack structure.

Examination of the fracture surfaces exposed when the tube sections were separated confirmed that all of the cracks in the tube, including those that penetrated through the wall as well as those that appeared only on the interior surface, were initiated at or near the interior surface. In addition, many of the fracture surfaces showed features that indicated that a thin layer of electrolyte at the interior surface was in a compressive stress state during formation of the crack.

To provide some insight into how extra-lattice sodium might be associated with the dark zones and with the cracks, one of the larger fragments of the tube was exposed to a silver nitrate solution. This treatment produced a dark layer, quite uniform in appearance, extending 50 to 70 μm into the interior surface of the tube (approximately the depth of the compressive layer described in the previous paragraph). The outside surface of the tube showed little discoloration except at the cracks. Examination of fracture surfaces revealed thin, dark deposits along cracks sometimes in layers parallel to the tube surface.

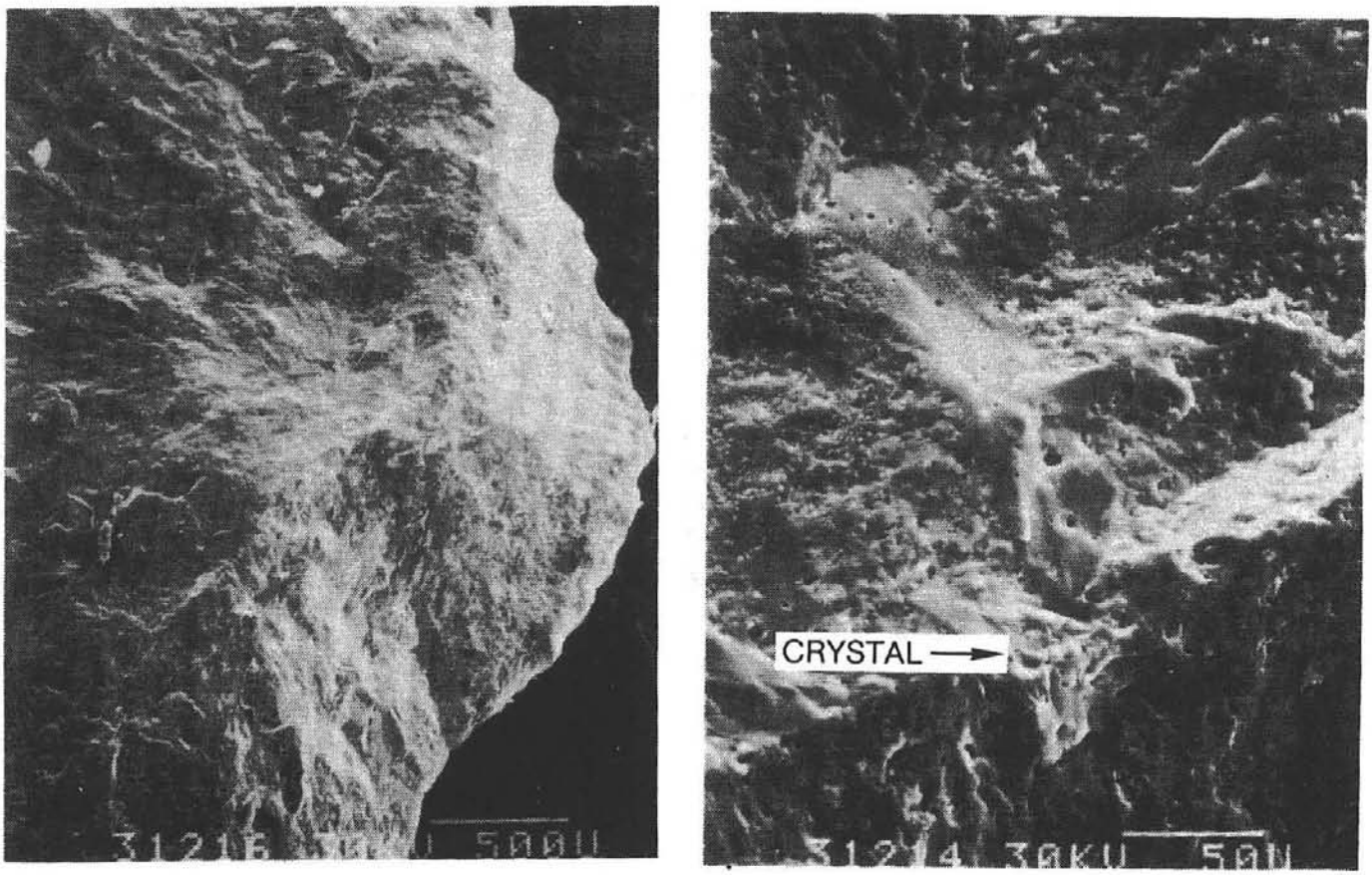

(a) Low Magnification

(b) High Magnification

Figure 5-3. Scanning Electron Micrograph of the Fracture Surface of Spalled Fragment from Sodium/Sulfur Cell 7498. The micrograph in part (b) of this figure is from the center of part (a). This fragment came from the spot to the left of arrow E in Figure 5-2b.

Cell 7436 Findings

Exterior Surface Features. Cell 7436 was the first CSPL cell to undergo post-mortem examination. X-ray examination prior to disassembly had shown no indication of fracture.

Large fragments from the bottom face of the electrolyte came off with the end of the can. A yellow deposit, presumably a sodium sulfide, was found in the anode (sodium electrode) region when this section was removed. Both of the saw-cuts produced some mechanical damage to the electrolyte, including some cracks. However, these cracks were generally easy to distinguish from those that had been present before the post-mortem procedure began.

When the cathode material was removed from the electrolyte, the tube fragmented into pieces with dimensions of several centimeters down to fragments of millimeter size. To obtain a record of fracture surface morphology of the fragments, silicone-rubber replicas were made of many of the surfaces. The fragments were then reassembled so that general information on the sequence of fracture events and on the fracture patterns could be obtained.

Virtually all of the fractures that could not be attributed to the damage induced in post-mortem disassembly initiated at the interior surface of the tube. On some of the fracture surfaces, a series of "arrest lines" produced when the crack stopped and restarted were found.

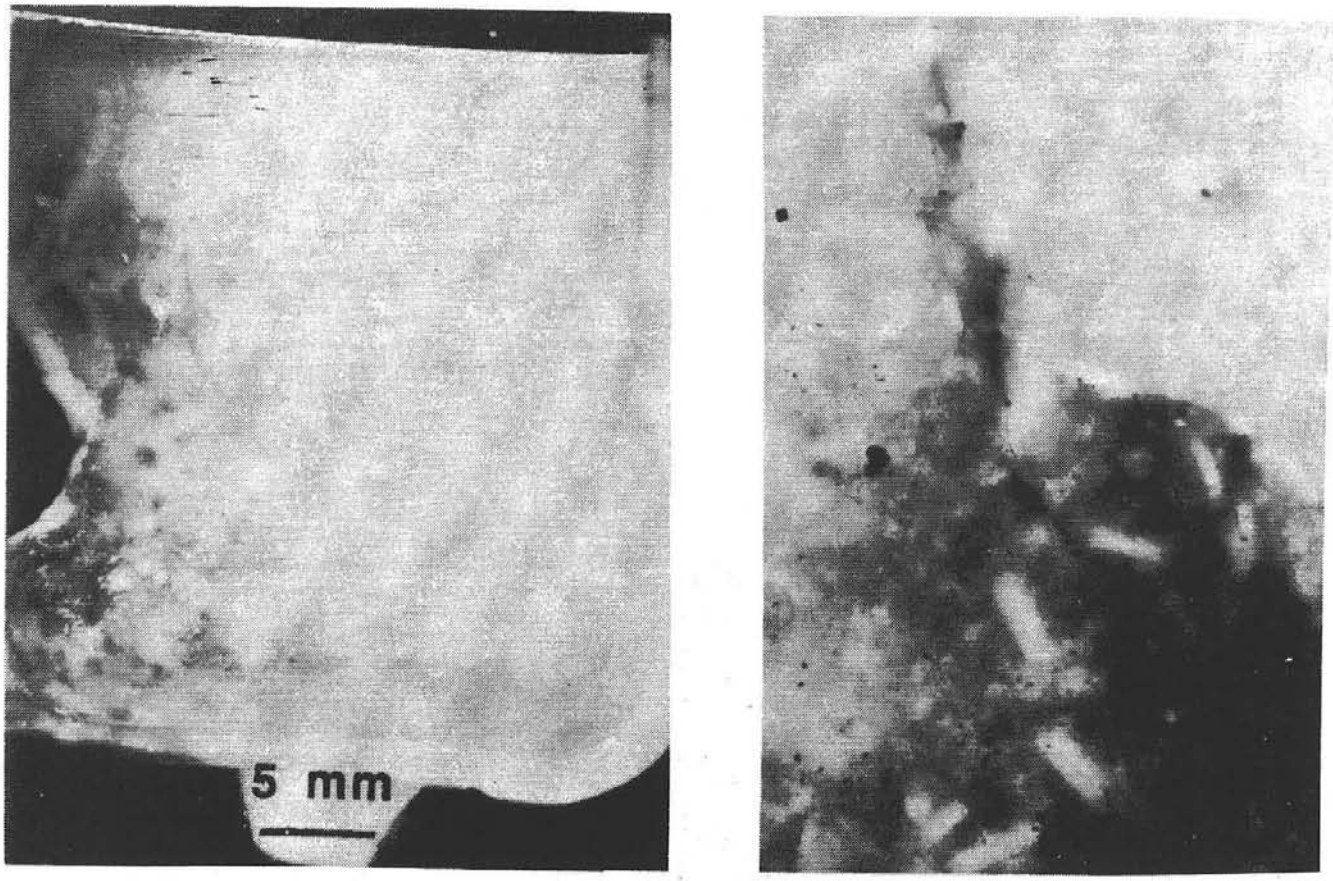

(a) Low Magnification

(b) High Magnification (100x)

Figure 5-4. Electrolyte Inner Surface from Cell 7498.

These features clearly indicated that the crack growth was not continuous. Probably, each of the steps corresponded to a charging cycle.

Interior Surface Features. Unlike the electrolyte in cell 7498, the interior surface of this electrolyte, after cleaning in alcohol, was white and nearly featureless when examined at low magnification. Using an optical microscope at magnifications of 50x and above, a number of cracks on the interior surface that had not penetrated to the outer surface were found. Many of these cracks showed a narrow trace of discoloration, but none showed the dark bands associated with the cracks in cell 7498, nor were any of the large grains seen in cell 7498 found.

After the preliminary examinations, some of the fragments were exposed to silver nitrate solution. The surface of one of the fragments is shown in Figure 5-5 after that exposure. In some respects, there is a resemblance to the interior surface of cell 7498, with cracks running through light-shaded linear features (Figure 5-4). However, these features are much larger than the oversized grains associated with the cracks in cell 7498 and indeed are not large grains.

The cracks that ran through the light-shaded features were decorated by exposure to the silver nitrate. Examination of fracture surfaces revealed, as in the electrolyte from cell 7498, that not all of the cracks starting perpendicular

Figure 5-5. Inner Surface of a Fragment from Cell 7436 after Silver Nitrate Treatment.

to the interior surface continued to move in the same direction through the tube wall. Many cracks turned and some eventually ran parallel to the interior tube surface. However, there were no spall fragments in this electrolyte like those associated with similar cracks in cell 7498.

Similar to cell 7498, the fracture surfaces showed features near the interior surface that indicated that a shallow layer in much of that surface was in compression when the fracture ran through it. However, in the vicinity of the light-shaded features seen on the interior surface, this compressive stress was apparently not present. It appears that the fractures initiated at the surface in the light-shaded areas and, after some penetration into the tube wall, propagated laterally, eventually extending through the compressive stress layers.

Suggested Fracture Process

Cell 7498. The mechanism that has evolved from this analysis of the failure of cell 7498 begins with generation of a compressive layer over much of the interior surface of the tube. Presumably, the compressive stress was generated by deposition of sodium in the layer--the process that ordinarily produces the discoloration of beta"-alumina after extended operation of a cell. Apparently, this stress was not developed in the very large grains that existed in this tube, and perhaps not in the thin layer of fine-grained material between most of the grains and the interior surface of the tube. As a consequence, portions of the large grains and perhaps the thin layer were put into tension. The fine-grained material might not have cracked under this low-level tensile stress, but the very weak cleavage plane in the large grains failed. During charging of the cell, that crack would have produced a local electric field enhancement, which would raise the local current density. The crack could then have propagated under the pressure developed in the crack by the sodium flowing into it in the manner of the electrolytic degradation process described by Virkar, de Jonghe, and others. (See the discussion on Electrochemical Degradation, which follows.)

The crack would have started out perpendicular to the interior surface, but would not necessarily continue in that direction through the wall. Some of the cracks changed direction until they were running approximately parallel to the tube surface. Eventually, pressure that developed from sodium flow into the crack was enough to produce the spall fracture. Presumably, the deposits found on the spall fragments were reaction products from this deposited sodium.

There are some additional facts that must be explained for the above description to be valid.

- First, although the large grains in this tube seem to be a critical element in the tube failure, there were other cells made with

electrolytes from the same lot as this one. Examination at CSPL, after the large grains were observed in this tube, confirmed that the other electrolytes in this lot also contained large grains. At least one of these cells had been tested at CSPL for a much longer time than cell 7498 without failing.

- Second, although the mechanism for propagating a crack under pressure of sodium flowing into it is a viable one for very high current densities, the currents that had been run through this tube were not high enough to degrade the electrolyte (assuming the current was uniformly distributed over the tube).

The major difference between cell 7498 and the "sister" cells on test at CSPL is that cell 7498 was shipped from Great Britain to New Mexico. It is possible that the mechanical impact loads during transit produced a leak in a seal large enough to allow some water vapor to enter the sodium space. Reaction of the water vapor with the electrolyte surface might have changed the wetting characteristics of the beta"-alumina enough to limit the effective current-carrying area. Local current densities could then be much higher than expected.

One problem with this explanation is that the resistance of cell 7498 during testing at SNL is not typical of a cell with a seal failure. Another discrepancy is that the silver nitrate staining indicated that the exposure of the electrolyte surface to sodium was quite uniform, which is not an expected characteristic of incomplete wetting.

Cell 7436. As with cell 7498, the failure in cell 7436 appears to be a result of stresses generated in the electrolyte wall by nonuniform current densities. In this instance, it is probable that nonuniform wetting was responsible for the nonuniform current densities. The resistance of this cell was high for the entire test period. As suggested for cell 7498, the nonuniform wetting might have resulted from contamination of the interior surface of the electrolyte by water vapor entering through a leaky seal, although a leak was not detected.

Initiation of the cracks probably involved a different driving force than their subsequent propagation. Possibly, in the regions where wetting of the surface was satisfactory, charge and discharge of the cell gradually developed a compressive stress layer whose depth increased with time. Apparently, adjacent to these compressively stressed zones, in the regions where wetting was inadequate, some areas were driven into tension and cracks initiated. These cracks were then extended by the current-focusing and sodium-pressurization processes described above. In addition to propagation through the wall, the cracks could extend laterally along the surface in zones that had not been carrying current. Because the stress to propagate the crack would only be generated when the cell was being recharged, the crack would extend in a series of steps as the bands on the fracture surfaces suggested.

Electromechanical Degradation

During 1987, compressive stresses were shown to potentially have an adverse effect on the electrolytic failure of the beta"-alumina material. This finding could be very important because of its impact on the logic behind using transformation-toughened beta"-alumina and the need to keep the electrolyte completely free of residual stresses. More detailed measurements are needed to confirm this finding. A new contract is planned for fiscal year 1988.

Background

Cationic solid electrolytes are subject to a type of degradation under electrolytic conditions that manifests itself in the form of thin metallic dendrites originating from the ion-neutralization surface. This phenomenon has been extensively studied in sodium/beta"-alumina. With respect to practical applications in sodium/sulfur cells, understanding this phenomenon is essential because it can lead to electrolyte failure. The fundamentals of this type of degradation process are reasonably well understood from both a qualitative and semiquantitative perspective.

Dendrite formation in the electrolyte depends on the presence of residual stress and the local current density. Residual stresses invariably exist

in sodium/sulfur electrolyte tubes. Kuribayashi and Nicholson observed that externally imposed stresses enhanced the propensity to degradation regardless of whether the residual stress was tensile or compressive (K. Kuribayashi and P. S. Nicholson, *Journal of Material Science*, 18, p. 1590 (1983). An explanation for this observation was pointed out by Virkar, who analytically examined the role of applied stresses on the propensity to degradation (A. V. Virkar, *Journal of Material Science*, 21, p. 859 (1986)). He showed that nonuniform compressive stress, which tends to pinch off the open end of the dendrite, promotes degradation in a natural way. Tensile stress enhances degradation for obvious reasons.

For the last two years, the objective of this work has been to investigate experimentally the effect of externally applied stresses on the degradation of sodium/beta"-alumina. During the first year, experiments were conducted at room temperature. These results were described in the previous annual report (*ETD Report for 1986*, pages 133 and 134). However, from the standpoint of the operation of the sodium/sulfur battery, experiments needed to be done at temperatures above the melting point of sodium. During the past year, experiments were conducted at temperatures as high as about 150°C. These experiments are considerably more complicated than the room-temperature experiments. Results from these high-temperature experiments provided further insight into the degradation process and the role of residual stresses.

Room-Temperature Measurements

The room-temperature measurements indicated that compression suppressed electrolytic degradation of unnotched samples, while tension accentuated it. The fact that degradation at room temperature was suppressed under compression would suggest that surface compressive stresses in the electrolyte would be beneficial in sodium/sulfur cells. This recommendation, however, is based on the assumption that similar effects are to be expected at temperatures where sodium is molten.

In contrast, notched samples showed a greater tendency towards degradation, even under compression, similar to the results of Kuribayashi and Nicholson. These results were rationalized on the basis of the Poiseuille (sodium pressure) model. At room temperature, sodium does not easily flow. As a result, the critical current density for dendrite formation (i_{cr}) is very low. But during the experiments the applied current density was too large. This factor may have also influenced the results on the unnotched samples.

High-Temperature Measurements

Based on the past year's high-temperature measurements, the observation was made that pristine (bar-shaped) samples did not easily degrade above the melting point of sodium. This is consistent with theoretical predictions using a three-dimensional model that predicts an i_{cr} in excess of 5 A/cm^2 for a flaw size of ≈200 μm. The maximum current density in these samples was typically 5 A/cm^2 and the flaw size was presumably much below 200 μm. However, when the samples were indented, flaws in excess of 200 μm were created. Further, coating all the sample except a 3-mm-diameter region with glass ensured that a current density as high as ≈11 A/cm^2 could be imposed. Under these conditions, dendrites were seen to form in agreement with theoretical predictions.

When these samples were subjected to a bending stress of ≈50 MPa (compressive stress at the indented flaw), it was observed that degradation initiated at current densities on the order of 1 A/cm^2, which is an order of magnitude lower than that of the samples not subjected to external stress during electrolysis. Bending created a nonuniform stress that tended to close the crack at the open end. Calculations have indeed shown that under such conditions propensity to degradation should increase under compression (A. V. Virkar, *Journal of Material Science*, 21, p. 859 (1986). These calculations show that nonuniform compressive stress may be detrimental.

With respect to the sodium/sulfur cell, these results show that the electrolyte may have to be

completely free of stress, be it tensile or compressive. Stresses can arise from phenomena such as nonuniform shrinkage during sintering, alignment-induced stresses during assembly, sodium deposition, or possibly contamination. These stresses may promote dendritic growth and cause premature failure of the cells.

Component Stress During Freeze/Thaw Cycling of Sodium/Sulfur Cells

Sodium/sulfur batteries used in both motive power and utility applications will be subjected to numerous thermal cycles during their lifetime. These cycles are expected and must not cause significant cell failures. To demonstrate the potential impact of a high failure rate, consider that the random failure of 1% of the cells per cycle within a battery constructed with four-cell strings could reduce its capacity by 20% after less than five freeze/thaw (F/T) cycles. Although substantial progress has been made in improving freeze/thaw durability during the past five years, most developers feel that it is not satisfactory.

Component failure can be caused by thermally induced stress generated during freeze/thaw cycling. Most F/T failures involve fracturing of the beta"-alumina electrolyte or seal breakage. Possible sources of stress that can lead to these types of failures include the following:

- Changes of state: incongruent sodium and/or sulfur melting; trapped sodium polysulfides with different freezing-points and volumetric-change characteristics; amorphous-to-crystalline transformations in positive electrode materials; and thermal gradients caused by sudden release of latent heat when sodium polysulfides freeze.

- Thermal expansion mismatches: container/positive-electrode/electrolyte; alpha-alumina-to-beta"-alumina glass seal; and thermocompression seal (alpha-alumina-to-metal).

- Discontinuities or anisotropy of properties at the electrolyte/positive-electrode interface.

Past experience with cells having a large length/diameter ratio has shown that freeze/thaw-induced failures can occur during the initial heatup of the cell. These infant-mortality problems can be avoided with proper cell design and fabrication/break-in procedures. The failures that are difficult to eliminate are those that occur after initial cell break-in. Factors that influence the F/T failure rate include cell lifetime, rate of heating/cooling, and the state-of-charge.

A task is being performed at SNL to assist developers in their efforts to improve the long-term durability of cells during these expected F/T events. The ultimate product of this activity will be a validated mathematical model that can be used to calculate stress within cell components and thus allow the susceptibility of various cell designs to both known and potential failure mechanisms to be determined. One objective of this task is to ensure that the results are applicable to many designs rather than focusing solely on a specific cell. A close tie is being maintained, however, with Chloride Silent Power, Ltd., (CSPL) because of their current contract with SNL for the development of the sodium/sulfur technology.

Two papers on the activities performed mainly in 1987 under this task were presented at the Beta Battery Workshop VII held in June 1988 at Toronto, Canada. (J. W. Braithwaite, et al., "Component Stress During Freeze/Thaw Cycling," and "Effects of Thermal Cycling on CSPL Sodium/Sulfur Cells," *Proc. Beta Battery Workshop VII*, Electric Power Research Institute, Toronto, June 1988.)

The initial effort of this task involved formulating and incorporating materials-behavior models based on known or believed properties of the cell components into a thermomechanical code and designing/constructing a laboratory sodium/sulfur cell. This cell is needed to facilitate instrumentation and failure-mode simulation and to allow the majority of the results to remain generic. In addition to the SNL cell, numerical analyses are being performed on

cell designs from CSPL and Ford Aerospace and Communications Corporation (FACC).

The approach that is currently being followed in this task encompasses the following steps:

1. Numerical simulation of known, yet simple, electrolyte-failure mechanisms to determine the status and basic requirements of the selected thermomechanical models.

2. Numerical study of the sensitivity of component stress to changes in cell operating and physical-property parameters. This study will allow the types of conditions and cell behavior that could lead to high component stress to be identified, thus establishing detailed information needs (physical property data and cell characteristics).

3. Measurement and/or empirical determination of the detailed information needs identified in step 2.

4. Measurement and mathematical modeling of expected cell behavior to validate the materials models contained in the thermomechanical code.

5. Modeling and in-cell testing of proposed failure mechanisms to determine their viability and applicability to various cell designs.

The results obtained from step 1 were reported in the previous annual report (*ETD Report for 1986*, pages 136 through 138). During 1987, the sensitivity calculations (step 2) were completed, the initial cell-behavior measurements (step 3) were performed, and the model validation studies (step 4) were started. A summary of the important findings from these activities follows, and the highlights of these findings are presented in Table 5-6.

Parametric Sensitivity Study

The objective of this initial part of component stress study was to determine the structural parameters of the cell materials that have the greatest effect on the stress in the electrolyte, the principal component of concern. Identification of these material parameters provides a guideline for establishing the level of effort that should be placed upon additional material characterization, and to what level that characterization should be pursued.

Another objective of this early study was to identify the types of thermomechanical processes that could induce tensile stresses in the electrolyte. Once such a process has been identified, it can be examined in detail by performing one- and two-dimensional numerical analyses of an actual cell configuration.

Property Variation

As reported last year, a numerical model of an FACC cell design was developed, and that model was used to successfully predict a postulated electrolyte failure mechanism (*ETD Report for 1986*, pages 136 through 138). As in any numerical simulation, the solution reflects not only the validity of the modeling assumptions, but also the uncertainties that exist in the material parameter data. With the exception of the active positive electrode materials (graphite/sulfur/Na_2S_x composite), the cell component materials have been well characterized. Therefore, the sensitivity of calculations to uncertainties in the properties of the positive electrode was considered.

To examine the trends in these sensitivities, a parametric study of the variation in electrolyte stress induced by a freeze cycle as a function of the thermal expansion coefficient and Young's modulus of the positive-electrode composite was performed. An axisymmetric section of an FACC cell was chosen as the model geometry. The same values of both the thermal expansion coefficient and Young's modulus that were used in the 1986 work were used as the reference values. Sodium polysulfide properties were taken from results published by Brown, Boveri, and Cie (BBC) (Gross, F., "Present Tasks of Research in Sodium/Sulfur Battery Development." Paper presented at The Electrochemical Society fall meeting, New Orleans, LA, October 1984. Knodler, R., and A.R. Nicoll, "Thermal

Table 5-6. Summary of Modeling Component Stress During Freeze/Thaw Cycling of Sodium/Sulfur Cells

Parametric Sensitivity Study	Numerical calculations were performed that showed: • electrolyte stress is most influenced by the thermal expansion coefficient (CTE) of the positive electrode; • electrolyte tensile stress can be produced in a cell with a homogeneous positive electrode if its CTE is high; • electrolyte failure in a cell with a homogeneous electrode is unlikely because of the limited tensile strength of the positive electrode. Localized volumetric changes caused by nonthermal amorphous-to-crystalline phase transformation were shown to cause electrolyte tensile stresses: • the magnitude of the stresses increased as the size of the crystallization region was reduced; • these results confirm that tensile stresses in the electrolyte are probably local phenomena caused by a material discontinuity.
Cell Behavior	Mechanical behavior of positive-electrode materials was characterized by measuring the strain on the cell case of SNL lab cells and CSPL-PB cells; the information obtained is needed to identify important stress-producing processes and to validate mathematical models. Overall observations: • net strain exists only with solidified positive electrode; • strain is design-dependent; • inconsistent solidification behavior leads to variable strain results; • no effect of thermal rate or cell lifetime could be identified.

Expansion Coefficient and Density of Amorphous and Crystallized Sodium Polysulfides." *J. Mat. Sci. Letters, 3*, 1984, pages 911-914.).

Other simplifying assumptions of this study included:

- A one-dimensional modeling approach was used to obtain acceptable and computationally economic solutions. The assumption of one-dimensional behavior implies that the hoop (circumferential) stress distribution is uniform both circumferentially and along the length of the cell.
- Material behavior of the cell components was assumed to be linear-elastic.
- Although the true strength of the materials will limit the magnitude of stress that can actually be developed, the materials were assumed to possess infinite strength.

The study was performed by fixing one of the reference parameters and then varying the other parameter over a range of values. Each model was then analyzed for an incremental temperature drop from 235°C to 25°C, over which thermal stresses can be induced.

Results of the parametric study indicated that the peak electrolyte stresses were more sensitive

Table 5-6. Summary of Modeling Component Stress During Freeze/Thaw Cycling of Sodium/Sulfur Cells (Continued)

Modeling of Cell Behavior	The goal of this modeling activity is to refine the material-behavior models in order that the measured strain will correlate with the calculated strain, thus allowing the state of stress within cell components to be determined reliably. The completed activity centered on explaining differences in observed hoop strain measured in various cell designs. Contributing factors include: • temperature dependence of thermal expansion coefficients of the various materials • interaction of materials possessing different thermal-expansion behavior.
Physical Properties of Positive Electrode Materials	The physical properties (Young's modulus, coefficient of thermal expansion, Poisson's ratio, compressive strength) of sulfur and sulfur/graphite composites has been measured using a variety of techniques; the important effect of the graphite felt on the properties of sulfur was shown.
Status	The significant findings obtained during 1987 included: • the feasibility and usefulness of modeling the F/T behavior of sodium/sulfur cells was demonstrated; • the first strain measurements on functioning cells were completed that help provide the information needed to understand F/T processes and validate the mathematical (thermomechanical) code. Final development of the thermomechanical code will be attempted once physical property and strain measurements are completed.

to variations in the thermal expansion coefficient than to variations in Young's modulus. This finding has significance for two reasons:

- First, it demonstrates that the value used for Young's modulus in the numerical calculations must be in error by nearly an order of magnitude to significantly affect the result. This situation is not likely because the experimental measurement techniques for obtaining Young's modulus are reliable.
- Second, it implies that the electrolyte stresses produced during a freeze cycle are primarily caused by the mismatch of thermal expansion coefficients among the cell components.

The results of the parametric sensitivity study showed that if a conservative fracture stress for the electrolyte of 20,000 psi is assumed, an increase of 2.5 times the reference thermal expansion coefficient would be required to produce the levels of stress that could cause

electrolyte failure (assuming a positive electrode composite with a very large tensile strength). Because the experimentally measured coefficients of thermal expansion are also unlikely to be this much in error, electrolyte failure caused by thermal expansion/contraction of a homogeneous and isotropic positive electrode is improbable. Thus one must conclude that the large, localized stresses that lead to electrolyte fracture are probably caused by differential thermal expansion and/or by inhomogeneities and that the maximum stress levels occurs when the minimum temperature is attained at the end of the freeze cycle. To further investigate this conclusion, the analyses on volumetric changes, which are reported below, were performed.

Volumetric Changes

In addition to the documented failure associated with discrete gaps, electrolyte failures are also known to occur in cells at various states-of-charge and in cells containing no gaps. Because many of the earlier programs to design and construct cells were plagued by structural problems related to volumetric effects that occurred during changes in phase (incongruent melting of sodium, for example), there is reason to believe that similar behavior could exist in current cell configurations.

BBC noted that the active positive electrode materials can undergo an amorphous-to-crystalline phase transformation that is accompanied by a change in density (Knodler, R., and A.R. Nicoll, "Thermal Expansion Coefficient and Density of Amorphous and Crystallized Sodium Polysulfides." *J. Mat. Sci. Letters, 3*, 1984, pages 911-914). These volumetric changes occur independently of the expansion/contraction of the positive-electrode material produced by variations in temperature. Because the mechanisms involved in the two processes are entirely different, their contributions to the structural behavior of the cell can only be measured by directly comparing their net effects.

In order to compare the nonthermal volumetric effects with those induced by thermal expansion, the volumetric change can be assumed to occur over a large temperature range rather than over a small one. By relating that change in volume to a percentage change in the linear dimensions of a reference volume, a linear strain associated with the volumetric change is obtained. If this straining is then considered to occur over a selected temperature range, a "pseudo" coefficient of thermal expansion associated only with the volumetric changes that occur during a phase transformation can be computed. The relative magnitudes of the two effects can then be measured directly through their corresponding expansion coefficients.

In the present comparison, the selected temperature change was chosen to be the same as that used in the previous numerical calculations: 210°C. Using the BBC experimental and the calculated "pseudo" thermal expansion coefficients, the strains attributable to the two mechanisms were found to be similar and of the same sign. Thus, the net effect of the combined mechanisms is to produce an "effective" coefficient of thermal expansion that is twice as large as the experimentally determined thermal expansion coefficient. Recalling that in the parametric study a 2.5-fold increase in the measured thermal expansion coefficient was required to produce electrolyte failure, indications are that during freeze/thaw of a cell with a homogeneous and isotropic positive electrode, these combined mechanisms will not lead to electrolyte failure. However, because the amorphous-to-crystalline transformation is not likely to occur uniformly throughout the entire positive electrode, this scenario warrants further examination.

Given the sensitivity of electrolyte stresses to volumetric change and thermal expansion/contraction, the potential effect of a solid-state volume change caused by an amorphous-to-crystalline transformation during a freeze cycle was numerically investigated. A single planar-section model of the FACC cell was used. Two-dimensional-plane strain analyses were then performed assuming that discrete portions of the positive electrode were composed of either purely amorphous and amorphous/crystalline regions of sodium polysulfide. Again, the material behavior was considered to be linear-elastic. The effect of the amorphous-to-crystalline phase change was included by using the effective thermal expansion coefficient discussed previously.

Because electrolyte behavior was the item of interest, the results of the analyses were examined in terms of the maximum principal stress. The cell model was analyzed for different size regions of amorphous and crystalline sodium polysulfide. Maximum stress contours for a quarter section of the FACC cell are shown in Figure 5-6 for one of the configurations considered. Results indicate that, as the extent of the crystallization region is reduced, the tensile stresses in the electrolyte increase slightly. The contours appear very similar to those calculated for the cell with a gap in the positive electrode. These results imply that tensile stresses generated in the electrolyte as a result of volumetric changes are a local phenomena caused by a material discontinuity.

Conclusions from Sensitivity Calculations

Two general conclusions can be gained from these initial studies:

- volumetric changes in the positive electrode can cause tensile stresses to develop in the electrolyte during a freeze cycle;
- discontinuities in the positive electrode (gaps, amorphous/crystalline phases, multiple phases with differing thermal expansion coefficients) may lead to electrolyte failure.

The stresses generated by volumetric changes and discontinuities can be used to qualitatively

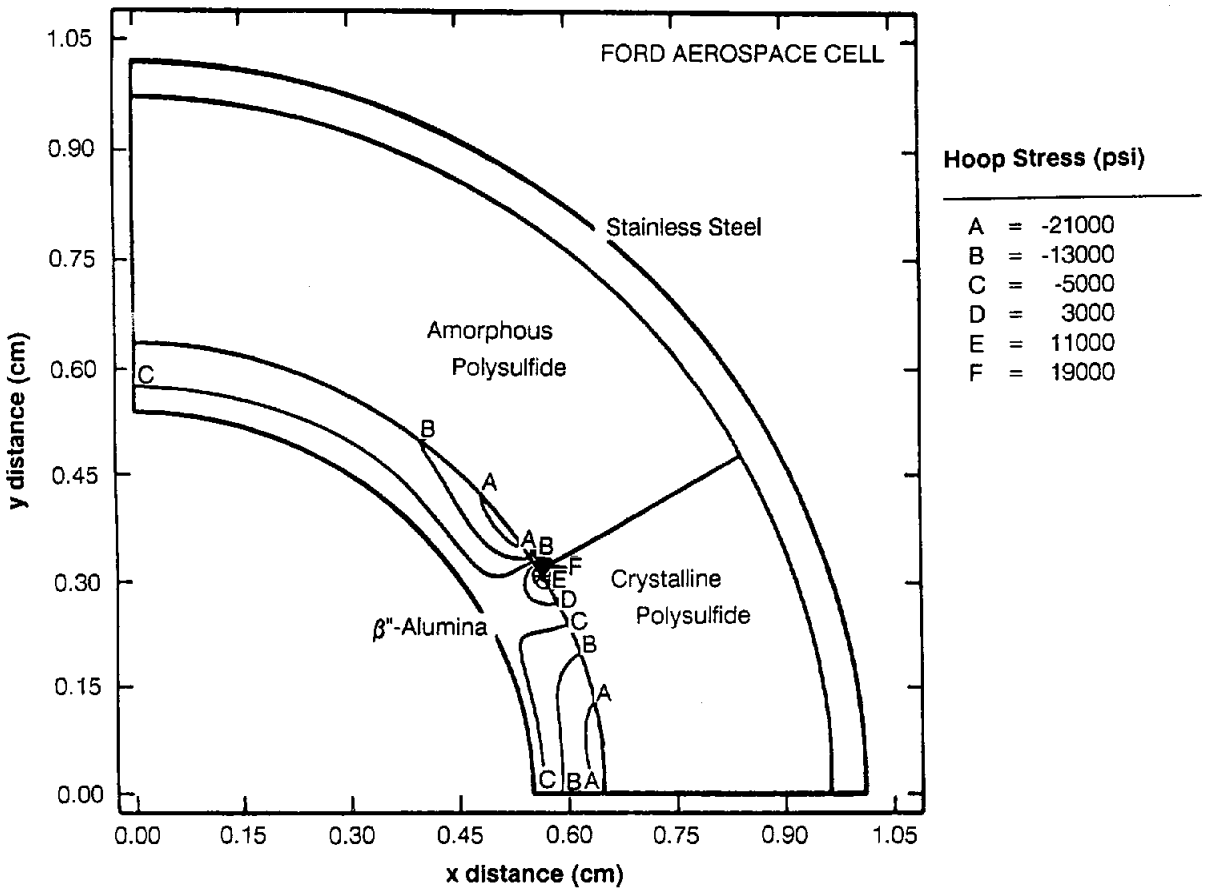

Figure 5-6. Stress Contours Calculated for an FACC Cell Design Containing Amorphous and Crystalline Polysulfide Phases When Cell Is Cooled to 25°C

explain many characteristics of actual freeze/thaw failures, including the effects of cooling rate and state-of-charge, the necessity to cool slowly around the melting point, and finally the infrequency or uncertainty associated with electrolyte failures.

Cell Behavior

Strain Measurements

Other than stresses generated solely by thermal gradients, thermomechanical processes occurring in the positive electrode, such as those discussed in the previous section, are believed to be responsible for long-term cell failure. Given this, the approach that is being followed in this subtask consists of measuring strain on the cell case, a component that should track the mechanical behavior of the positive electrode. The measurements made to date have utilized SNL lab cells and CSPL-PB cells that exhibit normal electrical-cycling characteristics. More detailed results for the CSPL cell are discussed in one of the papers from the Beta Battery Workshop (J. W. Braithwaite, et al., "Effects of Thermal Cycling on CSPL Sodium/Sulfur Cells." *Proc. Beta Battery Workshop VII*, Electric Power Research Institute, Toronto, June 1988).

Two lab-cell configurations have been used. The first one contained only crystalline sodium tetrasulfide in the positive electrode and no sodium in the negative electrode. The intent was to measure the strain behavior on a simpler system in order to facilitate interpretation and initial validation of the thermomechanical model somewhat. The second cell was a fully functional cell, broken in with a minimum of five electrical cycles.

Typical strain results obtained during the freezing of a CSPL cell and the two versions of the lab cell are shown in Figures 5-7 through 5-9. The data given in these figures are mechanical strain: the strain produced on the container attributable to the presence of the electrodes and the electrolyte.

As shown in Figures 5-7 through 5-9, not all aspects of the general strain characteristics of these three cells were similar. For example, the hoop strain in the CSPL cell and the full lab cell was moderately compressive, and in the modified cell (Na_2S_4 only) it was tensile. The axial strain in both lab cell configurations was tensile, yet it was near zero for the CSPL cell. Because of very different design and fabrication procedures, these results were not surprising. Possible explanations for some of these differences are found in the discussion on Modeling of Cell Behavior.

Several interesting overall observations can be made based on the strain measurements completed to date:

- Mechanical strain does not exist unless the positive electrode is solid, which is to be expected because a liquid electrode cannot support shear stress.
- The effect of cooling rate (from 6°C/h to 48°C/h) on strain is not statistically significant; however, the trend shows that the lower the rate, the lower the net strain.
- The magnitude of the mechanically induced strains are relatively small (less than 1000 μstrain) for cells that exhibit normal operating characteristics. For reference, thermally induced strain is approximately 3500 μstrain.

Thermal Gradients

One additional factor relevant to the F/T issue is the existence of thermal gradients. Such gradients are a potential concern because if their magnitude is large enough, electrolyte failure can occur because of (1) internally generated stresses, and/or (2) high shear stresses caused by nonuniform solidification patterns of the sodium polysulfide. During solidification of supercooled sodium polysulfides, container temperatures have been observed to increase rapidly by as much as 75°C.

To provide some additional needed experimental data about the gradient through the cell, a thermocouple was placed inside the sodium electrode of a lab cell at the bottom of the electrolyte tube. Even during exotherms and endotherms, the measured gradients were very small (a few degrees at 36°C/h), and conduction appeared to be the primary heat-transfer

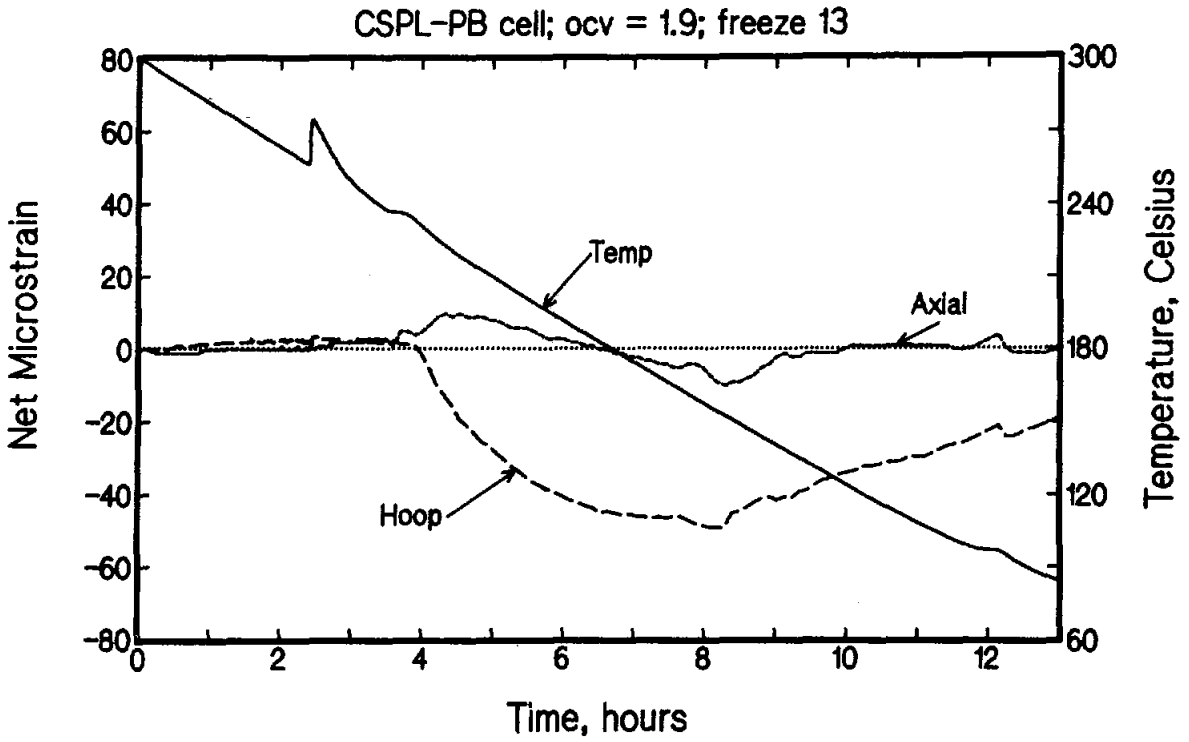

Figure 5-7. Average Mechanical Strain Measured During the Freezing of a Discharged CSPL-PB cell. OCV = 1.9 V.

mechanism. Based on these findings, it was felt that a detailed study of potential "thermal-only" effects probably was not needed.

The recent failure of a lab cell, however, placed renewed interest in the conclusion that purely thermal effects may not be important. The thermal, strain, and cell-voltage data collected during this event are shown in Figure 5-10. The rise in temperature, coincident with the decrease in open-circuit voltage, demonstrates that electrolyte fracture happened during the initial solidification of the supercooled sodium polysulfide. Because significant strain was not observed, this failure was probably not caused by the thermomechanical volumetric effects (see discussion on volumetric changes in Parametric Sensitivity Study). Rather, one of the two thermal effects discussed in the preceding paragraph is most probable. The observation, however, that electrolytes routinely survive sudden temperature increases during solidification would lead one to the conclusion that this failure was a result of nonuniform solidification.

Modeling of Cell Behavior

While the previous modeling efforts centered on an examination of electrolyte stresses internal to the cell, the goal of this work is to relate the strain state at the external surface of the cell to the state of stress within the cell. This is being accomplished by numerically simulating the response to F/T cycling of the container on a CSPL cell and the two different versions of the lab cell and comparing the predictions with observed cell behavior.

To date, these efforts have focused on establishing qualitative explanations for the following experimental result: how the hoop strain in the full lab and CSPL cell can be compressive and begin relaxing at about 150°C, whereas the hoop strain in the modified lab cell (Na_2S_4 only) could be tensile. Such explanations are required before quantitative validation can commence, because this process forces the identification of actual materials-behavior characteristics along with unknown mechanical properties.

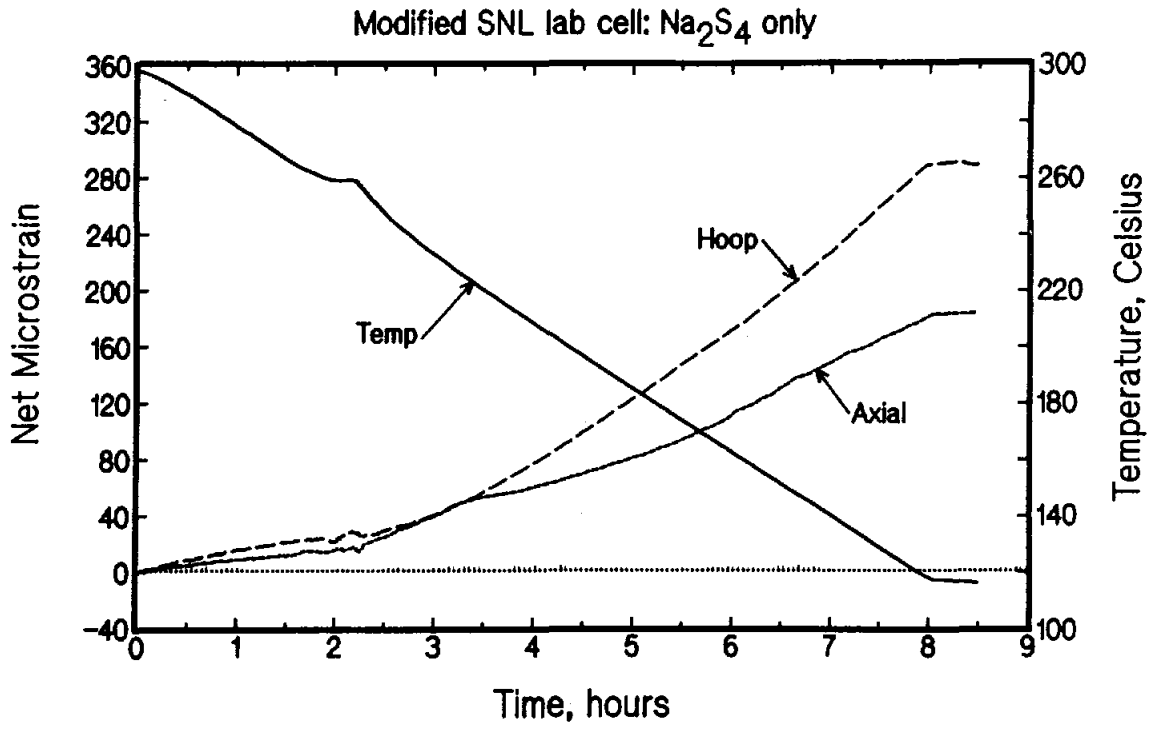

Figure 5-8. Average Mechanical Strain Measured During the Freezing of a Modified SNL Lab Cell. This cell was fabricated without any sodium and a positive electrode containing only Na_2S_4.

Axisymmetric models of the CSPL-PB cell and of the two laboratory cells were constructed and analyzed for the freeze portion of the temperature cycle. Again, the material behavior was considered to be linearly elastic. These models were unable to predict the experimentally measured strains. Given this deficiency, the materials models, physical properties, and cell functions were revisited.

An examination of the results showed that the temperature dependence of thermal expansion coefficients used in the analyses can have a marked influence on the computed strains. The thermal expansion coefficient of the electrolyte remains fairly constant over the temperature range used in these analyses, but the expansion coefficients of the sodium polysulfides and the cell container are somewhat temperature dependent.

BBC concluded that a constant-value thermal expansion coefficient of 35 μstrain/°C for all the sodium polysulfides was justified based on experimental error (R. Knodler and A.R. Nicoll, "Thermal Expansion Coefficient and Density of Amorphous and Crystallized Sodium Polysulfides." *J. Mat. Sci. Letters, 3*, 1984, pages 911-914). If, however, their measured temperature dependence of the thermal expansion coefficient for pure sodium polysulfides is included in the analyses, drastically different strain results are obtained. Similarly, inclusion of temperature dependence of the expansion coefficient of the cell container also influences the computed strains. Clearly the difference in the measured and computed strains can be partially attributed to the interaction of materials possessing temperature-dependent and uniquely different thermal-expansion behavior. For example, if the BBC data on the temperature effect on the thermal expansion coefficient are used, the compressive hoop strain behavior observed for the CSPL cell would result. However, if the thermal expansion coefficient is constant at values above 30 μstrain/°C, then tensile strain would exist (modified lab cell).

Both cases are possible. Thermal expansion values for the more relevant polysulfide/graphite composite materials have never been determined.

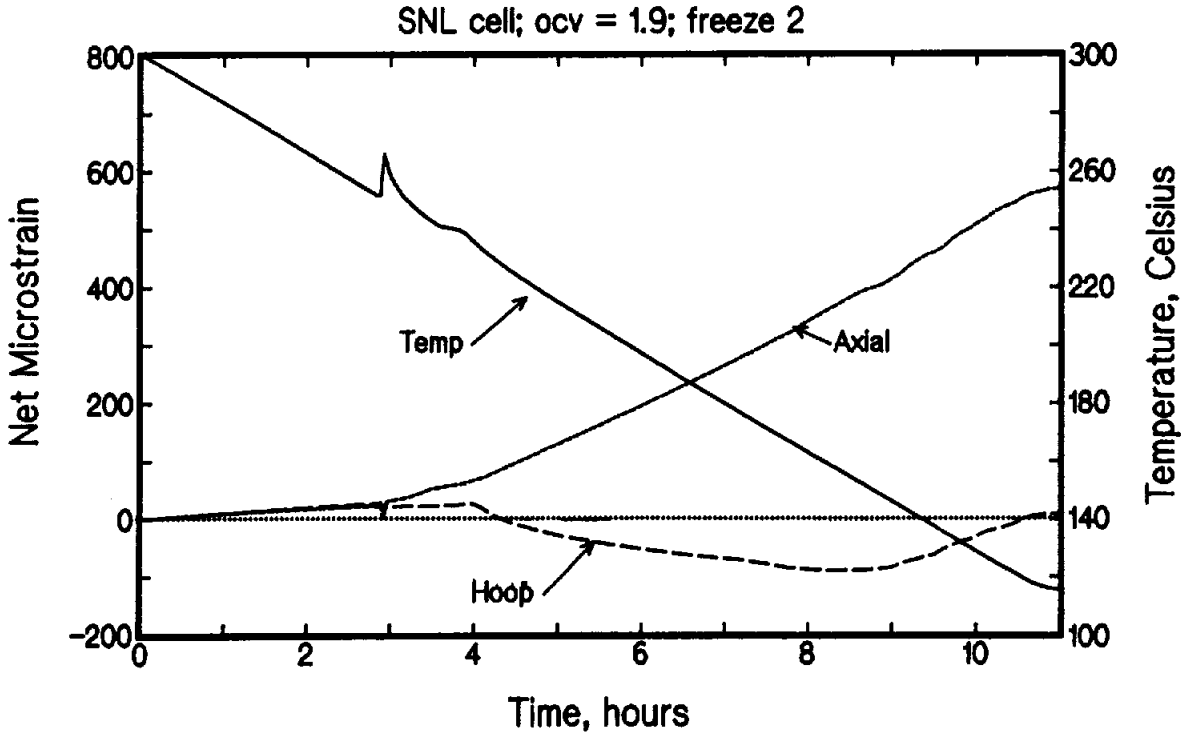

Figure 5-9. Average Mechanical Strain Measured During the Freezing of a Discharged SNL Lab Cell. OCV = 1.9 V.

Amorphous-to-crystalline transitions, phase distributions, and fiber orientation should also affect the actual values. The measurement of the important thermomechanical properties as a function of these variables is the objective of the study discussed below.

Physical Properties of Positive Electrode Materials

To provide the modeling effort with accurate values for the important physical properties of the positive-electrode materials, a complementary experimental study is being performed. The goal of this effort is to measure the thermomechanical properties (elastic modulus, Poisson's ratio, compressive strength, and thermal expansion coefficients) of sulfur, the single-phase sodium polysulfides, and the sulfur/graphite and sodium polysulfide/graphite composites as a function of temperature up to (near) their melting points. Thus far, the properties of sulfur and sulfur/graphite composites have been the focus of the study. This section will briefly describe the measurement techniques and present the results obtained to date.

The sulfur and sulfur/graphite composites were made by casting molten sulfur into heated teflon molds. Specific geometries for further testing were obtained by sectioning with a dry diamond wafering blade and polishing. X-ray diffraction disclosed that, prior to testing, all samples were predominantly in the equilibrium, room-temperature rhombohedral crystal structure (theoretical density of 2.07 g/cm^3) with varying amounts of the monoclinic structure (theoretical density 1.97 g/cm^3). Samples with observable surface flaws or voids were excluded from further experiments. Porosity, which is inevitably present in cast samples, was not specifically quantified; however, samples with low geometrical density (less than 1.92 g/cm^3) were not used.

Strength properties were measured by three different techniques: stress (compressive)-strain, ultrasonic attenuation, and dynamic mechanical analysis (DMA). All three were used because

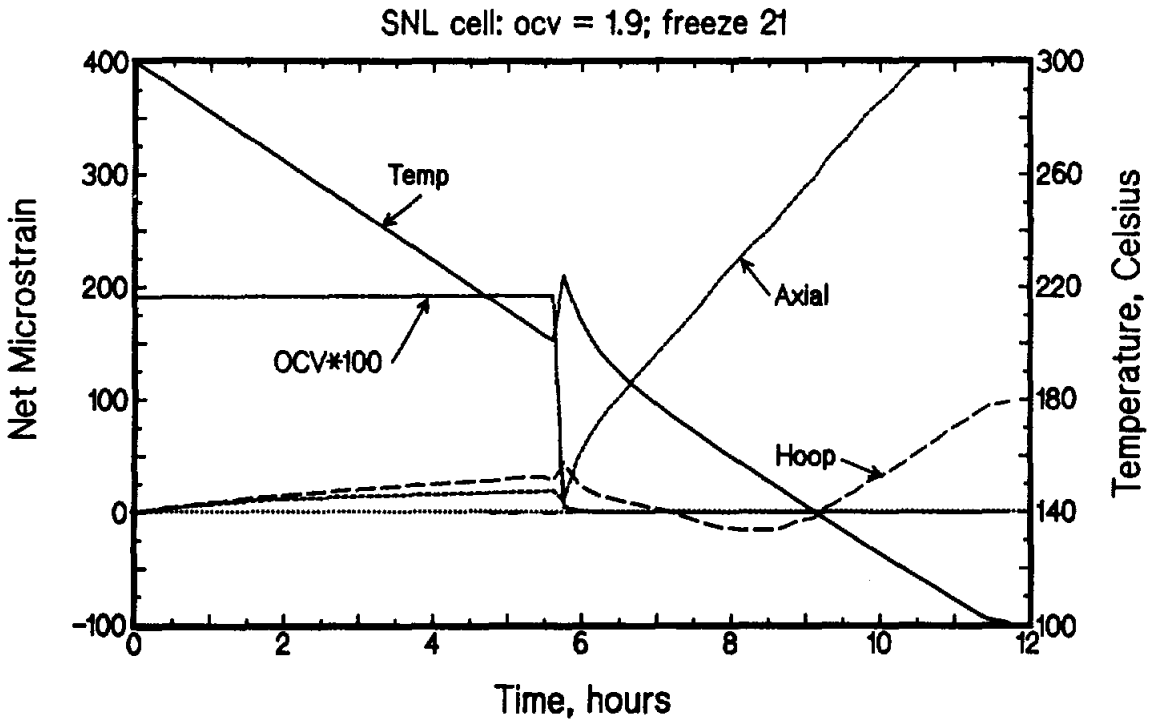

Figure 5-10. Average Mechanical Strain Measured During the Freezing of a Discharged SNL Lab Cell. Electrolyte failure was coincident with the freezing isotherm. OCV = 1.9 V.

each offers distinct advantages and applications relative to the others. Measurements were made on sulfur samples using all three techniques, but only stress-strain was applied to sulfur/graphite composite samples.

A typical (compressive) load-displacement curve for sulfur is shown in Figure 5-11. This trace is composed of four regions:

a. the elastic region in which the load increases linearly with displacement

b. a region in which the material appears to yield (displacement increases with only slight increase in load)

c. a second region in which load appears to increase linearly with displacement

d. a region in which the sample is compressed under decreasing load.

The elastic modulus calculated from the slope of region "a" is fairly representative of the material. The average elastic modulus is 619 ± 59 MPa. The values of maximum stress supported by each sample show a wider variation and probably reflect the fact that failure is controlled by flaws in the material that are not well characterized and probably accurately reflect sample-to-sample variations.

The average modulus for several different sulfur/graphite samples is 7.2 ± 1.1 GPa. The presence of the graphite felt appears to increase the modulus by about an order of magnitude. However, the values of maximum stress supported by the sulfur/graphite samples are only slightly greater than the maximum stresses supported by sulfur alone. The features of the load-displacement curves are, in general, different from the features of the curves for sulfur. Little yielding is observed (region 2), and failure (load falls abruptly to zero) occurs at the point of maximum stress.

The ultrasonic attenuation experiments yield a number of mechanical properties. For "pure" sulfur the properties derived from these measurements are: an elastic modulus of

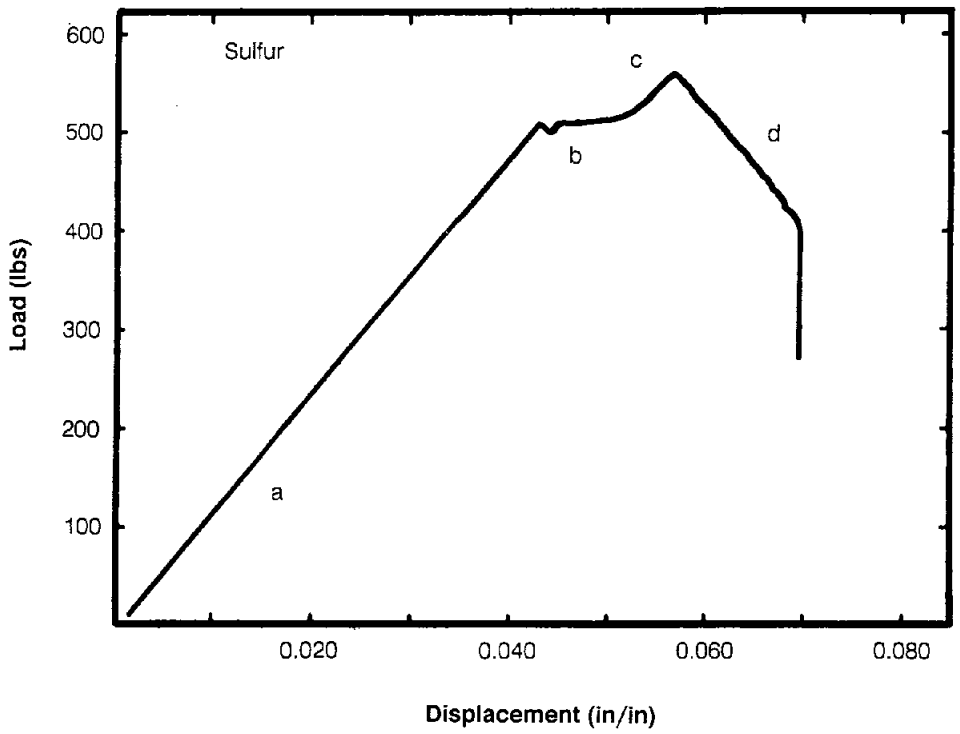

Figure 5-11. Results From the Compressive Load-Displacement Testing of Pure Sulfur

11.8 GPa; a shear modulus of 4.66 GPa; a Poisson's ratio of 0.27; and a bulk modulus of 8.5 GPa. DMA experiments, also on sulfur, in a dry argon atmosphere resulted in a room-temperature elastic modulus of 525 MPa and a shear modulus of about 200 MPa. Although a complete evaluation of the temperature dependence of these properties is still underway, preliminary results suggest that the moduli are essentially unchanged up to 50°C. The elastic modulus measured by this technique is in good agreement with that determined by the more classical stress-strain measurements.

The coefficient of thermal expansion of both sulfur and the sulfur/graphite composite was measured to be 65 μstrain/°C. Currently there is too much scatter in the data to tell if any significant differences exist between the two materials.

Status

During 1987, the feasibility and usefulness of mathematically modeling the processes occurring in sodium/sulfur cells during F/T cycling has been demonstrated. The first strain measurements on functioning cells have been completed. These measurements have shown the variable mechanical behavior of the processes occurring in the positive electrode, a factor that may account for the randomness of actual F/T-induced failures.

Once the physical property and ongoing strain measurements are completed, an attempt will be made to finalize the development of materials models contained in a thermomechanical code. The strain data will be used to validate the accuracy of the models. Finally, this code will be used to identify and

simulate important aspects of various design options and to determine the feasibility of proposed failure mechanisms.

Improved Chromium Plating of Sodium/Sulfur Cell Containers

A major unsolved materials problem associated with the development of the sodium/sulfur technology is the identification of suitable sulfur-container materials. The solution to this problem is difficult because the container must be very corrosion resistant, have good electrical conductivity and mechanical properties, and yet be light-weight and inexpensive. Corrosion is detrimental not only because of its potential effect on cell lifetime but also because corrosion products can cause cell performance to degrade.

The diverse and demanding requirements placed on the container have forced developers to select and use composite materials: usually an inexpensive substrate (such as aluminum, carbon steel, or stainless steel) that has been coated, plated, or sheathed with at least one corrosion-resistant material. The key to success of these composites is that the corrosion-resistant layer be defect-free, which prevents undermining, substrate attack, and spalling. An excellent review of the information available concerning the selection of materials for the sulfur container was compiled by A. R. Tilley (J. L. Sudworth and A. R. Tilley, *The Sodium Sulfur Battery*, Chapman and Hall, New York, 1985, pages 199-226.)

The ETD project has supported major sodium/sulfur development programs at Ford Aerospace and Communications Corp. (FACC) and currently at Chloride Silent Power, Ltd. (CSPL). In both of these programs, a chromium-containing layer was selected as the primary corrosion barrier.

One of the preferred methods for applying chromium onto sodium/sulfur containers is by electroplating. This process can be cost effective and theoretically can produce deposits with good chemical, physical and mechanical properties. However, in practice, electroplated chromium is typically a hard, brittle, and highly stressed deposit. Copious quantities of hydrogen gas are normally liberated during the plating operation, resulting in poor electrical efficiency (<15%) and formation of chromium hydride. The hydride and its associated defects produce high residual stress, which increases with increasing thickness. The stress is eventually relieved when the deposit cracks, at which point the process is repeated. Most problems with the quality of chromium deposits involve this process of hydride inclusion and the defects associated with them.

Although many sodium/sulfur developers have studied and used chromium electroplating, techniques have not yet been identified that produce reliable and effective platings. Based on this deficiency, a study is being performed at SNL to develop techniques to improve the quality and efficiency of chromium electroplating. This effort initially provided direct support to the FACC program and was prematurely suspended at the conclusion of their final contract. Because CSPL is seeking to improve its current corrosion-prevention scheme (chromized steel), this task was activated in mid-year and its scope was expanded.

A description of the intended program, preceded by a brief summary of the principal findings from the FACC study, follows. The FACC section is included to provide necessary background information. The FACC findings and the progress made on the current program are summarized in Table 5-7.

Results from Support to FACC

For terrestrial applications, FACC decided to construct their sulfur container with a moderately corrosion-resistant stainless steel (26% chromium, 1% molybdenum) that was electroplated with chromium. They selected M&T Unichrome CF-500, a proprietary electrolyte that could be used to produce crack-free deposits. In practice, the performance of their corrosion-protection scheme was very erratic, probably because of the significant cracking observed in the plating of many cells. The actual plating conditions were identified collectively by FACC and SNL as the critical factor affecting the cracking and ultimately the rate of container degradation.

Table 5-7. Summary of the Development of Improved Chromium Plating of Sodium/Sulfur Cell Containers

Results from Support to FACC	Conditions for electroplating chromium identified as the critical factor affecting cracking of deposit. SNL performed a factorial study to optimize electroplating process. Two cells with optimized deposits completed over 1200 cycles.
Support to CSPL	Present CSPL method (high-temperature packed-bed chromizing process) has limited durability and high cost; a high-quality electroplated chromium layer could overcome these disadvantages. Electroplated chromium layer could also be an initial step in a multistep process. Objective of CSPL support: continued development of improved electroplating of chromium. Planned tasks: • complete evaluation of FACC task; • add V_2O_5 to electroplating electrolyte; • use pulse and pulse-reverse plating techniques to reduce deposit stress; • investigate effectiveness of highly cracked deposit; • determine the feasibility of shot-peening the inside steel surface of the container; • characterize the quality and performance of the platings. Four different electrolytes prepared (two self-regulating solutions, one conventional solution, and one with V_2O_5 additive).

During the last year of DOE support to FACC (1985), a small study was performed at SNL to optimize the plating solution and operating conditions. Specifically, a factorial study that compared the effects of electrolyte composition, temperature, and current density to determine the best parameters for producing a crack-free deposit was used in the SNL research (Figure 5-12).

Results obtained using the original FACC and optimized plating conditions are shown in Figures 5-13 and 5-14, respectively. Prior to the conclusion of the contract, FACC plated four of its cells using the SNL parameters. Two of the

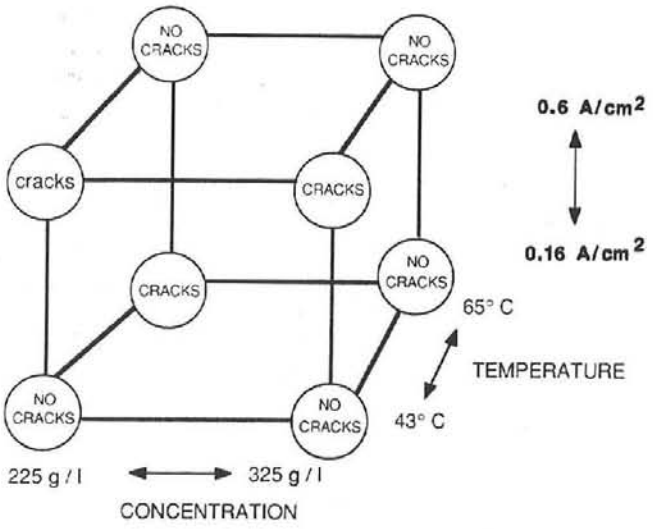

Figure 5-12. Schematic Diagram of the Factorial Study Performed to Determine the Influence of Plating Conditions on Cracking of the Chromium Deposit

cells were removed voluntarily from cycle testing for postmortem analysis; the other two cells completed over 1200 cycles during a 16-month period with stable performance. Although only four cells were tested, the consistent results demonstrated that a noticeable improvement had been achieved.

Support to CSPL

CSPL chose a different method for utilizing chromium in their protective barrier. Currently, CSPL chromizes drawn steel cans using a high-temperature packed-bed process. The durability of the duplex chromized layer is projected to be adequate for shorter term (≈5 year) EV applications if the depth-of-discharge and temperature are limited (open-circuit voltage > 1.9 V, temperature <380°C). However, for longer-life cells used in load-leveling batteries, a more durable layer will be needed. The other major disadvantage of this type of protection scheme is the relative high cost of the chromizing process. Both CSPL and SNL agree that a high-quality electroplated chromium layer could, by itself, not only improve durability and lower cost, but also could be an effective initial step in a multistep process (such as thermal treatment followed by carburizing).

The objectives of the new activity are to continue the development of improved techniques to electroplate chromium onto carbon and stainless steels and to identify methods to use these techniques to effectively plate containers from the two cell designs being considered by CSPL: PB and XPB. Although the process modification identified for the FACC application resulted in improved container performance, the deposits were still brittle and in a tensile-stressed condition. A ductile, stress-free or a compressively stressed deposit is more desirable because better longevity for the container should be attained. The thermal expansion coefficient for steel is approximately twice that for chromium. The ductility and compressive state will counter some of the negative effects caused by thermal expansion and should enhance plating integrity.

The specific tasks that are planned under this plating activity are as follows:

1. Complete the evaluation of the process used to plate the FACC cells.

2. Modify the electrolyte by adding vanadium pentoxide (V_2O_5). This chemical additive will reduce stress, improve ductility, and increase plating efficiency. An improvement in efficiency is important because it will allow thicker deposits to be produced in less time, thus reducing cost.

3. Develop pulse and pulse-reverse plating techniques as a method to reduce deposit stress. Published information has established that crack-free chromium is possible using either on- and off-times of approximately 1 ms or pulsed, reversed-current plating with short anodic periods and very low frequencies (<1 Hz). Deposits produced this way have a significant reduction in hardness and increased deposit quality over conventional plating methods.

4. Investigate the potential for utilizing a highly cracked deposit. This type of deposit may be desirable because the thermal expansion coefficients of the steel

Chromium Deposit Using FACC Conditions

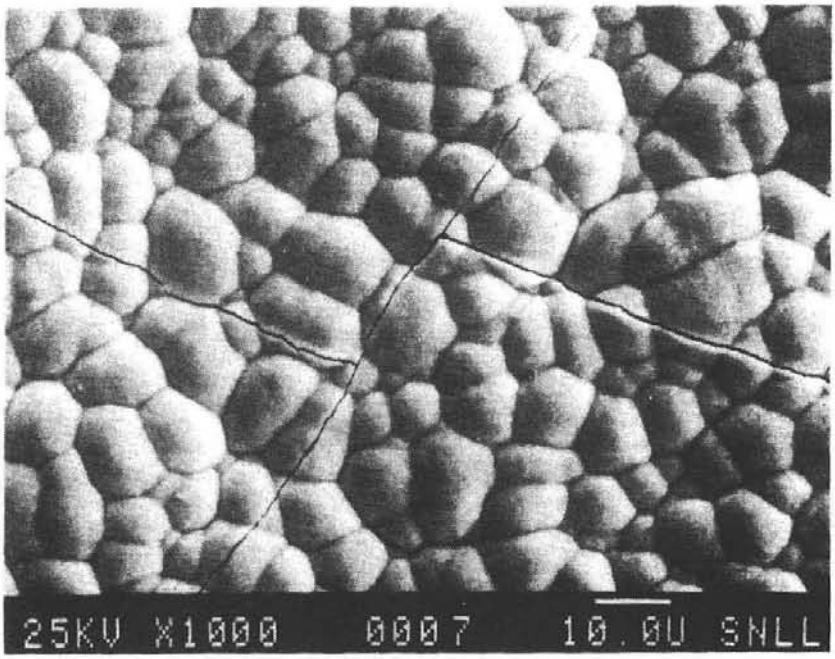

0.3 A/cm²
225 g/l
54°C

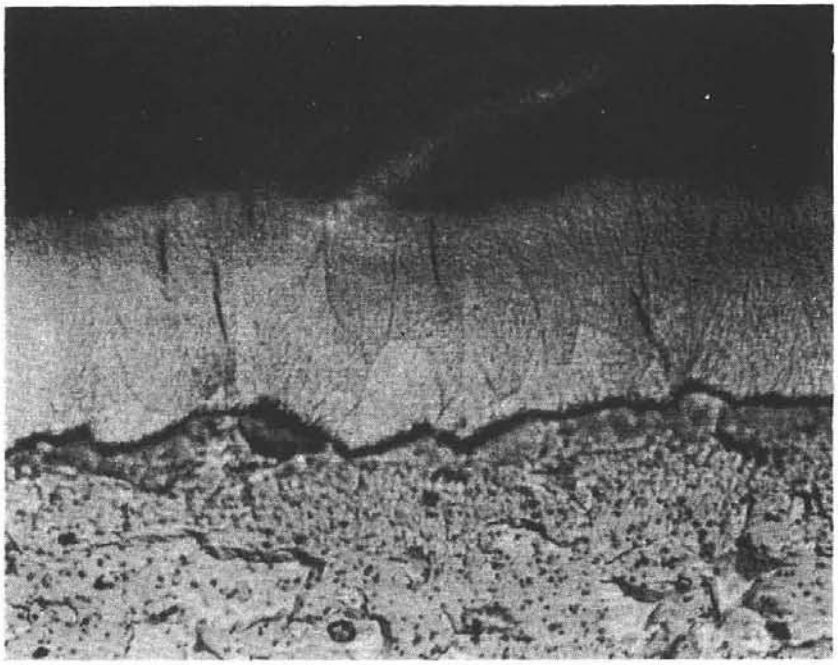

50μm
Chromium

Base Steel

0.3 A/cm²
225 g/l
54°C

Figure 5-13. Scanning Electron Micrographs and Optical Micrographs of Chromium Deposits Produced Using the Original FACC Plating Conditions

Chromium Deposit Using Parameters Developed by SNL

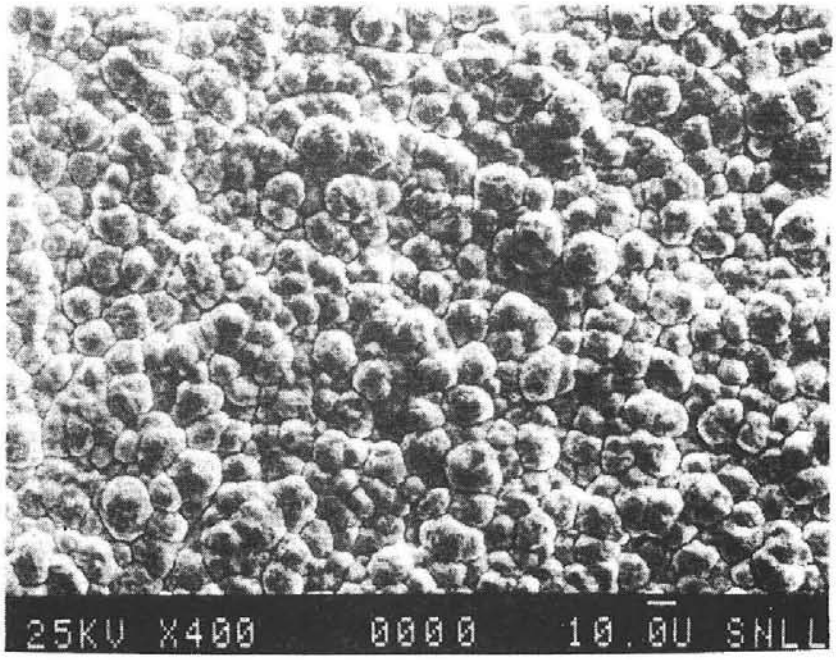

0.6 A/cm²
325 g/l
65°C

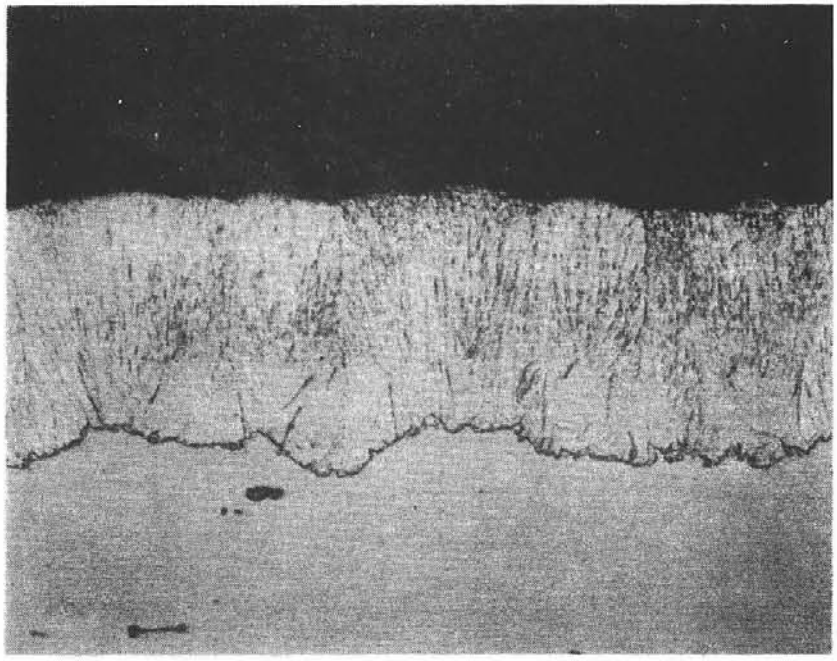

50μm
Chromium

Base Steel

0.6 A/cm²
325 g/l
65°C

Figure 5-14. Scanning Electron Micrographs and Optical Micrographs of Chromium Deposits Produced Using the Modified SNL Plating Conditions

and the chromium are better matched. Corrosion protection would come from a diffusion layer formed during a post-plating step. As such, the presence of a cracked surface may not be detrimental.

5. Determine the feasibility of shot-peening the inside steel surface of the container with glass beads prior to plating. This type of treatment may improve the quality of chromium deposits by putting the steel surface into a compressive state and providing a better surface for mechanical keying.

6. Characterize the quality and performance of the platings with a variety of techniques. Scanning electron and optical microscopy will be used to determine surface morphology and deposit integrity. Stress and hydrogen gas content will be measured to determine if reductions in hydriding were produced. (A more detailed discussion of the planned characterization activities follows.)

The performance of the platings will be evaluated both at SNL and CSPL:

- The CSPL evaluations will involve predominantly in-cell exposures, but some direct studies of plating performance will also be performed.

- The studies at SNL are being conducted mainly to quickly screen the effectiveness of the potential plating processes.

In-cell testing is recognized as being a mandatory requirement because corrosion in actual cells is usually more severe than in static tests and is the only way to determine if corrosion products can affect cell performance (J. L. Sudworth and A. R. Tilley, *The Sodium Sulfur Battery*, Chapman and Hall, New York, 1985, pp. 199-226.). To accomplish the in-cell testing, end plates for the SNL lab cell along with the inside of PB containers will be plated. The plated PB containers will be shipped to CSPL. Depending on the type of plating process used, the platings may be further processed. In either case, actual cells will then the assembled and tested. The performance of the platings at both SNL and CSPL will be determined during postmortem analyses.

Program Status

At the end of 1987, a chromium-plating facility had been assembled and was operational. In addition, four different electrolytes were prepared that will be used to determine the effect of composition on deposit quality. These include:

- M&T Unichrome CF-500, a proprietary, chemical self-regulating electrolyte, to be used with the procedures developed for the FACC cells. Initial plating of coupons for accelerated testing has been completed.

- M&T CF-500 with an addition of vanadium pentoxide. By adding 10 g/l of V_2O_5 to the electrolyte, the plating rate can be increased with no deterioration expected in quality.

- A conventional chromium-plating solution containing a 100:1 ratio of chromium to sulfuric acid. This solution will be being used in the pulse and pulse reverse-plating techniques as a method to reduce stress in the deposit and improve efficiency.

- M&T CR-110, another self-regulating electrolyte that will produce a compressively stressed deposit with approximately 1200 cracks/cm. This deposit should be a good candidate for the post-processing procedures being considered at CSPL.

Information obtained during the course of this task will be used to ultimately determine the feasibility (in terms of both performance and cost) of this type of corrosion protection scheme. Although the results obtained several years ago while working with the FACC program yielded good quality deposits and excellent performance during in-cell evaluations, only a few cells were plated and tested. The critical need to perform rigorous long-term and accelerated testing of sound, defect-free, deposits is clearly recognized. The approach being followed in this study should allow the required assessments to be completed.

APPENDIX

Publications and Presentations, 1987

Arnold, Jr., C., R.A. Assink, R.P. Hollandsworth (Lockheed Corp.), and J.A. Lee (RAI Research Corp.), "Chemically Stable Membranes Made from α-Methylstyrene by Radiative Grafting," SD-4573, S-66,636 (Disclosure 9 October 1987).

Arnold, Jr., C., and R.A. Assink, "Development of Sulfonated Polysulfone Membranes for Redox Flow Batteries," accepted for publication in *Journal of Membrane Science.*

Arnold, Jr., C., and R.A. Assink, "Materials Studies for the Zinc/Bromine Flow Battery," *Proceedings of the Eight Battery and Electrochemical Contractors' Conference*, (Conf-871121), 101, Vienna, VA, 15-19 November 1987.

Arnold, Jr., C., and R.A. Assink, "Sulfonated Polysulfone Battery Membrane for Use in Corrosive Environments," U.S. Patent No. 4,714,663 (22 December 1987).

Assink, R.A., and C. Arnold, Jr., "Effect of Tertiary Hydrogens on the Stability of an Ionic Membrane in a Chemically Aggressive Environment," *Proceedings of the 172nd Electrochemical Society Meeting*, Battery Division, Honolulu, HI, 18-23 October 1987.

Auxer, W., "Sizing Considerations for a Sodium Sulfur Load Levelling Battery," Presented at the 172nd Electrochemical Society Meeting, Honolulu, HI, 18-23 October 1987.

Beauchamp, R.L., and J.F. Sindorf, "Cost Reductions in the Nickel/Hydrogen Battery," Presented at the Space Electrochemical Research and Technology Conference, Cleveland, OH, 14-16 April 1987.

Beauchamp, R.L., "Nickel Hydrogen Battery Development," Presented at the Eight Battery and Electrochemical Contractors' Conference, Vienna, VA, 15-19 November 1987.

Braithwaite, J.W. "Sodium/Sulfur Studies at SNL," *Extended Abstracts: Eighth Battery and Electrochemical Contractors' Conference*, Vienna, VA, November 1987.

Bush, "Nickel/Hydrogen Testing at SNL," Presented at the Eight Battery and Electrochemical Contractors' Conference, Vienna, VA, 15-19 November 1987.

Bush, D.M., and J.F. Sindorf, "A Hydrogen/Nickel Oxide Battery for Remote Applications," Presented at the 172nd Electrochemical Society Meeting, Honolulu, HI, 18-23 October 1987.

Butler, P.C., and J.M. Freese, "Advanced Battery Systems Performance Evaluation," Presented at the Eighth Battery and Electrochemical Contractors' Conference, Vienna, VA, 15-19 November 1987.

Butler, P.C., and J.M. Freese, "Review of Sandia Battery Evaluation," Presented at the ETD Project Review Meeting, Washington, DC, 4 March 1987.

Butler, P.C., and C.E. Robinson, "Zinc/Bromine Battery Evaluation at SNL," Presented at the Eighth Battery and Electrochemical Contractors' Conference, Vienna, VA, 15-19 November 1987.

Chi, C., and M. Bilhorn, "Design and Economics of a Zinc-Bromine Utility Load Leveling Battery System," Presented at the 22nd Intersociety Energy Conversion Engineering Conference, Philadelphia, PA, 10-14 August 1987.

Chi, C., and M. Klein, "Zinc-Bromine Commercialization," Presented at the Eighth Battery and Electrochemical Contractors' Conference, Vienna, VA, 15-19 November 1987.

Delaney, W.C., and M.D. Eskra, "Zinc/Bromine Load Management Battery Development," *Extended Abstracts: Eighth Battery and Electrochemical Contractors' Conference*, Vienna, VA, November 1987.

Duncan, G.K., and A.R. West, "The Stoichiometry of Beta Alumina, Phase Diagram Studies in System Na_2O-MgO-Li_2O-Al_2O_3," Presented at the Sixth International Conference on Solid State Ionics, Garmisch-Partenkirchen, Federal Republic of Germany, September 1987.

Dunlop, J.D., et al., (COMSAT Laboratories) and W. Gentry et al. (Johnson Controls, Inc.) "Design and Development of a Multi-Kilowatt Hour Hydrogen/Nickel Oxide Battery," SAND87-7061 Albuquerque, Sandia National Laboratories, January 1987.

Dunlop, J.D., and R.L. Beauchamp, "Making Space Nickel/Hydrogen Batteries Lighter and Less Expensive," Presented at the AIAA/DARPA Meeting on Lightweight Satellite Systems, Monterey, CA, 4-6 August 1987.

Eden, E.A., "Corrosion and Protection Centre Industrial Services," University of Manchester Institute of Science and Technology, April 1987.

Freese, J.M., and P.C. Butler, "Results of a Wind Turbine/Sealed Lead-Acid Battery Experiment," Presented at the 172nd Electrochemical Society Meeting, Honolulu, HI, 18-23 October 1987.

Heavens, S.N., "Electrophoretic Deposition as a Processing Route for Ceramic," Accepted for publication in *Ceramic Processing Technique*.

Heavens, S.N., "Strength Improvements in Beta" by Incorporation of Zirconia," Accepted for publication to the *Journal of Materials Science*.

Kelsey, J., "Feasibility Study into Heat Recovery System Applied to a High Temperature Electric Storage Battery," Salford University Business Services Limited, Interim Report, 5 November 1987.

Knerr, L.A., E.J. Rudd, R.J. Coin, L.K. Mitchell, T.J. Schue, T. Turk, M.J. Niksa, and L.L. Frank, "Development of an Aluminum-Air Battery," Presented at the Eighth Battery and Electrochemical Contractors' Conference, Vienna, VA, 15-19 November 1987.

Leadbetter, A., "Thermal Enclosures for Advanced Electric Vehicle Batteries," *AICHE*, November 1987.

Leo, A., M. Klein, and C. Chi, "Status of Zinc-Bromine Battery Development at Energy Research Corporation," Presented at the 172nd Electrochemical Society Meeting, Honolulu, HI, 18-23 October 1987.

Leo, A., "Zinc-Bromine Core Technology Development," Presented at the Eighth Battery and Electrochemical Contractors' Conference, Vienna, VA, 15-19 November 1987.

Miller, J.F., and T.P. Mulcahey, "Evaluation of Advanced Lead-Acid Batteries Developed for Load-Leveling Applications," *Extended Abstracts: 172nd Electrochemical Society Meeting*, Honolulu, HI, 18-23 October 1987, Vol. 87-2, p. 146 (1987).

Miller, J.F., and T.P. Mulcahey, "Evaluation of Advanced Lead-Acid Batteries Developed for Load-Leveling Applications," *Extended Abstracts: 172nd Electrochemical Society Meeting*, Honolulu, HI, 18-23 October 1987, Vol. 87-2, p. 146 (1987).

Miller, J.F., T.P. Mulcahey, C.E. Webster, R.L. Hogrefe, and J.E. Kulaga "Experimental Evaluation of Nickel-Based Alkaline Batteries Developed for Electric Propulsion," *Extended Abstracts: 172nd Electrochemical Society Meeting*, Honolulu, HI, 18-23 October 1987, Vol. 87-2, pp. 212-13 (1987).

Miller, J.F., T.P. Mulcahey, C.C. Christianson, J.J. Marr, and J.A. Smaga, "Laboratory Evaluation and Analysis of Advanced Lead-Acid Load-Leveling Batteries," *Proceedings of the International Conference on Batteries for Utility Energy Storage*, West Berlin, Federal Republic of Germany, 9-11 November 1987, pp. 147-164 (1987).

Miller, J.F., T.P. Mulcahey, C.C. Christianson, J.J. Marr, and J.A. Smaga "Lead-Acid Load-Leveling Battery Testing at Argonne National Laboratory," *Extended Abstracts: Eighth Battery and Electrochemical Contractors' Conference*, Tysons Corner, VA, 16-19 November 1987, pp. 162-168 (1987).

Molyneux, J., G. Sands, S. Jackson, and I. Witherspoon, "Development and Testing of Sodium Sulphur Batteries for Electric Vehicle Application," Presented at the 22nd Intersociety Energy Conversion Engineering Conference, Philadelphia, PA, August 1987.

Mulcahey, T.P., J.F. Miller, C.E. Webster, and C.C. Christianson "Interim Technology Assessment of Research and Development Modules from Energy Research Corporation's Nickel/Cadmium Battery Contract," Presented at DOE EHP Contractors' Coordination Meeting, Las Vegas, Nevada, 1-2 December 1987.

Mulcahey, T.P., A.F. Tummillo, R.L. Hogrefe, C.C. Christianson, R.L. Biwer, C.E. Webster, J. Lee, J.F. Miller, J.J. Marr, and J.A. Smaga "Sodium-Sulfur Technology Evaluation at Argonne National Laboratory," *Extended Abstracts: Eighth Battery and Electrochemical Contractors' Conference*, Tysons Corner, VA, 16-19 November 1987, pp. 85-88 (1987).

Mulcahey, T.P., A.F. Tummillo, R.L. Hogrefe, C.C. Christianson, J.F. Miller, J.J. Marr, J.A. Smaga, C.E. Webster, and J. Lee "Zinc/Bromine Battery Evaluations at Argonne National Laboratory," *Extended Abstracts: Eighth Battery and Electrochemical Contractors' Conference*, Tysons Corner, VA, 16-19 November 16-19 1987, pp. 122-125 (1987).

Niksa, M.J., and D.J. Wheeler, "Aluminum-Air Batteries for Remote Applications," Presented at the ROV 1987, San Diego, CA, 10-12 March 1987. [This work was performed before ETD sponsorship.]

Niksa, M.J., and D.J. Wheeler, "Aluminum-Oxygen Batteries as Power Sources for Submersibles," Presented at the Fifth International Symposium on Unmanned, Untethered Submersible Technology, University of New Hampshire, 27 April 1987. [This work was performed before ETD sponsorship.]

Niksa, M.J., and D.J. Wheeler, "Aluminum-Oxygen Batteries for Space Applications," Presented at the Conference on Space Electrochemical Research and Technology at NASA-Lewis, Cleveland, OH, 14-16 April 1987. [This work was performed before ETD sponsorship.]

Riches, S.T., "Reliability of Resistance Welded Joints Between Joints Between Ni Shim and Inconel 600 Washer for Sodium Sulphur Battery," The Welding Institute, Report No. 24542/1/87, December 1987.

Rudd, E.J., Design Concept of the Aluminum-Air Battery for the DOE-EHP "Improved Dual Shaft Electric Propulsion" Van. Submitted to Sheladia Associates, Inc., Rockville, MD, 18 December 1987.

Sindorf, J.F., "Progress in the Development of A Low Cost Nickel Hydrogen Battery," Presented at the NASA/GSFC Battery Workshop, Greenbelt, MD, 4-5 November 1987.

Smaga, J.A., "Morphological Changes in Sulfur Electrode of Lifecycle-Tested Na/S Cells,"*Proceedings of the Symposium on Sodium-Sulfur Batteries*, San Diego, CA, 19-24 October 1986, Vol. 87-5, pp. 247-260 (1987).

Smaga, J.A., "Post-Test Analysis of CSPL Sodium/Sulfur Cells," *Extended Abstracts: Eighth Battery and Electrochemical Contractors' Conference*, Tysons Corner, VA, 16-19 November, 1987, pp. 69-72 (1987).

Zagrodnik, J.P., and M.D. Eskra, "Zinc/Bromine Battery Development," Presented at the 22nd Intersociety Energy Conversion Engineering Conference, Philadelphia, PA, 10-14 August 1987.

DISTRIBUTION

Argonne National Laboratory (8)
Attn: C. Christianson
W. DeLuca
J. Marr
T. Mulcahey (3)
P. Nelson
J. Smaga

Battelle (3)
Pacific Northwest Laboratories
Attn: D. Brown (2)
L. Kannberg
Battelle Blvd.
Richland, WA 99352

Battelle (7)
Pacific Northwest Laboratories
Attn: C.Imhoff
L. Fassbender (5)
R. Sen
2030 M Street NW
Washington, DC 20036

California State Air Resources Board
Attn: John Holmes
Research Division
PO Box 2815
Sacramento, CA 95812

Ceramatec
Attn: J. Rasmussen
163 West 1700 South
Salt Lake City, UT 84115

Chloride Silent Power, Ltd.
Attn: William L. Auxer (5)
Suite 1804
West Valley Road
Wayne, PA 19087

Dr. Robert Meredith
PO Box 164
Corvallis, OR 97339

EG&G Idaho, Inc.
Idaho National Engineering Lab
Attn: G. L. Hunt
PO Box 1625
Idaho Falls, ID 83415

Electric Power Research Institute (7)
Attn: R. Schainker
PO Box 10412
Palo Alto, CA 94303

Eltech Systems Corp.
Attn: E. Rudd
Research and Development Center
625 East Street
Fairport Harbor, OH 44077

Energetics (3)
Attn: J. Hurwitch
H. Lowitt
R. Scheer
9210 Route 108
Columbia, MD 21044

Energy Research Corporation
Attn: A. Leo
Three Great Pasture Road
Danbury, CT 06810

Johnson Controls, Inc. (3)
Attn: R. Beauchamp
M. Eskra
J. Zagrodnik
PO Box 591
Milwaukee, WI 53201

Lawrence Berkeley Laboratory (7)
University of California
Attn: E. Cairns
K. Kinoshita
F. McLarnon (5)
No. 1 Cyclotron Road
Berkeley, CA 94720

Martin Marietta Energy Systems, Inc.
Attn: J. Stovall
PO Box X
Oak Ridge, TN 37831

Science Applications International Corporation
Attn: B. Butler
10401 Roselle St.
San Diego, CA 92121

DISTRIBUTION (continued)

Wright Patterson AFB
Attn: W. Bishop
Air Force Wright Aeronautical Labs
AFWAL/POOC-1
Wright Patterson AFB, OH 45433

US Department of Energy (34)
Office of Energy Storage and Distribution
Attn: R. Eaton
M. Gurevich
K. Klein
A. Landgrebe
J. Quinn (30)
CE-32
FORSTL
Washington, DC 20585

US Department of Energy (4)
Office of Transportation Systems
Attn: K. Barber
P. J. Brown
R. Kirk
P. Patil
CE-152
FORSTL
Washington, DC 20585

US Department of Energy (5)
Albuquerque Operations Office
Attn: D. L. Krenz(2)
C. B. Quinn (2)
K. Smith
Energy Technologies Div.
Albuquerque, NM 87115

US Department of Energy
Sandia Area Office
Attn: A. R. Sneddon, Jr.
PO Box 5800
Albuquerque, NM 87115

20 O. E. Jones
140 W. W. Hollis
Attn: H. A. Romme, 143
400 A. N. Blackwell
1521 R. D. Krieg
1521 C. M. Stone
1524 A. K. Miller
1810 R. G. Kepler
1811 C. Arnold, Jr.
1811 R. L. Clough
1812 R. A. Assink
1812 J. M. Zeigler
1820 R. E. Whan
1840 R. J. Eagan
1845 E. K. Beauchamp
1845 R. P. Gerstle, Jr.
2000 L. K. Anderson
2500 D. B. Hayes, Actg.
2520 N. J. Magnani
2522 R. P. Clark
2523 J. Q. Searcy
2525 R. B. Diegle (75)
2526 R. C. Lincoln
3141 S. A. Landenberger (5)
3151 W. L. Garner (3)
3154-1 C. H. Dalin (8) for DOE/OSTI
3710 A. J. Arenholz
Attn: A. McConnell, 3714
6200 V. L. Dugan
6220 D. G. Schueler
6221 E. C. Boes
6223 G. J. Jones
8313 W. D. Bonivert
8313 L. R. Thorne
8524 P. W. Dean